Pavlov Institute of Physiology Russian Academy of Sciences
Ministry of Science and Higher Education of the Russian Federation
Institute of Electrical and Electronics Engineers (IEEE)
Neuroiconics Assistive Co. Ltd.
St. Petersburg State University of Film and Television

NEURAL NETWORKS AND NEUROTECHNOLOGIES

St. Petersburg, Russia
2019

UDC (Universal Decimal Classification) 001 Science and knowledge in general, 004 Computer science and technology, 004.5 Human-computer interaction, 159.91 Psychophysiology, 159.93 Sensation, 612.8 Neurophysiology and Sensory perception.

Authors: Aleksandrov A.A., Alizade M.R., Andreeva G.O., Andreeva I.G., Babenko V.V., Boiko A.A., Bondarko V.M., Chikhman V.N., Danilichev S.N., Dmitrieva E. S., Dobrov A.V., Dynin P.S., Emelin A.U., Glasman K.F., Gerasimov A.P., Gorbatov D.S., Grinenko E.N., Gvozdeva A.P., Harauzov A.K., Ikonopistseva K.A., Ivanova L.E., Knyazeva V.M., Koroleva I.V., Kozub K.E., Krasilnikov N.N., Krasilnikova O.I., Krivenchuk D.I., Kulchitsky V.A., Labutina O.V., Litvinenko I.V., Lobzin V.U., Malakhova K. Yu., Malashin D.O., Malashin R.O., Markin K.V., Merkulyeva N.S., Michalkin A.A., Moiseenko G.A., Murav'eva S.V., Naumov K.M., Ogorodnikova E.A., Pavlov A.V., Pechenchin D.V., Podvigina D.N., Pronin S.V., Puchkov N.A., Shalygin D. Yu., Shelepin E. Yu., Shelepin Yu.E., Shchemeleva O.V., Shepeleva I.P., Simarev A.N., Skuratova K.A., Smirnova V.A., Solnushkin S.D., Solovyev N.A., Soms L.N., Soms N.L,. Stankevich L.N., Tarumov D.A., Temniy A.V., Titarenko M.A., Varovin I.A., Vasiljev P.P., Yavna D.V., Zamaro A.S., Zhukova O.V., Zueva M.V.

Neural Networks and Neurotechnologies SPb, Publish by VVM, 2019, 294 p.

Editors: *Yuri Shelepin, Elena Ogorodnikova, Nikita Solovyev, Elena Yakimova*

Neurotechnology is the most important trend of intelligent technologies related to the study of brain activity such as: the perception and recognition, the decision-making mechanisms, the analysis of "maps" of neural network activity during planning and organizing targeted actions in real and virtual environment. Neurotechnologies are a part of the creation of the artificial intelligence systems, the convergence of man and autonomous intelligent artificial devices with targeted activities. This book reflects a wide range of investigations from biological and artificial neural networks to rehabilitation neurotechnologies for neurological patients (or patients with sensory and cognitive dysfunctions). Modern investigations and intellectual technologies open a new way of human cognition, purposeful behavior and «free will» (free choice) concept.

The material of this book has been discussed by the authors at the IEEE International Conference «Video and Audio Signal Processing in the Context of Neurotechnologies» May 27 — May 31, 2019 at I.P. Pavlov's Institute of physiology, St.-Petersburg, Russia, organized in collaboration with St.-Petersburg Electrotechnical University "LETI", St.-Petersburg State University of Film and Television, Neuroiconics Assistive Co. Ltd. The conference got the financial support of the Ministry of Science and Higher Education of the Russian Federation

Ministry of Science and Higher Education of the Russian Federation supported the edition of this book

ISBN 978-5-9651-1259-3

CONTENTS

PSYCHOPHYSICS AND PSYCOPHYSIOLOGY

Chapter 1.
Auditory adaptation to signals of biological value

I. G. Andreeva

Introduction

Prolonged presentation to an observer a constant or repeating visual stimulus can induce a transient alteration in the perception of following stimuli (afterimage or aftereffect). The cause of perceptual phenomena like afterimages or aftereffects is considered to be visual adaptation. Adaptation to signals of biological value matches processes in the visual cortex. A lot of auditory adaptation data to signals with biological significance has been received. It means that a sensory adaptation is the general principle of sensory tuning to the current structure of the information flow. Functionally, it is highly feasibly that adaptation may enhance the limited response range of neurons to encode sensory signals with much larger dynamic diapasons by shifting the range of stimulus amplitudes [Chung et al., 2002]. Perhaps, auditory adaptation to current information may be useful to take into consideration as an algorithm in artificial neural networks such as long short-term memory networks for separating acoustic flows and identifying new events in an acoustic environment.

Goal

The goal of the paper was to show that adaptation to signals of biological value is not only in visual but also in auditory modality and is implemented as the general principle of current information processing.

Auditory adaptation as a phenomenon

One example of auditory adaptation is the so-called "Zwicker tone," in which an illusory tonal sensation is heard for a few seconds following the presentation of a broadband noise containing a spectral notch about one-third octave in width [Zwicker, 1964]. The Zwicker tone has been described as a "negative auditory afterimage," because the pitch of the transient illusory tone corresponds roughly to the center frequency of the spectral notch in the preceding noise. Potential neural correlates for the phenomenon have been identified at the level of the auditory cortex [Hoke et al., 1996; Norena, Eggermont,

2003]. It appears that the aftereffect is related to a temporary enhancement of responsiveness, possibly related to a release from inhibition, in central auditory neurons with best frequencies within the spectral notch, which were least stimulated during the presentation of the inducer. Contrastive adaptation aftereffects were accounted not only for low-level stimulus qualities, but also for complex auditory stimuli. Auditory aftereffects have been identified for many features of auditory perception, including amplitude modulation [Rosenblith et al., 1947; Gutshalk et al., 2008], sound source location [Frissen et al., 2003; Phillips, Hall, 2005; Malinina, 2014], motion [Ehrenstein, 1978; Grantham, Wightman, 1979], phonemic category [Eimas, Corbit, 1973; Landahl, Blumstein, 1982; Sussman. 1993], voice gender [Schweinberger et al., 2008], voice timbre [Latinus, Belin, 2011], vocal emotion [Skuk, Schweinberger, 2013]. Perceptual aftereffects provide a unique psychophysical tool as evidence for the existence of specific feature detectors in the auditory system.

Auditory adaptation to motion cues

Human adaptation to sound source motion leads to a change in the perception of subsequent moving and stationary sound stimuli. After audition of repeated unidirectional adapting sound stimuli, a static test stimulus was perceived by listeners as shifting in the direction opposite to that of adapting stimuli. A test signal moving slowly toward the adapting stimuli was estimated by listeners as static (motionless). The fact that the auditory motion aftereffect is weaker than the visual aftereffect [Grantham, Wightman, 1979], as well as the multisensory interaction, when the motion of the visual adaptive stimulus causes changes in sound perception [Deas et al., 2008], suggests that the motion aftereffect is the result of central auditory system activity. The value of auditory motion aftereffect was maximal in case of real motion of sound sources. The auditory radial and azimuthal motion aftereffects depended on the motion simulation quality: how the motion simulation approximates real motion closely and also how the localization cues contained in the motion model are significant for the motion estimation. The effects were considerably less during motion simulation using only a single localization cue. The auditory motion aftereffect was demonstrated under different stimulation conditions: upon presentation of stimuli whose motion was simulated by varying the interaural differences in time or intensity of sound stimuli [Grantham, Wightman, 1979]; on the basis of the head-related transfer function or their simulation [Deas et al., 2008; Grantham, 1989; Neelon, Jenison, 2003; Shu et al., 1993]; upon presentation of stimuli really moving in the free field [Dong et al., 2000; Grantham, 1998]. The data

indicate a manifestation of the motion aftereffect in all coordinates of the acoustic space.

Studies of the auditory motion aftereffects during the sound azimuthal and radial motion revealed a spatial and frequency selectivity of this effect. For the spatially coinciding areas of adapting and test stimuli, the aftereffects magnitude proved to be the same on the motion trajectory ±35° relative to the head midline [Dong et al., 2000]. In another study addressing the spatial motion selectivity, the pronounced aftereffect was observed only for the adapting stimuli moving toward the head midline [Neelon, Jenison, 2003]. The auditory motion aftereffects of approaching and receding were larger when the trajectory of adapting and test stimuli ran within the limits of the certain coinciding trajectories [Malinina, Andreeva, 2013].

There were observed the significant differences in the magnitude of the motion aftereffect depending on the sound frequency and similarity/dissimilarity between spectral compositions of the adapting and subsequent test stimuli. The band low-frequency noise stimuli evoked the larger motion aftereffect in the horizontal plane than the high-frequency ones for which the effect was observed not in all listeners [Grantham, Wightman, 1979]. In another study, the noises with a bandwidth of one octave were applied to yield a several-fold reduction in the aftereffect magnitude with a discrepancy in the composition of adapting and test stimuli; and the larger the spectral distance, the weaker was the effect [Dong et al., 2000]. The effect reduction was more pronounced when the adapting stimulus had a higher frequency than the test one. Providing a coincidence between spectral compositions of adapting and test stimuli, a minimum magnitude of the effect was registered in the spectral range of 2–4 kHz where the binaural mechanisms of azimuthal localization, based on the interaural differences in time and intensity, function with lower efficacy. The above-presented data support the well-known fact of high significance of low frequencies for azimuthal localization. The radial coordinate aftereffect was observed in the event of coincidence between spectral compositions of adapting and test stimuli, while in the event of non-coincidence the radial motion aftereffect was not revealed [Andreeva, Nikolaeva, 2013]. For the high-frequency stimuli with a bandwidth of 3–20 kHz, the effect was obtained in the adaptation to approaching and receding sound stimuli, while for the low-frequency stimuli with a bandwidth of 0.05–1 kHz to approaching only. The data demonstrating spectral and spatial specificity reflect the known features of the human spatial hearing. Novel data were also obtained in studies of the optimal velocity ranges which cause a maximal aftereffect and correlate in literature

with optimal velocities at which a motion detection is performed in the auditory system most effectively [Deas et al., 2008; Andreeva, Malinina, 2011]. The motion aftereffects occurred independently of the spatial coordinate with the similarity of the adapting and test stimuli according to the main characteristics of the motion — spectral and temporal structure, spatial trajectory.

Auditory adaptation to speech cues

Thus, adaptation methods are widely used in sensory perception studies in order to investigate the mechanisms underlying the dynamic and environment-dependent processes of perception. Selective adaptation to linguistic features has been shown also for synthetic stimuli in speech perception [Eimas, Corbit, 1973; Coady et al., 2003]. Authors' works, mentioned below demonstrate the role of adaptation in calibrating properties of auditory representations of voices and show that recent perceptual experiences may significantly bias everyday perception of social information in voices. For instance, adaptation to nonlinguistic information in voices elicits systematic auditory aftereffects. Prior adaptation to male voices causes a voice to be perceived as more female (and vice versa), and these auditory aftereffects were measurable even minutes after adaptation [Schweinberger et al., 2008]. When sinusoidal tones (with frequencies matched to male and female voice fundamental frequencies) were used as adaptors, no aftereffects on voice perception were observed. This excludes explanations for the voice aftereffect in terms of both pitch adaptation and postperceptual adaptation to gender concepts and suggests that contrastive voice-coding mechanisms may routinely influence voice perception. The role of adaptation in calibrating properties of high-level voice representations indicates that adaptation is not confined to vision but is a ubiquitous mechanism in the perception of nonlinguistic social information from both faces and voices. Candidate regions for neural adaptation to voice gender remain to be determined, but based on previous neuroimaging results, one may expect such regions within auditory association cortex anterior to Heschl's gyrus and/or the superior temporal sulcus area of the right hemisphere [Belin, Zatorre, 2003; Lattner et al., 2005]. Adaptation may well be a general property of high-level auditory coding, and a full understanding of the mechanisms mediating auditory adaptation may ultimately benefit from progress in modeling sparse neural coding of auditory information [Smith, Lewicki, 2006].

Perceptual aftereffects to explore the representations of voice identity were used [Latinus, Belin, 2011]. A voice stimulus lying opposite to this voice relative to the average voice — i.e., its matched anti-voice — in a perceptual voice space yields aftereffects stronger than other adaptors, even though this

anti-voice is perceived as an unrelated identity. The results cannot simply be explained in terms of adaptation to low- level auditory representations: adaptation to low-level acoustical features would be expected to affect similarly the different adaptation conditions. Aftereffects were stronger for morph trajectories that pass through the average voice thus ruling out any explanation in terms of adaptation to low-level acoustic representations. The study provides empirical evidence supporting prototype-based coding of voice identity. Vocal emotion aftereffects for angry-to-fearful test voice continua were reported [Bestelmeyer et al., 2010; Skuk, Schweinberger, 2013]. Contrastive aftereffects were found for voice adaptation conditions, in that test voices were perceived as happier after adaptation to angry voices, and vice versa. A degree of variability in the data might be attributed to stimulus properties, such as differences in emotional expressiveness of individual stimuli. These data suggest that adaptation as a universal mechanism revealed in the central auditory system provides identification of the speaker during the processing of various stimuli, including non-linguistic speech information concerning gender and emotion of the speaker.

Conclusions

Auditory adaptation is a useful mechanism that allows flexible and quick change of the sensitivity to external stimuli in accordance with the environment. Adaptation, a mechanism by which specific neural responses decrease after prolonged stimulation, has been referred to as ‘‘the psychologist’s microelectrode’’ [Frisby, 1979] for its ability to reveal neuron populations tuned to the adapting stimulus. The versatility of adaptation with respect to various dynamic characteristics of the acoustic environment indicates the effectiveness of such a short-term tuning to the parameters of information about current events and the need to include this algorithm in the implementation of technical solutions in speech recognition systems and other dynamic processes.

The work was supported by state budget funding for 2013–2020 years (reg. no. AAAA-A18–118013090245–6).

References

1. Andreeva I. G., Malinina E. S. Auditory aftereffect of radial motion at different velocities of adapting stimuli // Fiziol. Chel. 2011. 37(1): 75–84.
2. Andreeva I. G., Nikolaeva A. V. Auditory motion aftereffect of approaching and receding sources of low- and high-frequency band noise // Fiziol. Chel. 2013. 39(4): 133–137.

3. Belin P., Zatorre R. J. Adaptation to speaker's voice in right anterior temporal lobe // Neuroreport. 2003. 14: 2105–2109.
4. Bestelmeyer P. E., Rouger J., DeBruine L.M., Belin P. Auditory adaptation in vocal affect perception // Cogn. 2010. 117: 217–223. doi:10.1016/j.cognition.2010.08.008.
5. Chung S., Li X., Nelson S. B. Short-term depression at thalamocortical synapses contributes to rapid adaptation of cortical sensory responses in vivo // Neuron. 2002. 34(3): 437–46. doi: 10.1016/s0896–6273(02)00659–1.
6. Coady J. A., Kluender K. R., Rhode W. S. Effects of contrast between onsets of speech and other complex spectra // J. Acoust. Soc. Am. 2003. 114: 2225–2235.
7. Deas R. W., Roach N. W., McGraw P. V. Distortions of perceived auditory and visual space following adaptation to motion // Exp. Brain Res. 2008. V.191. P. 473–485.
8. Dong C. J., Swindale N. V., Zakarauskas P., Hayward V., Cynader M. S. The auditory motion aftereffect: its tuning and specificity in the spatial and frequency domains // Percept. Psychophys. 2000. 62: 1099–1111.
9. Ehrenstein W. H. Direction-specific acoustical aftereffects // J. Acoust. Soc. Amer. 1978. 64: Suppl. 1. S35.
10. Eimas P. D., Corbit J. D. Selective adaptation of linguistic feature detectors // Cogn. Psychol. 1973. 4: 99–109.
11. Frisby J. P. Seeing: Illusion, Brain and Mind. 1979. 168 p.
12. Frissen I., Vroomen J., de Gelder B., Bertelson P. The aftereffects of ventriloquism: are they sound-frequency specific? // Acta Psychol. (Amst). 2003. 113(3): 315–327.
13. Grantham W. D. Auditory motion aftereffects in the horizontal plane: the effects of the spectral region, spatial sector and spatial richness // Acta Acustica. 1998. 84: 337–347.
14. Grantham W. D. Motion aftereffects with horizontally moving sound sources in the free field // Percept. Psychophys. 1989. 45(2): 129–136.
15. Grantham W. D., Wightman F. L. Auditory motion aftereffects // Percept. Psychophys. 1979. 26: 403–408.
16. Gutschalk A., Michey C., Oxenham A. J. The pulse-train auditory aftereffect and the perception of rapid amplitude modulations // J. Acoust. Soc. Am. 2008. 123(2): 935–945. DOI: 10.1121/1.2828057
17. Hoke E. S., Hoke M., Ross B. Neurophysiological correlate of the auditory after-image 'Zwicker tone' // Audiol. Neuro-Otol. 1996. 1: 161–174.
18. Landahl K. L., Blumstein S. E. Acoustic invariance and the perception of place of articulation: a selective adaptation study // J. Acoust. Soc. Am. 1982. 71(5): 1234–1241.

19. Latinus M., Belin P. Anti-voice adaptation suggests prototype-based coding of voice identity // Frontiers in Psychology. 2011. (2): 175. doi: 10.3389/fpsyg.2011.00175
20. Lattner S., Meyer M. E., Friederici A. D. Voice perception: Sex, pitch, and the right hemisphere // Hum. Brain Mapp. 2005. 24: 11–20.
21. Malinina E. S. Perception of approaching and withdrawing sound sources following exposure to broadband noise. The effect of spatial domain // Zh. Evol. Biokhim. Fiziol. 2014. 50(1): 59–68.
22. Malinina E. S., Andreeva I. G. Auditory motion aftereffect of receding and approaching sound source: a dependence on the trajectory and area of presentation of adapting stimuli // Zh. Evol. Fiziol. Biokh. 2013. 49(3): 211–223.
23. Neelon M. F., Jenison R. L. The effect of trajectory on the auditory motion aftereffect // Hearing Res. 2003. 180: 57–66.
24. Noren A. J., Eggermont J. J. Neural correlates of an auditory afterimage in primary auditory cortex // J. Assoc. Res. Otolaryngol. 2003. 4: 312–328.
25. Phillips D. P., Hall S. E. Psychophysical evidence for adaptation of central auditory processors for interaural differences in time and level // Hearing Res. 2005. 202(1–2): 188–199.
26. Rosenblith W. A., Miller G. A., Egan J. P., Hirsh I. J., Thomas G. J. An auditory afterimage? // Science. 1947. 106: 333–335.
27. Schweinberger S. R., Casper C., Hauthal N., Kaufmann J. M., Kawahara H., Kloth N., Robertson D. M. C., Simpson A. P., Zuske R. Auditory Adaptation in Voice Perception // Current Biology. 2008. (18): 684–688. DOI 10.1016/j.cub.2008.04.015
28. Shu Z. J., Swindale N. V., Cynader M. S. Spectral motion produces an auditory after-effect // Nature. 1993. 364: 721–723.
29. Skuk V. G., Schweinberger S. R. Adaptation Aftereffects in Vocal Emotion Perception Elicited by Expressive Faces and Voices // PLoS ONE2013 8(11): e81691. doi:10.1371/journal.pone.0081691
30. Smith E. C., Lewicki M. S. Efficient auditory coding // Nature. 2006. 439: 978–982.
31. Sussman J. E. Auditory processing in children's speech perception: results of selective adaptation and discrimination tasks // J. Speech. Hear. Res. 1993. 36(2): 380–395.
32. Zwicker E. 'Negative afterimage' in hearing // J. Acoust. Soc. Am. 1964. 36: 2413–2415.

Chapter 2.
Development of spatial frequency filters in ontogenesis

V. M. Bondarko

Introduction

Processing of visual signals is carried out by spatial-frequency channels [Campbell, Robson, 1968, Blakemore, Campbell, 1969]. Each channel consists of certain filters. It is possible to estimate the development of the highest-frequency filters in ontogenesis by measuring the minimal sizes of stimuli when their orientation is discriminated, and by studying crowding effect (deterioration of perception due to nearby surroundings).

The quantitative characteristic of the crowding effect at the resolution limit of visual system was measured by Flom, Weymouth and Kahneman in 1963 for adult subjects. The study showed that the recognition of the central test Landolt C deteriorated when it was flanked by four tangential bars at close distances. The distance between the test stimulus and flankers (or size of the inhibitory area where impairment was found) was equal about the size of the Landolt C. These researches [Flom et al., 1963] suggested that the distance over which spatial interaction occurs is related to the size of the receptive field that is most sensitive to the target.

To test this hypothesis many psychophysical experiments with different test stimuli and surroundings were carried out [Bondarko, Danilova, 1999, 2002; Danilova, Bondarko, 2000, 2007] for adult subjects. It was shown that the shape of the masking functions for test Landolt Cs in crowding effects at the resolution limit of the visual system is described well by a simple model. The model incorporates integration of the spatial profile of a receptive field (bar detector for symmetrical surrounding) with the luminance profile of the test Landolt C and distractors. These receptive fields correspond to the highest spatial frequency channel described by Wilson and Gelb (1984). The width of the excitatory area of the bar detector is almost equal to minimal size of Landolt C, when observers can discriminate its orientation. Moreover the size of inhibitory areas of crowding effect equal to the width of inhibitory areas of the minimal receptive fields. Correspondence was specified between the line spread function of bar detectors, the

optical scattering function and retinal cones mosaic [Shelepin, Bondarko, 2004]. It was shown also that high-frequency bar or grating detectors can perform initial processing of the test stimulus under different experimental conditions [Danilova, Bondarko, 2002, 2007].

But the dependence of minimal sizes of stimuli, when observers can discriminate their orientation, and sizes of inhibitory areas of crowding effect were unknown in ontogenesis. These values were measured partly in the early [Bondarko, Semenov, 2005] and in the present psychophysical experiments.

Method

Stimuli. Rectangular gratings or Landolt Cs were presented on a monitor screen as black images on a bright background. The background luminance was 80 cd/m^2 and the luminance of the bars was 5 cd/m^2. Landolt Cs were surrounded by tangential bars (Figure 1, a) or were presented alone. The gratings either were presented alone at the centre of the screen, or they were surrounded by four gratings having the same frequency (Figure 1, b). We changed distance (α) between the central stimulus and the surrounding ones. The duration of all stimuli was unlimited.

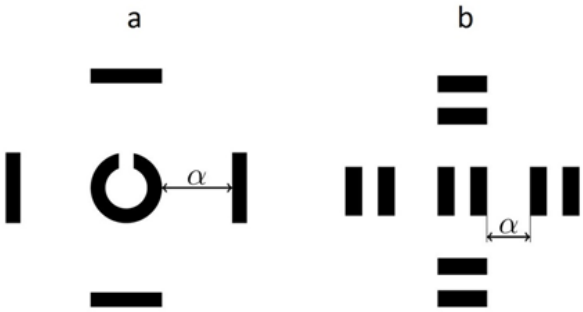

Figure 1. Examples of stimuli.

Procedure. Two experiments with each stimulus were carried out. The observer's task was to determine the orientation of the stimulus. The viewing distance was 4.1 m. The minimal sizes of rectangular gratings or/and Landolt Cs were measured at 75 % levels of correct responses for orientation discrimination, using the forced-choice staircase procedure 3:1. Playing situation was applied for little children. An example of a response card for such children is shown on figure 2 for the test Landolt Cs (a) and gratings (b, c). For Landolt

Cs used three-dimensional objects with parts removed. When the rectangular grating was presented the child said that the cat is lying or climbing a tree.

The influence of flanking stimuli in different separations (distances between edges of stimuli and distractors) on perception of these stimuli was studied as well. Flanking stimuli were bars for the test Landolt Cs and gratings surrounded the test gratings. We calculated right responses probability in each separation between the test stimuli and distractors and defined the sizes of the inhibitory areas by comparing the percent of correct responses obtained when the stimulus was surrounded by distractors with the percent of correct responses to the isolated stimulus (10 % level). Maximal separations were taken as the sizes of the inhibitory areas.

Subjects: 677 observers of 4–22 years old took part in study with normal vision.

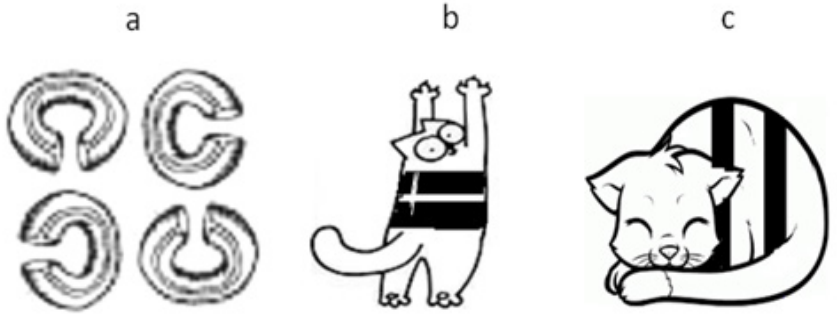

Figure 2. Response card for the little children.

Results

The minimal size and inhibitory area were measured for each observer. Figure 3 shows example of minimal sizes distribution for the test Landolt Cs. Then the data were averaged in age groups. Figure 4 represents mean values of minimal sizes and inhibitory areas in age groups for the test gratings (A) and the Landolt Cs (B).

The obtained minimal sizes gradually decreased when age increased and reached the adult level at 8–11 years for both stimuli. When the test stimuli were surrounded, deterioration in the identification of stimulus orientation for the short separations between stimulus and flanking patterns was found (crowding-effect). But age dependences were different for Landolt Cs and

gratings. These separations decreased until 16 years for gratings when age increased and did not change after 9–10 years for the Landolt Cs.

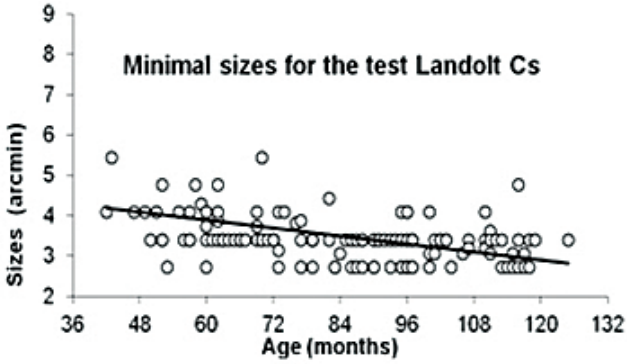

Figure 3. Example of distribution of the minimal sizes. Dependence on age (months).

These results have been specified on a large group of schoolchildren of 8–17 years old, which were tested by two stimuli. In one group of observers the first stimulus was Landolt C, for the other one it was grating. Then results of these groups were averaged. Significant decreasing of inhibitory areas for the test gratings were shown with age increasing until 16–17 years. But for the Landolt Cs inhibitory areas decreased until 12 years only. The minimal sizes did not change almost for these observers in dependence on age.

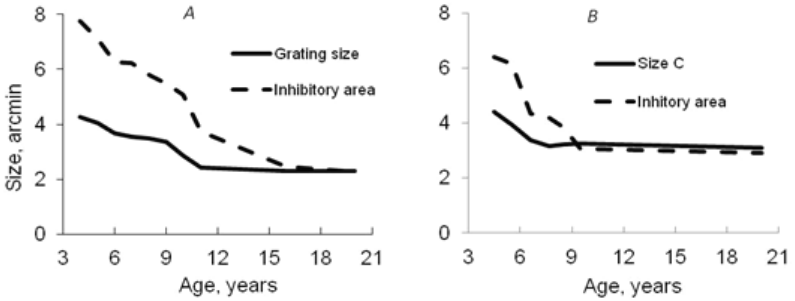

Figure. 4. Dependence on age of minimal sizes and inhibitory areas for the test gratings (A) and Landolt Cs (B).

As shown early, the minimal sizes almost equal to the width of excitatory areas of minimal receptive field (RF) while the inhibitory areas of crowding

effect correspond to RF inhibitory areas. Line spread functions were calculated using experimental data and parameters of model by Wilson and Gelb (1984). The line spread functions were approximated by the difference of two Gaussians for the little children and by the difference of three Gaussians for the other children. Their even line spread functions correspond to functions of RFs which are named lines detectors and have 3 and 5 separate excitatory and inhibitory areas respectively. The line spread function for the adult subjects was represented as Gabor element with equal width of excitatory and inhibitory areas. Its even function had almost 3.5 periods and similar to grating detectors in neurophysiology [Glezer, 1995].

We assume that such RFs form the highest spatial-frequency channels based on data for orientation sensitivity in ontogenesis [Bondarko, Semenov, 2017] because the dependence on age for orientation sensitivity was similar to the dependence for the gratings inhibitory areas.

Conclusions

We found different characteristics of crowding effects for test Landolt Cs and gratings and the same for minimal sizes of these stimuli. It is shown that the minimal sizes decrease with increasing age up to 8–11 years for both stimuli. But age dependences were different for the test Landolt Cs and gratings in crowding-effect. Separations between test stimuli and distractors where recognition was impaired decreased till 14–16 years for gratings and did not change after 10–12 years for Landolt Cs. The difference may be explained by considering different spatial elements or RFs of the visual system. Such elements in the first case may be the highest frequency grating detectors [Glezer, 1995] and the highest frequency line detectors [Wilson, Gelb, 1984] in the second case. These elements are lower frequency and broadband filters at younger age and higher frequency and narrowband filters among older observers. Our result develops the model by Wilson (1988) for the organization of spatial frequency channels in ontogenesis, which was elaborated for infant vision only.

References

1. Blakemore C., Campbell F. W. On the existence in human visual system of neurones selectively sensitive to the orientation and size of retinal image // J. Physiology. 1969. V.203. N1. P. 237–260.
2. Bondarko V. M., Danilova M. V. Relation between crowding-effect and functioning of high-frequency spatial elements // Sensory Systems. 2002. V.16. P. 89–99.

3. Bondarko V.M., Danilova M.V. Dependence of the size of the inhibitory zone on the shape of the test stimulus in the crowding effect // J. Optical Technology. 1999. V. 66. P. 865–868.
4. Bondarko V.M., Semenov L.A. Orientation Selectivity and Visual Acuity in Schoolchildren and Adults // Human Physiology. 2017. V. 43 (3). P. 259–264.
5. Bondarko V.M., Semenov L.A. Visual acuity and the crowding effect in 8- to 17-year-old schoolchildren // Human Physiology. 2005. V. 31 (5). P. 532–542.
6. Campbell F.W., Robson J.G. Application of Fourier Analyses to the Visibility of Gratings // J. Physiol. 1968. V. 197. P. 551–566.
7. Danilova M.V., Bondarko V.M. Foveal contour interactions and crowding effects at the resolution limit of the visual system // J. Vision. 2007. V. 7(2). N. 25. P. 1–18.
8. Danilova M.V., Bondarko V.M. Foveal crowding effect: Masking interactions or nature of the highest spatial-frequency mechanism? // Perception. 2000. V. 29. P. 51.
9. Flom M.C., Weymouth F.W., Kahneman D. Visual resolution and contour interaction // J. Opt. Soc. Am. 1963a. V. 53. P. 1026–1032.
10. Glezer V.D. Vision and mind: Modeling visual functions. 1995. Mahwah, NJ: Erlbaum.
11. Shelepin Y.E., Bondarko V.M. Resolving Ability and Image Discretization in the Visual System //Neuroscience and Behavioral Physiology. 2004. V. 34(2). P. 147–157.
12. Wilson H.R. Development of spatiotemporal mechanisms in infant vision // Vision Res. 1988. V.28. P. 611–628.
13. Wilson H.R., Gelb D.J. Modified line element theory for spatial frequency and width discrimination // J. Opt. Soc. Amer. A. 1984. V. 1. 124–131.

Chapter 3.
Can image statistics explain anomalous perception of length?

V. M. Bondarko, S. D. Solnushkin, V. N. Chikhman

Introduction

It is known that visual perception connects with environment. Setting of artificial neural networks also depends on the images which are presented during the learning. We considered from this point of view some illusions. Back in the 19th century, it was shown that vertical line appears to be longer than the same line presented horizontally (the vertical-horizontal illusion). But dependences of length estimation on lines orientation are different in various studies. In some investigations the maximum length being seen when the stimulus is oriented 20–30° from the vertical axis [e.g., Cormack, Cormack, 1974]. At these points line appear about 10–15 % longer than the minimum length seen by observers when the orientation of the stimulus is horizontal. In the other Studies, the maximum length seen by observers occurs when the line is vertical [e.g., Landwehr, 2017].

This dependence was tested by some researchers. The results were ambivalent. The reason of this discrepancy is unknown. But interpretation of the illusion connects with the nature of dependence and we tried to study the form of this dependence. We evaluated lines length varying their orientation, length and distance between them in a wide range.

Method

In psychophysical study four experiments were carried out with distances between lines 0.0 (connected lines), 2.4, 5.8 or 9.2 deg. In separate sets the lines length was equal to 0.7, 1.4 or 2.1 deg. The task of observers was to compare the length of horizontal and inclined lines. The lengths of inclined lines were fixed; but lengths of horizontal ones were varied. The forced-choice procedure was used. Three observers with normal vision took part in experiments.

Figure 1. Examples of stimuli of experiment *1* (a) and experiments *2–4* (b).

Results

We obtained different deviation of the length estimates for our observers. The highest illusion magnitude was 15–20 %. On Figure 2 data of observers S1, S2 and S3 are averaged. The dependence of illusion on orientation is shown. The distances between lines are equal to 0.0, 2.4, 5.8 or 9.2 deg (columns 1, 2, 3, 4).

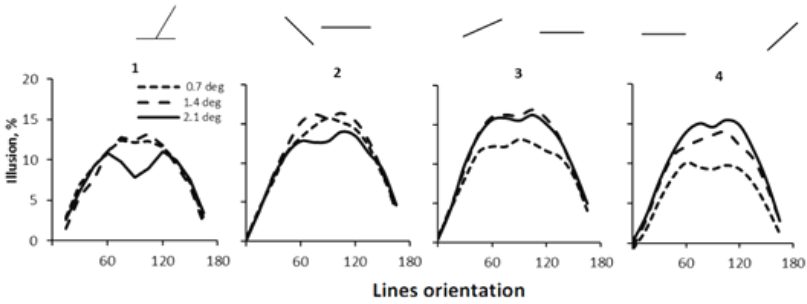

Figure. 2. Dependence of illusion on orientation. Lines length 0.7 deg, 1.4 deg and 2.1 deg. On top of the figure examples of stimuli are shown that were used in the experiments.

It was found that the magnitude of the illusion depended on the relative orientation of the lines and almost invariant to the line length. The illusion hardly changes with distance, but dependences were different. The illusion was a little less for abutting lines. In some cases, the longest lines seemed to be the lines with orientation 60 or 120° to the horizontal. But the tendency was not steady. Only for lines with length 2.1 deg and abutting lines the maxima were for orientations 60 or 120° for all observers.

On Figure 3 the averaged thresholds of observers S1, S2 and S3 are shown in dependence on orientation. 1 — adjoined lines, 2 — distance between lines 2.4 deg, 3–5.8 deg, 4–9.2 deg.

The thresholds were higher for those orientations for which there was a larger illusion. Minimal thresholds were found for adjoined lines and maximal ones for lines of minimal length (0.7 deg).

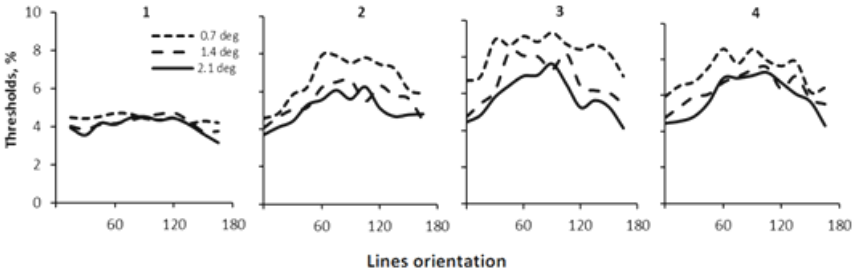

Figure 3. Dependence of averaged thresholds on orientation. Lines length 0.7 deg, 1.4 deg and 2.1 deg. *1* — adjoined lines, *2* — distance between lines 2.4 deg, *3* — 5.8 deg, *4* — 9.2 deg.

Discussion

We examined the variable perception of line length as a function of stimulus orientation and distance between them. Deviation of the length estimates was different for observers. The highest illusion magnitude was 15–20 %. It was found that Illusion depended on the relative orientation of the lines and almost invariant to separation between them. Refined dependences on orientation were individual. For the long (2.1 deg) adjacent lines, the illusion had maxima with orientations of 60 and 120º to the horizontal for all observers. In most other cases, the maximum was at 90º, i.e. in a vertical orientation. Thus we have not identified a common tendency.

The illusion was tried to be explained by various mechanisms. Several authors have proposed that the horizontal–vertical illusion is a consequence of a fixed distortion in the visual field. The basis for the distortion has been sought in (1) imperfections in the refractive properties of the eye [Avery & Day, 1969], (2) nonhomogeneous photoreceptor spacing in the retina [Begelman & Steinfeld, 1971], (3) no uniformities in retinal pigment distribution [Bayer & Pressey, 1972], and (4) the oval shape of the visual field [Künnapas, 1955].

Wolfe, Maloney and Tam (2005) considered the perspective theories [Gregory, 1968a, 1968b]. Perspective theories attribute such interactions to size constancy scaling: The configuration of line segments present in the visual field includes depth cues that trigger size scaling of each line segment. They

concluded that the available depth cues, even when supplemented by known biases in perspective interpretations, do not account for observed distortions in judgments of relative length.

Howe and Purves (2002) proposed other interpretation of illusion. They considered statistics of real images projections. An analysis of the natural images that included the three-dimensional location of every point in the scenes into two-dimensional projection showed that the average length of a physical interval in three-dimensional space changes systematically as a function of the orientation with maximums in 60 and 120°.

The absence of a general principle in our experimental data does not allow concluding about the mechanisms of the observed illusion.

Conclusions

Possible mechanisms for the appearance of an illusion are discussed, in particular, explaining the illusion by the statistics of two-dimensional projections of three-dimensional scenes, the theory of perspective or the connection of illusion with the elliptical form of the visual field.

Ambiguous dependencies may reflect the interaction of several mechanisms that manifest themselves in different observation conditions associated with the ellipsoid form of the visual field and the statistics of two-dimensional projections of three-dimensional real scenes. Thus, our data do not confirm direct connection between the projected images statistics and the variation of perceived length.

References

1. Avery G.C., Day R.H. Basis of the horizontal vertical illusion // J. Exp. Psychol. 1969. V.81. P. 376–382.
2. Bayer C.A., & Pressey A.W. Geometric illusions as a function of pigmentation of the fundus occuli and target size // Psvchonomic Science. 1972. V. 26. P. 77–79.
3. Begelman D.A., Steinfeld G. An investigation of several parameters of the horizontal-vertical illusion // Percept. Psychoph. 1967. V. 2 (11). P. 539–543.
4. Cormack E.O., Cormack R.H. Stimulus configuration and line orientation in the horizontal-vertical illusion // Percep. Psychophys. 1974. V. 16. P. 208–212.
5. Gregory R.L. Perceptual illusions and brain models // Proceedings of the Royal Society, B. 1968a. V. 171. P. 179–296.

6. Gregory R. L. Visual illusions // Scientific America. 1968b. V. 219 (5). P. 66–76.
7. Howe C. Q., Purves D. Range image statistics can explain the anomalous perception of length // Proc. Natl. Acad. Sci. USA. 2002. V. 99. P. 13184–13188.
8. Künnapas T. M. An analysis of the "vertical-horizontal illusion" // J. Exp. Psychol. 1955. V. 49. P. 134–140.
9. Landwehr K. Titchener's ⊥ with its lines tilted — A partial replication and extension of Cormack and Cormack (1974) // Atten. Percept. Psychophys. 2017. V. 79. P. 223–229.
10. Wolfe U., Maloney L. T., Tam M. Distortions of perceived length in the frontoparallel plane: Tests of perspective theories // Percept. Psychophys. 2005. V. 67(6). P. 967–979.

Chapter 4.
Comparison of the cosmonauts and the pilots visual system status after gravitational loads

S. N. Danilichev, Yu. E. Shelepin, S. V. Pronin

The consequences of the long-term effects of lowering of the level of gravity (conditions of hypogravity or microgravity) on the processes of visual perception are the most important factor in changing the working capacity of a person in orbit and on Earth [Bogomolov et al., 2015; Danilichev, Manko, 2018; Danilichev, Shelepin, 2013; Donina et al., 2013; Kuzmin, 2013; Mader et al., 2011]. The most sensitive method for assessing the state of the primary stages of the visual analyzer is visocontrastometry. To implement this method, visual stimuli with a precisely defined luminance profile are needed, suitable for measuring spatial frequency-contrast characteristics [Danilichev, Shelepin, 2013; Moiseenko et al., 2018; Shelepin, 2017; Vakhrameeva et al., 2013, Valiakh et al., 2017]. The synthesis of such stimuli on conventional liquid crystal monitors presents significant technological difficulties. For their synthesis, we have developed software (Ergotest-3), which allows for visocontrastometry using public laptops and tablet computers.

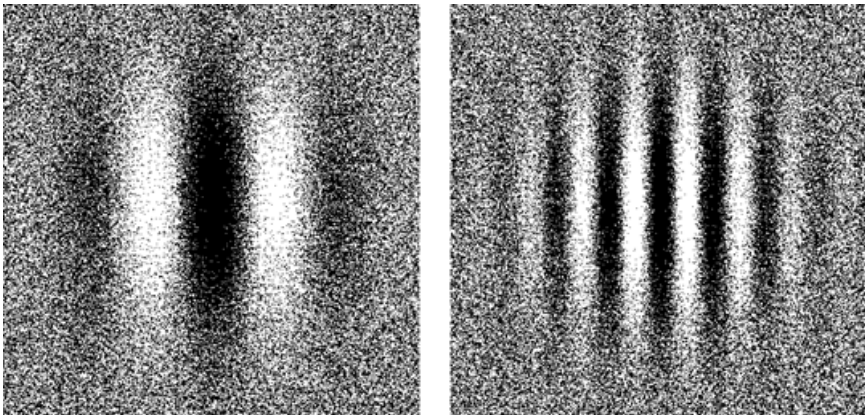

Figure 1. An example of test images — Gabor elements, as a function of modulating of the black and white pixels density.

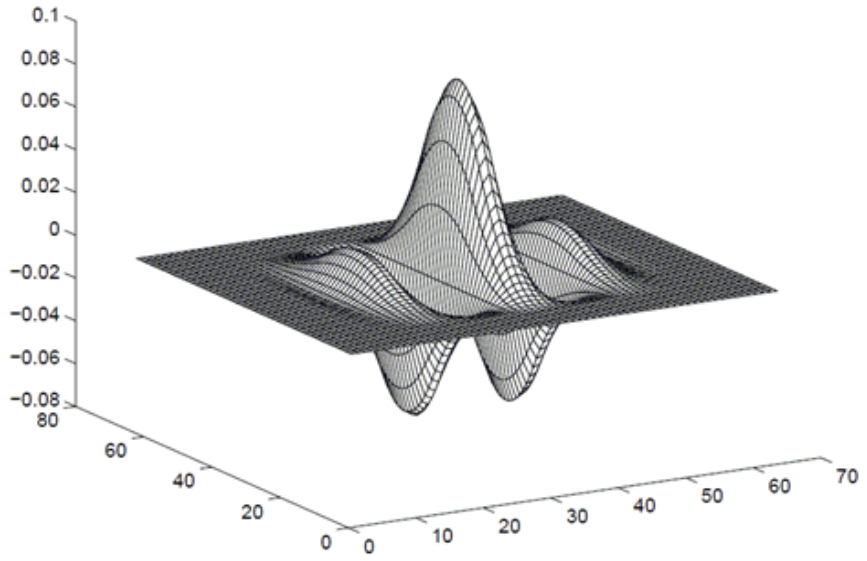

Figure 2. Three-dimensional image of a test stimulus — the Gabor element.

We analyzed the results of our measurement in two examined groups. The first group (70 measurements) was represented by astronauts flying into space at the age of 40 to 60 years. The second group (63 measurements) was represented by crew members of transport aircraft aged 40 to 60 who did not fly into space. The difference between the first group and the second was that the cosmonauts examined in this group were previously subjected to prolonged exposure to microgravity in space missions. The study of contrast sensitivity was carried out at frequencies of 0.3; 1.0; 4.0 and 8.0 cycle / city according to the program developed in the laboratory of physiology of vision of the Institute of physiology of the Russian Academy of Sciences (Pronin S. V., Shelepin Yu. E.). This method of conducting visocontrastometry is described in detail in the "Methodology for ophthalmological monitoring of the state of the organ of vision of operators" (Ergotest-3) approved by the "Federal State Budgetary Institution Scientific Research Institute of CPC named after Yu. A. Gagarin". Vision and comparison with data for optical coherence tomography of the eye (OCT) in persons associated with driving, including aircraft and spacecraft. The results of the measurements are presented in the figure 3. The 3-d group of the cosmonauts was 30–40 years old.

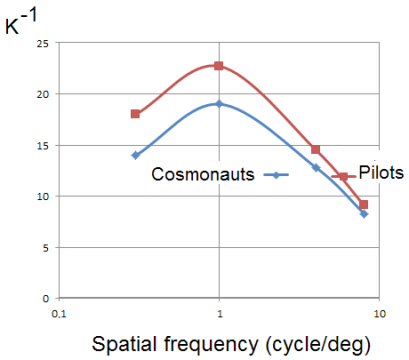

Figure 3. The contrast sensitivity of the cosmonauts, who made long space missions and the pilots, members of the aviation crews of the same age 40–60 years old.

Statistically significant differences according to the Student's criterion ($P < 0.005$) in the range of middle and low spatial frequencies between the groups of the cosmonauts (who made long space missions) and the pilots. The contrast sensitivity is on the ordinate K^{-1}.

To study the long-term effects of microgravity on the organ of vision of the astronauts, measurements were made of contrast sensitivity at frequencies of 0.3; 1.0; 4.0 and 8.0 cycle / degree before (background values), and on days 1, 3, 7 and 14 after long space flights (DCT). The results of the surveys are presented in figure 4.

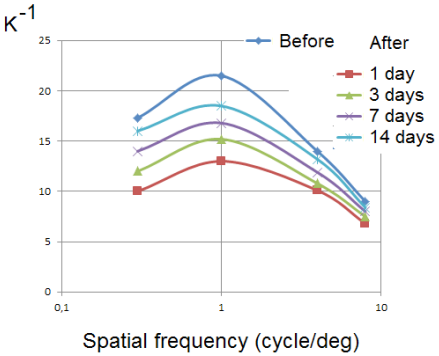

Figure 4. The contrast sensitivity of the cosmonauts (age 30-40 years old), before (top dark blue curve) and after long space missions.

Statistically significant ($P < 0.01$) differences of the cosmonauts before and after long space missions at different days (1, 3, 7, 14) after the end of the flight according to the The Wilcoxon Rank-Sum Tes criterion. The contrast sensitivity is on the ordinate K^{-1}.

Of particular interest is the change in contrast sensitivity in the region of low spatial frequencies. A decrease in sensitivity at low spatial frequencies reflects an increase in internal noise. In our subjects, the main factor that can lead to an increase in the level of internal noise is a change in hemodynamics. The combination of visocontrastometry and OCT makes it possible to give this explanation [Bogomolov et al., 2015; Danilichev, Manko, 2018; Danilichev, Shelepin, 2013; Donina et al., 2013; Kuzmin, 2013; Mader et al., 2011; Moiseenko et al., 2018; Shelepin, 2017; Vakhrameeva et al., 2013].

In the end, we propose such conclusions:

1. The method that measures contrast sensitivity of the visual system using public laptops was developed. The software presents the gradations of brightness on the monitor as a density of black and white pixels.
2. The method of measuring contrast sensitivity (visocontrastometria) made it possible to establish visual system status after gravitational loads by a long space flight. We provide the measurements during the first 14 days of rehabilitation after the end of the flight. We noted the decrease of contrast sensitivity at low and medium spatial frequencies, which reflects a change in the state of the nervous (not the optical) part of the visual system.
3. The decrease in contrast sensitivity is associated with a deterioration in the processing of visual information in the central nervous system and reflects an increase in the level of internal noise in the nervous system of the subjects.
4. It has been suggested that an increase in the level of internal noise in the nervous system occurs as a result of changes in blood circulation and the appearance of intracranial hypertension, recorded by optical coherent tomography (OCT).

References

1. Bogomolov V. V., Kuzmin M. P., Danilichev S. N. On the issue of intracranial hypertension in astronauts under conditions of prolonged weightlessness // Aerospace and Environmental Medicine, No. 4, Volume 49, 2015. S.54–58.
2. Danilichev S. N., Shelepin Yu. E. The study of frequency — contrast sensitivity of the organ of vision of astronauts in the process of biomedical training // Modern technologies for diagnosis and treatment of injuries of the organ of vision / Materials of the anniversary conference. SPb.: VMedA, 2013.S. 40.

3. Danilichev S. N., Manko O. M. “Neuroplasticity of the visual system in conditions of chronic stress” at the anniversary scientific-practical conference with international participation “General and military ophthalmology”, dedicated to the 200th anniversary of the foundation of the Department of Ophthalmology of the Military Medical Academy them. C. M. Kirov, which will take place on September 13–14, 2018.
4. Donina Zh.A., Baranov V. M., Alexandrova N. P., Nozdrachev A. D. Breathing and hemodynamics in modeling the physiological effects of weightlessness. St. Petersburg: Nauka, 2013, 182 p.
5. Kuzmin M. P. Risk assessment of increased intracranial pressure and edema of the optic nerve head in astronauts under conditions of prolonged weightlessness // Aerospace and Environmental Medicine, No. 4, 2013. S.85–86.
6. Mader T. H., Gibson G. R., Pass A. F. et al. Optic disc edema globe flattening, choroidal folds, and hyperopic shifts observed in astronauts after long-dyration space flight // Ophthalmology (American Academy of Ophthalmology Published by Elsevier Inc.) 2011. Vol. 118. P. 2058–2069.
7. Moiseenko G. A., Vakhrameeva O. A., Lamminpiya A. M., Pronin S. V., Maltsev D. S., Sukhinin M. V., Vershinina E. A., Kovalskaya A. A., Koskin S. A., Shelepin Yu. E. “The study of the relationship between the size of the foveola and the characteristics of visual perception.” // Human physiology. 2018.Vol. 44. No. 4.S. 22–29.
8. Shelepin Yu. E. Introduction to neuroiconics. SPb, 2017
9. Vakhrameeva O. A., Sukhinin M. V., Moiseenko G. A., Muravyova S. V., Pronin S. V., Volkov V. V., Shelepin Yu. E. Studying perception thresholds depending on the geometry of fovea // Sensory systems. 2013.Vol. 27. No. 2. P. 122–129.
10. Valiakh M. A., Katz D. V., Baranov M. V., Shpakov A. V., Merzlikin D. M. Influence on the hydrodynamics of the eye and the visual analyzer of conditions simulating “staying on the lunar surface”, a change in CFSM // Russian Medical Journal “Clinical Ophthalmology” No. 1 of 03/07/2017 p. 3–6.

Chapter 5.
Cross-modal interaction of visual and auditory components of media content

K. F. Glasman, E. N. Grinenko

Introduction

The current stage of the development of television broadcasting as a technical field is determined by the following main trends: the growing usage of audiovisual information in data networks, the increasing role of interactivity and the growing of mobile audiovisual services. The goal of current research in the field of quality assessment is to take into account all aspects of creating a holistic approach to quality assessment, which will determine the integral quality taking into account the characteristics of the user, system and context of use.

Today's television systems deliver programs that affect the organs of vision and hearing of the viewer. Quality assessment should be multimodal (in the framework of visual and audio modalities), giving a holistic description of the impression received by the final user. But television and other multimedia applications are not only the media, they also can be considered as parts of culture and art. Therefore, the assessment of the quality experience should be extended to the sphere of aesthetic perception and objects of art.

Progress in different applications of digital television broadcasting technologies is linked with the improvement of compression methods of digital video and audio data streams. Compression makes all new television services economically feasible because it allows consuming economically the most expensive resource of communication and information systems — the bandwidth of communication channels. However, compression causes distortions and artifacts of image and sound. The aim of this work is to study cross-modal interaction in assessing the quality of experience in digital television systems with data compression.

Cross-modal interaction of image and sound quality assessment

Existing methods do not meet the goals of current work, therefore, a new methodology for conducting psychophysical experiments was developed,

which can be used to study cross-modal interaction in assessing the quality of experience [Peregudov et al., 2010].

Quality assessment as a subjective quantity characterizing the degree of user satisfaction should take into account both semantic and aesthetic information contained in films and television programs. In the news and similar television programs, this is mainly semantic information. This information helps to decrease the degree of uncertainty (to increase viewer's knowledge) about any fact, event, phenomenon. Artistic and musical television programs contain mainly aesthetic information. Getting aesthetic information gives the viewer an aesthetic enjoyment. It is proposed to evaluate the degradation of integral quality caused by compression distortions as reducing the amount of semantic information and reducing the degree of aesthetic enjoyment (aesthetic information). In accordance with the proposed information approach, a double-stimulus quality assessment method was created, which uses of a new version of impermanent scale. A prototype of this method is described in Recommendation ITU-R BT.500 [Methodology for the subjective assessment of the quality of television pictures, 2012]. The evaluation process is regulated by the developed instruction for viewers, which is used in the process of experiments.

An important aspect of conducting subjective experiments is to choose a proper measurement standard: a scale and the determination of its properties. The scales proposed in the Recommendations developed by the International Telecommunication Union (ITU), including the scale of impairments [Methodology for the subjective assessment of the quality of television pictures, 2012], are ordinal scales. The numbers on such scales are ranks that allow ordering the values of the measured quality. But to use the results obtained in subjective experiments for solving mathematical modeling and optimization problems, it is necessary to have a scale that has the properties of an interval scale or, more preferably, a ratio scale. To build an impairment scale, which has the properties of scales of intervals or rations, the Thurstone method was used [Thurstone, 1925].

Statistical processing of data obtained in experiments by the Thurstone method showed that the impairment scale, built on the basis of the judgments "Degradation is imperceptible", "Degradation is perceptible, but does not hinder perception of information", "Degradation is perceptible and slightly hinders perception of information", "Degradation is perceptible and hinders perception of information", "Degradation is perceptible and hinders perception of information very much", "Distortion is extremely perceptible and extremely

hinders perception of information" has the properties of a scale of relations. The equivalents of judgments are the numbers 5, 4, 3, 2, 1, 0, that are used for all mathematical operations. The scale can be recommended for use in research and quality assessment of television broadcasting systems.

The developed methodology and scale ware used for integral quality assessment of compressed television materials [Peregudov et al., 2009; 2010, 2010a]. Three test audiovisual sequences were used in the study: a fragment of the news program ("talking head"), a music video clip and a sports report. Selected sequences have different audiovisual characteristics. The relevant factors in the video and audio domains that varied in the study were: video bit rate (video compression ratio), audio bit rate (audio compression ratio).

It was shown experimentally that cross-modal interaction exists. Distortions of both components (image and sound) caused by compression of video and audio signals influence the decision of experts when setting grades. One of the components can complement and modify the perceptual experience created by the other one. Evaluation of multimodal quality depends on the content (genre) of audiovisual work. Both modalities (visual and auditory) influence the quality perception, but one modality may be of high importance. In high motion sport programs the image quality has relatively higher weight compared to the sound. On the other side, in musical programs like music videos the sound quality is more significant. In head-and-shoulder news content the quality of sound is of greatest importance.

A quantitative assessment of the effects of cross-modal interaction was carried out as part of mathematical model creation that allows predicting the integral assessment of audiovisual quality of programs in television systems with data compression, taking into account the effect of cross-modal interaction.

Modeling the assessment of image and sound quality in modern multimedia systems is a complex task. Level decomposition can be used as an effective way to solve it. In this paper, it is proposed to use level decomposition when developing a model for integral quality assessment. At the first level, the model describes the relationship between image quality Q^*_V and sound quality Q^*_A and bit rates of compressed video and audio signals and these functions depend on the genre of audiovisual program, as it can be concluded on the basis of the experiments. The predicted quality at the first level of the model can be called monomodal ones. At the second level, the model describes the relationship of the integral quality Q^*_{AV} as a function of the image quality and sound found at the first level. The Q^*_{AV} integral quality predicted by the model at the second level can be called multimodal.

Finding the parameters of the subjective perception model describing the influence of audio and video bit rates on the integral quality is based on experimental research data, when viewers were asked to evaluate the image and sound quality, as well as to give a multimodal assessment of the same audio-visual clips: news program, sports reportage and music video clip.

At the second level, it is reasonable to use a polynomial approximation:

$$\begin{aligned} Q^*_{AV} = {} & c_0 + c_{A1} \cdot Q^*_A + c_{V1} \cdot Q^*_V + c_{AV} \cdot Q^*_A \cdot Q^*_V + \\ & + c_{A2} \cdot Q^{*2}_A + c_{V2} \cdot Q^{*2}_V + c_{AV2} \cdot Q^*_A \cdot Q^{*2}_V + \\ & + c_{A2V} \cdot Q^{*2}_A \cdot Q^*_V + c_{A3} \cdot Q^{*3}_A + c_{V3} \cdot Q^{*3}_V + \ldots \end{aligned} \quad (1)$$

Figure 1 represents the relationship between multimodal quality Q^*_{AV} and monomodal image quality Q^*_V and sound quality Q^*_A at various numbers of nonzero coefficients in the polynomial approximation and experimentally obtained data for a music video clip. The parameters of a multinomial model of subjective assessments of multimodal quality were obtained using the method of the least squares. As a parameter for the curves, the corresponding sound quality values are selected.

The linear model, when the values of monomodal image quality Q^*_V and sound quality Q^*_A are added up with weight coefficients c_{V1} and c_{A1}, generally describes the relationship obtained in the experimental studies. But according to the figure (Figure 1a), it can be concluded that the model does not fully correspond to the experimental results and does not take into account the interaction of two factors (the lines are parallel for each of the values of the Q_A parameter).

To describe the effect of two modalities interaction, the coefficient c_{AV} of the product of Q^*_V and Q^*_A must be nonzero. As can be seen from Figure 1b, straight lines are not parallel. In this case, the model will have the form of an incomplete quadratic model, which better describes the experimental data, reflecting the properties of mutual compensation of the quality of the components.

Numerical verification of the adequacy of the model using the criteria formulated by the VQEG (Video Quality Experts Group) image quality expert group: prediction accuracy, monotonicity of the prediction, prediction sequence. The value of the mean-square error characterizing the accuracy of prediction of the second-order polynomial model is 0.1568. Spearman's rank correlation coefficient characterizing the monotonicity of the prediction is 0.9883. The value of the emission factor, reflecting the consistency of the

model, is 0. Values of the metrics that determine the accuracy, monotonicity and consistency of prediction is sufficient, the second-order polynomial model well describes the multimodal assessment of quality of experience as a function of monomodal image and sound quality.

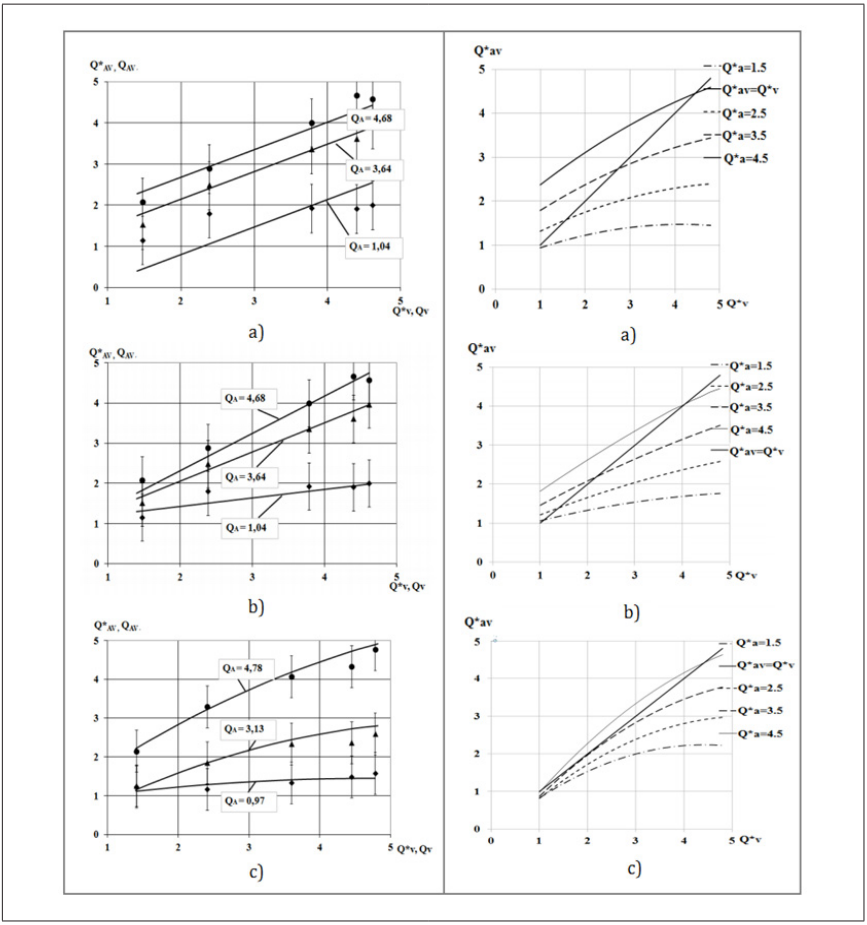

Figure 1. Relationship among Q*V, Q*A, and Q*AV for different numbers of terms of the polynomial approximation (*a* – co, cA1, and cv1 are non-zero coefficients; *b* — cO, cA1, cV1, and cAV are non-zero coefficients, *c* — cO, cA1, cV1, cAV, cA2, cV2 are non-zero coefficients

Figure 2. Relationship between multimodal quality (Q*AV) and monomodal video (Q*V) and audio quality (Q*A) for *a* — news; *b* — music video clip; *c* — sport

Audio and video quality interaction: quantitative estimates

Using the developed mathematical model of subjective assessments, it becomes possible to obtain quantitative estimates of the exchange relationships between audio and visual modalities and to reveal patterns of the interdependence of perception of audio and video information, for which only a qualitative description was previously known.

Figure 2 illustrates the relationship of the integral quality level predicted by the model as a function of monomodal image and sound quality for three sequences. Sound quality is selected as a parameter for the curves. An analysis of presented characteristics allows us to conclude that there are so-called neutral points. At these points, there is no decrease or increase in the level of subjectively perceived integral quality compared to monomodal image quality. Figure 2b represents the relationship between the integral quality predicted by the model and monomodal image and sound quality for music video. For example, if the values of image and sound quality are equal to $Q^*_V = 4$ and $Q^*_A = 4.5$, the level of integral quality will correspond to "4", i.e. equal to image quality. All neutral points lie on the line $Q^*_{AV} = Q^*_V$. For low image quality (i.e., for low video bit rates), the level of perception of integral quality will always be higher than the level of perception of image quality only for all three sequences. However, for medium and high values of image quality, the situation is not so simple and depends on the level of sound quality.

The developed model of multimodal quality assessment allows solving optimization problems that are very important for television broadcasting [Grinenko et al., 2014]. In television systems with data compression, including mobile television systems, that use the least broadband communication channels, the main task is to ensure an acceptable level of quality with limited channel bandwidth. For example, the task of achieving maximum multimodal quality with a fixed bandwidth of communication channel can be solved. The developed model of perception of multimodal quality will be used as an objective function in solving optimization problems. Using the optimal ratio between bit rates of digital audio and video data streams during the transmission of audio-visual programs can significantly increase the level of integral quality, especially in conditions of a narrow bandwidth of communication channel.

Conclusions

The effect of cross-modal interaction of two components of audiovisual program was studied. One modality (image or sound) can complement and modify the subjective perception created by the other one, also information

received by one sensory modality (visual or audio) affects the perception of information received by another sensory modality for different genres and contents of television programs. Quantitative estimates of exchange relationships between audio and visual modalities are obtained and the patterns of the interdependence of perception of audio and video information are revealed, for which only a qualitative description was previously known.

References

1. Grinenko E., Glasman K., Belozertsev A. Content-adaptive Bitrate Reduction in Mobile Multimedia Applications // Proceedings of 4th IEEE International Conference on Consumer Electronics — Berlin. 2014.
2. Methodology for the subjective assessment of the quality of television pictures, Rec. ITU-R BT.500–13. 2012.
3. Peregudov A., Glasman K., Belozertsev A., Grinenko E. Quality assessment of television materials in broadcast systems for mobile terminals // Scientific and Technical Journal of Information Technologies, Mechanics and Optics. 2009, No 04(62), pp. 102–108.
4. Peregudov A., Glasman K., Belozertsev A., Grinenko E.. Multimodal Quality Assessments of Compressed Television Materials for Portable and Mobile Devices // SMPTE Motion Imaging Journal. — January/February 2010. Pp. 42–51.
5. Peregudov A., Glasman K., Belozertsev A., Grinenko E. Model for assessing multimodal quality of audiovisual programs broadcast to mobile terminals // Scientific and Technical Journal “Radio Electronics Issues: Technology of Television”, 2010a, No. 1, pp. 21–33.
6. Thurstone L. L. A Method of Scaling Psychological and Educational Tests // Journal of Educational Psychology. 1925. 16. Pp.433–451.

Chapter 6.
The role of non-simultaneous masking in auditory perception of continuous and discontinuous sound images

A. P. Gvozdeva

Introduction

Many environmental sounds such as communicative signals of animals, sounds of steps and humans' speech have discontinuous temporal structure [Kozhevnikova, 1980; Catchpole, Slater, 1995; Wilden et al., 1998; Zellner, 1994]. In a simplified manner these signals can be presented as sequences of sound bursts with pauses between them, and durations of the bursts and pauses can vary in a wide range, depending on the type of the signal and its source. When approaching to a listener, sources of these signals produce a gradual increase of sound bursts amplitude in the place of listening. This can lead to a pronounced backward masking of sound bursts in a sequence, and, as a result, to the perception of continuous motion instead of discontinuous (or broken) one. The aim of this study was to determine threshold pauses for perception of broken and continuous approaching sound images in a wide range of sound bursts durations and to compare them with known temporal characteristics of backward masking.

Fifteen healthy adult individuals with clinically normal hearing participated in the study. Their hearing thresholds were assessed by pure-tone audiometry. All participants also successfully passed the random gap-detection test to ensure that they do not have impairments of temporal auditory analysis. Experiments were conducted in a soundproof anechoic chamber with the volume of 62.5 m^3 (5 × 5 × 2.5 m). Attenuation of external noise in the chamber was not less than 40 dB in the frequency range 0.5–16 kHz. Sound signals for modeling of sound source approaching were sequences of broadband noise bursts (0.03–20 kHz) with durations of 5, 10, 20, 40, 70 or 100 ms separated by 10–150 ms pauses. The noise bursts had trapezoidal shape with linear rise/fall times of 0.5 ms. Duration of sequences was 400 or 1000 ms. Amplitude of noise bursts increased from the beginning to the end of sequences for 40 dB. When played back through a loudspeaker placed in front of the listener at the distance of 1.1 m these sequences made an illusion of an approaching sound source. Maximum sound pressure level in the place of listening amounted 67

dB SPL and was the same for all stimuli. Assessment of threshold pause for perception of continuous and broken approaching sound images was carried out by the usage of adaptive transformed up-down method [Levitt, 1971]. For determining threshold of continuous motion, the experiment began from the sequences with the longest pause between sound bursts, and for thresholds of broken motion — from the sequences with the shortest pause. After listening to each of the sequences the subject had to push one of two buttons on a control panel to answer the question: "Does the sound image approach continuously or brokenly?" Threshold pauses for continuous and broken motion perception were determined at the level of 75 % of answers on the corresponding perceptive quality of motion. Significance of differences for the thresholds of continuous and broken motion perception was determined using Wilcoxon matched pairs test. The same approach was used to determine significance of differences between the thresholds of the same (continuous or broken) quality of motion in case of different durations of sound bursts.

Threshold pauses of broken and continuous approaching of sound images for the group of 15 subjects are presented at Figure 1.

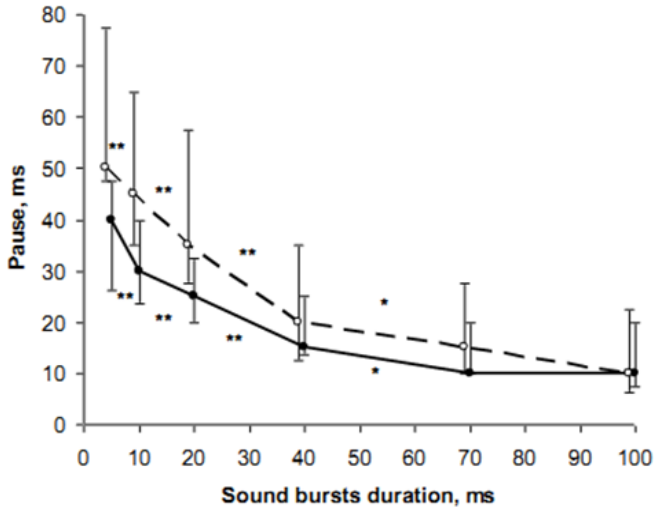

Figure 1. Median threshold pauses for perception of continuous (solid line) and broken (dashed line) approaching sound images by the group of subjects.

Asterisks show significant differences between the thresholds of the same quality of motion, but different sound bursts durations (**- $p<0.01$, *- $p<0.05$, Wilcoxon matched pairs test). 1st and 3rd quartiles are shown. N = 15.

For both continuous and broken motion the thresholds were highest in case of the shortest sound bursts (50 ms pause for broken motion and 40 ms — for continuous motion perception). Step-by-step increase of sound bursts duration from 5 to 70 ms led to a consistent statistically significant lowering of the threshold pause up to 10–20 ms. Subsequent increase of the sound bursts duration up to 100 ms did not cause significant changes of threshold pauses for both continuous and broken motion perception. The threshold pause of 40–50 ms for the shortest durations of sound bursts coincide with the results of Vartanian and Tchernigovskayas' (1980) study, which was carried out in close experimental conditions. The obtained lowering of threshold pause with an increase of sound bursts duration is in accordance with the data on backward masking, which was shown to have the longest duration for short masked signals and shorten with an increase of their duration [Pickett, 1959; Deatherage, Evans, 1969]. Comparison of perception thresholds of continuous and broken approaching sound images showed that threshold pauses for broken motion were significantly higher ($p<0.05$, Wilcoxon matched pairs test) than those for continuous motion in case of comparatively short noise bursts (5–20 ms). At the same time there were no significant differences between thresholds of continuous and broken motion for longer noise bursts. These facts can also be explained by properties of backward masking, more precisely by its logarithmic decay with time [Elliot, 1962]: for comparatively short pauses between a masked signal and a masker even a small increase of the pause can lead to a significant lowering of masking and, consequently, to the fast change of perceptual quality of motion which was observed for sequences with 40–100 ms noise bursts. In contrast, for shorter sound bursts durations (and longer pauses, starting from 25–30 ms) the same amount of unmasking can be achieved only when an increase of the pause is 10 ms or longer. Probably, that is why we found statistically significant differences between threshold pauses of continuous and broken motion perception for sequences with 40–100 ms noise bursts. Thus, auditory perception of continuous and broken moving sound images is considerably affected by non-simultaneous masking. It is possible, however, that thresholds of continuous and broken motion perception for receding sound images will be different from the ones for approaching sound images due to prevalence of different types of non-simultaneous masking in these cases: backward masking for approaching sound images, and forward masking for receding ones. This question is a topic of further research.

The work is supported by means of the state budget for 2013–2020 years (theme № AAAA-A18–118013090245–6).

References

1. Catchpole C. K., Slater P. J.B. Bird song: biological themes and variations // Cambridge university press. 2003. 348 p.
2. Deatherage B. H., Evans T. R. Binaural masking: Backward, forward, and simultaneous effects // The Journal of the Acoustical Society of America. 1969. V 46. PP. 362–371.
3. Elliott L. L. Backward and forward masking of probe tones of different frequencies // The Journal of the Acoustical Society of America. 1962. V. 34. P. 1116–1117.
4. Kozhevnikova E. V. Some characteristics of perception of an approaching sound image by human // Physiol. Journ. USSR. 1980. V.66. No. 1. P. 109–112 (in Russian).
5. Levitt H. T. Transformed Up-Down Methods in Psychoacoustics // The Journal of the Acoustical Society of America. 1971. V.49. P. 467–477.
6. Pickett J. M. Backward masking // The Journal of the Acoustical Society of America. 1959. V.31. P. 1613–1615.
7. Vartanian I. A., Tchernigovsaya T. V. Effects of different parameters of acoustic stimulation on estimation of changes of distances from the sound source by humans // Physiol. Journ. USSR. 1980. V.66. No 1. P. 101–108.
8. Wilden I., Herzel H., Peters G., Tembrock G. Subharmonics, biphonation, and deterministic chaos in mammal vocalization // Bioacoustics. 1998. V. 9. P. 171–196.
9. Zellner B. Pauses and the temporal structure of speech, in E. Keller (Ed.) Fundamentals of speech synthesis and speech recognition // Chichester: John Wiley. 1994. P. 41–62.

Chapter 7.
Dyslexia assessment model using the eye-tracker technique investigations

E. Yu. Shelepin, K.A. Skuratova

Dyslexia is a reading disorder, characterized by trouble with reading despite normal intelligence. Previously, it was common to call dyslexia "word-blindness". Dyslexia affects not only reading but also learning, writing, socializing. Modern theories associate dyslexia with lack of visual perception, disorders of the magnocellular pathway of the visual sensory system that affect the organization of eye movements and scene perception.

Objectives of our work were to study the influence of the visual text format on the spatial-temporal parameters of oculomotor activity on reading skills and to develop a prognostic model of reading skill disorder based on atypical oculomotor patterns while reading.

The purpose of the study was to analyse the oculomotor activity of the second-grade pupils and to reveal its connection with dyslexia and the visual format of the text display.

Our hypothesis was that dyslexia cause atypical patterns of oculomotor activity when reading texts aloud, increasing the number of fixations and their duration, increasing the frequency of regressive saccades, as well as reducing the amplitude of saccades.

Our study was standardized.

1. Instruction
2. Eye-tracker calibration
3. Reading aloud the stimulus text displayed on the screen
4. Interview on comprehension assessment
5. Repeat 2–4 for other stimulus (texts randomized)

Stimuli consisted of 5 texts of different.

1. **Normal**. Black font, white background, standard line length.
2. **Emoji**. Black font, white background, standard line length, illustrations in the form of pictograms, two in each line after the keywords.

3. **Beige on black**. Beige font (shade # f2c976), black background, standard line length.
4. **Colored syllables**. Accentuation of syllables using yellow (shade # e0d205), green (shade # 05e035), red (shade # e00505) and blue (shade # 0514e0) colors, white background, standard line length.
5. **Newspaper**. Black font, white background, shortened line length.

The sample (examples) of the stimuli is presented on the Figure 1.

Figure 1. The examples of the ordinary and reorganized texts images used as a stimulus.

The study was conducted in three secondary schools of St. Petersburg (№ 505, 567, 3).

The sample consisted of 77 second-grade students, normalized by gender. All subjects had normal or adjusted to normal vision and hearing. The intelligence of the subjects corresponded to the age norm (reading skill):

– 55 of them without a reading disorder
– 22 with dyslexia (based on psycho-medical pedagogical commission)

Results

The results of the eye tracks for normal and dyslexic patients are presented on the figure 2. These are not quantitative, qualitative data of visible differences in the characteristics of the eye movements of the two groups of subjects examined.

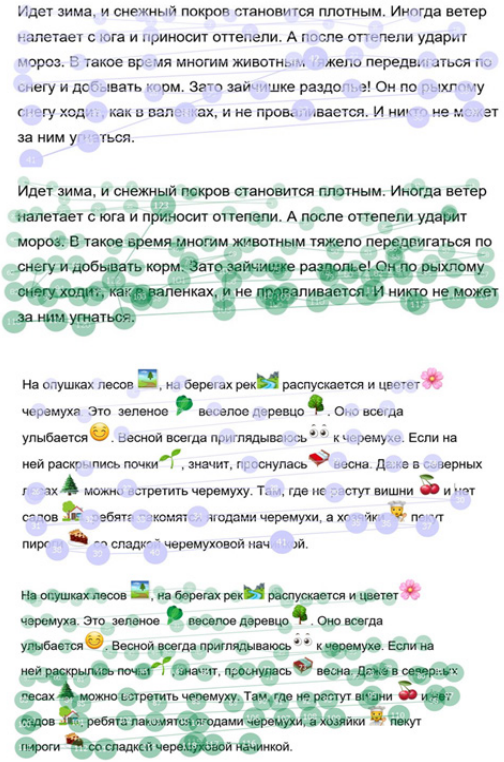

Figure 2. Example of scan paths of the eye movements for two groups of patients (violet — normal, green — dyslexia). The lines demonstrate the direction of saccades from the text beginning from the end of the text. The discs are the points of fixation.

You can see from the Figure. 2 that average typical patterns of the eye movements that belong to the dyslexia patients includes larger number of fixations smaller saccades.

On the next Figures 3 we present quantitative results on measured parameters of reading speed and the number of fixations per 1 word for of each text by two groups of school students. For each diagram, you can see a median, 25th and 75th percentiles, and minimum and maximum values.

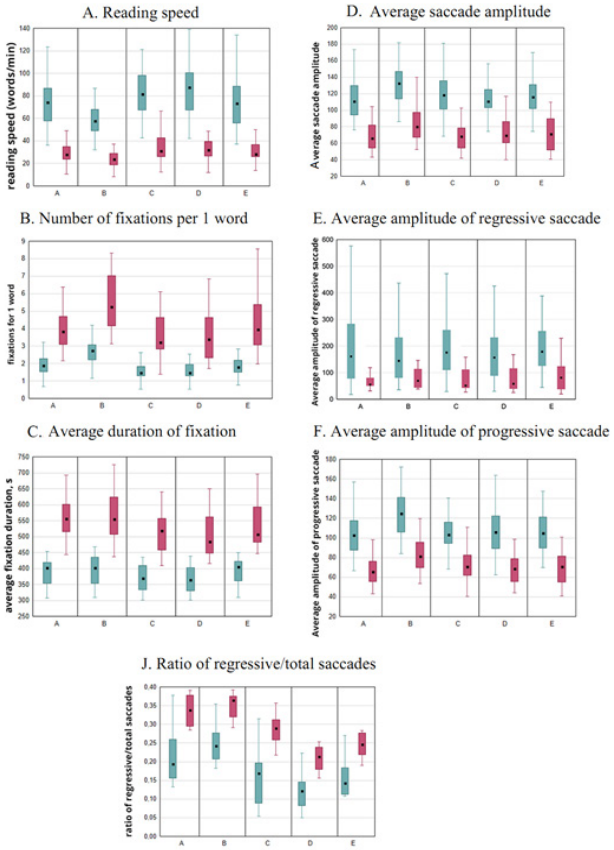

Figure 3. Parameters of reading speed and the number of fixations per 1 word of each text for two groups of school students. The median, 25th and 75th percentiles, and minimum and maximum values. The abscissa of *A, B, C, D, E* columns consists the stimuli 5 different variations of text formats.

Again, here is a scan path example for two groups.

Based on that data, we made two prognostic models. First one is a classification tree method. As a predictors, model includes fixation duration, fixations per 1 word, regressions ratio. That model describes 100 % of the sample. On the Figure.4 you can see the prognostic model based on the classification tree method.

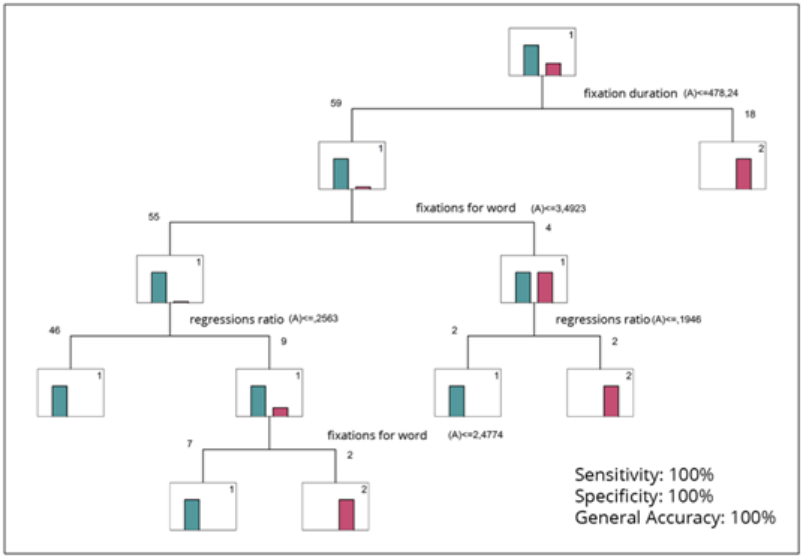

Figure 4. Prognostic model based on the classification tree method.

Using classification we developed the tree method and the discriminant analysis. Another model is based on the discriminant analysis, again it is very accurate. The results you can see in the Table 1.

Table 1

Prognostic model based on the discriminant analysis

N=77	Wilks' Lambda	Partial Lambda	F-remove (1,69)	p-value
reading speed	0,169300	0,989205	0,75298	0,388542
fixations per 1 word	0,215156	0,778379	19,64579	0,000034
fixation duration	0,233671	0,716702	27,27435	0,000002
saccade amplitude	0,167740	0,998408	0,11002	0,741123
progressive saccade amplitude	0,167619	0,999129	0,06015	0,806983
regressive saccade amplitude	0,167480	0,999957	0,00299	0,956581
regression ratio	0,240284	0,696980	29,99858	0,000001

We revealed possibility of using a prognostic method and the assessment of reading skills including dyslexia (for second-grades pupils), based on the spatial-temporal parameters of oculomotor activity as the:

- fixation duration
- ratio of regressive saccades
- fixations per 1 word.

This work is the demonstration of our way to develop a prognostic model of reading skill disorder based on the atypical oculomotor patterns during the reading.

References

1. Pinna B., Shelepin E., Deiana K.. Chromatic accentuation in Dyslexia: Useful implications for effective assistive technology. Materials of the IEEE International Symposium «Video and Audio Signal Processing in the Context of Neurotechnologies», pp. 34–36, St. Petersburg, Russia. ISBN 978-5-9651-1005-6

Chapter 8.
Investigation of the EEG variations during Verbal and Non-Verbal Communication during the Dialogue

O. V. Shchemeleva, O. V. Zhukova, P. P. Vasiljev, Y. E. Shelepin, G. A. Moiseenko

Comparison of various types of EEG indicators of brain activity of two interlocutors was conducted. The appropriate methodology and hardware-software complex has been developed for EEG hyperscanning: simultaneous EEG recording of two people with different location: face to face (with mimic observation of interlocutor) and back to back (without mimic observation) in terms of dialogue, monologue, listening and silence.

It was shown that the total EEG of interlocutors depends on the combination of verbal and nonverbal components.

The highest total EEG capacity of brain activity is shown for the interlocutors' location **"face to face**" compared to "back to back", when non-verbal information about the interlocutor was available. When comparing the conversation modes the largest total EEG power appeared in the **monologue** mode compared to silent, listening and dialogue mode.

Non-verbal communication of two people (not only mirror activity) leads to decrease in power of mu frequency band. During the "open eyes, silence" mode, a statistically significant difference in power values of **mu rhythm** between the face-to-face and back-to-back interlocutors was found (in the middle central and parietal areas).

Both verbal and non-verbal communication lead to an increase in power of beta 2 and gamma frequency band. It is interesting that changes in power during the «monologue» mode compared with the mode «open eyes, silently» were found only for location "**back to back**"

It is shown that the EEG of the speaker is different from the listener's EEG. There are statistically significant differences in power of **theta** frequency band in frontal channels (F7, F3) of the brain.

Event-related spectral perturbation (ERSP) (event-related shifts in the power spectrum) shows that more rhythmic spectral changes occur at channels FP1

and FP2 for both the speaker and listener. The ERSP image of speaker (channels FP1 и FP2) shows a rhythmic increase in power starting at about 1500 ms at 0–14 Hz (Δ, θ, α frequency ranges).

The ERSP image of the listener (channels FP1 и FP2) shows a rhythmic increase in power starting at 0 ms at 0–20 Hz (Δ, θ, α, β frequency bands).

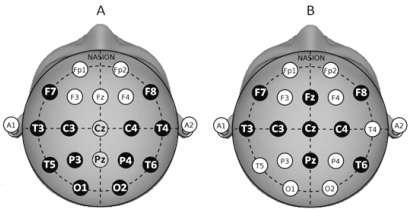

Figure 1. Compared power of EEG signals of the brain in different conditions:

A — «open eyes, silently» and B — «monologue». The data are averaged over 18 participants group. Grey color — increasing of signal power of gamma rhythm in condition «face to face». Black color — increasing of signal power of alpha rhythm in condition «back to back».

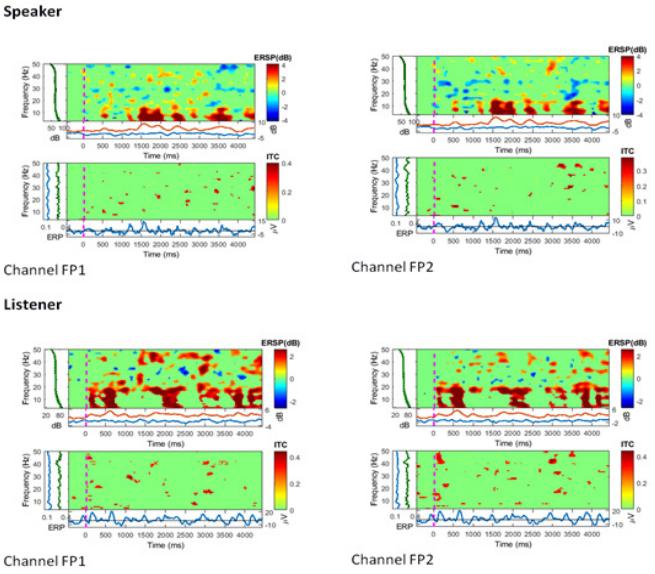

Figure 2. Example of event-related spectral perturbation (ERSP) images for speaker and listener for channels FP1 and FP2.

These results are interesting to compare with the previous hyperscanning studies that demonstrated a greater correlation between different structures of the speaker's and listener's brain.

It is shown that the EEG indicators can serve as markers reflecting different modes of communication.

References

1. Fox N. A., Bakermans-Kranenburg M.J., Yoo K. H. et al. Assessing Human Mirror Activity With EEG Mu Rhythm: A Meta-Analysis // Psychological Bulletin. 2016. V. 142. № 3. P. 291.
2. Liu D., Liu S., Liu X. et al. Interactive Brain Activity: Review and Progress on EEG-Based Hyperscanning in Social Interactions // Frontiers in Psychology. 2018. V. 9. P. 1.
3. Liu Y., Piazza E. A., Simony E., Shewokis P. A., Onaral B., Hasson U., Ayaz H. Measuring speaker–listener neural coupling with functional near infrared spectroscopy // Scientific Reports. 2017. 7. P. 1.
4. Montague P. R., Berns G. S., Cohen J. D. et al. Hyperscanning: simultaneous fMRI during linked social interactions // Neuroimage. 2002. V. 16. P. 1159.
5. Sänger J., Müller V., and Lindenberger U. Intra-and interbrain synchronization and network properties when playing guitar in duets. Front. Human Neurosci. 2012. V. 6. P. 1.
6. Zhukova O., Shelepin Y., Shchemeleva O., Vasilijev P., and Moiseenko G. Influence of verbal and nonverbal signals on an interlocutors electroencephalogram // J. Opt. Technol. 85, 455–462 (2018).

Chapter 9.
Speech detection in spatially distributed speech-like noise

V.A. Smirnova, O.V. Labutina, A.P. Gvozdeva

Introduction

The human auditory system has an ability to separate a target sound source from other sound sources. This ability plays a great role in speech communication in noisy and crowded environments and allows an individual to concentrate on a certain speaker while neglecting other speakers or noises. The problem solved by the auditory system in this case is referred as "the cocktail-party problem" and several physiological mechanisms which underlie its solving are currently known. One of them is connected with properties of speech itself.

Speech is a very convenient communicative signal for noisy environment because it concentrates energy in limited spectral regions, which makes it resistant to masking by background noise [Diehl, 2008]. In addition speech is a highly redundant signal which gives one an ability to "reconstruct" its missing (or masked) parts [Kalikow, Stevens, & Elliot, 1977]. The other mechanism involved in solving "the cocktail-party problem" is based on the fact that sources of the target speech signal and masking signals are usually separated in space. Thus, the effects of spatial release from masking improve speech detection and intelligibility in noisy crowded environment, and the improvement arises from differences in the binaural cues of the target speech signal and the masking signal [Andreeva et al., 2019; Sutojo et al., 2018]. For example, the separation of sources of the target speech signal and the masker by the azimuthal coordinate can lead to the release from masking up to 12 dB [Best et al., 2013; Culling et al., 2004]. Separation by distance also improves speech detection: spatial release from masking amounts up to 2–3 dB when sources of target speech signal and speech-like noise masker placed in front of a listener and separated by 3 m distance [Andreeva et al., 2019]. Authors of this work assume that there is a possibility of auditory spatial tuning to egocentric distance characterized by a certain opening angle, under which the sound wave arrives to the left and right ears, when the source placed directly in front of the listener. I.e. spatial release from masking for the speech signal and the speech-like noise masker separated by distance is also determined by

a binaural mechanism. However in real conditions, for example in a crowded café, or a market place, the source of speech-like noise has no certain position and typically it is distributed in space. The present study was conducted to assess the impact of spatially distributed (internalized) speech-like noise on target speech signal detection threshold for typical communicative distances (1–4 m).

Goal

The goal of the study was to determine detection probabilities of speech signals from the sources placed at distances of 1, 2 or 4 m in case of spatially distributed speech-like noise of different intensities.

Method

Psychoacoustic experiments were conducted in accordance with International Ethical Guidelines for Biomedical Research Involving Human Subjects.

Subjects: 17 individuals aged 20–34 years (8 men and 9 women). Hearing conditions of subjects were estimated by using a pure-tone audiometry (AA-02 audiometer) and a random gap-detection test.

In experiments target speech signal was located directly in front of a subject at different distances — 1, 2 and 4 m. The sources of internalized babble-noise were placed around the head of the listener (Figure. 1).

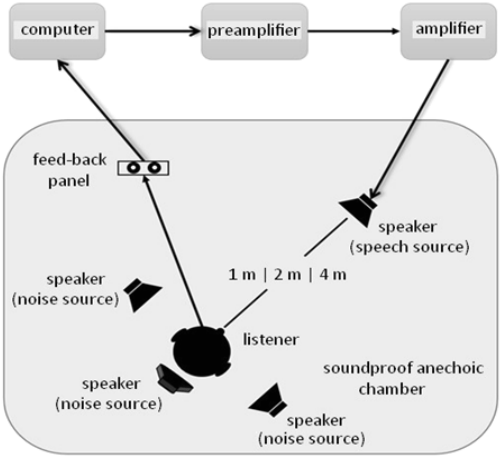

Figure 1. Experimental apparatus diagram.

The stimuli were eight disyllabic Russian words (“pochva”, “stroka”, “rubezh”, “plata”, “vypusk”, “kredit”, “ruchka”, “nabor”) with a low frequency of usage in accordance with the national corpus of the Russian language. These words were pronounced by four native speakers — two men (whose fundamental frequencies were 117 and 139 Hz) and two women (fundamental frequencies 208 and 234 Hz). Monophonic audio recording of words was made in a quiet room, the background noise level was 30 dB SPL. In this way, 32 different speech files were recorded using Sennheiser E845 vocal microphone with a cardioid pattern and an external USB audio interface Creative E-MU 0202 connected to a desktop PC with Adobe Audition 1.5 software. As a speech-like masker, the result of mixing 32 audio files with duration of 10 s was applied, in each of which one of the words was repeated several times successively without pauses. While listening to this speech-like masker, the subjects has an auditory sensation similar to those he/she experiences being in a room where many people speak at the same time. The technique for creating such crowd noise is described in more details in the paper [Best et al., 2013].

Ten randomly selected fragments of 2 s duration each with 100 ms rise and fall times were cut from the received sound file. These fragments were used in experiments as masking signals. Duration of 32 speech stimuli was in the range from 515 to 935 ms while duration of maskers was 2 s.

Experiments to evaluate probabilities of speech signals detection were carried out under conditions of a soundproof anechoic chamber with a volume of 62.5 m^3. The attenuation of external noise in the chamber was not less than 40 dB in the frequency range 0.5–16 kHz. Acoustic measurements were conducted using microphone 4145, preamplifier 2639 and amplifier 2606 of Bruel and Kjaer Company in a mode of averaging the mean square power over a time interval of 1000 ms.

Speech stimuli were played back on MicroXperts PC with external USB audio interface Creative E-MU 0202, the analog signals from which were fed to ONKYO power amplifier, and then to loudspeaker SONY XSF1720 located in the chamber in front of the listener at the level of his/her ears (azimuth 0º, elevation 0º) at one of the following distances: 1, 2 or 4 m. Speech-like noise maskers were played back using the same equipment except they were fed to three loudspeakers placed at distances of 1 m in front of left and right ears of the listener and above his/her head.

There were three experimental series of stimuli which differed from each other by position of the source of target speech stimuli (1, 2 or 4 m). Each series was a sequence of 40 pairs of speech-like maskers, which varied in intensity be-

tween pairs. One of 32 target speech stimuli was presented during sounding of one of the two speech-like maskers in each pair. The pause between the pairs of signals was 5 s, and the pause between the signals in the pair was 1 s. Formation of sequences of experimental series and their subsequent reproduction was carried out automatically with the help of an original computer program. As a result of equalizing the meansquared power of all speech stimuli at the listening position, their level was 50 dB of sound pressure level (SPL) and was the same in all experimental series. The level of the speech-like masker at the listening position was changed in 3 dB increments and was equal to 55, 58, 61 or 64 dB (SPL). More details of the method are in [Andreeva et al., 2019].

Subjects listened to each of the experimental series once. After listening to a pair of speech-like maskers, the subject had to answer the question: "During which period of noise, first or second, a speech signal appeared?" by pressing one of two buttons on a control panel. The answer of the subject was recorded automatically.

Probabilities of correct judgments were assessed for each subject at each of three spatial configurations and signal-to-noise ratios (SNRs): -5,-8,-11 and -14 dB. The reliability of changes in the probability of detecting speech stimuli depending on SNR and the distance between the speech sound sources and speech-like noise was estimated using non-parametric Wilcoxon pair test.

Results

Probabilities of detection of speech signals under condition of their frontal placement at distances of 1, 2 and 4 m from the listener (typical distances for a communication situation) were determined in case of different intensities of spatially distributed (internalized) speech-like noise masker.

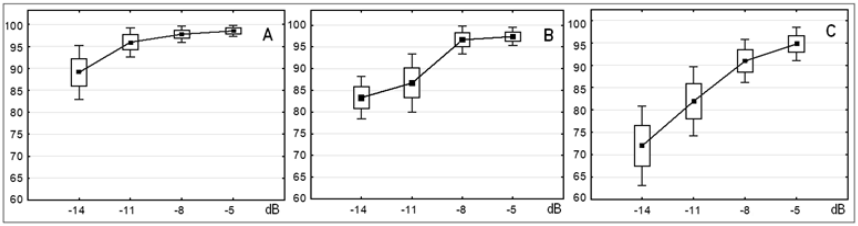

Figure. 2: Group mean probability of target speech signal detection at various SNRs for three different distances: A — 4 m, B — 2 m, C — 1 m. The SNR, dB, is on the X axis, the signal detection probability,%, is on the Y axis.

At 4 m distance from the target speech signal source and SNR of -14 dB, the average value of the signal detection probability was 89 % and then reliably increased ($p < 0.01$) to 96 % for -11 dB. For -8 and -5 dB SNRs probabilities amounted 98 % and 99 % respectively (Figure 2, A). For 2 m distance from the listener to the speech signal source, the average probability of detection at -14 dB SNR was 83 %, and increased up to 87 % at -11 dB SNR, and then reliably increased ($p < 0.01$) to 97 % at -8 dB SNR and 98 % at -5 dB SNR (Figure 2, B). The data on the detection probability at different SNRs for the distance to the source of the target speech signal of 1 m are presented in Figure 2, C. At -14 dB SNR the probability was 72 %, at -11 dB it amounted 82 %, and for SNRs of -8 and -5 dB — 91 % and 95 % respectively. There was a tendency to a difference ($p < 0.01$) between the probabilities at the SNRs of -8 and -5 dB.

Comparison of the relative changes in the probabilities of detecting the target speech signal at 4 (Figure 3, A) and 2 m (Figure 3, B), revealed a number of significant differences, discussed below.

For both 4 and 2 m distances to a source of speech signals probabilities of speech detection were higher than for 1 m distance. The decrease was statistically significant for SNRs of -14 and -11 dB SNRs in case of 4 m distance (17 and 14 % respectively, $p<0.01$, $p<0.05$) and only for -14 dB SNR under condition of 2 m distance to the source of speech signals (11 %, $p<0.05$).

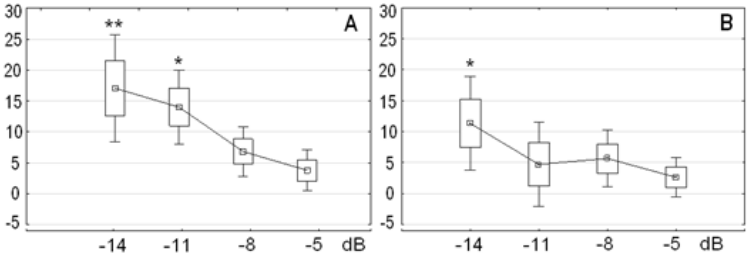

Figure 3. Relative change of detection probability for 4 m (A) and 2 m (B) distances as compared to detection probability at 1 m distance. The S/N ratio, dB, is on the X axis. The relative detection probability change (%) is on the Y axis. (** – $p<0.01$; * – $p<0.05$, comparison with corresponding values for 1 m distance)

Conclusions

The probability of signal detection decreases proportionally to the SNR decrease for all tested distances. The most prominent decrease was observed for 1 m distance to the target speech stimulus, and the least prominent — for 4

m. Distance is a crucial factor for speech detection at low SNRs: an increase of distance from 1 to 2 m leads to a significant improvement of speech detection at -14 dB SNR, and increase from 1 to 4 m significantly improves speech detection for both -11 and -14 dB SNR. Thus, speech stimuli from distant sources are more likely to be detected in spatially distributed speech-like noise at low SNRs than stimuli from closer sources. It is possible that the way of making spatially distributed noise that was used in present work produced a sound image of internalized noise and consequently was more efficient as a masker for closer (more internalized) than for farther (more externalized) sources of speech signals.

References

1. Andreeva I.G., Dymnikowa M., Gvozdeva A.P., Ogorodnikova E.A., Pak S.P. Influence of separation by the distance of the sources of speech and noise on speech signal detection// Acta Acust united Ac. 2019. V.105. P. 484–491.
2. Best V., Thompson E.R., Mason C.R., Kidd G.J. An energetic limit on spatial release from masking // J. Assoc. Res. Otolaryngol. 2013. V. 14. P. 603.
3. Culling J.F., Hawley M.L., Litovsky R.Y. The role of head-induced inter-aural time and level differences in the speech reception threshold for multiple interfering sound sources // J. Acoust. Soc. Am. 2004. V. 116. P. 1057.
4. Diehl R.L. Acoustic and auditory phonetics: the adaptive design of speech sound systems // Philos Trans Royal Soc. 2008. V.363. P. 965–978.
5. Kalikow D.N., Stevens K.N., Elliott L.L. Development of a test of speech intelligibility in noise using sentence materials with controlled word predictability // J Acoust Soc Am. 1977. V.61. N.5. P. 1337–1351.
6. Sutojo S., van de Par S., Schoenmaker E. Contribution of binaural masking release to improved speech intelligibility for different masker types // Eur. J. Neurosci. 2018. doi:10.1111/ejn.13980

SENSORY PHYSIOLOGY AND NEURAL NETWORKS

Chapter 10.
Effects of trace amine-associated receptors (TAARs) agonists on the mismatch negativity (MMN) and sensory gating

A.A. Aleksandrov, V.M. Knyazeva, E.S. Dmitrieva, L.N. Stankevich

Trace amines (TAs) have long been known to be present in low concentrations in the mammalian nervous system. TAs are related by structure to classical biogenic amines and violation of their concentration is associated with different psychiatric impairments [Branchek and Blackburn, 2003; Burchett and Hicks, 2006; Berry et al., 2017; Gainetdinov et al., 2018]. The so-called trace amine associated receptors (TAARs) belong to the family of G protein-coupled receptors and are divided into three subgroups: TAAR1–4, TAAR5 and TAAR6–9 [Lindemann et al., 2005]. TAARs family members, which are relatively well represented in the central nervous system, are TAAR1 and TAAR5.

TAAR1 is the best studied member of the TA receptor family [Bradaia et al., 2009; Lindemann et al., 2008; Revel et al., 2011; Leo et al., 2014]. TAAR1 is mainly expressed in the limbic system and monoaminergic systems regions [Lindemann et al., 2008; Panas et al., 2010]. Large amount of data suggest that TAAR1 is an important dopaminergic, serotonergic and glutamatergic neuromodulator [Lindemann et al., 2008; Revel et al., 2011; Miller, 2011; Espinoza et al., 2015]. Some data indicate TAAR1 role in a number of pathological conditions, including schizophrenia [Gainetdinov et al., 2018]. Currently, the promising drugs for the schizophrenia treatment, based on TAAR1 agonist as a therapeutic target, are at the stage of clinical trials [Berry et al., 2017].

The co-expression of mouse TAAR1 and TAAR5 in the amygdala, arcuate nucleus and ventromedial hypothalamus have been recently reported by Dinter and co-workers [Dinter et al., 2015]. TAAR5 has been found to be a target of 3-iodothyronamine [Dinter et al., 2015], a neuromodulator that affects adrenergic and histaminergic neurons and improves learning and memory [Zucchi et al., 2014]. Furthermore, recent studies have discovered the effect of TAAR5 agonist on brain monoamine systems, electrical and locomotor activity in mice [Efimova et al., 2019].

Thus, at the moment, research into the role of trace amines receptors in the pathophysiology of psychiatric impairments, including schizophrenia, is one of the key areas of neuropharmacology. The research work of our laboratory was focused on the effects of TAAR1 and TAAR5 agonists on the schizophrenia electrophysiological endophenotypes, such as mismatch negativity (MMN) and sensory gating (SG) in rodents.

Electrocorticogram was recorded on mice and rats with implanted epidural electrodes before and after the injection of TAARs agonists: alpha-NETA, the TAAR5 agonist, and RO5263397, the TAAR1 agonist. The paired-click and oddball paradigms were presented acoustically for SG and MMN researches, respectively.

The results obtained indicate that the TAAR1 agonist RO5263397 and TAAR5 agonist alpha-NETA have the opposite effect on schizophrenia biomarkers. We found a significant enhancement of SG index [Aleksandrov et al., 2019c] and an increased MMN-like response [Aleksandrov et al., 2019a] after the TAAR1 agonist administration in mice. Conversely, the TAAR5 agonist causes a significant SG index decrease in rats [Aleksandrov et al., 2018] and an additionally amplitude decline and latency increase in mice ERPs [Aleksandrov et al., 2019d]. In the MMN research paradigm the TAAR5 agonist has been found to decrease an MMN-like response that resulted from the N40 increase to standard stimuli without corresponding changes in the response to deviant stimuli (unpublished data). It should be noted, that TAAR5 agonist administration also increased the amplitude of the late positive ERP component both in mice (unpublished data) and rats [Aleksandrov et al., 2018b].

Previous studies have established that TAAR1 is localised in dopaminergic and serotonergic regions of the brain and acts as a neuromodulator for dopaminergic, serotonergic and glutamatergic systems [Lindemann et al., 2008; Revel et al., 2011; Miller, 2011; Espinoza et al., 2015]. TAAR1 agonists are known to have the unique ability to normalize the glutamatergic and monoaminergic neurotransmission [Gainetdinov et al., 2018]. Studies of TAAR5 agonist cognitive and behavioral effects show that the alpha-NETA administration leads to a decreased sensory gaiting in rats, as well as behavioral abnormalities in mice that are similar to human tardive dyskinesia [Aleksandrov et al., 2018a; Aleksandrov et al., 2019b]. Furthermore, TAAR5 agonist causes an increase in dopamine (DA) and its metabolites levels [Efimova et al., 2019]. These results allow us to assume that TAAR5 may presumably affect the dopaminergic system.

It can be assumed that the SG index and MMN-like response changes under the TAAR1 and TAAR5 agonist's action is due to the influence of the classical monoamine neurotransmitters. An increased SG index and MMN-like response in mice after the RO5263397 injection gives us a reason to suggest that TAAR1 activation may help to normalize the SG index and MMN in various pathological conditions, including schizophrenia. Otherwise, a decrease of ERP response amplitudes and latency in paired-click paradigm as well as the MMN-like response after the alpha-NETA injection allows us to suggest the potential TAAR5 contribution in the pathophysiology of schizophrenia spectrum disorders.

This work was supported by the Russian Foundation for Basic Research (Grant No. 17-04-00082).

References

1. Aleksandrov A.A., Dmitrieva E.S., Volnova A.B., Knyazeva V.M., Gerasimov A.S., and Gainetdinov R.R. (2018a). TAAR5 receptor agonist affects sensory gating in rats. Neuroscience letters, 666, 144–147.
2. Aleksandrov A.A., Knyazeva V.M., Volnova A.B., Dmitrieva E.S., Korenkova O., Espinoza S., Gainetdinov R.R. (2018b). Identification of TAAR5 agonist activity of alpha-NETA and its effect on mismatch negativity amplitude in awake rats. Neurotoxicity research, 34, 442–451.
3. Aleksandrov A.A., Knyazeva V.M., Volnova A.B., Dmitrieva E.S., Polyakova N.V., Gainetdinov R.R. (2019a). Trace amine-associated receptor 1 agonist modulates mismatch negativity-like responses in mice. Frontiers in Pharmacology, 10, 470.
4. Aleksandrov A.A., Polyakova N.V., Vinogradova E.P., Gainetdinov R.R., and Knyazeva V.M. (2019b). The TAAR5 agonist α-NETA causes dyskinesia in mice. Neuroscience letters, 704, 208–211.
5. Aleksandrov A., Dmitrieva E., Volnova A., Knyazeva V., Gainetdinov R. and Polyakova N. (2019c) Effect of trace amine-associated receptor 1 agonist RO5263397 on sensory gating in mice. NeuroReport, 30(15), 1004–1007.
6. Aleksandrov A.A., Dmitrieva E.S., Volnova A.B., Knyazeva V.M., Polyakova N.V., Ptukha M.A. and Gainetdinov R.R. (2019d) Effect of alpha-NETA on auditory event related potentials in sensory gating study paradigm in mice. Neuroscience Letters, 712, 134470.
7. Berry M.D., Gainetdinov R.R., Hoener M.C., Shahid M. Pharmacology of human trace amine-associated receptors: therapeutic opportunities and challenges. Pharmacol Ther. 2017; 180: 161–180.
8. Bradaia A., Trube G., Stalder H., Norcross R.D., Ozmen L., Wettstein J.G., et al. (2009). The selective antagonist EPPTB reveals TA-

AR1-mediated regulatory mechanisms in dopaminergic neurons of the mesolimbic system. Proc. Natl. Acad. Sci. 106, 20081–20086.
9. Branchek T.A., and Blackburn T.P. (2003). Trace amine receptors as targets for novel therapeutics: Legend, myth and fact. Curr. Opin. Pharmacol. 3, 90–97.
10. Burchett S.A., Hicks T.P. (2006). The mysterious trace amines: Protean neuromodulators of synaptic transmission in mammalian brain. Prog. Neurobiol. 79, 223–246.
11. Dinter J., Mühlhaus J., Wienchol C.L., Yi C.X., Nürnberg D., Morin S., and Krude H. (2015). Inverse agonistic action of 3-iodothyronamine at the human trace amine-associated receptor 5. PLoS One, 10(2), e0117774.
12. Efimova E.V., Gerasimov A.S., Sukhanov I., Antonova K.A., Ptuha M.A., Volnova A.B. and Gainetdinov R.R. (2019). Identification of the agonist of trace amine-associated receptor 5 (TAAR5) and its action on brain physiology and neurochemistry. European Neuropsychopharmacology, 29, S571-S572.
13. Espinoza S., Lignani G., Caffino L., Maggi S., Sukhanov I., Leo D., … and Medrihan, L. (2015). TAAR1 modulates cortical glutamate NMDA receptor function. Neuropsychopharmacology, 40(9), 2217.
14. Gainetdinov R.R., Marius C.H., Mark D.B.. Trace Amines and Their Receptors. Pharmacol Rev. 2018; 70: 549–620
15. Leo D., Mus L., Espinoza S., Hoener M.C., Sotnikova T.D., and Gainetdinov R.R. (2014). Taar1-mediated modulation of presynaptic dopaminergic neurotransmission: Role of D2 dopamine autoreceptors. Neuropharmacology 81, 283–291.
16. Lindemann L., Ebeling M., Kratochwil N.A., Bunzow J.R., Grandy D.K., and Hoener M.C. (2005). Trace amine-associated receptors form structurally and functionally distinct subfamilies of novel G protein-coupled receptors. Genomics 85, 372–385.
17. Lindemann L., Meyer C.A., Jeanneau K., Bradaia A., Ozmen L., Bluethmann H., … and Hoener M.C. (2008). Trace amine-associated receptor 1 modulates dopaminergic activity. Journal of Pharmacology and Experimental Therapeutics, 324(3), 948–956.
18. Miller G.M. (2011). The emerging role of trace amine-associated receptor 1 in the functional regulation of monoamine transporters and dopaminergic activity. Journal of neurochemistry, 116(2), 164–176.
19. Panas H.N., Lynch L.J., Vallender E.J., Xie Z., Chen G.L., Lynn S.K., et al. (2010). Normal thermoregulatory responses to 3-iodothyronamine, trace amines and amphetamine-like psychostimulants in trace amine associated receptor 1 knockout mice. J. Neurosci. Res. 88, 1962–1969.
20. Revel F.G., Moreau J.L., Gainetdinov R.R., Bradaia A., Sotnikova T.D.,

Mory R., … & Metzler V. (2011). TAAR1 activation modulates monoaminergic neurotransmission, preventing hyperdopaminergic and hypoglutamatergic activity. Proceedings of the national academy of sciences, 108(20), 8485–8490.

21. Zucchi R., Accorroni A., & Chiellini G. (2014). Update on 3-iodothyronamine and its neurological and metabolic actions. Frontiers in physiology, 5, 402.

Chapter 11.
Comparative analysis of event related potentials in monkeys and humans

A. K. Harauzov, I. A. Varovin, L. E. Ivanova, D. N. Podvigina

Neurophysiological basis of human brain functioning is difficult to study without using animal models. Monkeys are the closest animals to humans in evolutionary terms, as well as anatomical structure and physiological characteristics. Here we present comparative research of humans' and monkeys' electrophysiological reactions during visual pattern discrimination.

Visual stimuli were rectangular matrices each composed of 100 Gabor patches having different orientations. Matrices differed in the number of Gabor patches with vertical, or horizontal, orientation [Kharauzov et al., 2008; Shelepin et al., 2009; Figure 1].

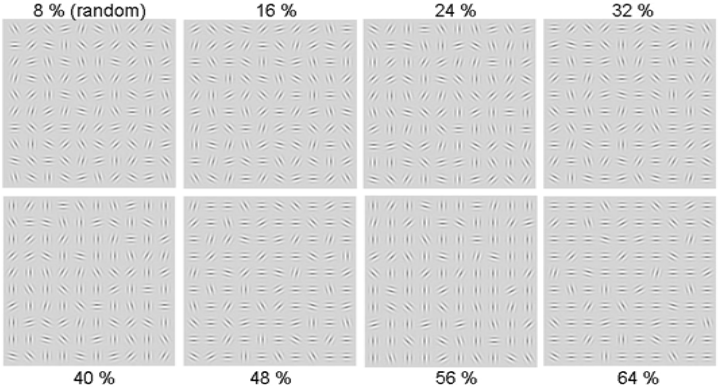

Figure 1. Examples of the test matrices with different degree of orderliness of the Gabor patches' orientation in percentages.

The observers' task was to discriminate the dominant orientation (vertical or horizontal); therefore the difficulty of perceptual tasks depended on the degree of order in the matrix. While humans were presented 7 different types of stimuli and were required to press the left or right mouse button to indicate their choice, the monkey's task was to choose the vertical matrix out of the two ones

presented on a touchscreen; four most difficult matrices were used. Percentage of correct responses, reaction times and event related potentials (ERPs) were recorded while subjects performed the task. In total, 25 human subjects participated once in the experiment, and one macaca mulatta monkey repeated the same experiment 21 times. The data obtained from all 25 human subjects and from all 21 experiments on monkey were averaged and then compared.

Figure 2 illustrates dependencies of the accuracy and the median reaction time of humans' (left) and monkey's (right) on the number of co-oriented Gabor patches in the matrix. As for humans and monkey, the percentage of correct responses was low (70 %) for less ordered matrices and sharply increased with the degree of "orientational orderliness", reaching a plateau (95 %) where matrices contained 40 or more co-oriented elements. In contrast, reaction time gradually decreased with increasing numbers of co-oriented gratings, demonstrating a shorter duration of stimulus processing for

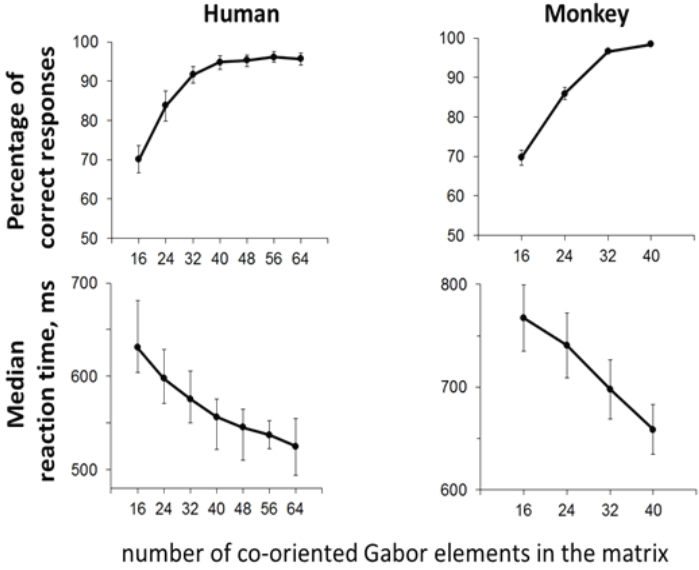

Figure 2. Percentage of correct responses (up) and median reaction time (down) as a function of the number of co-oriented Gabor elements in the matrix for humans (left) and monkey (right). For humans each trace is averaged across 25 participants [data taken from Harauzov et.al, 2016]. For the monkey the data were averaged across 21 experiments hold on different days. Error bars indicate 95 % percentile bootstrap confidence intervals with 1000 bootstrap samples (for humans) and SEM for monkey.

highly ordered matrices. Note the similarity of the humans' and monkey's responses with exception of the slight increase of the monkey's reaction time comparatively to humans, which is most probably explained by the difference in the response acquiring methods (mouse button press for humans and touch the screen for monkey).

Comparison of the shape of ERPs recorded from humans and monkey revealed much earlier responses in monkey's ERPs which appeared in occipital area as early as 40 ms after stimulus presentation, whereas in humans' ERP the first prominent wave we observed at 90 ms after stimulus onset. In the time interval of 90–230 ms after stimulus onset the components' polarity and latency in occipital area were similar in humans and monkey. Both species showed positive waves at 90–100 ms and at 220–230 ms and negative wave at 150–160 ms after stimulus onset. However, later waves showed different polarities between humans and monkey. ERPs recoded from central areas of the brain were quite different in humans and monkey both in shape and polarity of the main waves (see figure 3).

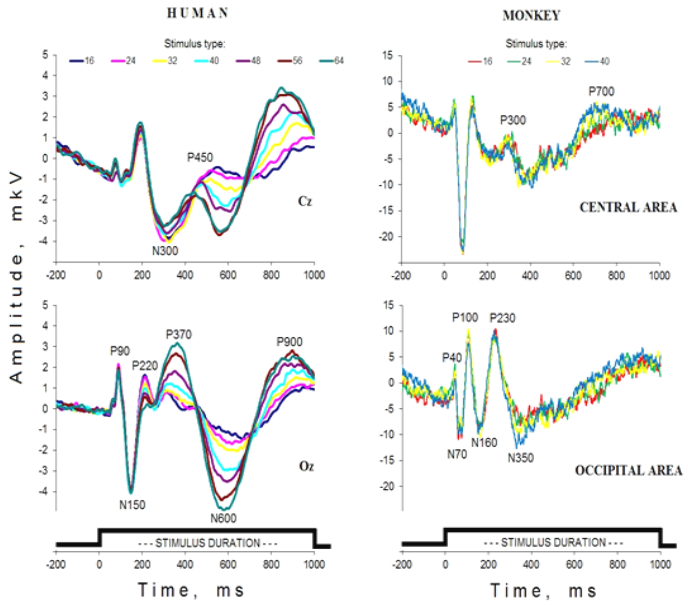

Figure 3. Human (left) and monkey (right) evoked potentials to matrices recorded at central and occipital areas. Grand average data: for humans $N=25$ (subjects), for monkey $N=21$ (experiments).

Whereas ERP's shape between human and monkey can be explained by different position of recording electrodes relatively to the source of the activity in the brain, the most intriguing question is when and how the task difficulty affects the ERPs obtained from two species. As it is seen in figure 3, stimulus type has much earlier effect on human ERPs as compared to monkey ERPs. However, additional study performed on human subjects with the same stimuli but with different instruction that changed the difficulty curve (the task was to detect collinear elements in the matrix) showed that the amplitude of ERP wave P220 in occipital areas correlated only with image complexity, but not with task difficulty. The first effects on the human ERPs amplitude arising from decision difficulty were observable at 400 ms after stimulus onset [see Harauzov et.al, 2016]. The first effects of the decision difficulty on ERPs latency was observed in central areas of the human brain at approximately 300 ms after stimulus onset (N300 and P450 in the figure 3).

We than compared dependencies of the amplitude and latency of the main ERPs components on the stimulus type, which were obtained for humans and monkey. In human ERP the earliest wave that showed significant decrease of its amplitude with the stimulus degree of orderliness was P220, but the analogous wave in the monkey ERP (P230) did not depend on the stimulus type (see figure 4). Such discrepancy can be explained by the difference in the gaze fixation conditions between humans and monkey. If the humans' task was to keep their gaze on the fixation point in the center of the screen, monkey was trained to look towards the screen after the warning sound without any fixation points. Therefore, for humans the projection of the image on the retina was always constant, whereas for monkey the image could appear with a variable shift at any direction from the central point of the retina. Taking in account that P220 wave in humans' ERPs depended on the stimulus properties such as degree of orderliness, but not on the task difficulty, we suppose that this wave is sensitive to the position of the image projection onto retina.

Next waves affected by the stimulus type were N300 (for humans) and P300 (for monkey) recorded in central areas. Their latency decreased with the number of co-oriented elements in the image (see figure 4). Note that the analogous decrease we observed for the reaction times (see figure 2). We suppose that these waves reflect activation of the decision making mechanisms, because the more difficult the task is, the later the decision takes place which in turns increases the reaction time.

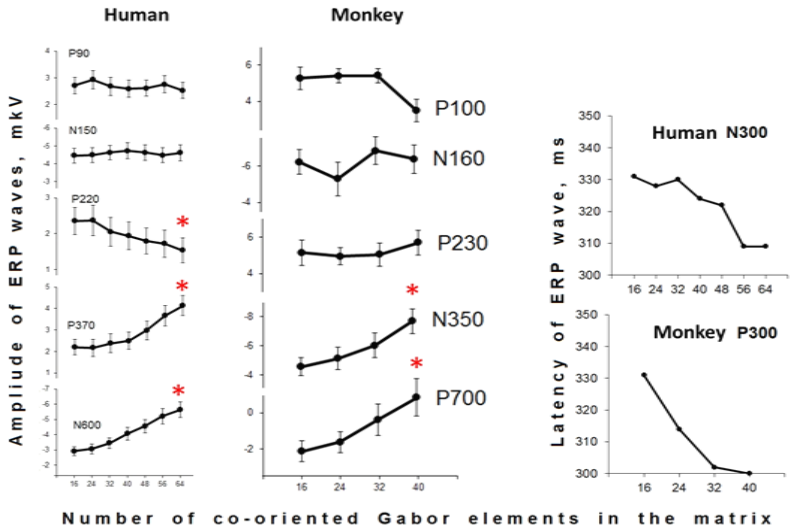

Figure 4. Dependence of mean amplitude (left) and latency (right) of some ERP components on the number of co-oriented elements in the matrix. Stars above data points indicate significant changes in amplitude with the stimulus type (*T*-test, $P<0.01$).

The amplitude of the later ERP waves with the latency of 350–370 ms and 600–700 ms similarly depended on the number of co-oriented elements in the image both for humans and monkeys, though these waves differed in polarity between two species. The fact that the appearance and duration of N600 and P900 waves (for humans) and P700 waves (for monkey) exceeds the reaction time implies that they reflect some post-decision processes. The characteristics of these late components seem to be consistent with Sutton and colleagues' original idea of "uncertainty resolution" [Sutton et al, 1965]. Indeed, the lager the amplitude of these waves, the higher the participants' categorization accuracy and, therefore, self-confidence in their decision. In summary, the first electrophysiological signature of the task difficulty both in humans and monkeys was observed at approximately 300 ms after stimulus presentation. At this time, the latency of ERPs waves started to increase with the task difficulty, that implies that decision about the dominant orientation in the matrix takes place at the same time in both species. The amplitude of late ERPs waves recorded in humans and monkey decreased with the task difficulty in the similar way. The similarity of behavioral and electrophysi-

ological responses in humans and monkeys in pattern discrimination tasks and a possibility to register electrical activity in monkeys directly from brain structures involved in decision-making processes opens up broad prospects for studying this issue.

References

1. Harauzov A. K., Shelepin Y. E., Noskov Y. A., Vasilev P. P., Foreman N. P. // The time course of pattern discrimination in the human brain // Vision Research 125 (2016) 55–63
2. Kharauzov A. K., Shelepin Y. E., Pronin S. V., Sel'chenkova T.V., Noskov Y. A. // Electrophysiological studies of texture recognition mechanisms // Neuroscience and Behavioral Physiology (2008) 38(3):219–226.
3. Shelepin Yu. E., Fokin V. A., Harauzov A. K., Pronin S. V., Chikhman V. N. // Location of the decision-making center during image shape perception // Doklady Akademii Nauk, (2009) Vol. 429, No. 6, pp. 835–838.
4. Sutton S., Braren M., Zubin J., John E. R. // Evoked potential correlates of stimulus uncertainty // Science. (1965). 150, pp. 1187–1188

Chapter 12.
Electrophysiological indices of emotional arousal in monkeys

L. E. Ivanova, D. N. Podvigina, I. A. Varovin, A. K. Harauzov

Electrophysiological assessment of emotional arousal is a rapidly developing area of the brain research. This work aims to identify the electrophysiological signs of a high arousal state of Macaca Mulatta monkeys using conventional EEG spectral analysis.

We recorded EEG at the occipital, parietal, central, and frontal regions of the monkey skull. Two conditions were compared: resting state without any excitatory factors and viewing videos about the life of monkeys in the wild nature. Watching videos caused strong behavioral reactions — the monkey kept a close look at the screen, occasionally making sounds and showing signs of communication. This was a confirmation that the arousal state of the monkey was indeed heightened while watching the video compared to the state of rest. Each recording session lasted for 20–30 minutes. In total, 33 EEG records were made in rest condition and 23 records were obtained when monkey was watching a video. Figure 1 represents averaged EEG spectra obtained from one animal J8 in two conditions.

EEG spectra obtained at rest showed one noticeable peak at a frequency of about 10 Hz, which was maximal at central occipital area and resembled the alpha rhythm in humans. Watching the video led to a significant reduction in the oscillation power of 10 Hz in EEG recorded at all electrodes, but at the same time, a new peak at a frequency of 17 Hz appeared in the EEG spectra, which was most prominent at lateral parietal sites. The two small peaks also appeared at lateral occipital areas with frequency 25 and 30 Hz, which most likely reflect monitor flickers.

To get statistical proof of changes in EEG spectra caused by high arousal state, we calculated areas of two peaks as is shown in figure 2 (left) for each recording session. The results were then averaged for each of the two conditions and compared (Figure 2, right). Statistical analysis revealed high significance of the peaks' power difference in the two conditions ($P<<0.001$, *t*-test; Figure 2, left).

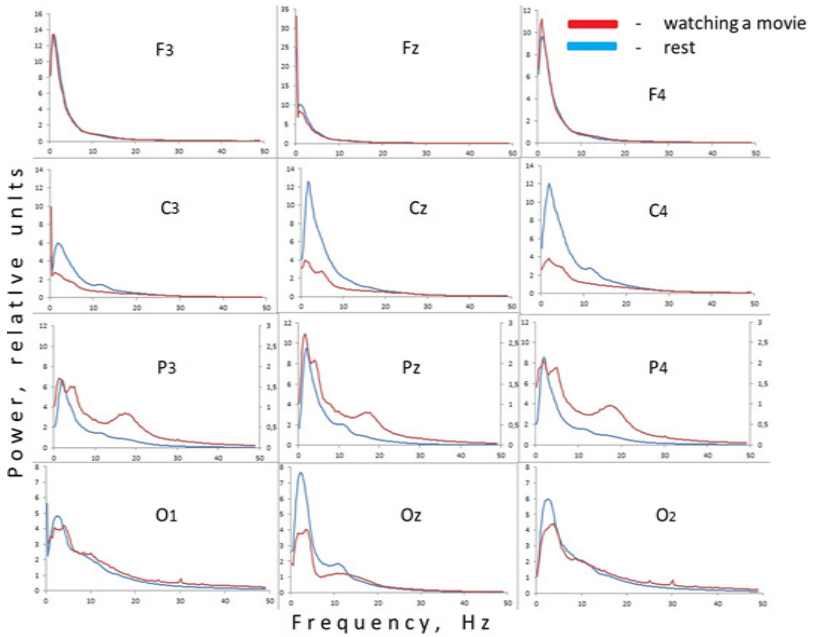

Figure 1. EEG spectra recorded in animal J8 in two conditions: at rest (blue line, 33 records averaged) and during watching video (red line, 23 records averaged). Electrodes placement roughly matches International 10–20 system for human EEG recordings.

Another animal L9 took part in 10 electrophysiological sessions at rest condition and only in 4 sessions during watching movies. EEG spectra of animal L9 at rest resembled those obtained in animal J8 with dominant frequency at 9 Hz. As well as for animal J8, watching a movie resulted in appearance of higher frequency peak of 18 Hz. However, unlike in animal J8, the power of 9 Hz oscillation in EEG of animal L9 substantially increased during watching a movie (see Figure 3).

Thus, during watching a movie in EEG spectra of animal L9 we observed two peaks at the same time: at 9 and at 18 Hz correspondingly. This fact together with differences in topographic distribution over skull of the two peaks indicate that emotional arousal in monkeys leads not to a simple shift in the frequency of the existing brain oscillations, but causes the appearance of new, highly prominent rhythms of the brain at higher frequency. This is unusual feature for human EEG spectra. Explanation of that difference between human and monkey is a matter of further experiments.

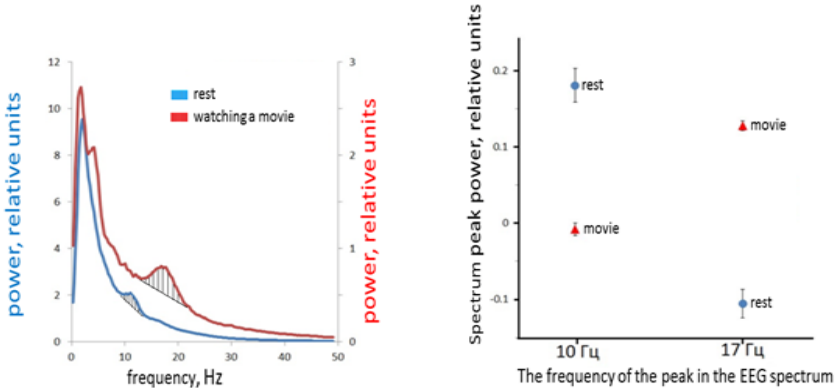

Figure 2. Changes in the EEG spectra (left) and in the power of two peaks of the spectrum at frequency 10 and 17 Hz (right) depending on the emotional arousal during watching the movie. Error bars on the right figure represent SEM. Animal J8. Central parietal area (Pz).

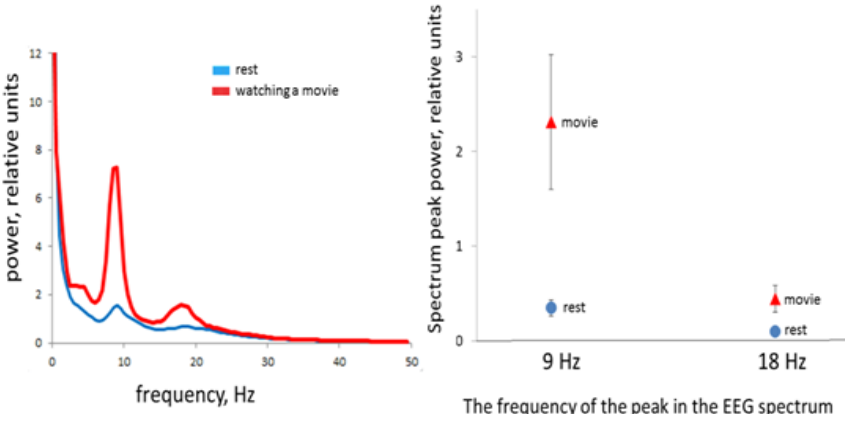

Figure 3. Changes in the EEG spectra (left) and in the power of two peaks of the spectrum at frequency 9 and 18 Hz (right) depending on the emotional arousal during watching the movie. Error bars on the right figure represent SEM. Animal L9. Central parietal area (Pz).

Chapter 13.
SMI-32 labeling in the perigeniculate nucleus

N. S. Merkulyeva, A. A. Michalkin

Introduction

The main transition zone between the retina and visual cortex is dorsal thalamus, and its main part is dorsal lateral geniculate nucleus (LGNd) [Berson, Graybiel, 1983; Sherman, Guillery, 2002]. The communication of the LGNd and primary visual cortex is under strong modulatory influence of the perigeniculate nucleus (PGN) located dorsally to the LGNd [Sanchez-Vives et al., 1996; Guillery, Harting, 2003]. Neurons of the PGN are mainly GABAergic [Fitzpatrick et al., 1984; Stichel et al., 1988] and underlie recurrent inhibition of the LGNd [Dubin, Cleland, 1977; Friedlander et al., 1981]. Despite the importance of relationships between LGNd, PGN and visual cortex, postnatal development of the PGN, especially its neurochemical features, still have been poor understood. Since neurofilaments are strongly important for the development and structural maturation of neurons [Kutcher, Duffy, 2007], in the present work we investigated the postnatal development of the neurofilaments labeling in the perigeniculate neurons using SMI-32 antibody used for the detection of the non-phosphorylated isoform of the heavy-chain neurofilaments [Sternberger, Sternberger, 1983].

Materials and Methods

All experimental procedures were approved by the Ethics Commission of the Pavlov Institute of Physiology (№ 12/03/2019) and were performed in accordance with the requirements of Council Directive 2010/63EU of the European Parliament on the protection of animals used in experimental and other scientific purposes. Four normal pigmented kittens, of either sex, aged 4 (n=2) or 28 (n=2) postnatal days, and one adult (1.5 years old) cat were used. All animals were reared in a standard "12 hrs dark/12 hrs light" environment. Under deep anesthesia (a mixture of 2 mg/kg Zoletil and 20 mg/kg xylazine), all animals were transcardially perfused with 0.9 % NaCl, followed by 4 % paraformaldehyde. After perfusion, brains were removed from the skull, stored in sucrose and subsequently cut on a freezing microtome (50 μm sagittal slices). The detailed procedure of the immunohistochemical staining was described

previously [Merkulyeva et al., 2016; 2018). In brief, slices had been incubated for 70 hours in an anti-mouse monoclonal primary antibody SMI-32 (Sigma-Aldrich, USA, 1:5000 dilution), and thereafter for 1 day — in biotinylated secondary horse anti-mouse antibody (Vector Laboratories, UK, 1:600 dilution). After processing for an avidin-biotin horseradish-peroxidase complex (ABC Elite system, Vector Laboratories, UK) for 1 hour, and diaminobenzidine (DAB)-NiCl-H_2O_2 reaction, slices were mounted, dehydrated, cleared and placed into mounting media (Bio Mount HM, Bio-Optica, Italy). Slices were analyzed with an Olympus microscope (Olympus CX33, Olympus Corporation, Japan) using a Nikon camera (Nikon Corporation, Japan). The number and the sizes of the immunopositive neurons were manually estimated in free software Fiji [Schindelin et al., 2012]. Data were presented as mean±SD; the Mann-Whitney test was used to characterize the statistical significance.

Results and Discussion

Only scared SMI-32(+) neurons (7±10 cells per slice) having triangle soma and multiple long and ramified dendrites both weak stained were visualized in the PGN of the neonatal kittens (P4) (Figure 1A). In contrary to them, a gross amount of SMI-32(+) neural somas was observed in 28-days old kittens (up to 210±15 cells per slice (Figure 1B)). These neurons were dark stained and had highly developed dendritic arborization forming dense neuropil (Figure 1A). A dramatic drop in the number of the SMI-32(+) neurons was observed in adult cat, having only solitary SMI-32(+) neurons (0–2 cells per slice) (Figure 1A).

As it was said above, an SMI-32 antibody recognizes the non-phosphorylated epitope of the heavy-chain neurofilaments [Sternberger, Sternberger, 1983]. Heavy-chain neurofilaments participate in the maintenance of the axonal caliber [Hoffman et al., 1987; Sánchez et al., 2000], and it was proposed previously that SMI-32 is expressed in descending output neurons [Campbell, Morrison, 1989; Fuentes-Santamaria et al., 2006]. These facts allow proposing a transient participation of the SMI-32-labeled perigeniculate cells in the long-lasted projections during particular period of the ontogenesis. According to the literature, reciprocal axonal projections of the PGN in adult animals are restricted to the LGN [Uhlrich et al., 1991]. But some unidirectional connections are known, for example, direct projections from the visual cortex to the PGN [Murphy, Sillito, 1996]. Can these communications be transiently bidirectional, is a question that only waiting to be answered. Since a great number of the SMI-32(+) cells were observed by us in kittens at P28 — the peak of the critical period plasticity [Crowley, Katz, 2002], a transient SMI-32 labeling

in the PGN can be related to the transient plasticity-dependent interneural communication of the perigeniculate cells with the sources that only expected to be observed.

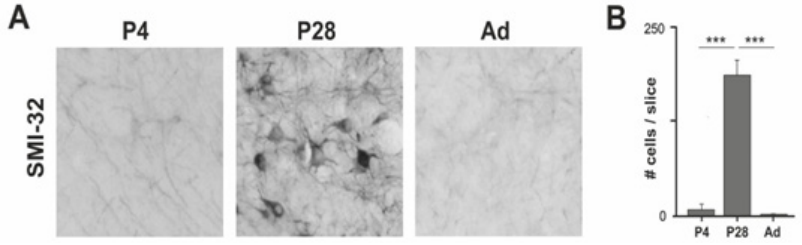

Figure 1. SMI-32-labeling in the perigeniculate nucleus of kittens aged 4 days (P4), 28 days (P28), and in adult cat (Ad). A*—representative examples of the immunostaining at sagittal slices.* B*—an amount of the SMI-32-immunopositive cells per slice in three age groups. ***—p<0.001.*

In other side, it was proposed that SMI-32 antibody selectivity label so-called Y visual neurons related to the motion processing channel [Gutierrez et al., 1995; Bickford et al., 1998]. But up today we don't know, is an input from the Y cells predominant for the PGN cells or all principal geniculate cells have equal contribution to them [Friedlander et al., 1981; Cucchiaro et al., 1991]. But we can expect that a balance in these inputs can be modified during the ontogenetic development.

References

1. Berson D. M., Graybiel A. M. (1983) Organization of the striate-recipient zone of the cat's lateralis posterior-pulvinar complex and its relations with the geniculostriate system. Neuroscience 9:337–372.
2. Bickford M. E., Guido W., Godwin D. W. (1998) Neurofilament Proteins in Y-Cells of the Cat Lateral Geniculate Nucleus: Normal Expression and Alteration with Visual Deprivation. J Neurosci 18:6549–6557.
3. Campbell M. J., Morrison J. H. (1989) Monoclonal antibody to neurofilament protein (SMI-32) labels a subpopulation of pyramidal neurons in the human and monkey neocortex. J Comp Neurol 282:191–205.
4. Crowley J. C., Katz L. C. (2002) Ocular dominance development revisited. Curr Opin Neurobiol 12:104–109.
5. Cucchiaro J. B., Uhlrich D. J., Sherman S. M. (1991) Electron-microscopic analysis of synaptic input from the perigeniculate nucleus to the A-laminae of the lateral geniculate nucleus in cats. J Comp Neurol 310:316–336.

6. Dubin M. W., Cleland B. G. (1977) Organization of visual inputs to interneurons of lateral geniculate nucleus of the cat. J Neurophysiol 40:410–427.
7. Fitzpatrick D., Penny G., Schmechel D. (1984) Glutamic acid decarboxylase-immunoreactive neurons and terminals in the lateral geniculate nucleus of the cat. J Neurosci 4:1809–1829.
8. Friedlander M. J., Lin C. S., Stanford L. R., Sherman S. M. (1981) Morphology of functionally identified neurons in lateral geniculate nucleus of the cat. J Neurophysiol 46:80–129.
9. Fuentes-Santamaria V., Stein B. E., McHaffie J.G. (2006) Neurofilament proteins are preferentially expressed in descending output neurons of the cat the superior colliculus: A study using SMI-32. Neuroscience 138:55–68.
10. Guillery R. W., Harting J. K. (2003) Structure and connections of the thalamic reticular nucleus: Advancing views over half a century. J Comp Neurol 463:360–371.
11. Gutierrez C., Yaun A., Cusick C. G. (1995) Neurochemical subdivisions of the inferior pulvinar in macaque monkeys. J Comp Neurol 363:545–562.
12. Hoffman P. N., Cleveland D. W., Griffin J. W., et al (1987) Neurofilament gene expression: a major determinant of axonal caliber. Proc Natl Acad Sci 84:3472–3476.
13. Kutcher M. R., Duffy K. R. (2007) Cytoskeleton alteration correlates with gross structural plasticity in the cat lateral geniculate nucleus. Vis Neurosci 24:775–785.
14. Merkulyeva N., Mikhalkin A., Zykin P. (2018) Early Postnatal Development of the Lamination in the Lateral Geniculate Nucleus A-Layers in Cats. Cell Mol Neurobiol 38:1137–1143.
15. Merkulyeva N., Veshchitskii A., Makarov F., et al (2016) Distribution of 28 kDa calbindin-immunopositive neurons in the cat spinal cord. Front Neuroanat 9:166.
16. Murphy P., Sillito A. (1996) Functional morphology of the feedback pathway from area 17 of the cat visual cortex to the lateral geniculate nucleus. J Neurosci 16:1180–1192.
17. Raczkowski D., Rosenquist A. (1983) Connections of the multiple visual cortical areas with the lateral posterior-pulvinar complex and adjacent thalamic nuclei in the cat. J Neurosci 3:1912–1942.
18. Sanchez-Vives M.V., Bal T., Kim U., et al (1996) Are the interlaminar zones of the ferret dorsal lateral geniculate nucleus actually part of the perigeniculate nucleus? J Neurosci 16:5923–5941.
19. Sánchez I., Hassinger L., Sihag R. K., et al (2000) Local control of neuro-

filament accumulation during radial growth of myelinating axons in vivo: Selective role of site-specific phosphorylation. J Cell Biol 151:1013–1024.
20. Schindelin J., Arganda-Carreras I., Frise E., et al (2012) Fiji: an open-source platform for biological-image analysis. Nat Methods 9:676–682.
21. Sherman S. M., Guillery R. W. (2002) The role of the thalamus in the flow of information to the cortex. Philos Trans R Soc Lond B Biol Sci 357:1695–708.
22. Sternberger L. A., Sternberger N. H. (1983) Monoclonal antibodies distinguish phosphorylated and nonphosphorylated forms of neurofilaments in situ. Proc Natl Acad Sci USA 80:6126–6130.
23. Stichel C. C., Singer W., Heizmann C. W. (1988) Light and electron microscopic immunocytochemical localization of parvalbumin in the dorsal lateral geniculate nucleus of the cat: evidence for coexistence with GABA. J Comp Neurol 268:29–37.
24. Uhlrich D. J., Cucchiaro J. B., Humphrey A. L., Sherman S. M. (1991) Morphology and axonal projection patterns of individual neurons in the cat perigeniculate nucleus. J Neurophysiol 65:1528–1541.

Chapter 14.
Neurophysiological mechanisms of images classification invariant to their size

G.A. Moiseenko, S.V. Pronin

The mechanisms of objects classification are crucial for the humans being. The classification process is invariant to the size transformation. General description of the image is provided in occipital (BA17-BA19, BA37) cortex [Glezer et al, 1975; Shelepin, 1973]. In recent years, interest has increased in the study of the mechanisms of invariance in connection with the creation of artificial intelligence systems [Baranov, 2012; Cecotti, 2015; Lowe, 1999; Wiskott, 2003; Wiskott, 2002].

In our previous two series of studies, we studied the influence of the intuitions of the observer on the classification processes in the human brain. Subjects were shown images filtered at different spatial frequencies, projected into the fovea region, and were given instructions to classify images according to physical (clear / blurred object) and semantic characteristics of images (animate/inanimate object). As a result of the research, components of cognitive evoked potentials associated with the semantics of images were identified. Differences in the components of evoked potentials from image semantics were significant with frontal (in P200 components), temporal and occipital areas (in N170 components) even in those conditions when the test subject's task was to classify the physical properties of the images of objects [Moiseenko et al., 2015].

Aim

The aim of our research was to investigate the influence of images size on characteristics humane visual cognitive evoked potentials in classification tasks.

Methods

The study involved 35 healthy subjects aged 20 to 38 years. Using a cognitive evoked potentials method, 2 experiments series were carried out. The angular dimensions of the objects images for observer was 3 angular degree in first

series and 0,4 angular degrees in the next series. In both series, the observer's get the instruction to classify the images: animate and inanimate. Time of images presentation was 100 ms with an interval of 1 second. Registration of evoked potentials carried out according to the scheme 10–20 with reference ear electrodes.

Figures 1 and 2 show examples of stimuli images for the first and second series of studies.

Figure 1. Sample images of stimuli in 1 research.

Figure 2. Sample images of stimuli in 2 research.

Results

If we compare the results of the 1st and 3rd studies, it turned out that in both series of studies the amplitude of the P200 component in the frontal (F7, F8) areas differed in semantic features ("animate-inanimate"). Figures 3a and 3b show examples of grand average of evoked potentials (electrode F7) for the first and second series of studies.

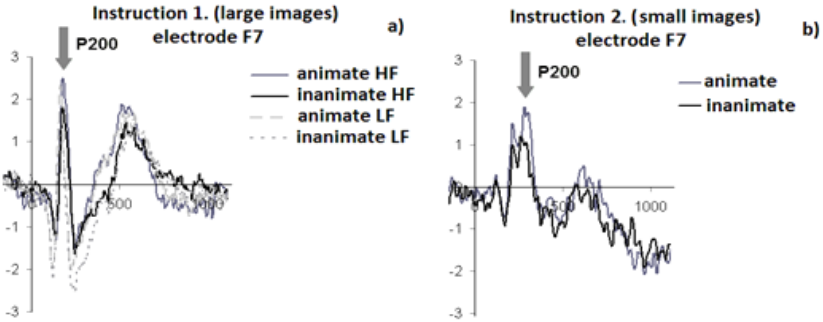

Figure 3. Examples of grand average of evoked potentials (electrode F7) for the first research (instructions 1: "animate/inanimate", large images) (3a) and second series research (instructions 2: "animate/inanimate", small images) (3b). The arrow indicates the component (P200) where differences were expressed in terms of "animate/inanimate" objects.

Discussion

Probably, in the areas of the frontal cortex established by us comes information that is invariant to large-scale transformations. Therefore, it becomes possible to classify images according to semantic characteristics, regardless of the image size and its spatial frequency spectrum. It can be assumed that in the frontal area, which provides decision making when performing image classification tasks, the brain uses the scale-invariant transformation of images already formed at previous levels. This statement is based on specific experimental data. Previously, amplitudes of evoked potentials were measured, according to which, in predators without a pronounced frontal region, an invariant description is carried out in the Claire-Bishop zone, parietal-temporal-occipital region of the cortex [Glezer et al, 1975; Shelepin, 1973].

In the works of Shelepin Yu. E., Vakhrameeva O. A. and Chikhman V. N. when studying the perception thresholds of fragmented contour images, it was shown that when the image is reduced less than 1 angular degree and with an increase in the size of the incentives over 50 angular degree, there is an increase in the perception thresholds of incomplete images. The minimum values of the perception threshold of incomplete images correspond to the domain of perception invariance [Vakhrameeva et al., 2008; Shelepin, 2008; Chikhman et al., 2009].

In our data in this study, the sizes of the images corresponded to the sizes of foveolita (central area of foveola) and fovea sizes, the visual acuity of the observ-

ers was 1, respectively, based on the probability of correct answers and localization of significant differences in the amplitude of evoked potentials, the size invariance was more expressed in the 1st study, where the image sizes were within the limits of foveola sizes, than in the 2nd study, where the image sizes corresponded to the foveola sizes. This is consistent with the data obtained in our laboratory data Shelepin Yu.E., Vakhrameeva O.A. and Chikhman V.N. [Vakhrameeva et al., 2008; Shelepin, 2008; Chikhman et al., 2009].

Conclusions

The role of P200 evoked potentials components in the frontal regions of the brain in stimuli images size transformation is shown. Thus, it was shown that the neural networks of the frontal cortex use an invariant description of images to ensure the classification of objects.

References

1. Baranov R.P., Belokon' A.V. Opredeleniye i prioretizatsiya priznakov ob'yektov na izobrazhenii v sistemakh raspoznavaniya // Aktual'nyye problemy aviatsii i kosmonavtiki. 2012. S. 328–329.
2. Cecotti H. Toward shift invariant Detection Of Event-related potential is non-invasive brain-computer interface // Pattern Recognition Letters. 2015. V. 66. pp. 127–134.
3. Chikhman V.N., Shelepin Yu.Ye., Foreman N., Pesmor P. Vospriyatiye fragmentirovannykh izobrazheniy ugla nablyudeniya // Rossiyskiy fiziologicheskiy zhurnal im. I.M. Sechenova. S. 324–334.
4. Glezer V.D., Dudkin K.N., Podvigin N.F. Nevskaya A.A. Zritel'noye opoznaniye i yego neyrofiziologicheskiye mekhanizmy. M.: Nauka, 1975. 272 s.
5. Lowe D.G. Object recognition from local scale-invariant features.// Proceedings of the International Conference on Computer Vision. 1999. pp.1150–1157.
6. Moiseenko G.A., Shelepin Yu.E., Kharauzov A.K., Pronin S.V., Chikhman V.N., and Vakhrameeva O.A. Classification and recognition of images of animate and inanimate objects // Journal of Optical Technology. V. 82. Is. 10. P. 685–693.
7. Shelepin Yu.Ye. Lokalizatsiya oblastey zritel'noy kory koshki, dayushchikh invariantnyy otvet pri izmenenii razmera izobrazheniya // Neyrofiziologiya. 1973. T. 5. № 2. S. 115–121.
8. Shelepin Yu.Ye., Chikhman V.N., Vakhrameyeva O.A., Pronin S.V., Foreman N., Pesmor P. Invariantnost' zritel'nogo vospriyatiya // Eksperimental'naya psikhologiya. 2008. T 1. № 1. S. 7–33.

9. Vakhrameyeva O.A., Shelepin Yu.Ye., Mezentsev A. Yu., Pronin S. V. Izucheniye vospriyatiya nepolnykh konturnykh izobrazheniy razlichnogo razmera // Rossiyskiy fiziologicheskiy zhurnal im. I. P. Sechenova. 2008. T. 94. № 10. S. 1158–1170.
10. Wiskott L. How does our visual system achieve shift and size invariance? In Problems in Systems Neuroscience, J.L. van Hemmen and T. J. Sejnowski, eds. (Oxford: Oxford University Press). 2003.
11. Wiskott L., Sejnowski T. Slow feature analysis: unsupervised learning of invariances // Neural Computation. 2002. V.14. pp. 715–770.

Chapter 15.
A comparative analysis of the camera-like eyes of gastropod mollusks and humans

I. P. Shepeleva

Vision is a complex multi-level process carried out by the visual system and allows to obtain information about the world. It begins in the peripheral part of the visual system — the eyes — with the formation of an image on the retina and the conversion of light energy by photoreceptor cells into the energy of nerve impulses and ends in the central part — the cerebral cortex — by deciding what kind of object the organism met [Hubel, 1990]. It is often difficult to study the visual system in vertebrates for technical reasons or impossible for ethical considerations [Kandel, Kupfermann, 1970]. For research, model organisms are needed, which can serve as invertebrate animals — gastropod mollusks [Chernorizov, Sokolov, 2010]. Among invertebrates, gastropod mollusks are one of the few groups whose representatives have camera-like eyes, and the first group whose representatives have camera-like eyes adapted to vision in a terrestrial environment and at a high level of illumination in the same way as typical representatives of vertebrates — humans. At the same time, camera-like eyes and the visual system in general in mollusks are much simpler [Vavilov, 1961; Shepeleva, 2011, 2013, 2018; Land, Nilsson, 2002]. Further study of the model requires the identification of similarities and differences between the eyes of mollusks and humans. Therefore, the aim of the work is to compare the camera-like eyes of terrestrial gastropods pulmonate mollusks and humans and to reveal similarities and differences in the structure and functions of their common components.

In mollusks and humans, the eyes are spherical as well as ellipsoid in shape along or perpendicular to the optical axis. With an average length of about 300 microns, the eyes of the mollusks consist of a shell surrounding the eye; the lens; the vitreous body and the retina, the edges of which form a pupil of constant diameter [Shepeleva, 2011, 2013; Land, Nilsson, 2002] (Figure 1A). The eyes of humans with an axial length of about 24 mm consist of a shell surrounding the eye; anterior chamber filled with aqueous humor; the iris, in which there is a pupil of variable diameter; a back chamber filled with aqueous humor; the lens suspended on ligament of Zinn; vitreous body; retina and

choroid [Grüsser, Grüsser-Gornehls, 1996; Basinsky, Egorov, 2007] (Figure 1B). Thus, the camera-like eyes of mollusks and humans vary significantly in structure, but contain common components — the shell, lens, vitreous body and retina. Therefore, the work analyzes the known structure and functions of these components.

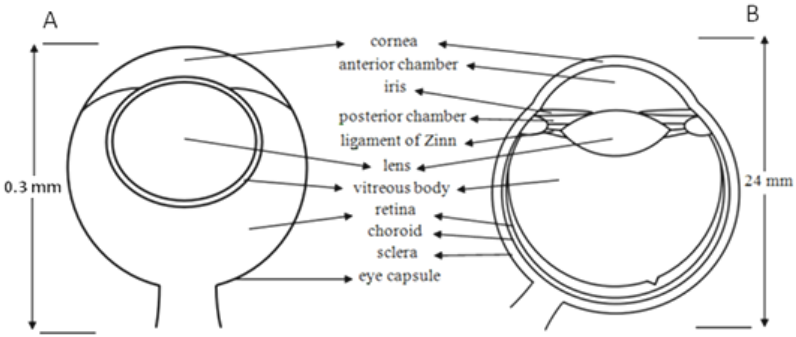

Figure 1. Schematic drawing of the camera-like eyes of mollusks (A) and humans (B). The diameter of the eye of the mollusk is 0.3 mm, the human eye is 24 mm. The difference is about 100 times. The vertical thickness of the retina of the mollusk in the center is about 0.1 mm, in the human fovea — about the same — 0.1–0.2 mm.

The shell of the eyes of mollusks and humans is divided into two sections: a smaller anterior, formed by the cornea, and a larger posterior, formed by the sclera.

The cornea of the eyes of mollusks and humans is a convex-concave transparent colorless optically homogeneous lens with a similar refractive index. In mollusks, the cornea has a hemispherical shape; in humans, it has an aspherical shape of refractive surfaces. The cornea of mollusks consists of a single layer of epithelial cells lying on the basement membrane. There are 5 layers in the cornea of humans: the surface layer, represented by a multilayer epithelium; front border membrane; the stroma, which is a connective tissue of intercellular substance — plates of collagen with a carbohydrate-protein complex and the main type of cells — keratocytes; Dua layer — a thin high-strength layer of collagen; posterior border membrane; endothelial cell layer. In mollusks and humans, the cornea performs several common functions: light-refracting, light-transmitting, shaping, supporting and protective, while in humans it is still involved in the correction of spherical aberration and is a light filter for ultraviolet rays [Atchison, Smith, 2000; Basinsky, Egorov,

2007; Shepeleva, 2011, 2013, 2018; Majdi et al., 2014]. Thus, the cornea of mollusks and humans has more similarities than differences both separately in structure and functions, and in general — taking into account structure and functions.

The eyes of the mollusks are surrounded by a transparent eye capsule, the human eyes are surrounded by an opaque sclera, which are connective tissue membrane. The eye capsule is formed by collagen fibers with the main substance, fibroblasts and smooth muscle tissue cells. In the sclera, from the inside out, 4 layers are distinguished: 1 layer, which is formed by endothelial cells, and 3 layers — a brown plate, stroma and episclera, which differ in the density and composition of the components and are formed by collagen and elastic fibers with a carbohydrate-protein complex and the main type of cells — fibroblasts. In mollusks and humans, these shells perform the shaping, supporting and protective functions [Basinsky, Egorov, 2007; Shepeleva, 2011, 2013]. Thus, the eye capsule of mollusks and sclera of humans completely differ in structure, but are similar in function and in general have more similarities than differences.

The lens of the eyes of mollusks and humans is a biconvex transparent lens with a relatively soft consistency of different colors: colorless in mollusks and pale yellow in humans. In mollusks, the lens lies behind the cornea and occupies a significant part of the cavity of the eye, in humans it is located at a distance from the cornea and occupies a much smaller part of the cavity of the eyeball. The lens of mollusks has a spherical as well as an ellipsoidal shape along or perpendicular to the optical axis with a hemispherical shape of the refracting surfaces and is not capable of accommodation. The lens of people participates in accommodation, during which its shape changes — from an ellipsoid perpendicular to the optical axis with a flattened anterior and convex posterior surfaces of an aspherical shape to a round one with more convex both surfaces of equal curvature. In mollusks, the lens does not have a shell and is characterized by a non-cellular structure, granular structure, lamination and vesicles, and the quality of the images of test objects formed by isolated lenses indicates the possible refractive index gradient in some species of mollusks. In the lens of humans, a capsule is distinguished; a layer of epithelial cells on the inner front surface of the capsule; and lens material from spindle-shaped epithelial cells forming layers of different densities with a variable refractive index. In mollusks and humans, the lens performs light-refracting, light-transmitting, shaping, supporting and protective functions, while in humans it also participates in the accommodation process, attenuates spherical

aberration and is a light filter for ultraviolet rays [Grüsser, Grüsser-Gornehls, 1996; Atchison, Smith, 2000; Basinsky, Egorov, 2007; Shepeleva, 2011, 2013, 2018; Majdi et al., 2014]. Thus, the lens of mollusks and humans has more differences in structure and more similarities both separately in functions and in general.

In the eye cavity of mollusks and humans is the vitreous body. In mollusks, the vitreous body surrounds the lens in the form of a thin uniform layer and separates it from the cornea and retina, in humans it lies behind the lens, occupies a significant part of the eye cavity and delimits it only from the retina. Both in mollusks and in humans, the vitreous body is a transparent, colorless optically homogeneous substance of a gel-like consistency with a similar refractive index. In mollusks, the vitreous body has no membrane and has a granular homogeneous structure. In humans, it is surrounded by a membrane and is a connective tissue of intercellular substance — collagen fibers with a solution of organic and inorganic compounds and the main type of cells — hyalocytes. The density of the arrangement and composition of the components is divided into three zones: external, intermediate and central. In mollusks and humans, the vitreous body performs several functions: light-refracting, light-transmitting, shaping, supporting and protective, and in humans also metabolic [Atchison, Smith, 2000; Basinsky, Egorov, 2007; Shepeleva, 2011, 2013]. Thus, the vitreous body of mollusks and humans has more similarities than differences both separately in structure and functions, and in general.

After passing through the vitreous body, light enters the retina, which follows the shape of the eyes and is divided into two parts: the non-optic and the optic. The non-optic part in mollusks is the area near the pupil, in humans — the area of the ciliary body and iris. In the optic part, the central and peripheral regions are distinguished. Both areas are homogeneous in the mollusk and are divided into zones in humans. The central region, or macula, contains a fovea with a foveola, surrounded by parafovea and perifovea, and in the peripheral region, the near, middle, far and extreme periphery are distinguished [Hubel, 1990; Kolb, 2003; Schubert, 2009; Shepeleva, 2011, 2013].

In mollusks, the retina is not inverted; in humans, it is inverted. The retina of mollusks includes 4 types of cells — photoreceptor, pigment, glial and ganglion cells, which form 4 layers. In the retina of humans, there are 8 types of cells, which form 10 layers and of which all 4 of the listed cell types are common with mollusks [Hubel, 1990; Wandell, 1995; Kolb, 2003; Shepeleva, 2011, 2013].

Photoreceptor cells in mollusks and humans have a different structure, and also belong to different groups and are divided into two different morphological types, each of which is represented by one species. In mollusks, photoreceptor cells consist of a body and a photosensitive part, belong to the rhabdomeric group and are represented by the first and second type. Both types of cells contain the same visual pigment, so the mollusks have monochromatic vision. In humans, photoreceptor cells consist of a synaptic region with second-order neurons, the nuclear part, the inner segment, the connecting cilia and the photosensitive outer segment, are ciliary and are represented by rods and cones. All rods contain the same visual pigment, and cones are divided into three types — each with its own visual pigment, which forms the basis of color vision of humans. In mollusks, photoreceptor cells of both types are located in each region of the retina. In humans in foveola there are two types of cones, and in the remaining zones of the central region, as in all zones of the peripheral region, there are rods and three types of cones. The photoreceptor cells of the first type in mollusks and rods in humans are characterized by a higher light-collecting and lower resolving ability than photoreceptor cells of the second type and cones, respectively, both in the central and peripheral regions of the retina. The area with the minimum light-collecting and maximum resolving ability in mollusks and humans is the central region and foveola, respectively [Polyak, 1941; Hubel, 1990; Wandell, 1995; Grüsser, Grüsser-Gornehls, 1996; Kolb, 2003; Basinsky, Egorov, 2007; Shepeleva, 2011, 2013, 2018].

Pigment cells in mollusks and humans differ in location and certain functions. In mollusks, they are located between the photoreceptor cells, but they do not isolate their photosensitive parts of each other. However, they form a screen that prevents the penetration of light into the eye from any direction, and also participate in the synthesis and secretion of substances from which the lens and vitreous body are formed. In humans, they form a separate layer of cells whose apical processes isolate the outer segments of adjacent rods and cones adjacent to them and absorb the scattered light, and also perform a number of other functions [Polyak, 1941; Hubel, 1990; Kolb, 2003; Basinsky, Egorov, 2007; Shepeleva, 2011, 2013, 2018].

Glial cells in mollusks and humans can vary in location and function and vary in the number of types. In mollusks, they are located in two layers on the periphery of the retina, perform supporting and trophic functions, and are represented by 2 types. In humans, they are located near the inner and outer borders, and also permeate all layers of the retina, perform a larger set of functions and are represented by 3 types [Polyak, 1941; Wandell, 1995;

Kolb, 2003; Basinsky, Egorov, 2007; Shepeleva, 2011, 2013; Reichenbach, Bringmann, 2015].

Ganglion cells vary in location and number of types. In mollusks, they along with glial cells are in two layers on the periphery of the retina, as well as in the expanded part of the optic nerve and are represented by 1 type, in humans they form a separate layer and are represented by more than 20 types [Polyak, 1941; Hubel, 1990; Wandell, 1995; Kolb, 2003; Basinsky, Egorov, 2007; Shepeleva, 2011, 2013, 2018].

Thus, the retina of mollusks and humans has more differences than similarities both separately in structure and functions, and in general.

A comparative analysis of the camera-like eyes of mollusks and humans on the basis of their own and published data revealed similarities and differences in structure and functions of their common components (Table 1). Of the 4 components examined, 3 components — the shell (cornea and eye capsule/sclera), the lens and the vitreous body — have more similarities than differences and 1 component — the retina — shows more differences than similarities.

Table 1.

The similarities and differences in structure and functions of the common components of the camera-like eyes of mollusks and humans

Eye components	Structure	Functions	Structure and functions
Shell: Cornea	more similarities	more similarities	more similarities
Shell: Eye capsule/sclera	only differences	only similarities	more similarities
Lens	more differences	more similarities	more similarities
Vitreous body	more similarities	more similarities	more similarities
Retina	more differences	more differences	more differences
All components	more differences	more similarities	more similarities

Together, the components of the camera-like eyes of mollusks and humans are less similar in structure and more similar in function, but taking into account both structure and functions show more similarities than differences. The pre-

sented data on the peripheral part of the visual system of gastropod mollusks allow us to consider these invertebrates as a convenient model for studying the functioning of the visual system. Additional advantages of mollusks are availability in nature, abundance, ease of maintenance and cost-effectiveness. Also, the results of the comparative analysis made it possible to identify gaps in our knowledge about the eyes of mollusks and determine areas for further research, the purpose of which will be to study the unknown structure and functions of the components of the eyes, as well as assess the factors affecting the vision of mollusks, and through a comparative analysis with humans to create the most complete picture of gastropods as model organisms for the study of vision

References

1. Atchison D. A., Smith G. Optics of the human eye. Oxford. 2000. 269 p.
2. Basinsky S. N., Egorov E. A. Clinical lectures on ophthalmology. Moscow: GEOTAR-Media. 2007. 209 p. [in Russian].
3. Chernorizov A. M., Sokolov E. N. Mechanisms of achromatic vision in invertebrates and vertebrates: a comparative study // The Spanish J. Psychol. 2010. V. 13. No 1. P. 18–29.
4. Grüsser O.—J., Grüsser-Gornehls U. Vision // R. F. Schmidt, G. Thews (ed.). Human Physiology. Moscow: Mir. 1996. V. 1. P. 235–275 [in Russian].
5. Hubel D. H. Eye, brain and vision. Moscow: Mir. 1990. 239 p. [in Russian].
6. Kandel E. R., Kupfermann I. The functional organization of invertebrate ganglia // Annual Review of Physiology. 1970. V. 32. P. 193–258.
7. Kolb H. How the retina works // American scientist. 2003. V. 91. P. 28–35.
8. Land M. F., Nilsson D.—E. Animal eyes. Oxford: Oxford University Press. 2002. 221 p.
9. Majdi M., Milani B. Y., Movahedan A., Wasielewski L., Djalilian A. R. The role of ultraviolet radiation in the ocular system of mammals // Photonics. 2014. V. 1. P. 347–368.
10. Polyak S. L. The retina. Chicago: The University of Chicago Press. 1941. 607 p.
11. Reichenbach A., Bringmann A. Retinal glia // A. Verkhratsky, V. Parpura (ed.). Colloquium lectures on neuroglia in biology and medicine. From physiology to disease. Philadelphia: Morgan&Claypool Life sciences. 2015. P. 83–103.
12. Shepeleva I. P. Camera eyes of gastropod mollusks // Bulletin of Mordovian State University. 2011. No 4. P. 230–240. [in Russian].

13. Shepeleva I. P. A comparative analysis of the camera eyes of gastropod mollusks and humans // Sensory systems. 2013. V. 27. No 2. P. 317–326. [in Russian].
14. Shepeleva I. P. Comparative analysis of the resolving power of the camera eyes of gastropod mollusks and human // Russian journal of physiology. 2018. V. 104. No 4. P. 412–424. [in Russian].
15. Schubert H. D. Structure and function of the neural retina // Ophthalmology/Ed. by Yanoff M., Duker J. S. Edinburgh: Mosby Elsevier, 2009. P. 510–514.
16. Vavilov S. I. Eye and sun. Moscow: Academy of Sciences of USSR. 1961. 294 p. [in Russian].
17. Wandell B. A. Foundations of vision. Sunderland. 1995. 476 p.
18. Webvision: The Organization of the Retina and Visual System. Kolb H, Fernandez E, Nelson R, editors. Salt Lake City (UT): University of Utah Health Sciences Center; 1995-https://www.ncbi.nlm.nih.gov/books/NBK11556/

Chapter 16.
Development of non-invasive methods of primates' head fixation based on computed tomography data

I. A. Varovin, L. E. Ivanova, D. N. Podvigina, A. K. Harauzov

The modern concept of brain functioning is based on a network approach in which distant regions of the brain are connected on the basis of their synchronous activity and performing the same functions. Using the fMRI method to study brain functional connections ones managed to describe a number of large-scale neural networks in the human brain that are involved in performing certain cognitive functions, which are characterized by a remote arrangement of components, but at the same time a high level of coherent activity between them. For example, the areas of the dorsolateral prefrontal cortex and the posterior parietal cortex are connected into a so-called "central executive network" associated with memory functioning and decision-making. There are also neural networks responsible for detecting and switching attention to significant signals (salience network), for memory functions, language skills, sensory information processing, and so on. A common feature of all large-scale neural networks of the brain is internal functional coherence and opposite interactions with the so-called default mode network (DMN), which is believed to coordinate their work by maintaining a balance between activated and deactivated brain areas [Raichle, et al., 2001, 2006; Fox and Raichle, 2007; and many others including Kharauzov et al., 2018].

Localization of functionally connected areas of the brain, forming large-scale neural networks, is also possible in monkeys using fMRI methods [Vincent et al., 2007; Mantini et al., 2011]. There are two important requirements for a successful fMRI experiment: the subject must be conscious, and must lie motionless in the scanner. Unlike humans, it is quite difficult to get an animal to not move. Learning is one way to solve this problem, but it is time consuming. Another way is to fixate the head of the animal with a mask that exactly matches the shape of its face.

We have developed our own monkey head fixation system using two plastic masks — internal (soft) and external (solid). The inner mask corresponds to the individual shape of the head of the animal. It is molded of soft silicone to create comfortable conditions for the animal. The inner mask is created in

several stages. First, a three-dimensional model of the virtual head is formed on the basis of the CT data, which is then printed on a 3-D printer. Based on the printed model, casting from a two-component silicone, a mask is made in several stages, which is an exact copy of the monkey's head. The outer mask only roughly repeats the individual features of the monkey's head; it is universal in shape and size for fixing different monkeys. The outer mask is molded from durable plastic, so that inside you can insert any inner mask of various sizes. As a result, the head of the animal is tightly but comfortably fixed, which is necessary for performing tomographic studies. Figure 1 illustrates some stages of individual mask making.

Figure 1. Three-dimensional model of the virtual head based on the CT data (left). First stage of individual face mask creating on the basis of 3-D printed model of the head (right).

In order to tightly and comfortably fixate the monkey's body the special suit with belts was sewn on the basis of individual CT data of the whole body. Then a universal box compatible with MRI scanner was made from amagnetic materials (see Figure 2).

It is obviously that prolonged immobilization provokes stress in an untrained monkey. That would lead to unexpected patterns of functional connections peculiar to stress conditions which can differ from functional connections in rest conditions. To avoid this issue we performed two training sessions in two days with a week interval where a monkey was fixated for 2.5 hours on each day. Additionally, sound of working MRI scanner was sent though speakers in order to habituate an animal to loud sounds.

As an indirect indicator of a stress level we used heart rate registration with ECG. Figure 3 illustrates mean heart rate values obtained during two training sessions and during two fMRI recording session in conscious and uncon-

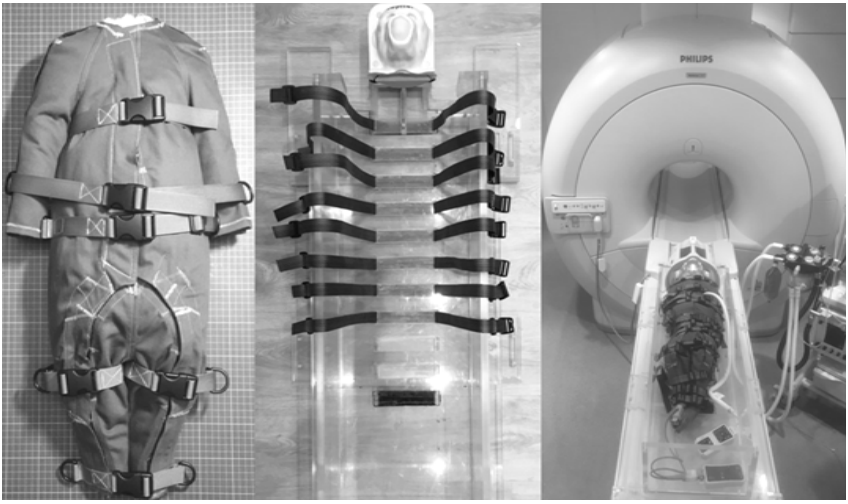

Figure 2. Experimental setup for tight and comfortable fixation of a monkey in MRI scanner.

scious states. At the beginning of training the heart rate was 180 beats per minute (bpm) which is the upper limit of this value for Rhesus monkeys. At the second training session the heart rate decreases up to 160 bpm, and at the third time of fixation (when the fMRI was recorded) the heart rate was about 140 bpm which is close to normal range for animals of this species. Immediately after fMRI recording in conscious state, the isoflurane anesthesia (1 %) was given to the animal and the second fMRI measure in unconscious state was performed. During unconscious state the mean heart rate value was 120 bpm which is close to lower limit for the Rhesus monkeys. Therefore, the heart rate data indirectly confirms that at the third time of fixation the animal was already habituated to immobilization and to loud sounds produced by the scanner. This allows us to consider the fMRI data obtained in conscious state close to the rest state of these specie animals.

The fMRI data was processed with a toolbox for Data Processing & Analysis for Brain Imaging (DPABI). To explore functionally connected areas in the monkey's brain, a seed-based correlation analysis was used. Based on the time series of a seed voxel, connectivity was calculated as the correlation of BOLD signal time series for all other voxels in the brain. Figure 4 illustrates preliminary data obtained in one monkey in consciousness state and under isofluran anesthesia.

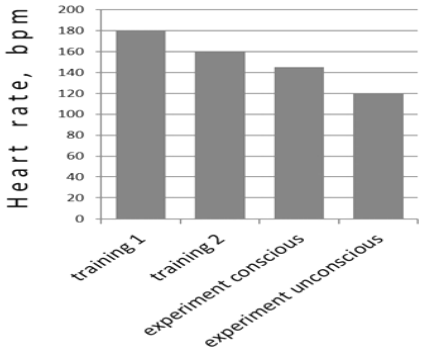

Figure 3. The monkey's mean heart rate data obtained during training session and during fMRI recording in conscious state and under isoflurane anesthesia.

As it is seen from the figure 4, in the brain of awake animal frontal and parietal areas are functionally connected. Loss of consciousness evoked by isofluran gas significantly changed the pattern of functional connectivity. We observed the strongest correlation of the BOLD signal between temporal and occipital areas of the brain.

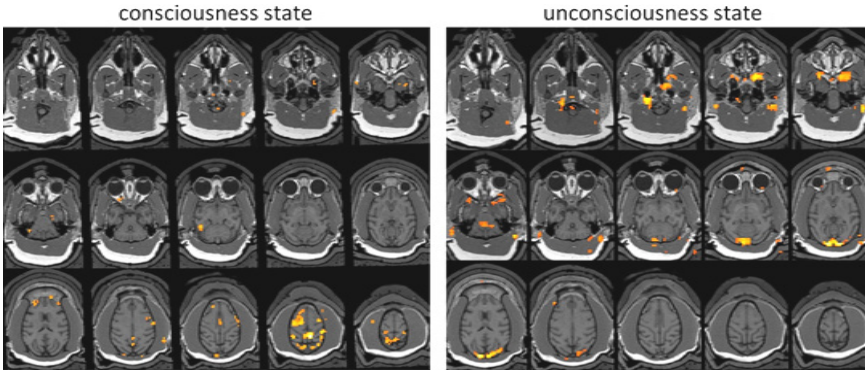

Figure 4. Functionally connected areas in the monkey brain.

In summary, the data obtained provide us additional information about the differences in brain functioning in consciousness and unconsciousness states. Moreover, the developed method opens a perspective to investigate neurophysiological basis of functional connectivity between distant brain regions. Next step is implantation of electrodes into discovered areas that show strong

correlation of the BOLD signal and registration of electrocorticogramm which has much finer time scale comparative to fMRI methods.

References

1. Fox M.D. and Raichle M.E. (2007) Spontaneous fluctuations in brain activity observed with functional magnetic resonance imaging. Nat. Rev. Neurosci. 8, 700–711
2. Kharauzov A.K., Vasil'ev P.P., Sokolov A.V., Fokin V.A., and Shelepin Yu.E. // Functional magnetic resonance imaging analysis of the human brain in texture recognition tasks // Vol. 85, Issue 8, pp. 463–467 (2018)
3. Mantini Dante, Gerits Annelis, Nelissen Koen, Durand Jean-Baptiste, Joly Olivier, Simone Luciano, Sawamura Hiromasa, Wardak Claire, Orban Guy A., Buckner Randy L. and Vanduffel Wim (2011) Default Mode of Brain Function in Monkeys. The Journal of Neuroscience, September 7, 31(36):12954–12962
4. Raichle M. (2006). Neuroscience. The brain's dark energy. Science 314, 1249–1250
5. Raichle M.E. et al. (2001) A default mode of brain function. Proc. Natl. Acad. Sci. U.S.A. 98, 676–682
6. Vincent J.L., Patel G.H., Fox M.D., Snyder A.Z., Baker J.T., Van Essen D.C., Zempel J.M., Snyder L.H., Corbetta M., Raichle M.E. (2007) Intrinsic functional architecture in the anaesthetized monkey brain. Nature. May 3;447(7140):83–6.

NEURAL NETWORKS AND FREE WILL (CHOICE)

Chapter 17.
Superpositional Model for Natural Language Understanding of Ambiguous Texts by Means of Ontological Semantics

A. V. Dobrov, N. L. Soms

Abstract

Algorithms for Natural Language Understanding tasks, which perform the full stack of analysis procedures (from graphematics or phonetics level through morphology, syntax, semantics, and up to pragmatics), have more than exponential complexity due to ambiguity of natural language on all of its levels. This article describes an approach to reduce computational complexity significantly within some restrictions for formal grammar and ontology based on superpositional packing of ambiguous structures.

Introduction

Natural Language Understanding (NLU) is a type of natural language processing, in which a machine performs the complete sequence of text analysis procedures at all its levels (graphematics or phonetics, morphology, syntax, semantics, and pragmatics), leading to the integration of its semantic content into the used knowledge base / ontology. NLU technologies aim to successfully perform disambiguation and work correctly under the conditions of uncertainty.

There are different types of ambiguity that NLU technologies deal with. From the linguistic perspective, the main of them are morphological ambiguity, syntactic ambiguity, and semantic ambiguity.

Morphological ambiguity can be caused by coincidence in spelling of wordforms of different lexical items that may have even different pronunciation, like in (1a) and (1b), or in (2a) and (2b), and it can also be caused by formal coincidence in word formational and/or inflectional models with no difference in pronunciation, like in (3a) and (3b), or in (4c) and (4d), and, finally, it can be just a complete coincidence in spelling and pronunciation without any rational reasons, like in (4a) and (4b).

(1a)	желез-а	(1b)	желез-а
	zheléz-a		zhelez-á
	iron-GEN.SG		gland-NOM.SG
	‘of iron’		‘gland’
(2a)	пот-ом	(2b)	потом
	pót-om		potóm
	sweat-INS.SG		after
	‘by sweat’		‘after’
(3a)	отёк-	(3b)	отёк--
	otjok-		otjok--
	edema-NOM.SG		swell-PST-M.SG
	‘edema’		‘swelled’

(4a)	при	(4b)	пр-и	(4c)	пр-и	(4d)	пр-и
	pri		pr-i		pr-i		pr-i
	at		go.baldheaded-IMP		feud-NOM.PL		feud-ACC.PL
	‘at’		‘go baldheaded!’		‘feuds’		‘feuds’

Morphological ambiguity is actually ubiquitous, especially in morphologically rich languages like Russian, but rarely obvious: whereas software products that perform morphological analysis have difficulty in choosing any interpretation of each ambiguous word form and need special add-ons for disambiguation, native speakers rarely even notice any ambiguity, especially when provided with context; at least, they tend not to verbalize the process of choice of interpretation.

Syntactic ambiguity can be caused by morphological ambiguity like in (5a) and (5b), or only by intrinsic structural ambiguity of specific natural language constructions, cf. different possible interpretations of (6): (6a), (6b), and (6c).

(5a)	Отёк--	*глаз-*.		(5b)	Отёк-*глаз-*.		
	otjok--	glaz-			otjok-	glaz-	
	swell-PST-M.SG	eye-NOM.SG			edema-NOM.SG	eye-GEN.PL	
	‘Eye swelled’				‘Eyes edema’		
(6)	Меркель-	встрети-*л-а*	*Трамп-а*	*в*	*её*	*костюм-е*	
	Merkel-	vstreti-l-a	Tramp-a	v	jejo	kostyum-e	
	Merkel-NOM.SG	meet-PST-F.SG	Trump-ACC.SG	in	her	suit-LOC.SG	

(6a) ‘Merkel met Trump who put on her suit for some reason’

(6b) ‘Merkel was wearing her suit when she met Trump’

(6c) ‘Merkel and Trump met each other within the inner space of Merkel’s suit’

Within NLU, syntactic ambiguity manifests itself in a possibility to build two or more different syntactic structures for the same phrase, e.g., AIIRE natural language processor (cf. [1]) builds two trees depicted on Figure 1 for (5a) for (5b), correspondingly.

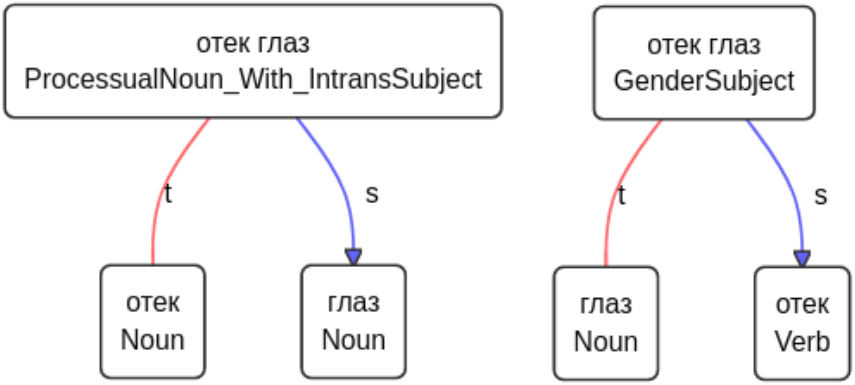

Figure 1. Syntactic ambiguity.

These diagrams and those below are screenshots from AIIRE natural language processor web-UI available at http://aiire.org website.

Syntactic ambiguity is almost inevitable: e.g., (6) is a very typical construction for SVO-languages like English or Russian, and it has, at least, three different possible structural interpretations, which means that any sentence, which has subject, object, and a prepositional phrase, is syntactically ambiguous. Nevertheless, syntactic ambiguity is, again, rarely obvious for a native speaker, who, most likely, does never even suppose that options like (6a) and (6c) can be possible. With a vanishingly low degree of probability, he may yet casually imagine that the eccentric American president, without ceremony, used the clothes of his German colleague, but, apparently, only an NLU system or its developer can imagine the costume of Angela Merkel, which she would use not just to crowd into together with the US president inside it, but also to negotiate with him on the sidelines of this costume.

Semantic ambiguity can be caused by lexical polysemy like in (7a), (7b), (7c), and (7d), by semantic relations indeterminacy, like in (8a) and (8b), or by them both, as in (9a) and (9b).

(7) *I saw bats*

(7a) 'I cut flittermice with a saw'

(7b) 'I cut cudgels with a saw'

(7c) 'I spotted flittermice'

(7d) 'I spotted cudgels'

(8) *Bob's hand*

(8a) 'hand being part of Bob's body

(8b) 'someone else's hand belonging to Bob'

(9a) *сосуд-ы* *пациент-а*
sosud-y pacient-a
blood.vessel-NOM.PL patient-GEN.SG
'blood vessels in a patient's body'

(9b) *сосуд-ы* *пациент-а*
sosud-y pacient-a
jar-NOM.PL patient-GEN.SG
'jars belonging to a patient'

Within the above-mentioned NLU pipeline, semantic interpretation is performed for syntactic trees. Thus, if a syntactic structure is semantically ambiguous, then two or more different semantic interpretations can be built for this structure, e.g., two semantic graphs depicted on Figure 2 are built by natural language processor for the same syntactic tree in (9), and correspond to interpretations (9a) and (9b). Some modern systems claim to perform semantic analysis without syntax parsing. The analysis these systems perform should not be confused with semantic interpretation or 'understanding': these kinds of analysis include statistical analysis of the thematic structure of the text (latent-semantic analysis, statistical classification, including deep-learning) or statistical sentiment analysis; thus, these systems should not be confused with NLU systems, although they are often mistakenly referred to as such.

Figure 2. Semantic ambiguity.

These diagrams are, again, screenshots from AIIRE natural language pro-

cessor that uses Russian labels for concepts in semantic graphs for Russian texts. The first (left) graph depicts ‘patient’ concept with ‘have material part’ relation directed at ‘blood vessel’ concept with the following description: ‘tubular organ in animals and plants, where a liquid medium moves’. The second (right) graph depicts ‘patient’ concept with ‘be owner of a thing’ relation directed at ‘jar’ concept with another description: ‘container for liquid and loose bodies’.

Besides the above-mentioned types of ambiguity, which are the most important from the point of view of linguists, there are also some other types, which are not less important from technical point of view and should be mentioned, at least, to complete the picture.

Segmentation (tokenization) ambiguity arises when there are no explicit delimiters between tokens. This applies to languages, which have such writing systems, that do not provide spaces or any equivalents thereof, like Chinese or Tibetan (cf. [2]), or most ancient languages; to tasks where tokens are parts of word forms like morphemes or stems (cf. [3]), and to speech recognition tasks, where boundaries of individual speech sounds themselves are ambiguous, not to mention the boundaries of morphemes and word forms. Segmentation ambiguity also applies to some phenomena even in languages with spaces: character spacing can be made in the form of spaces between characters like in (10), and inscriptions of this type can be parsed correctly only assuming ambiguity of spaces themselves; in addition, spaces can be missing by mistake, and if the NLU system tries to perform understanding of real texts, it must deal with mistakes of this kind.

(10) З А Я В Л Е Н И Е
Z A JA V L E N I E
application
‘application’

Encoding ambiguity takes place when the input encoding is not specified or is incorrectly specified, and the system tries to determine it on it’s own. This type of ambiguity is typically resolved with low-level procedures and, therefore, will not be considered in this paper, but it can also be resolved within the upper levels of NLU pipeline, and this solution can be a subject of a separate study.

Computational complexity problem

When processing real texts, all types of ambiguity operate simultaneously and in multiple places of each sentence, which leads to the problem of combinato-

rial explosion (cf. [4]). The following is an attempt to mathematically assess the impact of ambiguity on classical NLU performance.

$$]T_n \in Al^n \tag{1}$$

is text, i.e. a finite vector of symbols of a finite alphabet;

$$A = \{(i,j) : i \in [1,n] \wedge j \in [i+1,n]\} \tag{2}$$

are atomic units boundaries;

$$MI : A \to 2^{GC \times L} \tag{3}$$

is a morphological interpretations function, which associates each atomic unit with a set of interpretation vectors, where *GS* is a family of grammar classes, and *L* is lexicon;

$$S = \left(A, \{((i,j),(j,k)) : (i,j) \in A \wedge (j,k) \in A\}\right) \tag{4}$$

is a graph representing all possible segmentations of into atomic units;

$$E(S) \quad \text{is the set of } S \text{ edges} \tag{5}$$

$$SM \quad \text{is a set of all simple chains on } S; \tag{6}$$

$$\forall M \in SM, |M| = m : SyI : \prod_{i=1}^{m} MI(M_i) \to 2^{Tr} \tag{7}$$

is a syntactic interpretation function, which associates each combination of morphological interpretations of atomic units in each segmentation with a set of corresponding syntactic trees; *Tr* is the set of all possible syntactic trees of the language;

$$SemI : T_r \to 2^{Sem} \tag{8}$$

is semantic interpretation function, which associates each syntactic tree with a set of semantic graphs, *Sem* being the family of all possible semantic graphs;

Then:

Algorithmic complexity for segmentation is

$$O(|A| + |E(S)|); \tag{9}$$

$$\forall \mu \in \prod_{i=1}^{m} MI\left(M_i\right) : \left|SyI\left(\mu\right)\right| \le C_{m-1} = \frac{\left(2\left(m-1\right)\right)!}{m!\left(m-1\right)!} \tag{10}$$

Factorial complexity of syntactic interpretation makes its algorithmic complexity more than exponential, or more than $O(N^N)$;

$$\forall t \in SyI\left(\mu\right) : \left|SemI\left(t\right)\right| \le \prod_{i=1}^{m} MN\left(\mu_i\right), \tag{11}$$

where $MN(\mu)$ is the set of meanings of μ_1 lexical item;

In total, algorithmic complexity of classical NLU is determined as:

$$O\left(\left(\left|A\right| + \left|E\left(S\right)\right|\right) \cdot \frac{\left(2\left(m-1\right)\right)!)}{m!\left(m-1\right)!} \cdot \left|\prod_{i=1}^{m} MN\left(\mu_i\right)\right|\right). \tag{12}$$

Thus, with the classical implementation of the NLU pipeline, a more than exponential increase in the number of versions of the interpretation (understanding) of the text occurs, depending on the size of this text, which falls under the definition of a combinatorial explosion. In practice, this leads either to the inability of the system to process texts within the allowable time (which is typical of the rule-based systems) and to the memory overflow, or to the fact that the system developers artificially exclude some versions or even all but the first one (which is typical of the statistical solutions, especially deep learning, e.g., neural machine translation pipelines), which inevitably leads to inaccuracy and incompleteness of the analysis.

The choice of one version of the interpretation of a fundamentally ambiguous text in a natural language cannot be correct by definition. Moreover, the choice of one, even the most probable version of the interpretation of a certain fragment of the text, may in no way correspond to its context, which inevitably leads to the impossibility of parsing or semantic interpretation of the whole text. For this reason, ambiguity resolution can only be performed based on context.

Context-driven disambiguation implies inter-level interaction: syntactic analysis rejects ungrammatical morphological interpretations by means of formal grammar; semantic analysis rejects nonsense syntactic interpretations by means of semantic valencies imposed by the underlying semantic dictionary or ontology (cf. [1]).

Experiments show that inter-level interaction is, indeed, necessary, if the system does try to build all possible interpretations of texts, but solves the prob-

lem of combinatorial explosion only on grammars and ontologies of relatively small volume; when expanding them to cover the corpora of real texts, the factorial growth in the operation time of the algorithms is reproduced with all the restrictions introduced. This fact can be illustrated with a simple example: in (11), there is a series of homogeneous adjectives, each of which can be either an attribute of the noun in the end of the phrase (11a), or an independent noun phrase with an ellipsed head (11b). This phrase can also be part of a larger noun phrase series; moreover, Russian syntax allows conjunctionless enumerations, thus, different combinations (11c-d) are possible.

(11)	умн-ый,	*красив*-ый	*и*	*богат*-ый	*мужчин-а*
	umn-yj,	krasiv-yj	i	bogat-yj	muzhchin-a
	clever-NOM.SG	hansome-NOM.SG	and	rich-NOM.SG	man-NOM.SG

(11a) ‘a clever, handsome, and rich man’

(11b) ‘a clever (man), a handsome (man), and a rich man’

(11c) ‘a clever (man), a handsome and rich man, ...’

(11d) ‘a clever and handsome (man), a rich man, …’

Different parses lead to completely different understandings of the phrase meaning: in (11a), there is only one man, who has three features, whereas in (11b) there are three different men, each of which has his own property.

The peculiarity of this example is that the ambiguity in it is fundamentally not resolvable, and the number of adjectives can be arbitrarily large, the number of possible arrangements in the series of homogeneous noun phrases increasing as the Catalan number, see formula (10).

Of course, if the underlying language model does not take into account ellipsis or conjunctionless homogeneity, then interpretations like (11c) and (11d) do not arise, and this phenomenon can not be detected. Thus, context-driven linguistic constraints and inter-level interaction reduce the scale of combinatorial explosion, but in reality not only do not exclude its possibility, but also completely fail to reduce it anyhow when the recall of the model gets higher.

Thus, combinatorial explosion is a fundamental property of classical NLU, and not just a problem for which a workaround can be found without significant loss of recall or precision. In this regard, a more correct formulation of the problem seems to be such, that the goal is not to eliminate the unresolvable ambiguity, but rather to create such models and algorithms that would operate with this ambiguity with acceptable algorithmic complexity, i.e., without exponential or higher time, and without possible memory overflow.

Superpositional packing

A model for efficiently representing ambiguous syntactic structures was first proposed by Masaru Tomita in 1987 ([5]). The main idea was called 'packing': instead of building two different parse trees for an ambiguous phrase, a single 'packed' tree can be built, which allows the inner structure of each constituent to be ambiguous, i.e., each constituent can have multiple versions of child constituents. This representation requires less memory, because each constituent is stored only once. Moreover, when several constituents are ambiguous, the total amount of stored versions equals the sum of the amounts of versions of inner structure of these constituents, whereas in the classical model with a separate tree for each parsing version, the whole tree is copied for each version of each ambiguous inner structure, which means that the sets of versions get multiplied, and the cardinality of the resulting set is product, but not the sum of the cardinalities of the original sets. Thus, the 'packing' method can reduce the complexity from factorial to polynomial.

To implement this idea, an effective procedure is needed to determine that two subtrees that were built independently are actually two versions of the same tree, and can be combined into one packed tree. In the Tomita model, it was assumed that two trees should be combined if they have the same root constituent symbols and the same terms (tokens). Unfortunately, this criterion was not successful enough to work with languages with rich morphology: firstly, in addition to the symbol (class), each constituent has a number of morphological features, and if two trees have the same class of the root constituent, but different features, then merging them into one packed tree cannot be correct, and secondly, in languages with rich morphology, the morphological ambiguity is also 'rich', and, therefore, many different versions of a tree term can correspond to each token, whereas merging trees built from different combinations of these versions turns out to be quite correct.

In fact, combining different syntactic structures into one 'packed' ambiguous structure is correct if and only if the structures being merged have absolutely identical syntactic properties, i.e., they can be embedded into the same parent constituents by joining or being joined to the same siblings. A more universal formal criterion to detect such structures was proposed and tested on Russian with CYK algorithm by Andrei Popov et al. in [6] and [7]: Two different structures should have exactly the same classes, morphological properties, and spans, where spans are pairs of left and right boundaries (and not tokens like in [5]).

The resulting formalization turned out to be perfectly compatible with the

data structures used in the AIIRE project (the idea behind AIIRE original neighbor-binding algorithm is compatible with CYK, although, unlike CYK, AIIRE does not need necessarily Chomsky normal form grammars, deals with ellipsis and ambiguity), where it was adopted and generalized as superpositional model not only for syntax, but also for morphology (morphosyntax) and ontological semantics.

In the classical AIIRE implementation, (12) has two parsing versions, depicted on Figure 3, which correspond to (12a) and (12b) interpretations, respectively.

(12)	Николай-	встрети-*л*-	*гост-ей*	*в*	*коридор-е*
	Nikolaj-	vstreti-l-	gost-ej	v	koridor-e
	Nick-NOM.SG	meet-PST-M.SG	guest-ACC.PL	in	hallway-LOC.SG

(12a) ‘Nick met the guests who were in the hallway (whereas Nick could be anywhere else)’

(12b) ‘Nick met the guests, and the meeting took place in the hallway’

In the superpositional model, which is proposed in this paper, different versions of the same structure are treated as its discrete states.

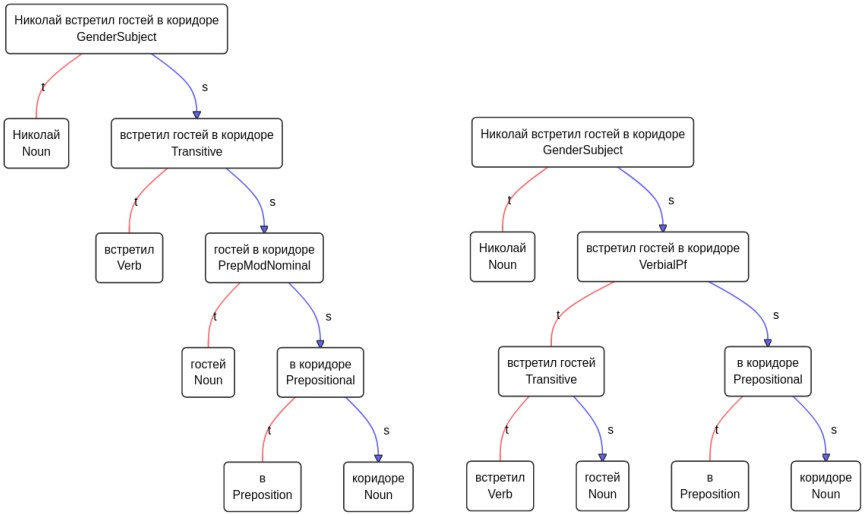

Figure 3. Two parsing versions of (12). For the purposes of compactness, these trees are artificially collapsed to Chomsky normal form, i.e., to binary structures, whereas the real trees are much larger, because of multiple single-branching constituents.

Thus, each tree on Figure 3 is treated as a possible discrete state of the same ambiguous phrase structure, and this structure itself is treated as superposition of these states. An ambiguous phrase structure, until it is put into a context, like Shroedinger's cat, is in a superpositional state, which means it is in all it's possible states simultaneously. Each of these states can be built by combining a pair of child constituents, thus, interpretation of a complex structure is superposition of possible states of its components, and the syntactic interpretation function can be redefined as:

$$SyI(t) = \sum_{i=1}^{n} A_i \ |C_i(t_{i_1}, t_{i_2})\rangle, t_{i_1} + t_{i_2} = t\,, \tag{13}$$

where t is the text (vector on the alphabet set), i is the number of the state, A_i is the square root of the probability of the state i, t_1 is a pair of two possible constituents of t, and C_i is a function which maps such a pair to a tree.

The Dirac notation used here can be used as such, because both trees and semantic graphs can be represented as vectors in a Hilbert space (see below).

E.g., there are two possible pairs of constituents that form the ambiguity in (12) with the following meanings: ('met the guests', 'in the hallway'), and ('met', 'the guests in the hallway'). Together they form, however, the same packed constituent, which is a perfective verb phrase like on Figure 4.

From the diagrams on Figure 3, it can seem that *GenderSubject* constituent also has two possible states that correspond to two possible pairs of child constituents: (*Noun*, *Transitive*) and (*Noun*, *VerbialPf*). In fact, the diagrams on Figure 3 are contracted to binary trees from much larger diagrams by omitting all single-branching nodes; in fact, the first tree also has (*Noun*, *VerbialPf*) structure, but in this case *VerbialPf* has only one child, and is therefore omitted.

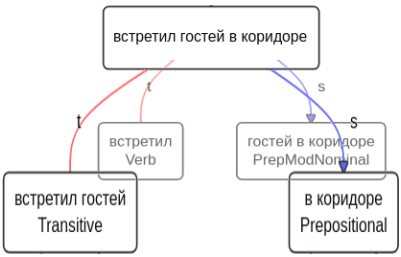

Figure 4. Superposition of tree states.

Semantics packing

The same applies to ontological semantics.

While the grammar defines classes of constituents and child-parent relations between them, the ontology defines classes of concepts and various semantic and conceptual relations between them.

Ontological relations restrict valencies (i.e., the properties of concepts of being able to have specific relations with other concepts) and form a multigraph which resembles a huge neural network; e.g., Figure 5 depicts the 'economics' concept from AIIRE ontology.

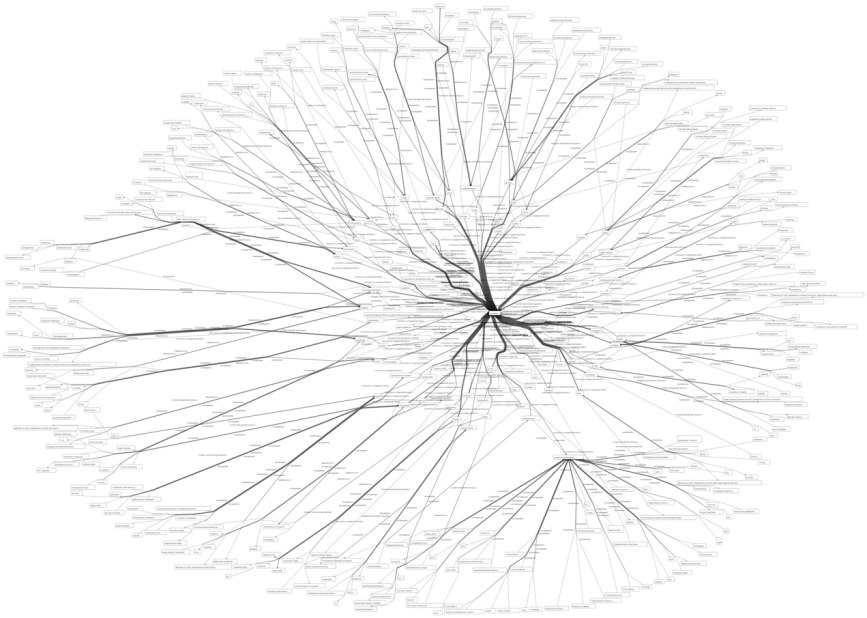

Figure 5. Visualization of ontological relations of 'economics' concept in AIIRE. Due to the large size of the graph, the image size is strongly reduced. Figure 6 shows a small part of this visualization, but in a larger scale.

Ontological relations are different and include not only classes of real-world objects or processes interactions, but also such relations that form the hierarchy of concepts themselves. The 'class-superclass' relation is one of the relations of this kind. Moreover, this is an inheritance relation, which means that each class inherits relations from all its superclasses. This relation reflects

the hypo-/hypernymy relation between word meanings in natural language and allows to define all other relations on basic classes of concepts and to evaluate the properties of particular concepts from the properties of its superclasses. Moreover, the classification itself, at least, in AIIRE ontology, is performed according with properties, which are relations with other concepts. E.g., physical objects are divided into artificial objects and objects of natural origin by relation to their origin; when relation can lead to two different object subclasses that are disjoint (which is another relation, actually), then the class itself also has two corresponding subclasses (this phenomenon is called classification parallelism). This approach allows to convert relations to dimensions of a Hilbert space and to define concepts as regions of this space.

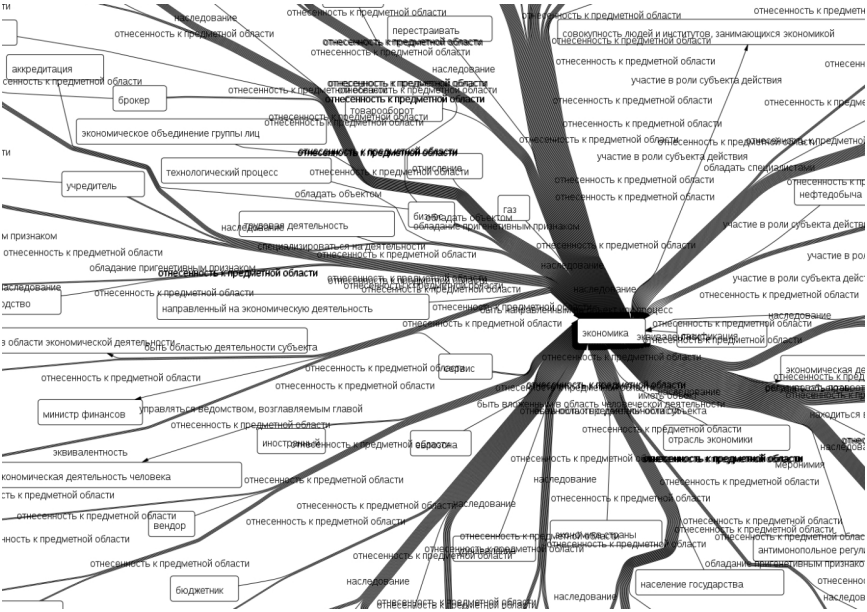

Figure 6. Larger scale of ‘economics’ concept visualization.

As a vector space, the ontology itself can be defined as a cartesian product of all independent dimensions defined by the properties (relations) of its concepts; for each such dimension, a bijection exists between the set of its possible values and the field of real numbers. This approach applies not only to obviously scalable attributes that can be measured, but also to qualitative attributes like ‘being pregnant’, usually treated as binary, but easily scaled in

the linguistic world view in jokes like *a little pregnant* or *completely pregnant*. In fact, natural language allows degree adverbs to be used with any adjectives, which confirms the scalability of all ontological dimensions, and, therefore, also the fact that it is a Hilbert space in which the scalar product operation is defined. Since AIIRE grammar is though separate, but still a full-scale part of this ontology (classes of immediate constituents are concepts, too, they have their own inheritance hierarchy and their own relations), the same also applies to the grammar.

Like in the grammar, in the rest of the ontology individual concepts, which have the same class, also have identical semantic properties, in that they can have the same relations with other concepts; then, if two concepts have the same class and correspond to the same span of the text, then they can be merged into a single concept with multiple possible sets of relations to other concepts.

Figure 7 depicts two possible semantic interpretations of the second tree, which corresponds to (12b): Russian word *гость* (‘guest’) has two different meanings that can fit into the context, one of them being defined as ‘the one who came to visit someone, spend time with someone or for some other purpose’, and the other being defined as ‘(plur.) (sports) sports team serving not in its native locality’.

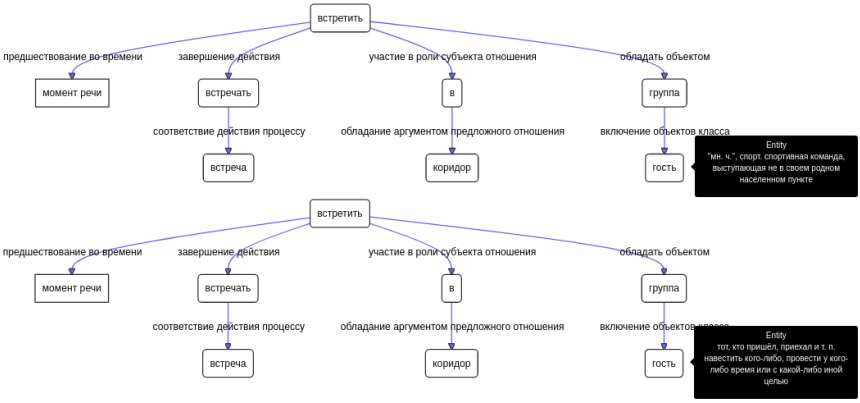

Figure 7. Two semantic interpretations of (12b).

These two interpretations differ only in one concept, thus, the whole semantic graph is actually unambiguous, except for the ‘guest’ concept, which may be either someone who came to visit someone, or a sport team, thus, these two

graphs are merged into one packed graph with one ambiguous concept.

Interpretation of an ambiguous lexical unit is, again, a superposition of its unambiguous interpretations (states):

$$QMN\left(\mu_i\right) = \sum_{i=1}^{n} A_i \left|\phi_i\right\rangle . \tag{14}$$

Thus, any ambiguous word, until it is put into a context, is in a superpositional state and simultaneously in all its possible states (meanings). Then, as the Compositionality principle says, the meaning of the whole is a function on the meanings of the parts and the way they are put together (cf. [8]), and the semantic interpretation function can be redefined as:

$$SemI\left(t\right) = f\left(t_1, t_2, C\right), \tag{15}$$

where t is a tree, f is a function that maps t_1, t_2, and C to the meaning of t_1, t_2 and t_2 are child constituents of t, and C is the function that maps t_1 and t_2 to t, determining the way they are put together.

Unfortunately, this redefinition does not apply directly to superpositional syntactic structures: individual parts and the way of putting them together are unknown for them. Whereas syntactic properties of the tree do not depend on its inner structure, its meaning does depend on it. Thus, in order to solve this problem, the function should be again redefined via the actual (non-superpositional) states (versions) of the syntactic tree:

$$SemI\left(t = \sum_{i=1}^{n} A_i \left|C_i\left(t_{i_1}, t_{i_2}\right)\right\rangle\right) = \sum_{i=1}^{n} A_i \; B_i \left|f\left(t_{i_1}, t_{i_2}, C_i\right)\right\rangle, \tag{16}$$

where B_i is the square root of probability of the semantic interpretation.

This approach imposes, however, some restrictions on linguistic data:

1. The grammar must be CNF (Chomsky Normal Form), strictly binary;
2. Both the grammar and the ontology must conform with the following general rule: external properties (including compatibility) of any entity (syntactic tree, concept) must not depend on its internal properties

Evaluation

The current implementation of the superpositional model in the AIIRE is intermediate: since the underlying linguistic data currently does not fully satisfy the limitation 1 above, the gain achieved using this model can be accurately calculated only for parsing, but even these figures confirm the

above estimations. Table 1 represents the amounts of immediate constituents in memory for different ambiguous phrases in Russian with classical model in comparison with superpositional packing, both with all syntactic and semantic limitations enabled and with inter-level interaction; the algorithmic complexity, and, therefore, execution time is directly proportional to these amounts.

Table 1

Amount of constituents in memory for classical model versus superpositional packing

Classical model	Superpositional packing
81	29
933	96
2382	125
32205	212
166485	270

Conclusion and further work

Despite the above limitations that do not influence precision and recall anyhow, the superpositional model allows not only to reduce multiplication to summation, moving from more than factorial algorithmic complexity to polynomial and retaining the possibility of restoring all those versions that the classical model could generate, but also to determine the mechanism of probabilistic ranking of these versions in the presence of a certain probability measure. This model has been actually developed in AIIRE project since 2007 as a so-called 'solver' model, where solver is an agent that generates individual solutions of possible object states ordered by their probability from the superpositional representation of this object. The main advantage of the solver model is that it can be used not only to quickly (in a nearly linear time) produce the most probable version, but also to switch to next version if needed, or to generate all possible versions one by one without keeping them all in the memory.

Current experimental implementations of superpositional solver model prove the algorithm complexity gain described above. Unfortunately current implementations are not production-ready and are still unstable with current linguistic data which violates requirement 1 mentioned above; however, as the whole AIIRE project, they are open-source and available under the terms of GNU General Public License at AIIRE project repository and can be tested with any other linguistic data.

References

1. Dobrov, A. Semantic and Ontological Relations in AIIRE Natural Language Processor. In Computational Models for Business and Engineering Domains. — ITHEA, Rzeszow - Sofia 2014 — pp. 147—157 — ISBN: 978-954-16-0066-5, 978-954-16-0067-2
2. Dobrov A., Dobrova A., Grokhovskiy P., Soms N., 2017. Morphosyntactic Parser and Textual Corpora: Processing Uncommon Phenomena of Tibetan Language. In: Proceedings of the International Conference IMS. Saint Petersburg, pp. 143-153 (2017). ISBN: 978-1-4503-5437-0 doi>10.1145/3143699.3143719.
3. Haspelmath M. 2011. The indeterminacy of word segmentation and the nature of morphology and syntax. In Folia linguistica. Voll. 45, Iss. 1, pp. 31–80.
4. Krippendorff Klaus. “Combinatorial Explosion”. [http://pespmc1.vub.ac.be/ASC/Combin_explo.html] Web Dictionary of Cybernetics and Systems. PRINCIPIA CYBERNETICA WEB.
5. Tomita M. 1987. “An Efficient Augmented Context-Free Parsing Algorithm,” Computational Linguistics, 13, 31-46.
6. Popov A., Protopopova E., Bukiya G. 2016. Once more on ways to overcome structural homonymy: selection of the only structure in the Hurma parcer [Esche raz o sposobah snyatiya strukturnoy omonimii: vybor edinstvennoi struktury v parsere Hurma // Collection of scientific articles of the 19th Joint Conference “Internet and modern society” [Sbornik nauchnih statei 19 Obyedinennoy konferenzii “Internet i sovremennoe obscchestvo] IMS-2015, Saint-Petersburg, June 22 - 24, 2016.
7. Popov A., Enikeeva E. 2017. Template Search Algorithm for Multiple Syntactic Parses. In Proceedings of the International Conference IMS-2017 (IMS2017). ACM, New York, NY, USA, 164-170. DOI: https://doi.org/10.1145/3143699.3143732
8. Pelletier F.J. Topoi. 1994. 13: 11. Springer Netherlands. https://doi.org/10.1007/BF00763644

Chapter 18.
Social induction and a problem of choice in conditions of uncertainty

D. S. Gorbatov, N. A. Solovyev, L. N. Soms

Introduction

Recently, quasi-physical approaches are actively developed in application for psychological and social problems. A particular interest is attracted to a problem of choice under conditions of uncertainty; deviations from classical paradigm based on logic and statistics were noticed. Thus, a violation of the conjunction law was found [Tversky, 1983] at answers of subjects for sequential range of questions, such violation is impossible to explain within classical theory of probability. An attempt of solution led to an alternative interpretation based on the quantum logic [Busemeyer, 2011]. The essence of this interpretation was that a certain vector of state was assigned to human's state of mind for the moment of making the answer, this vector represented a superposition of two alternative answers. After the decision of a definite answer is made, the vector of the state of mind collapsed into one of two possible final states.

The possibility of description of human's state of mind in terms of quantum mechanics induced a number of works in which a society was treated as laser-like system [Khrennikov, 2015]: here a human being was an analogue of an atom which excited state could either decay spontaneously to one of final states, or could undergo a stimulated transition under an influence of the choice of other members of society.

A similarity between complex biological systems and multimode lasers was pointed out in [Danilov, 2016].

In spite of the fact that ideas of laser-like features of social behaviour exist for a relatively long time, until present there are nor their experimental evidence neither theoretical models corresponding to a laser specificity of a decision making at the presence of several interacting individuals.

The goals of our study were:

1. to develop the scheme of a social experiment for quantitative evaluation of degree of a "social pressure" influencing the choice of a partici-

pant in conditions of uncertainty, and to perform the experiment;

2. to formulate a laser-like model of the experiment;
3. to determine, by fitting parameters of the model to the results of experiment, empirical numerical values of parameters of the model.

The presented work describes results of an experiment of computer testing in which participants were shown a series of images accompanied by two not evident alternative answers for a question "what is this?", and were prompted to make their choice under different conditions, viz.:

i. the free individual choice ("control" group);

ii. the choice when each participant sees the results of real answers (response promptings) of other subjects of his experimental group ("true" group);

iii. the choice when the participants see false response promptings generated by a special computer program ("false" groups).

A quasi-physical model was developed in which the process of choice was presented as an aggregation of spontaneous and stimulated transitions of the state of mind from "excited" into one of alternative "lower" states..

Experiment

A general scheme of the experiment is shown in Figure 1.

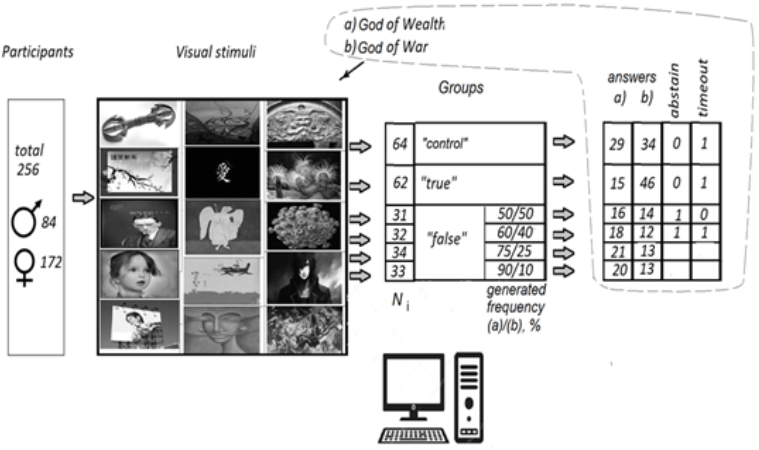

Figure 1. General scheme of the experiment.

Participants

A group of 265 volunteers (bachelor students of 1st –4th years of St.Petersburg State Institute of Psychology and Social Work), including 84 male youths and 172 girls, was divided into 6 groups and was subjected to a computer-controlled test.

In order to minimize an influence of sex and age of the participants to the results of the experiment, each group included persons of both sexes proportional to their relative part in the whole set of participants, and consisted of approximately even number of students from junior and senior classes.

A standard computer class of the Institute was used for the experiment. Each session of the experiment was in the end of the 4th of 6th hour of routine education process and lasted for 16–17 minutes. The number of participants in each session was limited by the number of computers in the classroom.

The numbers of participants in each group N_i ("control", "true", and "false" groups) are shown in Figure 1.

Software

A specialized proprietary software was developed and used in the experiment. The software was designed as a WEB-application with necessary stack of technological instruments.

Front-end — HTML5, CSS3, JavaScript, jQuery library. Back-end: — PHP5. Data manager — MySQL. The WebSocket technology was introduced for global synchronization with HTTP protocol.

The software complex included three blocks:

(1) operator control panel: to create, edit, load/unload the tasks; to control the WebSocket server; to set time intervals for answers and number of participants. This block provided also varying the regime of experiment: (a) free individual choice (for the "control" group); (b) response promptings by demonstration of real answers of other participants of the group ("true group"); (c) response promptings by demonstrating false answers of other participants of the group, with predetermined arbitrary frequency of occurrence of alternative answers (four "false" groups).

The answers and their statistical characteristics were displayed.

An algorithm of generation false promptings was as follows: just after the moment of answer of a participant, a generated false response prompting ap-

peared on displays of all other participants. The frequencies of appearance of the false promptings to alternative answers N_a/N_b, for different groups in our experiment, were equal to 50/50, 60/40, 75/25, 90/10.

2) user interface (a sequential disdplay of visual stimuli and questions to be answered, with or without real or false response promptings)

3) WebSocket-server — provided the interactive real-time exchange of information

Stimuli

In the course of the experiment, 15 cognitive-undetermined tasks were used. Each task included a picture, a question, and two alternative answers (a) and (b) for the question.

A participant could: (i) to choose one of the answers; (ii) to abstain from the answer (push an "answer" button without choosing); (iii) not to answer during 40 seconds given for each stimulus.

In order to eliminate or minimize a possible influence of the order of presentation of a stimulus and the order of suggested answers (a) or (b), the order of presentation of stimuli and of the answers changed from group to group.

Examples of several stimuli and alternative answers are shown in Figure 2.

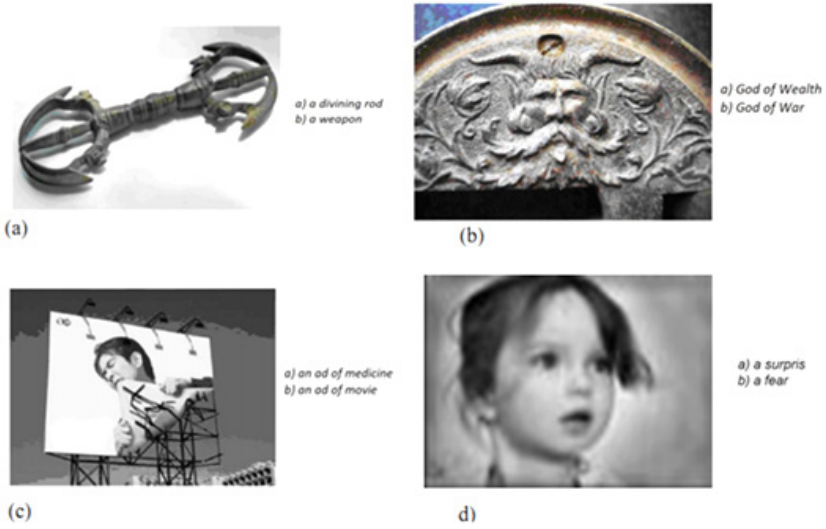

Figure 2. Examples of visual stimuli and alternative answers.

The information about response promptings was represented as a colored strip (red for (a) and blue for (b)) in the lower part of the screen, the length of the strips showed the number of corresponding answers. Besides, the percentage of (a)/(b) was shown.

Instructions and motivation of participants.

The participants were warned that the test did not pursue on an evaluation of erudition or intellectual capacity of a person and that it had no relation to teaching process. It was noted that the registration of the answers was "blind", no personal identification is applied.

In order to hide the independent variable of the study, the participants were told about a false target of the study as a reveal of influence of a type of cognitive uncertainty on the success of the task fulfillment.

The participants were instructed that the time allocated for each task was equal to 40 seconds and the rules of answering, as described above. The participants were informed that the evasion from an answer was not desirable since it makes the interpretation of the experimental results difficult.

The motivation was limited to a reference to *"results of previous studies which have shown that the bachelor students of our institute were as good in solution of cognitive-undetermined tasks as masters of a prestigious university*".

The first task in the series (see Figure 2, a) was presented to participants as a training, with the comments of the experimenter as follows:

"So, what do you see at the picture? Consider what is a material from which the thing is manufactured? What could be the age of the thing?

If this is a weapon is it a contact or it can act distantly? How could a warrior held it? How he could use it against an enemy?

If it is divining item, to what cult—polytheistic or monotheistic could it relate? Does it bear some esoteric symbols? How could it be used by a priest?

Please do not discuss the task with other participants and make your personal choice.

As for the next pictures, make your analysis and choice on your own".

Talks and discussions were announced as not desirable. Often, expressions of bewilderment aroused, which were parried by reference to a specificity of cognitive-indetermined tasks and advises were given to examine the picture more thoroughly.

The input briefing and registration of the group took not more than six minutes, and the further execution of the tasks — ten minutes. No final debriefing was provided.

Results of experiment and discussion

As the result, for each visual stimulus the experimenter got a set of answers, an example of the set is given in Figure 1, the area inside dotted line.

The total fraction of abstained and refused answers was 11 %, and these cases were excluded from further calculations.

The ratio of frequencies of occurrence of alternative answers (a) and (b) $K_0 = N_a / N_b$ obtained for the "control" group represents the degree of equiprobability of the answers. For all set of stimuli, the absolute value of deviation of K_0 from unity $|\Delta| = |K_0 - 1|$ varied from $|\Delta|_{max} = 2{,}5$ (for the stimulus #1, Figure 2, a) to $|\Delta|_{min} = 0{,}05$ (for the stimulus #7, the second row in the middle column, Figure 1; the task for this stimulus was: *what means this hieroglyph: (a) a luck, (b) a sorrow*), and for 70 % of stimuli this value $|\Delta|_{min} < 0{,}5.$.

At analysis, Pearson's chi-squared χ^2-test was applied: the differences between data distribution are considered as statistically valid if empirical value $\chi^2 \geq \chi^2_{0.05}$, and as highly authentic if empirical value $\chi^2 \geq \chi^2_{0.01}$. In the experiment, the number of participants in each session was limited by the number of computers in the classroom. This, for small groups (at $N - 1 = 14$, which is just our case) critical values χ^2 are between $\chi^2_{0.05} = 23.685$ to $\chi^2_{0.01} = 29.141$ (see [Sidorenko, 2002]). The results of χ^2 –test are shown in Figure 3.

The main findings of the analysis performed are as follows:

(1) the presence of statistically valid differences between "control" and "true" groups testifies to the possibility of registering the phenomenon of social inductance in the experiment performed;

(2) in our experiment, there were no significant difference between the behaviour of "true" and "false" groups: the real manifestations of the social inductance are similar to those for mocked ones.

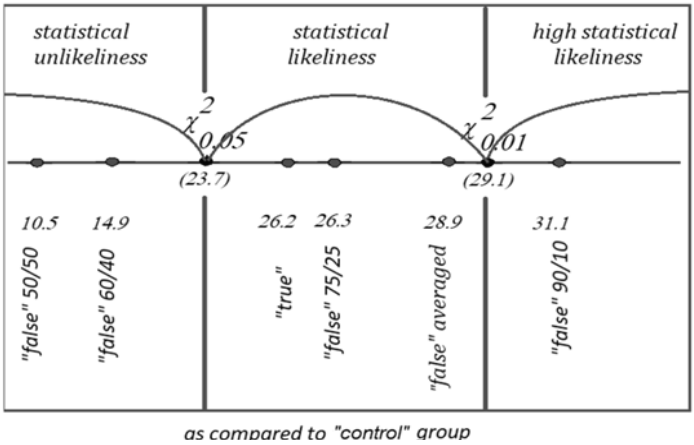

Figure 3. Results of χ^2 –test.

(3) the experiment have shown the statistically valid increase of value K_0 for benefit of an answer which frequency of occurrence on the screen (be it in the "true"or in the "false"groups) was prevalent.

Thus, a "strong" answer increased, a "weak" answer was suppressed. One can see this effect in the table of answers for the stimulus #11 in Figure 1: starting from $\Delta_0 = -0{,}15$ for the "control" group (for which the frequency of occurrence of the answer (a) is less than that of the answer (b)), under the influence of false hints 90/10, the initially less probable answer prevails, $\Delta_{90/10} = +0{,}54$.

In Figure 4, experimental values of ratio of "strong" to "weak" answers for all groups are shown. It is interesting that the deviation of numbers of answers from the average of distribution was observed much larger for "true" group than for all other groups ("control" and "false"). Let us remind that in the "true" group during all sessions and for all stimuli, participants saw real answers of other participants of their groups.

An interpretation of this phenomenon within our model will be given below.

Laser-like model.

In the model, we consider that at the moment of making decision, human mind is in a certain non-equilibrium state analogous to an excited state of a quantum object (atom, molecule, ion…)

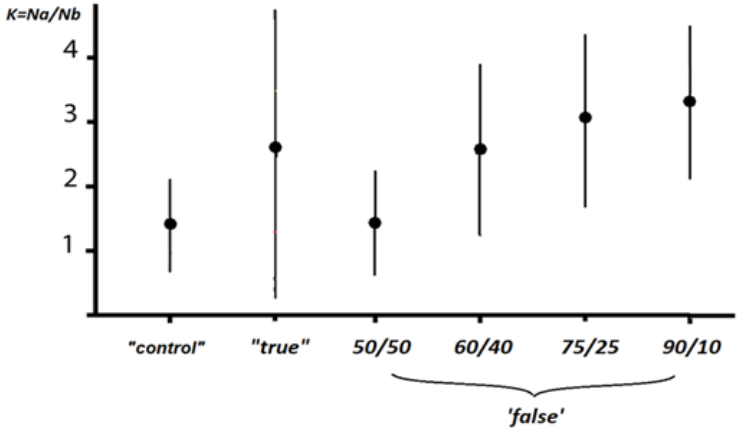

Figure 4. Experimental values of $K = N_a / N_b$.

This non-equilibrium state of the mind occurs when a participant agrees (“is pumped”) to take part in the experiment, is conserved in a kind of metastable state until the start of the experiment, is activated at the moment of appearance of a stimulus, and relaxes to a calm “lower” state after answering the question. Under conditions of choice between alternatives, this relaxation can happen by two “channels” corresponding to answers (a) or (b).

This process has a certain likeliness to a spontaneous decay of excited state of an atom to two final states through two different channels.

The answers are registered by a computer and become known to other participants in the real (“true” group) or in a biased form (“false” groups).

Let us suppose that the answers that are sensed by other participants are capable to act similar to an external radiation that caused a stimulated emission. The information about answers done by other participants influences the choice done by recipient of this information, similar to hints and prompts in earlier experiments [Asch, 1956.]. Thus, one can plot a scheme (Figure 5) similar to schemes of quantum transitions from excited states, usual for laser studies, and apply a corresponding mathematics to this scheme.

Populations on different levels in this scheme can be described by a system of so called kinetic equations.

For the case when prompting responses are visible to participants, for the “control” and “false” cases, this system can be written as follows:

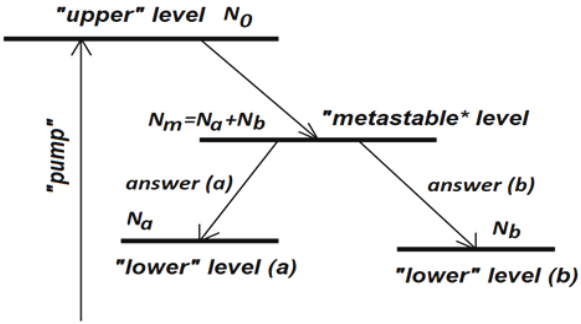

Figure.5. Laser-like scheme of states of mind.

$$\frac{dN_m}{dt} = -N_m\left(A_a + A_b\right) - N_m\left(B_aW_a + B_bW_b\right)\left(N_a + N_b\right) \quad (1)$$

$$\frac{dN_a}{dt} = N_mA_a + B_aW_aN_m\left(N_a + N_b\right) \quad (2)$$

$$\frac{dN_b}{dt} = N_mA_b + B_b \cdot W_bN_m\left(N_a + N_b\right) \quad (3)$$

Here: N_m, N_a, N_b — populations of "metastable" and "lower" levels; A_a, A_b — coefficients depicting frequencies of occurrence of answers (a) and (b) under conditions of individual choice (correspond to "control" group), similar to Einstein coefficients A for spontaneous decay of excited atoms; B_a, B_b — analogues of Einstein coefficients B for induced transitions for channels (a) and (b), correspondingly (see, e.g. [Svelto, 2008]); W_a, W_b — coefficients which provide the frequency of occurrence for mocked answers (a) or (b) specified and predetermined by the experimenter. It is clear that for the "control" group one shall set $W_a = W_b = 0$.

The initial conditions: $N_m\left(0\right) = N_0; N_a\left(0\right) = N_b\left(0\right) = 0$

In the equation (1) the member $N_m\left(B_aW_a + B_bW_b\right)\left(N_a + N_b\right)$ describes the decay of "metastable" level under the influence of prompting responses, since $W_a\left(N_a + N_b\right)$ represents the number of generated false prompts for the answer (a); for the equations (2) and (3) similarly.

The example of calculation for one of stimuli for the "control" group is shown in Figure 6.

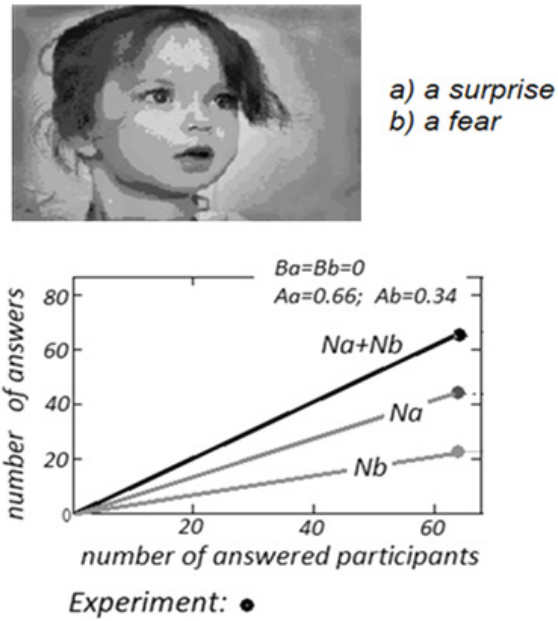

Figure 6. Example of calculation for the "control" group.

By numerical calculations, one can fit values B_a, B_b for getting the best agreement with experimental data. It was found that for all set of experimental data, all stimuli and all groups, the best agreement was obtained for $B_a = 6 \cdot 10^{-2}; B_b = 4 \cdot 10^{-2}$

As an example, for the same stimulus as in Figure 6, the results of experiment and calculations with the parameters B_a and B_b mentioned above are given in Figure 7. In the figure: lines — calculation; dots — experimental data (total number of answers for the group); straight line 1 — sum of answers (a) and (b); curves 2–3 — values of N_a for the "false 90/10" group (2) and "true"group (3); curve 4 — N_a for "control" group normalized for $N_0 = 34$; curve 5 — the value of N_b for the "false 90/10" group.

The results of calculations of $K = N_a / N_b$ together with experimental data are presented in Figure 8. One can see a satisfactory correspondence between

the results of calculation and experimental data. Let us try to explain, in the frames of the model, the mentioned above feature of experimental results for the "true" group: much larger value of the deviation of answers from the average than that for all other groups. This can find its explanation in the difference of action of promoting responses.

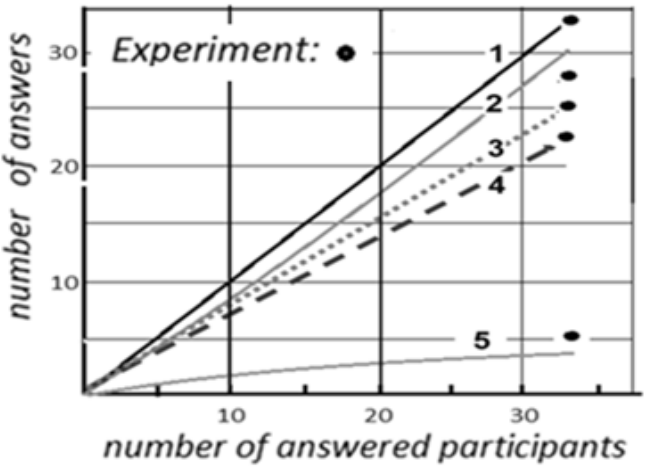

Figure 7. Results of calculation for the stimulus of Figure 6.

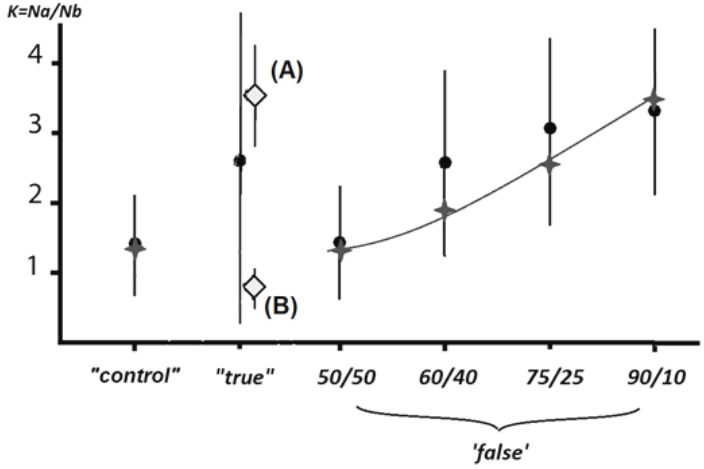

Figure 8. Results of calculation and experimental values of $K = N_a / N_b$.

For the "true" groups a random repeating set of first answers immediately provoke shift of subsequent answers to one of alternatives, thus operating as a positive feedback. At the same time, it is no such strong dependence of the final result to initial answers in the case of "false" groups; on the contrary, a constant relation $K = N_a / N_b$ set by the experimenter stabilizes final results against initial fluctuations of choice.

For the case of "true" hints the equations (1–3) were modified as follows:

$$\frac{dN_m}{dt} = -N_m\left(A_a + A_b\right) - N_m\left(B_a N_a + B_b N_b\right) \tag{4}$$

$$\frac{dN_a}{dt} = N_m A_a + B_a N_a \tag{5}$$

$$\frac{dN_b}{dt} = N_m A_b + B_b N_b \tag{6}$$

These equations, in a fact, are standard kinetic equations for populations of levels in the presence of stimulated emission (see, e.g., [Svelto, 2008]).

Taking initial conditions as $N_a(0) = 6, N_b(0) = 0$ one can get a theoretical solution indicated as A in Figure 8; taking them as $N_a(0) = 0, N_b(0) = 15$ we get the solution B in Figure 8. There was no monitoring of sequence of answers during the experiment, so one can suppose that such random initial conditions took place during the sessions. So the overall large deviation of results in the "true" case can be regarded as an illustration of high sensitivity of solutions of the system of equations (4–6) to initial conditions.

Conclusion

The scheme and results of our experiment gave some quantitative data concerning an influence of "social pressure" to individual choice in conditions of uncertainty. These data allowed to apply to our experiment a laser-like model of kinetic equations describing populations of excited and final states. Satisfactory results of comparison of theory and experiment give a hope to further development and productive application of laser-like models to problems of humans' social behaviour thus answering the vital needs of society (see e.g. [Sergeev, 2019]).

Several immediate questions are arising directly for the experiment, for instance:

- are the determined values of "stimulating influence" coefficients B_a and B_b applicable only for our experiment?
- will they vary with a different set of participants (ours were students; what for workers, office managers, artists…)?
- do they depend on sex of participants?;
- will they change if discussions between participant were allowed during the sessions?;
- how to apply similar theoretical model for more vivid problems, as, e.g., choice between candidates at municipal elections?; etc.

It is clear that the described experiment had a very specific and artificial character, and its immediate goal was to provide empirical background for justification a laser-like model. Surely, much wider research program shall be developed and fulfilled in order to reach an adequate description of social behaviour; we believe that the presented results could help in this.

References

1. Asch S.E., 1956: Asch S.E. Studies of independence and conformity. A minority of one against a unanimous majority. Psychological Monographs. 1956. Vol. 70 (9). P. 1–70.
2. Busemeyer J., 2011: Busemeyer J., Pothos E., Franco R., Trueblood J. A quantum theoretical explanation for probability judgment "errors". Psychological Review. 2011. 118 (2): 193–218.
3. Danilov O.B., 2016: Danilov O.B., Rozanov N.N., Solov'yev N.A., Soms L.N. Mnogomodovyye lazery kak analogi slozhnykh biologicheskikh sistem. Optika i spektroskopiya. 2016. 120: 682–69
4. Khrennikov A., 2015: "Social Laser": Action Amplification by Stimulated Emission of Social Energy // arXiv:1512.05386v1 [physics.soc-ph] (2015)
5. Sergeev A., 2019: Sergeyev A. «Sotsial'nyy» lazer i oranzhevyye revolyutsii: interv'yu prezidenta RAN, http://лазер. рф/2019/01/11/10816/
6. Sidorenko Ye.V., 2002: Sidorenko Ye.V. Metody matematicheskoy obrabotki v psikhologii.— SPb.: Rech', 2002.— 350 s..
7. Tversky A., 1983: Tversky A., Kahneman D. Extensional versus intuitive reasoning: the conjunction fallacy in probability judgment. Psychological Review. 1983. 90: 293–315
8. Svelto O. Printsipy lazerov / Per. pod nauch. red. T. A. Shmaonova. 4-e izd. — SPb.: Izd. «Lan'», 2008. — 720 s.

Chapter 19.
Models of light conversion by the visual system

N. N. Krasilnikov, O. I. Krasilnikova

Introduction

The hypothesis of a matched spatial filtering of noisy images by the observer's visual system was first expressed and experimentally confirmed by the author of this work in 1956. According to this hypothesis, the process of matched filtering of a noisy image is carried out not in the retina, but in higher sections of the visual system. In studies of the visual system, the Bayesian approach was used, i.e. the available a priori information about the investigated phenomenon or process was used to the maximum. For example, for engineers specializing in the field of radiolocation, it is expressed in the use of criteria for minimum average risk, an ideal observer, Neumann-Pearson criteria, and. etc. When developing systems designed for transmitting and reproducing images, a serious problem hindering the work is their coordination with the observer's vision. Using models allows to automate the selection of its optimal parameters using one of the optimization methods, for example, belonging to the class of gradient methods. In this paper we consider the models of transformation of light stimuli by the visual system.

Converting of the distribution of effective illumination on the retina to the distribution of excitations

At first, let us consider the simplest case when the effective illumination of all cones of the retina of the type in question (for example, the effective illumination I_R of a cone of type R)

$$I_R = \int_{\lambda_1}^{\lambda_2} \phi(\lambda)\varepsilon_R(\lambda)d\lambda \qquad (1)$$

is maintained at I_{0R} for a long time, and let us determine the output signal of the *i*-th bipolar cell associated with the *i*-th cone.

Here we use the notation: $\varphi(\lambda)$ is the spectral intensity of light, λ_1 and λ_2

are the wavelengths of light that determine the range of visible electromagnetic radiation, $\varepsilon_R(\lambda)$ is the spectral sensitivity of a cone of type R.

Since the photochemical processes in the cones are in equilibrium, the rate of formation of the product of fading of the visual pigment at the exit of the bipolar cell and, therefore, the excitation of the bipolar cell $S_{iR} = 0$, i.e. the *i*-th bipolar cell is in an unexcited state [Krasilnikov et al., 1999]. We encounter this phenomenon in experiments with a stabilized retinal image, when the image, after its stabilization on the retina, "fades" over time and becomes invisible, since the photochemical processes in the photoreceptors come into equilibrium. Now, let at the time $t = 0$ the effective illumination of the *i*-th cone change and become equal to I_{iR}. Since the values of the relative amount of discolored pigment x_{i0R} and the amount of the intermediate decomposition product y_{i0R} in the *i*-th cone at the first moment of time does not change due to the inertia of photochemical processes, the new value y'_{iR} becomes equal to

$$y'_{iR} = \frac{b_R\left(1 - x_{i0R}\right)I_{iR}}{k_{1R}} - \frac{y_{ioR}}{k_{3R}}, \qquad (2)$$

where b_R and k_{3R} are constant coefficients.

Considering that in the case under consideration, the average amount of the intermediate product of the decomposition of visual pigment $\bar{y}_R$ coincides with the value y_{i0R} at $t < 0$, we can write

$$y_{i0R} = \frac{b_R k_{3R}\left(1 - x_{i0R}\right)I_{0R}}{k_{1R}}. \qquad (3)$$

where k_{1R} is a constant coefficient.

Considering that y'_{iR} and $\bar{y}_R = y_{i0R}$, as follows from (2) and (3), we write the expression for the signal at the output of the i-th bipolar cell

$$S_{iR} = \frac{c_{0R}}{k_{3R}} \frac{I_{iR} - I_{0R}}{I_{0R}},$$

where c_{0R} is a constant coefficient.

In real conditions, due to the continuous displacement of the axis of vision and the inertia of photochemical processes, practically the same averaged values are set in all the considered retinal cones $x_{iR} = \overline{x}_R$ and $y_{iR} = \overline{y}_R$, and their values are determined by the average effective illumination $\overline{I}$. Moreover, as it is not difficult to see,

$$\overline{y}_R = \frac{b_R k_{3R} \left(1 - \overline{x}_R\right) \overline{I}_R}{k_{1R}}. \tag{4}$$

Carrying on with the same sort of discourse, we get the expression for the signal at the output of the *i*-th bipolar cell

$$S_{iR} = \frac{c_{0R}}{k_{3R}} \frac{I_{iR} - \overline{I}_R}{\overline{I}_R}, \tag{5}$$

and similarly for signals at the outputs of bipolar cells associated with the cones of types G and B

$$S_{iG} = \frac{c_{0G}}{k_{3G}} \frac{I_{iG} - \overline{I}_G}{\overline{I}_G}, \tag{6}$$

$$S_{iB} = \frac{c_{0B}}{k_{3B}} \frac{I_{iB} - \overline{I}_B}{\overline{I}_B}, \tag{7}$$

where c_{0G}, k_{3G}, c_{0B}, k_{3B} are the coefficients.

According to modern concepts, during the observation of achromatic and chromatic objects under threshold conditions, matched filtering takes place in the visual system [Krasilnikov et al., 2002]. According to Rushton [Rushton, 1962], under such conditions, the adaptation of each of the retinal cone systems (R, G, B) occurs independently of each other. In this case, the distribution of the effective illumination of I_R, I_G, and I_B on the corresponding cones of the retina is converted into signals: achromatic S_{iA}, as well as color-difference S_{iRG}, S_{iYB} at the outputs of the corresponding bipolar cells, which are proportional to the distribution of contrasts. Further, in the subsequent sections of the visual system, there are transformations of the primary signals into achromatic and two color-difference signals. These transformations are demonstrated by the model in Fig. 1, explaining the conversion of the signal

from the cone to the signal at the output of the bipolar cell by the triad: cone, horizontal cell system, bipolar cell. Figure 1 demonstrates a model of these transformations.

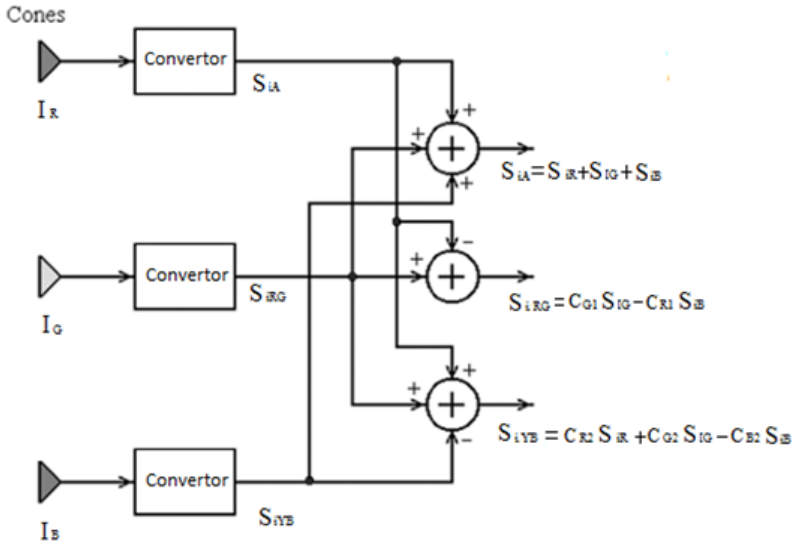

Figure 1. Model explaining the conversion of the signal from the cone to the signal at the output of the bipolar cell.

In this model, the values and signs of the signals S_{iA}, S_{iRG}, S_{iYB}, at the outputs of the corresponding bipolar cells are determined by the effective illuminances I_R, I_G, and I_B of the corresponding cones. Note that when the spectral composition of lighting changes in these expressions, only $\varphi(\lambda)$ changes. The expression for S_{iRG} through transformations is reduced to

$$S_{iRG} = D_{GC}\phi(\lambda)\varepsilon_G(\lambda) - D_{RC}\phi(\lambda)\varepsilon_R(\lambda),$$

where D_{GC} and D_{RC} —are the coefficients that are equal to

$$D_{GC} = \frac{A_G\varepsilon_G(\lambda)}{\bar{I}_G},\ D_{RC} = \frac{A_R\varepsilon_R(\lambda)}{\bar{I}_R},$$

the values of which are found from the condition of the minimum mean

square of the discrepancy between theoretical calculations [Krasilnikov et al., 1999] and experimental data [Handbook of physiology, 1971], for example, when determining the dependence of the magnitude of the change in the background impulse of the response of a two-phase neuron of a geniculate nucleus of a macaque to equal-energy stimuli, on the wavelength. These dependencies are shown in Figure 2: 1 — without a colored background, 2 — with a red background, 3 — with a green background.

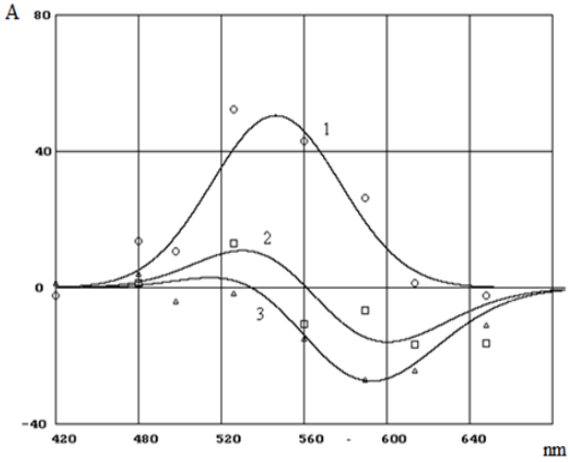

Figure 2. Dependences the magnitude the background activity of a macaque two-phase geniculate nucleus neuron to equal-energy stimuli and different wavelength.

From the performed calculations, we can understand that if an intense red background is added to the white adaptive background, this leads to a shift of the entire curve up, while the addition of an intense green background to the white adaptive background entails a downward shift of the curve.

The values of the corresponding coefficients in the formula for S_{iYB} are determined in a similar way, but due to the length of calculations, we do not present the described transformations here, but refer the reader to [Krasilnikov et al., 1999, pp. 39–43].

In the case of an achromatic stimulus, the resulting signal is obtained by summing the following components S_{iR}, S_{iG} and S_{iB}

$$S_{iA} = S_{iR} + S_{iG} + S_{iB}.$$

Let us now consider the case when the lighting is achromatic. In this case, according to modern concepts

$$S_{iA} = S_{iR} + S_{iG} + S_{iB}\,.$$

Figure 3 demonstrates a model of the conversion of a signal from cones to a signal at the output of a bipolar cell by a triad: a cone, a system of horizontal cells, a bipolar cell.

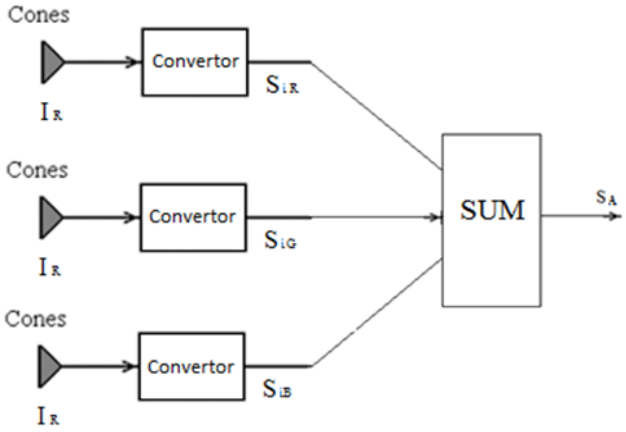

Figure 3. Model of achromatic signal transformation from cones to a signal at the output of a bipolar cell.

Because

$$\left(\varepsilon_R(\lambda)+\varepsilon_G(\lambda)+\varepsilon_B(\lambda)\right)\int_{\lambda_1}^{\lambda_2}\varphi(\lambda)d\lambda =$$

$$= \int_{\lambda_1}^{\lambda_2}\varphi(\lambda)\varepsilon_R(\lambda)d\lambda + \int_{\lambda_1}^{\lambda_2}\varphi(\lambda)\varepsilon_G(\lambda)d\lambda + \int_{\lambda_1}^{\lambda_2}\varphi(\lambda)\varepsilon_B(\lambda)d\lambda$$

S_{iA} can be written down as

$$S_{iA} = D_A\int_{\lambda_1}^{\lambda_2}\varphi(\lambda)d\lambda\,, \qquad (8)$$

where D_A is a coefficient, which value is determined by the spectral sensitiv-

ity of the photoreceptor and the spectral composition of the radiation.

$$D_A = \frac{C_A}{\bar{I}_A}\left(\varepsilon_R(\lambda)+\varepsilon_G(\lambda)+\varepsilon_B(\lambda)\right)\int_{\lambda_1}^{\lambda_2}\varphi(\lambda)d\lambda.$$

Value D_A can be found from the condition of minimum mean square discrepancy between theoretical calculations and experimental data [Van Esch et al., 1984] for dependence of the threshold increment of wavelength $\Delta\lambda$ on wavelength λ. This dependence [Krasilnikov et al., 1999] is shown in Figure 4.

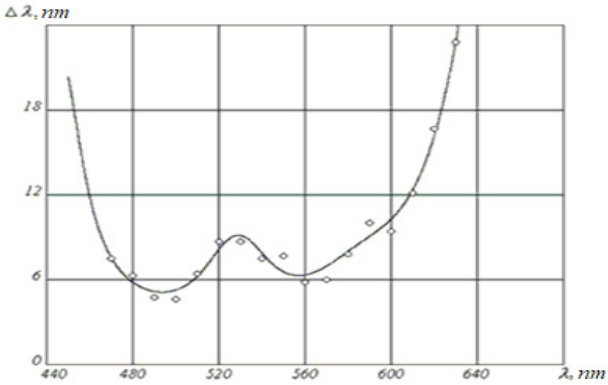

Figure 4. The dependence of the threshold increment on wavelength.

The model shown in Figure 1 also explains a number of illusions related to the perception of color, for example, the simultaneous color contrast manifested in the phenomenon of colored shadow. It can be observed if you direct a bright beam of red rays onto a white screen evenly illuminated by white light and install a small opaque object in the path of the beam, where in the viewer will think that the shadow cast on the screen by an opaque object is colored green. The lack of red in the shadow area is equivalent to the excess of green for the visual system. Similarly, the simultaneous color contrast is explained.

In further theoretical studies with subsequent experimental verification published by the author in [Krasilnikov et al., 1999], we used the models shown in Figure 1 and Figure 3.

Formulas (5–8) present two important features of the conversion of the distributions of effective illumination on the retinal cones to the signal distribution

at the outputs of the corresponding bipolar cells carried out by the triad of the cone — a system of horizontal cells — a bipolar cell:

- an n times increase in the illumination of the image does not lead to a change in the signals at the outputs of the bipolar cells, since the numerators and denominators in (5–7) increase by the same number of times, what actually allows adaptation to occur;
- signals at the outputs of bipolar cells are linear functions of the effective illumination of the corresponding cones, i.e. transformations are linear.

Due to the linearity of transformations (5–8), the basic laws of colorimetry are implemented, in particular, the perception of color tone and saturation in a wide range of values are independent of brightness, and the stimulus brightness is a weighted sum of color components. And finally, we note that since, as a result of the transformations, described (5–8), both positive and negative values of signals appear at the outputs of bipolar cells, this creates the basis for two systems: *on* and *off*, operating in opposite directions from the zero level.

Adaptation to lighting

Let us consider the case when for detection the observer is presented with a test object in the form of a disk, the average brightness of which is equal to $L_D + \Delta L$.

We accept the following assumptions:

- there is no noise in the visual system;
- there are three types of cones in the retina, which differ in spectral sensitivity (R, G, B);
- adaptation to illumination occurs independently of each color in the retina;
- adaptation time is not limited,

Since the luminous flux incident on the lens contains noise, it will cause detection errors for the test object. As you know, the noise of the luminous flux includes two components: a component whose average square depends on the intensity of the luminous flux, and a component whose average square does not depend on the intensity of the luminous flux.

Due to some simple transformations, which are given in the publication [Krasilnikov, 1997], for $\Delta L / L_D$ we get the formula:

$$\frac{\Delta L}{L_D} = \delta(\alpha, \tau) \sqrt{1 + \frac{G_0}{L_D}}, \qquad (9)$$

where the values: $\delta(\alpha,\tau)$ depends on the angular dimensions of the stimulus τ and the duration of its presentation τ) and G_0 are determined by two points of experimentally obtained dependence that are not on the same level. In particular cases, it follows that with an increase in L_D, when the second term under the square root (9) can be neglected in comparison with unity, it can be represented as

$$\frac{\Delta L}{L_D} = \delta(\alpha,\tau). \tag{10}$$

In this case, the ratio $\Delta L / L_D$ represents the Weber-Fechner law. For large values of G_0 / L_D, when the unit under the square root can be neglected, formula (9) takes the form of

$$\Delta L / L_D = \delta(\alpha,\tau)\sqrt{G_0 / L_D}\,. \tag{11}$$

In other words, for small values of L_D, the ratio $\Delta L / L_D$ represents a fluctuation law.

Figure 5 shows the experimental points [Handbook of physiology, 1971] and presents the dependence that was obtained and then published by the author in [Krasilnikov, 1997].

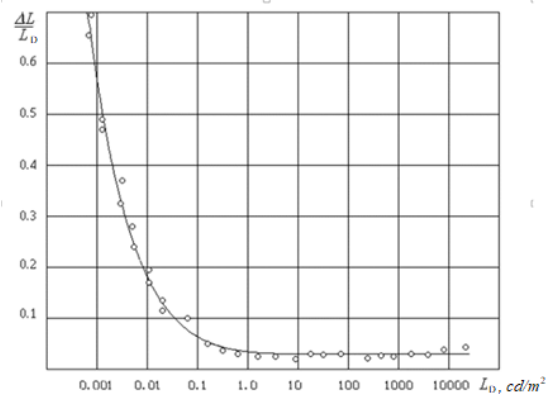

Figure 5. The dependence of the brightness increment $\Delta L / L_D$ on the background brightness L_D. For small values of L_D it represents the fluctuation law, which with increasing L_D, becomes a Weber-Fechner law.

The dependence of threshold intensity on time

Let us now turn to a completely different case, when the observer is presented with a test object in the form of a disk with an average brightness $L_D + \Delta L$, but for a limited observation time. As in the previous case, a number of assumptions are made, the difference in them consists only in the fact that the adaptation time is fixed and after it passes the test image is erased. Figure 6 shows the experimental points [Rushton, 1962] and the dependence, which was obtained and then published by the author in [Krasilnikov, 1997]. For small values of time, it can represent the Bloch-Charpentier law, and then, as time increases, it becomes the Blondel-Ray law.

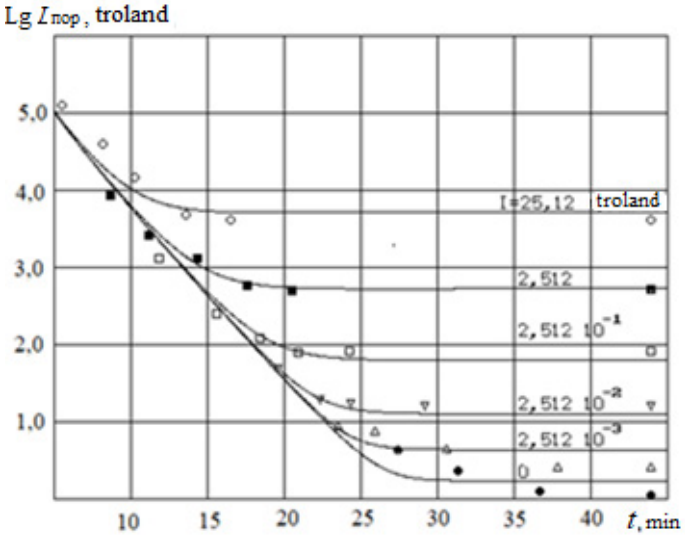

Figure 6. The dependences of $Lg\ L_{пор}$ on time t for the rod retina at various values of the background illumination *L: 1*—25.12 troland, *2*—2.512, *3*—0,251, *4*—0,025, *5*—0,0025, *6*—0.

Threshold contrast with full adaptation

Let us now consider the classical task of determining the threshold contrast under conditions of complete adaptation, assuming that the stimulus image is presented in the form of a disk divided into two halves, the brightness of which is $L_s + \Delta L_s / 2$ and $L_s - \Delta L_s / 2$, while the average brightness of the

disk is equal to L_s. The disk is placed on the field surrounding it, the brightness of which is L_a. Since the illumination on the retina is directly proportional to the brightness of the corresponding portion of the test image, the average illumination of the retina will be equal to

$$\bar{L} = a_0 \left(c_d L_a + L_s \right),$$

where a_0 is a constant coefficient, c_d is the coefficient by which the additive is taken into account, which is contributed by the brightness of the field surrounding the stimulus into the average value. We assume the angle α, at which the diameter of the disk is visible, and the duration τ unchanged during the experiment.

As is known, noise in the visual system that causes stimulus detection errors includes two components: the first is due to quantum fluctuations of the luminous flux from the stimulus, as well as fluctuations that occur in the photoreceptor when the signal is amplified, and the second exists due to fluctuation processes in subsequent neurons of the visual system. The average square of the first noise component is directly proportional to the average brightness of the stimulus L_s. The average square of the second component does not depend on the brightness of the stimulus.

As a result of simple transformations, which, we do not give here due to their length, and which are described in detail in [Krasilnikov, 1997], we obtain the expression

$$\frac{\Delta L_s}{L_s} = \delta(\alpha,\tau)\left(1+\frac{c_d L_a}{L_s}\right)\sqrt{1+\frac{G_0}{\left(1+c_d L_a / L_s\right)^2 L_s}}, \qquad (12)$$

where the values: $\delta(\alpha,\tau)$ depends on the angular dimensions of the stimulus α and the duration of its presentation τ) and G_0 are determined by two points of experimentally obtained dependencies that are not on the same level. In particular cases, it follows that with an increase in L_s, when the second term under the square root (12) can be neglected in comparison with unity, it can be represented as

$$\frac{\Delta L_s}{L_s} = \delta(\alpha, \tau). \tag{13}$$

In this case, the ratio $\Delta L_s / L_s$ represents the Weber—Fechner law. For large values of G_0 / L_s, when the unit under the square root can be neglected, equation (12) takes the form

$$\Delta L_s / L_s = \delta(\alpha, \tau)\sqrt{G_0 / L_s}. \tag{14}$$

In other words, for small values of L_s, the ratio $\Delta L_s / L_s$ represents a fluctuation law.

Figure 7 shows the experimental points and the dependence that was obtained and then published by the author in [Krasilnikov, 1997].

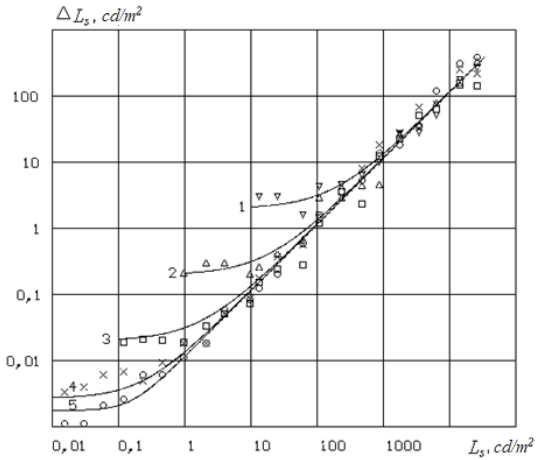

Figure 7. The dependence of the difference threshold ΔL_s on the average brightness of the stimulus L_s for various brightnesses L_a of the field surrounding the stimulus: 3426 cd/m² (1), 343 cd/m² (2), 34 cd/m² (3), 3,4 cd/m² (4), 0 cd/m² (5). In the calculations it was assumed $a = 1{,}5^\circ$, $d_1(a, t) = 0{,}0115$, $G = 0{,}46$ cd/m², $c_d = 0{,}057$.

Brightness inducing

We now consider the phenomenon of brightness inducing, which consists in

the fact that if an inducing stimulus area is placed near the test stimulus area, when the brightness of the inducing field changes, the visible brightness of the test field changes. By setting as equal the brightness of the test field and the brightness of the comparison field, which is placed at a certain distance from the test field, it is possible to estimate the apparent brightness of the test field by changes in the visible brightness of the comparison field.

It should be considered that since in the experiments in the study of brightness inducing the observer fixed eyes on the areas including both the test and the inducing fields, averaging should be performed over both areas. In view of the aforementioned, the illumination value will be proportional to the time intervals during which the photoreceptors are illuminated by the test and inducing fields due to incessant movements of the axis of view.

Arguing similarly, we find the formula for the signal $L_{\text{т}}$ at the output of the bipolar cell associated with the photoreceptor illuminated by the comparison field. Performing simple transformations, which due to the bulkiness we do not give here, they are presented in [Krasilnikov, 1997, pp.43–44], we find:

$$L_{\text{т}} < c_1 L_{\text{с}} + c_2 L_{\text{и}} \ .$$

Figure 8 shows the experimental points [Handbook of physiology, 1971], as well as the dependences [Krasilnikov, 1997] obtained theoretically. When calculating accepted $c_1 = 1.05$, $c_2 = 0.394$.

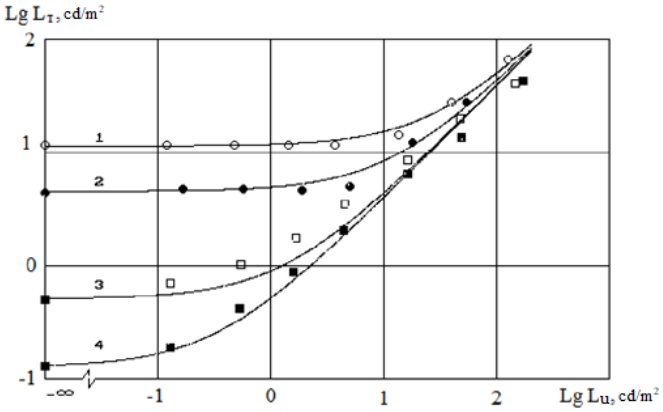

Figure 8. The dependencies of $Lg\ L_{\text{т}}$ on $Lg\ L_{\text{и}}$, when $L_{\text{с}} = 11{,}2$ cd/m² (1), 4,47 cd/m² (2), 0,5 cd/m² (3), 0,13 cd/m² (4).

In conclusion, it should be noted that to "adjust" the models used in our studies of the human visual system, it is sufficient to specify two points of experimentally obtained dependence, which do not lie on the same level, in order to ensure the correct prediction of the model (extrapolation and interpolation) of the entire dependence. As long as the model provides the correct "prediction" there is no need to make any changes to it. Otherwise, it is necessary to replace it with more perfect model, or to add "superstructure" like that which was made in due time, Bohr.

References

1. Handbook of physiology. Physiology of sensory systems. Part One. The physiology of vision. Ed. V.G. Samsonova. L.: Nauka 1971. 416 p.
2. Krasilnikov N.N. The mathematical model of the dark adaptation of the human visual system //. Journal of Optical Technology 1997. T. 64. № 11, pp. 38–44.
3. Krasilnikov N.N., Shelepin Yu.E., Krasilnikova O.I. Filtering in the human visual system under threshold-observation conditions.// Journal of Optical Technology, 1999. Vol. 66, Issue 1, pp.3–11
4. Krasilnikov N.N., Krasilnikova O.I., Shelepin Yu.E. Mathematical model of the color constancy of the human visual system Journal of Optical Technology, 2002. Vol. 69, Issue 5, pp.327–332.
5. Rushton W.A.H. Visual adaptation // The Ferrier Lecture. Physiological Laboratory, Cambrige University. 1962. P. 20–46.
6. Van Esch J.A., Koldenhof E.E., Van Doorn A.J., Koenderink J.J. Spectral sensitivity and wavelength discrimination of the human peripheral visual field // JOSA. 1984. Vol.1, № 5. P. 443–450.

Chapter 20.
Neural Networks Mechanisms for the Quantum-like Phenomenon "Linda"

A.V. Pavlov

Abstract. Two classical neural networks mechanisms for cognitive phenomenon "Linda" implementation upon the algebra of Fourier-dual operations is shown. The first mechanism implements the model of successive projections of the state vector onto the subspaces. It is implemented due to the nonlinear recording of the interconnection weighs, that allows the neural ensembles that were not associated by the learning to be linked by the neural network itself. The second one doesn't need noncommutativity of the logical operators and operates under linear characteristics of the media for interconnections weights recording. Thus, the two: subjectivity of perception and fatigue of synaptic transmission play the key role in the mechanism.

Keywords: Quantum-like phenomena, cognitive phenomena, quantum logic, neural networks, associative memory, nonlinearity, Fourier-duality, conjunction, activation function of neuron, free choice.

Introduction

Last years, both in physics and cognitive science, there is an increasing interest in the long-standing hypothesis about the quantum nature of the brain, mind and consciousness [Menskii, 2000; Busemeyer et al., 2011, Trueblood et al., 2014; Meijer & Raggett, 2014; Khrennikov, 2015; Moreira & Wichert, 2016; Asano et al., 2015; Bhattacharyya et al., 2017; Zheltikov, 2018]. The discussion was activated by the successful application of quantum logic to the description of human manner for judgment under uncertainty. In 2011 [Busemeyer et. al., 2011] have demonstrated an application of quantum logic apparatus to explain the experimentally obtained by Tversky and Kahneman violations of the laws of classical (Kolmogorov's) probability at the conjunction of independent events ("Linda" phenomenon) [Tversky & Kahneman, 1983].

The experiment [Tversky & Kahneman, 1983] was that the respondents were told about a fictional person named Linda: "Linda is 31 years old, single, outspoken and very bright. She majored in philosophy. As a student, she was deeply concerned with issues of discrimination and social justice, and also participated in anti-nuclear demonstrations". Then they were asked "who is

Linda?", and a list of fixed answers was proposed to choose the most adequate one. Only three answers were under consideration in the framework of the problem, as follows:

1. Linda is active in the feminist movement (*F*),
2. Linda is a bank teller (*T*),
3. Linda is a bank teller and is active in the feminist movement (*F*&*T*).

The answers were statistically processed and the order of their probabilities was obtained $P(F) > P(F\,\&\,T) > P(T)$. However, according to the Kolmogorov's theory of probability, conjunction of independent events cannot exceed the probability of individual events [Kolmogorov, 1974].

At the same time, the order $P(F\,\&\,T) > P(T)$, considered for independent events in the framework of the classical approach as a gross logical error, is valid in quantum logic, in which the procedure of logical conclusion is mathematically described by successively projecting the system current state vector onto the subspaces in which reference patterns "Feminist" and "Teller" are stored (Figure 1). This gave reason to apply quantum logic to the description of a hypothetical formal mechanism of the phenomenon [Busemeyer et al., 2011; Trueblood et al., 2014].

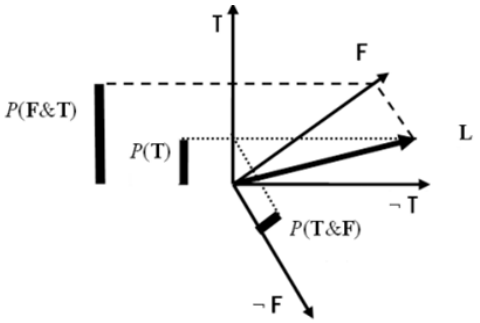

Figure 1. Implementation of the conjunction in quantum logic: state of the system by perceiving the story is described by vector L, the state vector L is firstly projected onto the subspace F, then from F onto T, as a result the conjunction probability is higher than probability of answer "Teller" [Busemeyer et al., 2011; Trueblood et al., 2014].

However, the proposed quantum logic application to the phenomenon doesn't address the physical, chemical or biological essence of the described mech-

anism. It is noncommutativity of the logical inference operators that plays a key role in that quantum-logical formalism [Busemeyer et al., 2011], but noncommutativity is not yet quantumness as such. Moreover, no real either quantum or classical mechanism to implement the concept of sequential projection of the vectors, that operates in biological neural networks, was neither shown, no proposed. Khrennikov [Khrennikov, 2007] has proposed a model of noncommutative probability where noncommutativity arose by introduction of "interference term" into the formula of total probability. But real either physical or biological mechanism for interference term appearance in the formula wasn't proposed.

As judgement is implemented by biological neural network (NN), then the model is to be adequate to real mechanisms implemented by the NN. Regarding the "Linda" phenomenon, it would be useful to answer two questions:

1. what is real NN's mechanism for noncommutativity arising?
2. do we need in noncommutativity to implement "Linda" phenomenon by NN?

In this article the neural networks' mechanisms for the "Linda" phenomenon is analyzed to answer the above stated questions. Firstly, it is demonstrated the noncommutativity may be arose by nonlinearity of the media for neural interconnections weights recording (nonlinearity of synaptic plasticity). It means not quantum, but fully classical mechanism can cause to the violations of classical probability laws. Then an implementation of the "Linda" phenomenon by a neural network under linear weights of the interconnections is demonstrated. The two real attributes of biological neural networks play the key role here: subjectivity of perception and fatigue of synaptic transmission.

2. An approach

Let us consider implementation of the judgment by NN in order to determine the framework of our approach by taking into account a number of biologically motivated statements.

2.1. Inner representation of information in NN, either biological or artificial, is realized by space-time patterns of neural activity, i.e. neural ensembles (NE), activated by perceived, recalled or generated information [Borisyuk et al., 2002]. Within the framework of this approach, the result of the reasoning is also NE, which is formed by the NN.

2.2. The simplest model of a neuron as a nonlinear summator is sufficient for our consideration.

2.3. According to Born rule probability of an event B_{xy} is calculated as a scalar product

$$P_{\psi}\left(B_{x,y}\right)=\psi\left(x,y\right)\psi^{*}\left(x,y\right),$$

where ψ is a wave function (amplitude of a probability) [Feynman, Leighton & Sands, 1963]. Thus, the probability in [Busemeyer et al., 2011; Trueblood et.al., 2014] under assumption the hypothesis of ergodicity is mathematically equivalent to the power (intensity) that is the measure of a logical conclusion. Thus, having accepted the ergodicity hypothesis, the symbol *P* we will use to denote the quadratic measure in general: both the probability and the power of the NE.

2.4. According to the experimental results [Glezer et al., 1972, 1973, 1975; Glezer, 1993, 1999, 2000], double Fourier-transform is implemented by the brain's neural structures. So, we are to take it into account by using the algebra of Fourier-dual operations and model of NN that stores interconnections weights in the Fourier domain.

Let us use the simplest model of NN to store reference pattern — auto-associative memory formed by two conjugated Grossberg stars: Instar-Outstar. To store two reference patterns "Feminist" and "Teller" to AAM are needed as it is shown in Figure 2.

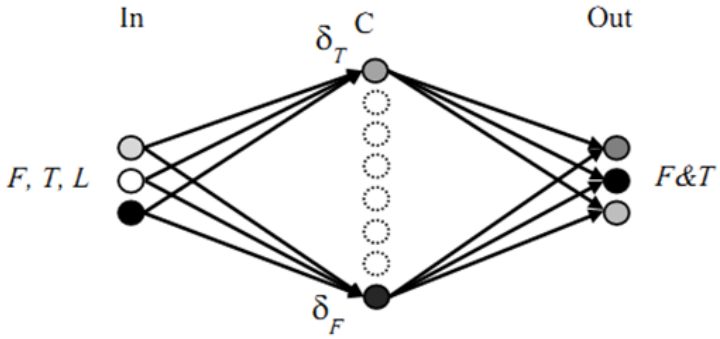

Figure 2. The principal structure of the auto-associative memory based in the NN HC «Grossberg star»: In, C and Out are the input, correlation and output layers, respectively; lines show connections formed by learning as the successive presentation of the NE pairs: *F* and δ_F, *T* and δ_T; $In \to C$ are Instars, $C \to Out$ are Outstars; dotted circles — the neurons in the Grossberg layer that are not assigned by the learning to any reference pattern, but are necessary for the sequential projection mechanism.

To implement the formal mechanism used in quantum logic for sequential projection of the current state vector onto the subspaces that store the references (Figure 1), it is necessary to ensure the connection of these subspaces. Since, according to the experimental conditions, these subspaces are considered as formed independently, then in the NN model of Figure 2, they are not related to each other as a result of learning. Thus, it is necessary to find a mechanism for self-formation by the NN connection between the NE *F* and *T*.

The problem of interpreting experimental results [Tversky & Kahneman, 1983] is largely related to the fact that, following the Kolmogorov approach, probability is an additive measure on the algebra of events [Kolmogorov, 1974]. Quantum probability that adequately describes "Linda", by contrast, is not additive [Kholevo, 1991; Khrennikov, 2003]. But according to Kolmogorov, the additivity of the measure is only an axiom: it is postulated, but not justified. From the standpoint of constructive substantiation of the property additivity — non-additivity of a measure, the work [Trillas, Alsina & Valverde, 1982] is relevant. In [Trillas, Alsina & Valverde, 1982] it is shown that the negation operation, as a special case of an operation defining the duality of the operations defining the model, uniquely determines the measure on algebra due to the fact that under certain reasonable assumptions the same additive generator as the operation $\bullet$ included in the axiomatic definition of measure g:

$$\forall a,b \in \mathcal{F}(X): g(a \oplus b) \bullet g(a \odot b) = g(a) \bullet g(b),$$

where $\mathcal{F}(X)$ is the set of elements of the model, $\oplus$ and $\odot$ are abstract addition and multiplication.

In particular, if the operation defining the duality $\oplus$ and $\odot$ is linear, then the operation $\bullet$ is the operation of arithmetic addition +, i.e. and the measure g is additive. If, on the other hand, the defining duality operation is nonlinear, then the measure g is nonadditive. This result can be generalized to other, except for negation, operations that define duality, including the Fourier transform [Pavlov, 2001]. Thus, the problem of finding the mechanism of results [Tversky & Kahneman, 1983] in terms of the noncommutativity property is mathematically reduced to finding the measure that is adequate to the NA model, which, in turn, reduces to defining the duality-specifying operation as the root cause of additivity — non-additivity of the measure.

2. The model

2.1. Auto-associative memory

Let us consider the NN model, presented in Figure 2. Registration of the interconnections weights «Instar» ($In \to C$) in the Fourier domain is carried out in two steps.

In the first step, the weights of the interconnections are formed according to the Hebb's learning rule as a pattern of the interference of wave fronts from the reference neural ensemble "Feminist" and "Teller", and delta neurons, $\delta_F(x_F)$ and $d_T(x_T)$, correspondingly, the power measure of the pattern to be recorded by the recording medium in the second step is described as follows

$$W(\nu) = \left[R_F \exp\left(j2\pi\nu x_F\right) + \mathfrak{F}\left(F(x)\right)\right] \cdot \left[R_F \exp\left(j2\pi\nu x_F\right) + \mathfrak{F}\left(F(x)\right)\right]^* + \\ + \left[R_T \exp\left(j2\pi\nu x_T\right) + \mathfrak{F}\left(T(x)\right)\right] \cdot \left[R_T \exp\left(j2\pi\nu x_T\right) + \mathfrak{F}\left(T(x)\right)\right]^*. \tag{1}$$

where $F(x)$ and $T(x)$ are row vectors describing NE "Feminist" and "Teller", correspondingly (we use functions of only one coordinate to avoid unnecessary cluttering of formulae), ν denotes spatial frequency, j — is the imaginary unit, R_F and R_T — are the amplitudes of excitations received from the neurons $\delta_F(x_F)$ and $\delta_T(x_T)$, x_F and x_T are the coordinates of the lasts, $\mathfrak{F}$ and * denote Fourier-transform and complex conjugating, correspondingly. Decomposition of each of the members in the brackets in (1) gives four terms, of which only one describes the link of the NE in the input layer In with the corresponding δ-neuron, and let us leave only these terms for the further analysis:

$$W(\nu) = W_F(\nu) + W_T(\nu) = \mathfrak{F}^*\left(F(x)\right) R_F \exp\left(j2\pi\nu x_F\right) + \\ + \mathfrak{F}^*\left(T(x)\right) R_T \exp\left(j2\pi\nu x_T\right). \tag{2}$$

The second step is registration of the interconnections (2) as a matrix of the weights. Recorded weights matrix depends on parameters of both learning procedure and recording medium (synaptic sensitivity). For simplicity but without loss of generality let us assume linear model of registration in the spectral range of matched filtration, that is denotes by letter L in superscripts:

$$W^L(\nu) = W_F^L(\nu) + W_T^L(\nu) = \Lambda_F\left(\mathfrak{F}^*\left(F(x)\right), R_F\right)\exp\left(j2\pi\nu x_F\right) + \\ + \Lambda_T\left(\mathfrak{F}^*\left(T(x)\right), R_T\right)\exp\left(j2\pi\nu x_T\right). \quad (3)$$

where Λ is the operator that takes into account the dependence of the interconnections weights on the ratio of the linked NEs R_F and $\delta_F(x_F)$, as just as R_T and $\delta_T(x_T)$ Fourier-spectra amplitudes:

$$\Lambda_A\left(\mathfrak{F}^*\left(A(x)\right), R_A\right) = \begin{cases} \dfrac{\mathfrak{F}^*\left(A(x)\right)}{R_A} \ \textit{if} \ \dfrac{\left|\mathfrak{F}^*\left(A(x)\right)\right|}{R_A} \le 1 \\ \Lambda_A^{inv}\left(\mathfrak{F}^*\left(A(x)\right), R_A\right) \ \textit{if} \ \dfrac{\left|\mathfrak{F}^*\left(A(x)\right)\right|}{R_A} > 1 \end{cases}, \quad (4)$$

where $\Lambda_A^{inv}\left(\mathfrak{F}^*\left(A(x)\right), R_A\right)$ describes the inverse filtration. The simplest model of the operator Λ for inverse filtration range is $\Lambda_A^{inv}\left(\mathfrak{F}^*\left(A(x)\right), R_A\right) = \dfrac{2R_A\left|\mathfrak{F}^*\left(A(x)\right)\right|}{R_A^2 + \left|\mathfrak{F}^*\left(A(x)\right)\right|^2}$, but often either sigmoidal or Gauss function $\Lambda_A^{inv}\left(\mathfrak{F}^*\left(A(x)\right), R_A\right) = \exp\left(\dfrac{-(\nu-\nu_0)^2}{2a^2R_A^2}\right)$ may corresponds to the properties of the both pattern and recording media, ν_0 — is the frequency at which the condition $\left|\mathfrak{F}^*\left(A(x)\right)\right| = |R_A|$ is met.

So, taking into account above mentioned remarks, we will denote the reference patterns stored in interconnections by letter R in superscripts and letter L will mark the interconnections are recorded linearly: $F^{\mathrm{RL}}(x) = \Lambda_F\left(\mathfrak{F}^*\left(F(x)\right), R_F\right)$, and the same for the $T^{\mathrm{RL}}(x)$, as just as for all other terms and expressions.

As NE "Linda" is presented into the input layer In, it passes through the links (1) and forms the excitations at the inputs of δ-neurons in layer C (the inputs are marked by In in the superscripts), their amplitudes are determined by the characteristics of the both NEs: stored $F_R(x)$ and $T_R(x)$, and input $L(x)$, as follows:

$$\begin{aligned}\delta_F^{\mathrm{InL}} &= \left\langle L(x), F^{\mathrm{RL}}(x)\right\rangle = \rho_{LF}\cdot\mu_F^{2\mathrm{RL}}\cdot N_F^{\mathrm{RL}} = \rho_{LF}\cdot P_F^{\mathrm{RL}}\\ \delta_T^{\mathrm{InL}} &= \left\langle L(x), T^{\mathrm{RL}}(x)\right\rangle = \rho_{LT}\cdot\mu_T^{2\mathrm{RL}}\cdot N_T^{\mathrm{RL}} = \rho_{LT}\cdot P_T^{\mathrm{RL}},\end{aligned} \tag{5}$$

where $\langle\ \rangle$ denotes scalar product, ρ is the correlation coefficient, μ^2 is the raw moment of the second order.

Excitations from δ-neurons, passing through the "Outstar" interconnections, conjugated to the corresponding "Instar" ones (3), form the amplitude distribution at the inputs of the Out-neurons:

$$\begin{aligned}&Out^{\mathrm{In}}(x) =\\ &= \mathcal{F}\left\{\begin{array}{l}\left[S^{\mathrm{C}}\left(\rho_{LF}\cdot P_F^{\mathrm{RL}}\right)\cdot\exp\left(j2\pi\nu x_F\right)\right]\cdot\left[\mathcal{F}\left(F^{\mathrm{RL}}(x)\right)\cdot\exp\left(-j2\pi\nu x_F\right)\right]+\\ +\left[S^{\mathrm{C}}\left(\rho_{LT}\cdot P_T^{\mathrm{RL}}\right)\cdot\exp\left(j2\pi\nu x_T\right)\right]\cdot\left[\mathcal{F}\left(T^{\mathrm{RL}}(x)\right)\cdot\exp\left(-j2\pi\nu x_T\right)\right]\end{array}\right\} =\\ &= \mathcal{F}\left\{S^{\mathrm{C}}\left(\rho_{LF}\cdot P_F^{\mathrm{RL}}\right)\cdot\mathcal{F}\left(F^{\mathrm{RL}}(x)\right)+S^{\mathrm{C}}\left(\rho_{LT}\cdot P_T^{\mathrm{RL}}\right)\cdot\mathcal{F}^{\mathrm{RL}}\left(T(x)\right)\right\} =\\ &= \left\{S^{\mathrm{C}}\left(\rho_{LF}\cdot P_F^{\mathrm{RL}}\right)\cdot F^{\mathrm{RL}}(x)\right\}\&\left\{S^{\mathrm{C}}\left(\rho_{LT}\cdot P_T^{\mathrm{RL}}\right)\cdot T^{\mathrm{RL}}(x)\right\} = F^{\mathrm{OutL}}(x)\&T^{\mathrm{OutL}}(x),\end{aligned} \tag{6}$$

where $S^{!}$ denotes activation function of the δ-neurons in layer C, and by transition to the line 2 we left only the terms that describe the NEs localized in the region of our interest in the output layer. The conjunction symbol & in the final expression appear due to the fact that expression (6) represents a case of the de-Morgan law for the operations + and & under their duality is given by the Fourier transform.

The power ratio jointly activated in the output layer of $T^{OutL}(x)$ and $F^{OutL}(x)$ without taking into account the activation function of neurons of the output layer $S^{Out}(P)$ is represented by the expression:

$$\begin{aligned}\Omega_{TF}^{\mathrm{L}} &= \frac{P\left(T^{\mathrm{OutL}}(x)\right)}{P\left(F^{\mathrm{OutL}}(x)\right)} = \frac{\left\langle\left\{S^{\mathrm{C}}\left(\rho_{LT}\cdot P_T^{\mathrm{RL}}\right)\cdot T^{\mathrm{RL}}(x)\right\},\left\{S^{\mathrm{C}}\left(\rho_{LT}\cdot P_T^{\mathrm{RL}}\right)\cdot T^{\mathrm{RL}}(x)\right\}\right\rangle}{\left\langle\left\{S^{\mathrm{C}}\left(\rho_{LF}\cdot P_F^{\mathrm{R}}\right)\cdot F^{\mathrm{R}}(x)\right\},\left\{S^{\mathrm{C}}\left(\rho_{LF}\cdot P_F^{\mathrm{R}}\right)\cdot F^{\mathrm{R}}(x)\right\}\right\rangle} =\\ &= \frac{\left[S^{\mathrm{C}}\left(\rho_{LT}\cdot P_T^{\mathrm{RL}}\right)\right]^2\cdot\left\langle T^{\mathrm{RL}}(x), T^{\mathrm{RL}}(x)\right\rangle}{\left[S^{\mathrm{C}}\left(\rho_{LF}\cdot P_F^{\mathrm{RL}}\right)\right]^2\cdot\left\langle F^{\mathrm{RL}}(x), F^{\mathrm{RL}}(x)\right\rangle} = \frac{\mu_T^{2\mathrm{RL}}\cdot N_T^{\mathrm{RL}}}{\mu_F^{2\mathrm{RL}}\cdot N_F^{\mathrm{RL}}}\cdot\frac{\left[S^{\mathrm{C}}\left(\rho_{LT}\cdot P_T^{\mathrm{RL}}\right)\right]^2}{\left[S^{\mathrm{C}}\left(\rho_{LF}\cdot P_F^{\mathrm{RL}}\right)\right]^2}\cdot\end{aligned}$$

. (7)

If the value (7) is less the relative dynamical range of the $S^{Out}(P)$, then the output neurons are activated by both NEs: $T^{OutL}(x)$ and $F^{OutL}(x)$ — the resulting NE represents their conjunction. Otherwise, only one of the two NEs is excited: either $T^{OutL}(x)$ or $F^{OutL}(x)$, depending on what measure falls into the dynamical range of the $S^{Out}(P)$. So, from (3), (4), and (5) it follows the resulting NE, activated in the Output layer, depends on a number of parameters defined by: the NEs properties: reference ones as just as inputting, their correlation coefficients, neurons activated functions, recording media exposition characteristics, and the weights recording (the network learning) conditions.

2.2. Noncommutativity as a result of the interconnections weighs nonlinear recording

Let us assume that the nonlinear characteristic of synaptic sensitivity can be approximated by a power series and restrict our consideration to the first two terms of the decomposition: linear and quadratic. Then a valid representation of the stored connections (1) in the following form:

$$W(\nu) = \eta_1 \cdot W^{L}(\nu) + \eta_2 \cdot \left[\begin{array}{l} \left(R_F \cdot \exp(j\omega x_F) + \mathfrak{F}(F(x))\right) \cdot \left(R_F \cdot \exp(j\omega x_F) + \mathfrak{F}(F(x))\right)^* + \\ + \left(R_T \cdot \exp(j\omega x_T) + \mathfrak{F}(T(x))\right) \cdot \left(R_T \cdot \exp(j\omega x_T) + \mathfrak{F}(T(x))\right)^* \end{array} \right]^2, \quad (8)$$

where η_1 и η_2 are the coefficients. We are interested in a quadratic term. Its decomposition (we omit bulky calculations) gives, among other things, also two terms describing the necessary links of not associated by the learning procedure references NE $F_R(x)$ and $T_R(x)$:

$$W_{FT}^{\mathrm{Nl}}(\nu) = \eta_2 \cdot \left[\begin{array}{l} \Lambda_{FT}\left(\mathfrak{F}^*(F(x)) \cdot \mathfrak{F}(T(x)) \cdot R_F \cdot R_T\right) \cdot \exp\left(j\omega\left(x_F - x_T\right)\right) + \\ + \Lambda_{TF}\left(\mathfrak{F}(F(x)) \cdot \mathfrak{F}^*(T(x)) \cdot R_F \cdot R_T\right) \cdot \exp\left(-j\omega\left(x_F - x_T\right)\right) \end{array} \right]. \quad (9)$$

Expression (9) describes a new structure in the composition of the interconnections, which was not specified at all during learning, but appeared by itself

due to the quadratic nonlinearity of the sensitivity of synapses, similar to the appearance of holograms between images recorded at different times shown in [Orlov, 2004, Pavlov & Orlov, 2019]. These interconnections are in our specific interest because of the terms $\exp\left(j\omega\left(x_F - x_T\right)\right)$ and $\exp\left(-j\omega\left(x_F - x_T\right)\right)$ describe the connections between the NEs "Teller" and "Feminist", that are necessary for the concept of sequential vector projections, that is used in the quantum logic [Busemeyer et al., 2011], to be implemented. Further, for brevity, we will call structure (9) quadratic connections.

NE "Linda" passing through the quadratic substructure (9) activates at the input of layer C amplitudes:

$$T^{\mathrm{CIn}(9)}\left(\Delta\right) = \\ = \eta_2 \cdot \mathcal{F}\left[\mathcal{F}\left(L\left(x\right)\right) \cdot \Lambda_{FT}\left(\mathcal{F}^{*}\left(F\left(x\right)\right) \cdot \mathcal{F}\left(T\left(x\right)\right) \cdot R_F \cdot R_T\right) \cdot \exp\left(j\omega\left(x_F - x_T\right)\right)\right] = \\ = \eta_2 \cdot \left[T^{\mathrm{RNl}}\left(x\right) * \left(L\left(x\right) \otimes F^{\mathrm{RNl}}\left(x\right)\right) * \delta\left(x_F - x_T\right)\right], \tag{10.a}$$

and

$$F^{\mathrm{CIn}(9)}\left(\Delta\right) = \\ = \eta_2 \cdot \mathcal{F}\left[\mathcal{F}\left(L\left(x\right)\right) \cdot \Lambda_{TF}\left(\mathcal{F}\left(F\left(x\right)\right) \cdot \mathcal{F}^{*}\left(T\left(x\right)\right) \cdot R_F \cdot R_T\right) \cdot \exp\left(-j\omega\left(x_F - x_T\right)\right)\right] = \\ = \eta_2 \cdot \left[F^{\mathrm{RNl}}\left(x\right) * \left(L\left(x\right) \otimes T^{\mathrm{RNl}}\left(x\right)\right) * \delta\left(x_T - x_F\right)\right], \tag{10.b}$$

where Δ is a coordinate in the C layer, $*$ and $\otimes$ denote convolution and correlation, respectively.

Let us pay attention that, according to expressions (10), quadratic connections (9), unlike linear ones (3), do not activate the only ones δ-neurons in layer C, but the ensembles, that are the images of reference NEs $F(x)$ and $T(x)$. This implies the requirement for the NN architecture—to implement the model, the free neurons are to be in the layer C, i.e. the neurons not involved in learning, shown in Figure 2 by the dotted cycles: there must be at least the total number of neurons in the reference $NEsF\left(x\right)$ and $T(x)$. For clarity of the main idea presentation, we neglect the restored images (8.a) and (8.b) blurring

described by the convolution with the correlation functions (loss of resolution) and present them as follows:

$$T^{\mathrm{CIn}(9)}(\Delta)=\eta_2\cdot\left[T^{\mathrm{RNl}}(x)\cdot\left\langle L(x),F^{\mathrm{RNl}}(x)\right\rangle * \delta(x_F-x_T)\right], \quad (11.a)$$

$$F^{\mathrm{CIn}(9)}(\Delta)=\eta_2\cdot\left[F^{\mathrm{RNl}}(x)\cdot\left\langle L(x),T^{\mathrm{RNl}}(x)\right\rangle * \delta(x_T-x_F)\right]. \quad (11.b)$$

Denote the ratio of scalar products in (11) by $k=\dfrac{\left\langle L(x),F^{\mathrm{RNl}}(x)\right\rangle}{\left\langle L(x),T^{\mathrm{RNl}}(x)\right\rangle}$ and rewrite (11.a):

$$T^{\mathrm{CIn}(9)}(\Delta)=k\cdot\eta_2\cdot\left[T^{\mathrm{RNl}}(x)\cdot\left\langle L(x),T^{\mathrm{RNl}}(x)\right\rangle * \delta(x_F-x_T)\right]. \quad (12)$$

Pattern (12) passing throughout the quadratic "Outstar", that is conjugated to the quadratic "Instar" (9), forms the amplitude distribution at the inputs of neurons of the Out layer:

$$T^{\mathrm{OutIn}(9)}(x)=$$
$$=\mathfrak{F}\left(\eta_2\cdot\mathfrak{F}\left[S^{\mathrm{C}}\left(T^{\mathrm{CIn}(9)}(\Delta)\right)\right]\cdot\begin{bmatrix}\Lambda_{FT}\left(\mathfrak{F}^{*}\left(F(x)\right)\cdot\mathfrak{F}\left(T(x)\right)\cdot R_F\cdot R_T\right)\cdot\exp\left(j\omega(x_F-x_T)\right)+\\ +\Lambda_{TF}\left(\mathfrak{F}\left(F(x)\right)\cdot\mathfrak{F}^{*}\left(T(x)\right)\cdot R_F\cdot R_T\right)\cdot\exp\left(-j\omega(x_F-x_T)\right)\end{bmatrix}\right)\cdot \quad (13)$$

Decomposition of this expression gives three terms, only the terms describing the NE localized in the position, that counterparts with the positions of restored by the linear weights matrix corresponding reference NE images (6) is of interest for us:

$$T^{\mathrm{OutIn}(9)}(x)=$$
$$=\mathfrak{F}\left(\eta_2\cdot\mathfrak{F}\left[S^{\mathrm{C}}\left(T^{\mathrm{CIn}(9)}(\Delta)\right)\right]\cdot\Lambda_{TF}\left(\mathfrak{F}\left(F(x)\right)\cdot\mathfrak{F}^{*}\left(T(x)\right)\cdot R_F\cdot R_T\right)\exp\left(j\omega(x_T-x_F)\right)\right)=$$
$$=\eta_2\cdot S^{\mathrm{C}}\left(T^{\mathrm{CIn}(9)}(\Delta)\right)*\left(F^{\mathrm{RNl}}(x)\otimes T^{\mathrm{RNl}}(x)\right)*\delta(x_T-x_F), \quad (14.a)$$

$$F^{\mathrm{OutIn}(9)}(x)=$$
$$=\mathfrak{F}\left(\eta_2\cdot\mathfrak{F}\left[S^{\mathrm{C}}\left(F^{\mathrm{CIn}(9)}(\Delta)\right)\right]\cdot\Lambda_{FT}\left(\mathfrak{F}^{*}\left(F(x)\right)\cdot\mathfrak{F}\left(T(x)\right)\cdot R_F\cdot R_T\right)\cdot\exp\left(j\omega(x_F-x_T)\right)\right)=$$
$$=\eta_2\cdot S^{\mathrm{C}}\left(F^{\mathrm{CIn}(9)}(\Delta)\right)*\left(T^{\mathrm{RNl}}(x)\otimes F^{\mathrm{RNl}}(x)\right)*\delta(x_F-x_T). \quad (14.b)$$

Let us estimate the ratio of the "Teller" and "Feminist" NEs jointly formed in the Out layer by both linear (3) and quadratic (9) interconnections, as was done in (7), without taking into account the activation function of the output layer neurons. Omitting intermediate bulky calculations, the ratio can be presented as follows:

$$\Omega_{TF}^{\mathrm{L+Nl}}=\frac{P_T^{\mathrm{Out(L+Nl)}}}{P_F^{\mathrm{Out(L+Nl)}}}=\left(\frac{\rho_{LF}\cdot P_T^{\mathrm{RL}}}{\rho_{LF}\cdot P_F^{\mathrm{RL}}}\right)^2\frac{\left\langle T^{\mathrm{RL}}(x),T^{\mathrm{RL}}(x)\right\rangle}{\left\langle F^{\mathrm{RL}}(x),F^{\mathrm{RL}}(x)\right\rangle}\frac{\left(1+\left(k\cdot\omega_{21}\cdot\omega_{PT}\right)^2\cdot\omega_T\right)}{\left(1+\left(\frac{\omega_{21}\cdot\omega_{PF}}{k}\right)^2\cdot\omega_F\right)}, \tag{15}$$

where the activation function S' of the δ -neurons in layer C is assumed linear, and we use the following notation:

$$k=\frac{\left\langle L(x),F^{\mathrm{RNl}}(x)\right\rangle}{\left\langle L(x),T^{\mathrm{RNl}}(x)\right\rangle}\gg 1,$$

$$\omega_{21}=\frac{\eta_2^2}{\eta_1},$$

$$\omega_{PT}=\frac{P_T^{\mathrm{RNl}}}{P_T^{\mathrm{RL}}},$$

$$\omega_T=\frac{\left\langle T^{\mathrm{RNl}}(x)*\left(F^{\mathrm{RNl}}(x)\otimes T^{\mathrm{RNl}}(x)\right),T^{\mathrm{RNl}}(x)*\left(F^{\mathrm{RNl}}(x)\otimes T^{\mathrm{RNl}}(x)\right)\right\rangle}{\left\langle T^{\mathrm{RL}}(x),T^{\mathrm{RL}}(x)\right\rangle},$$

and

$$\omega_F=\frac{\left\langle F^{\mathrm{RNl}}(x)*\left(T^{\mathrm{RNl}}(x)\otimes F^{\mathrm{RNl}}(x)\right),F^{\mathrm{RNl}}(x)*\left(T^{\mathrm{RNl}}(x)\otimes F^{\mathrm{RNl}}(x)\right)\right\rangle}{\left\langle F^{\mathrm{RL}}(x),F^{\mathrm{RL}}(x)\right\rangle}.$$

In order to separately evaluate the role of the quadratic connections in changing the power of the restored images, let us consider the relation of the values (15) and (7):

$$\Omega=\frac{\Omega_{TF}^{\mathrm{L+Nl}}}{\Omega_{TF}^{\mathrm{L}}}=\frac{\left(1+\left(k\cdot\omega_{21}\cdot\omega_{PT}\right)^2\cdot\omega_T\right)}{\left(1+\left(\frac{\omega_{21}\cdot\omega_{PF}}{k}\right)^2\cdot\omega_F\right)}=\frac{1+k^2\cdot\left[\left(\omega_{21}\cdot\omega_{PT}\right)^2\cdot\omega_T\right]}{1+\frac{1}{k^2}\left[\left(\omega_{21}\cdot\omega_{PT}\right)^2\cdot\omega_T\right]}. \tag{16}$$

Since the "Linda" story has been specially constructed so that condition $k = \dfrac{\langle L(x), F^{\mathrm{RNl}}(x)\rangle}{\langle L(x), T^{\mathrm{RNl}}(x)\rangle} \gg 1$ is met, then the ratio (16) shows an increasing of the "Teller" power measure relative to the "Feminist" one due to the contribution of the quadratic interconnections.

2.3. Short discussion

Thus, from the presented consideration it follows that nonlinearity of synaptic sensitivity, or, in general nonlinearity the media for interconnections weights recording, is a cause for noncommutativity as an attribute of a model. The nonlinearity generates new interconnections between the reference NEs, that were not linked during the learning procedure, since they were presented for training independently and at difference time. It is these interconnections provide projections from the subspace of one reference NE to the subspace of another reference NE, changing the ratio between power measures of the restored reference NEs so that the weaker NE is strengthened, and *v. v.* strong weakens.

This mechanism plays a key role in the model of successive projections of the vector from one subspace onto the another and it is classical mechanism, not requiring an appeal to quantum mechanics. However, it is not enough to choose the final decision from the three possible proposed to the respondents: *F*, $F \,\&\, T$, or *T*. Below we demonstrate that the final choice is provided be the output neurons activation function.

3. Final choosing of the decision: numerical illustration

The NN presented in Figure 2 was modeled for a number of activation functions of neurons, characteristics of the recording media (synaptic sensitivity), and NE. Figure 3 shows the results: the responses (NEs in the output layer) of the learned NN Fig 2, obtained by varying only one parameter — the activation function of the neurons of the output layer $S^{Out}(P)$. The activation functions of the δ-neurons, as well as the characteristics of the weights for recording medium were assumed linear, i. e. quadratic interconnections (9) were not involved. All NE had a size of $N = 256 \times 256\ px$. For clarity, inscriptions on a black background were used: for reasons of biological motivation to account for the presence of a fractal structure in NE [Molchatskii, 2015], the inscriptions are filled with realizations of two-dimensional fractal Brownian motion,

the Hirst parameter was $H = 0.1$. For greater visibility of the results, the inscriptions themselves are localized in different areas of the NEs, and the localization of the maxima of the cross-correlation functions coincided with the localization of the global maxima of the autocorrelation functions of the references.

Figure 3 shows the results obtained under the following experimental conditions:

To meet the experimental conditions [Tversky & Kahneman, 1983] that NE of the "Feminist" is subjectively brighter than the "Teller" one, the following relations of the parameters of the reference NE (inscriptions) $F(x)$ and $T(x)$ were set:

- power ratio $P(F) / P(T) = 1.943$,
- the ratio of the number of neurons $N_F / NT = 2$,
- the ratio of the correlation coefficients with NE "Linda": $\Omega_{LF} / \Omega_{LT} = 2$.

Three biologically inspired models of activation functions for output neurons were used:

- Figure 3.a presents the NE, obtained under the sigmoidal activation function usage:

$$S^{\text{Out}}(P,a,b,d) = \left[1 + \exp\left(a\left(\frac{-P}{b} + 1\right)\right)\right]^{-1} - d,$$

  where a, b and d are parameters, b sets the fixed point $S^{Out}(P) = P$, d sets the value $S^{Out}(0)$;

- Figure 3.b presents an output NE, obtained under linear activation function usage;
- Figure 3.c presents an output NE, obtained under usage of sigmoidal activation function with an inverse slope instead of saturation in the range of higher powers, the last was added to model the fatigue of synaptic transmission that implements a mechanism of overexcitation protect in biological neurons [Tversky, Kahneman, 1983]:

$$S^{\text{Out}}(P,a,c,d) = P^c \cdot exp\left(\frac{-(I+d)^2}{2 \cdot a^2}\right), \qquad (17)$$

where a is the function's radius at the level 0.606, c determines the steepness of the direct and inverse sections, *d* specifies the position of the function's maximum.

Figure 3.a. Output *NE «*Linda is active in the feminist movement», power of the *NE:* $P^{Out} = 2.469 \cdot 10^8$.

Figure 3.b. Output *NE* «Linda is a bank teller and is active in the feminist movement», power of the *NE:* $P^{Out} = 1.328 \cdot 10^8$.

Figure 3.c. Output NE «Linda is a bank teller», power of the *NE:* $P^{Out} = 9.642 \cdot 10^7$.

Figure 4 presents the results, obtained by modeling the implied condition of the Tversky and Kahneman experiment that the "Feminist" pattern in the inner representation of the reasoning agent was subjectively brighter than the "Teller" one. For this goal the reference NEs' parameters were established as follows:

- ratio of the power measures $P(F) / P(T) = 31$;
- ratio of the neurons' numbers in the inscriptions $N_F / N_T = 2.5$;
- ratio of the correlation coefficients with "Linda" $\Omega_{LF} / \Omega_{LT} = 62$.

Only the model of the activation function of the output layer neurons with the inverse slope in the saturation range (17) was used, only two parameters of the function (17) were varied: the exponent *c* and the radius of the Gauss function *a*, their values are given in the figures captions.

NE in Figure 3.c and 4.c are given specifically for those values of the parameters at which a part of the inscription "Feminist" is still visible, but the inscription itself is no longer readable. NEs in the Figures 3.b and 4.b represent the conjunction *F*&*T*.

Figure 4.a. Output *NE* «Linda is active in the feminist movement», c = 6, $a = 150$, power of the *NE:* $P^{Out} = 3.011 \cdot 10^8$

Figure 4.b. Output *NE* «Linda is a bank teller and is active in the feminist movement», $c = 0.1$, $a = 300$, power of the *NE:* $P^{Out} = 2.167 \cdot 10^8$

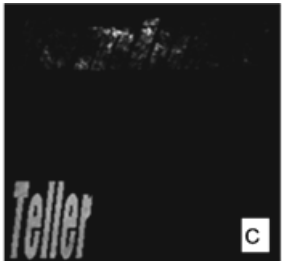

Figure 4.c. Output *NE* «Linda is a bank teller», $c = 0.4$, $a = 150$, power of the NE: $P^{Out} = 5.349 \cdot 10^7$

Thus, in Figure 3 and Figure 4 we have the order of the measures of the NEs representing the judgments $P^{Out}(F) > P^{Out}(F \,\&\, T) > P^{Out}(T)$, that coincides with the obtained by Tversky and Kahneman one: the measures of two events' conjunction are greater than measures of one. Let us note that the values of the measures of each of the three types of conclusions presented can vary within wide limits depending on the values of the parameters of both the activation functions and the reference NAs. Similar results were obtained for other models of activation functions and their parameters, the power ratios of the reference NEs and their correlation coefficients with the input NE. Thus, we have obtained the implementation of the "Linda" phenomenon by the classical method, without referring not only to quantum physics in its essence, but also to quantum formalism.

As the choice of final decision is implemented by output neurons activation function, the property of non-commutativity of operators describing the output in quantum logic is not essence to implement the phenomenon: the property is useful in order to strengthen the weaker neural ensemble by using quadratic interconnections arising due to nonlinear recording of the interconnections.

4. Conclusion

Thus, currently attributed to the category of quantum-like, the "Linda" phenomenon, which consists in violating the laws of classical probability theory for the conjunction of independent events, can be based on two completely

classical mechanisms that are implemented by neural network and do not require appeals to quantum physics, neither in substance nor formally:

- at linear recording of the weights of interconnections, the key factor is the type of activation functions of the output neurons — the mechanism of fatigue of synaptic transmission can give a measure of one of the independent events (responses) lower than the measure of their conjunction; the presence or absence of the property of noncommutativity is irrelevant in this case;
- when nonlinearly recording weights of interneuron connections, as shown earlier [Pavlov, Orlov, 2019], the mechanism of sequential projection of current state vectors onto subspaces storing reference images is actual; the nonlinearity of the recording media (synaptic sensitivity) generates properties of noncommutativity of operations and nonadditivity of a measure that are inherent in quantum logic.
- -whether there is noncommutativity or not the choice of the final decision neural ensemble is implemented by the activation function of the output neurons

Funding. This work was supported by the Russian Foundation for Basic Research, grant 18–01–00676-a.

Acknowledgments. Author would like to thank Prof. Igor B. Fominykh, Dr. Nikita A. Soloviev and Dr. Vyacheslav V. Orlov for the fruitful and helpful discussions.

References

1. Asano M., Basieva I., Khrennikov A. et al. Quantum Information Biology: From Information Interpretation of Quantum Mechanics to Applications in Molecular Biology and Cognitive Psychology // Foundations of Physics. 2015. V. 45. № 10. P. 1362–1378. https://doi.org/10.1007/s10701–015–9929-y
2. Borisyuk G. N., Borisyuk R. M., Kazanovich Ya.B., Ivanitskii G. R. Models of neural dynamics in brain information processing — the developments of 'the decade' // Phys. Usp. 2002. V.45. № 2. PP. 1073–1095. DOI: 10.1070/PU2002v045n10ABEH001143
3. Busemeyer J. R., Pothos E., Franco R., Trueblood J. S. A quantum theoretical explanation for probability judgment "errors" // Psychological Review 2011. V.118. № 2. P. 193–218. doi: 10.1037/a0022542
4. Feynman R., Leighton R., Sands M. Feynman Lectures on Physics. 1963, V. 3. Quantum Mechanics / http://www.feynmanlectures.caltech.edu

5. Glezer V. D. Matched filtering in the visual system // Journal of Optical Technology. V.66, № 10, October 1999, Pages 853–856.
6. Glezer V. D. The Role of Spatial–Frequency Analysis, Primitives, and Interhemispheric Asymmetry in the Identification of Visual Images // Human Physiology. 2000. V.26. № 5. P. 636–640.
7. Glezer V. D. Zrenie I myshlenie. SPb.: Nauka, 1993. 341 P.
8. Glezer V. D., Ivanov V. A., Sherbach T. A. Issledovanie retseptivnykch poleii neironov zritel’noii kory koshki kak filtrov prostranstvennyh chastot // Phys. Journal USSR. 1973. V.59. № 2.
9. Glezer V. D., Ivanov V. A., Sherbach T. A. Otvet retseptivnykch poleii zritel’noii kory koshki na slognye stimuly // Phys. Journal USSR. 1972. V.58. № 3.
10. Glezer V. D., Dudkin K. N. et al. Zritel’noe opoznanie I ego neiropfiziologicheskie mechanizmy. L.: Nauka, 1975.
11. Kholevo A. S. Quantum probability and quantum statistics. (Russian) // Itogi Nauki Tekh., Ser. Sovrem. Probl. Mat., Fundam. Napravleniya 83, 5–132 (1991). Zbl 0739.46049
12. Khrennikov A. Yu. Quantum-like modeling of cognition // Frontiers in Physics. 2015. 3: 77. DOI: 10.3389/fphy.2015.00077
13. Khrennikov A. Yu. A Formula of Total Probability with the Interference Term and the Hilbert Space Representation of the Contextual Kolmogorovian Model // Theory of Probability and its Applications, 2007, 51:3, 427–441. https://doi.org/10.1137/S0040585X97982505
14. Khrennikov A. Yu. NonKolmogorov Theories of Propability and Quantum Physics. M.: Fizmatlit, 2003. 208 p. (In Russian)
15. Kolmogorov A. N. Osnovnye poniyatiya teorii veroyatnosteii. M., 1974.
16. Meijer D. K.F., Raggett S. Quantum Physics in Consciousness Studies // In book: Quantum Mind UK, 2014. Ed.: Raggett S. PP.180.
17. Menskii M. B. Quantum mechanics: new experiments, new applications, and new formulations of old questions // Phys. Usp. 2000. V. 43. #6. PP. 585–600. DOI: 10.1070/PU2000v043n06ABEH000771
18. Molchatskii S. L. Fractal Organization and Self-organization of Brain Neural Structures — Samara: PGS-GA, 2015. 133 P. (In Russian)
19. Moreira C., Wichert A. Quantum Probabilistic Models Revisited: The Case of Disjunction Effects in Cognition // Frontiers in Physics. 2016. 4: 26. https://doi.org/10.3389/fphy.2016.00026
20. Orlov R. S. Normal Physyology — 2-d ed., imroved. — M.: GEOTAR-Media, 2010. —832 P. (In Russian)
21. Orlov V. V. Gratings Formed During Nonlinear Recording of Superimposed Holograms // Technical Physics letters. 2004. T. 30. #. 12. PP. 1054–1056.

22. Pavlov A. V. On Algebraic Foundations of Fourier Holography // Optics and Spectroscopy. 2001. V.90. P. 452
23. Pavlov A. V., Orlov V. V. Quantum Logic Mechanisms Modeling by Superimposed Fourier-holograms, Based on Holographic Recording Media Nonlinearity Usage // Quantum Electronics. 2019. T. 49. № 3. P. 246–252.
24. Quantum Inspired Computational Intelligence. Research and Applications / Eds.: Siddhartha Bhattacharyya, Ujjwal Maulik, Paramartha Dutta. Elsevier, MK.: Amsterdam, N.Y. 2017 https://doi.org/10.1016/B978–0–12–804409–4.09988–5
25. Trillas E., Alsina. C., Valverde L. Do we need in MAX, MIN and 1-j operations in fuzzy set theory? Нужны ли в теории нечетких множеств операции MAX, MIN и 1-j? // in book: Fuzzy Set and Possibility Theory. Recent Developments. Ed. by Ronald R. Yager, Jona College. Pergamon Press. 1982. NY, Oxford, Toronto, Sydney, Paris, Frankfurt.
26. Trueblood J. S., Pothos E. M. and Busemeyer J. R. Quantum probability theory as a common framework for reasoning and similarity // Frontiers in Psychology, 11 April 2014 https://doi.org/10.3389/fpsyg.2014.00322
27. Tversky A., Kahneman D. Extensional versus intuitive reasoning: The conjunction fallacy in probability judgment // Psychological Review. 1983. V. 90. Issue 4. P. 293–315. doi:10.1037/0033–295X.90.4.293
28. Zheltikov A. M. The critique of quantum mind: measurement, consciousness, delayed choice, and lost coherence // Phys. Usp. 2018.V. 61. #10. PP.1016–1025; DOI: 10.3367/UFNe.2017.06.038155.

Chapter 21.
Quantum neurophilosophy and the problem of free will

N.A. Solovyev

Patricia Churchland introduced the notion of the term «neurophilosophy». It defines the field of research, which explores the connection of neurobiology with philosophy of mind. Though supporters of neurophilosophy are criticized, because they deny the very existence of consciousness. Neurophilosophy deals with different aspects of the problem brain-consciousness. However, the investigation of free will is one of the most urgent issues in this research area. The problem of free will belongs to the eternal questions of philosophy. Its urgency is largely determined by the fact that it is closely related to the issues of social organization, as almost every state in its Constitution affirms the important role of human freedom, and politics is somehow connected with the fight for freedom and the interpretation of this idea. The situation is exacerbated, because the modern neurophysiology tends, in fact, to deny free will. For example, in work [Klyucharev, 2017] «Freedom of will: neuroeconomics approach» V.A. Klyucharev says: «From my point of view, the definition of free will as an opportunity to do otherwise leaves no space for the existence of freedom within the framework of determinism, however, as well as the presence of stochastic processes in the brain activity… I note that the deterministic decision-making is understood by me in this article as a tangle of genetic, physiological, social and evolutionary factors that strictly determine human decision-making». The situation with the phenomenon of free will becomes so challenging, that V.A. Klyucharev continues: «The circle is closed — determinism is so incompatible with the concept of free "to do otherwise" that some philosophers seriously suggest to hide this fact from the masses, "it may get wrong"» [Klyucharev, 2017]. These contradictions make neurobiologists and philosophers refer to phenomenon of freedom again. One of the illustrative examples is the research in the field of neurophilosophy of free will initiated in the USA in 2019 in the Brain Institute. One of the project participants Uri Maoz, Ph.D., assistant professor of psychology and computational neuroscience at Chapman University, defines project goal so: "This grant aims to create a new field in the study of the brain — the neurophilosophy of free will" [Maoz].

As shown above, the main obstacle to the recognition of the existence of free will of the person is the determinism of Descartes-Laplace, by which the phase trajectory of a physical object is unique and has no branching points. However, as is well known, this argument applies to classical systems, and quantum systems have branching points of the phase trajectory. They are connected with the collapse of the wave function of the system, when the system, that realizes deterministic evolution according to the Schrodinger equation, goes into one of the states of the world of potential opportunities, Figure. 1. It should be noted, that the reasoning about free will and quantum effects in the brain are often reduced to the question of the existence of stochastic processes in neural networks. This approach simplifies the problem and leaves out of consideration the existence of branching points of the phase trajectory. There should be more correct statement of the problem. The quantum system at the branching points may with different probabilities go into various states, which are chosen from the world of potential possibilities. It should be kept in mind that the very concept of probability makes sense either for an ensemble of identical particles (objects, systems), or for a large number of measurements carried out over the system, which must be in the same initial state. It is clear that during the research of free will none of these conditions can be acceptably fulfilled. Experiments are usually carried out either with different test persons, which quite differ from each other (there are no identical people), or with one test person, who cannot be in the same state many times in a row. In ordinary life, making a conscious decision is always a single event for which the very concept of probability is not inapplicable. And this, in turn, means that a person can choose very unlikely behavior, that is, in terms of work [Van Inwagen, 1975], to do otherwise.

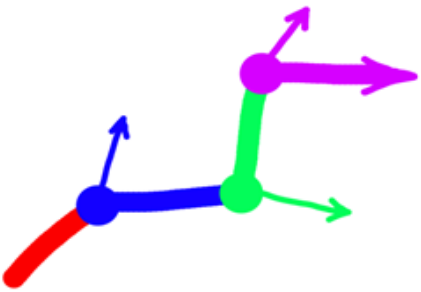

Figure 1. Schematic view of the evolution of a quantum system with branching points of the phase trajectory.

Based on the foregoing, we can define free will as the possibility of making an unlikely decision or, metaphorically speaking, as an opportunity "to freeze the ears to spite the mother». Thus, the assumption of the possibility of quantum effects in the brain allows us to solve the problem of free will from the philosophical point of view, but this solution brings difficulties from philosophical field in the physical one. The point is that quantum effects are known to play a significant role in the microworld, and for macroscopic objects, which is the brain, the role of quantum effects is usually questioned. This is associated with the phenomenon of decoherence, which leads to the destruction of quantum coherence and the manifestation of the classical properties of the system (see, for example [Zurek, 2002]). However, despite these limitations, there are a number of phenomena in the neural structures of the brain that can be considered as candidates for a positive solution to the quantum brain problem. Studies of the possibility of the existence of quantum phenomena in the brain relating to the problem of free will are conducted for a long time. One of the most well-known approaches to the issue is the approach, which is developed by the Australian neurophysiologist, Nobel laureate in physiology and medicine in 1963, John Eccles and the German physicist Friedrich Beck [Beck, Eccles, 1992], where quantum effects are considered in the synaptic gaps. It is assumed that mental activity controls the probabilities of the signal passing through synaptic gaps, and this process occurs coherently in a large number of gaps.

Another approach to the issue is developed in the works of the well-known physicist Roger Penrose (see, for example [Penrose, 2005]). In these works tubulin microtubules are considered as a source of quantum effects. Tubulin microtubules have different functions in cells, including transportation of various particles and formations. Despite its originality and attractiveness, Penrose's hypothesis has obvious weaknesses. First of all, it assumes that the characteristic frequencies of processes, which have a quantum nature, are about 10^{11} Hz, which is 9–10 orders higher than the characteristic frequencies of the brain. Such a huge difference in frequencies gives grounds for doubts about the general nature of the phenomena, which occur in the microtubules and macroscopic structures of the brain. Secondly, mental activity in the brain, according to Penrose's hypothesis, is connected with the objective reduction of the wave function due to the processes of quantum gravity. It is clear that objective reduction excludes the participation of the subject in decision-making and, in that sense, it cannot be accepted to explain the phenomenon of free will. It should be pointed out, that Roger Penrose is still a acknowledged authority in the field of quantum neurophilosophy. So in 2008

he wrote a foreword to the book Quantum Aspects of Life [Abbott, Davies, Arun, 2008], which deals with a wide range of issues related to the problem of the existence of quantum effects in nature.

One of the most attractive hypotheses, in our opinion, is the hypothesis of the quantum nature of the processes occurring in the ion channels of the cell membranes of neurons and axons, since it is the processes of opening and closing the ion channels and determine the timelines for the work of the neural networks. A discussion of the possibility of quantum effects in the operation of ion channels can be found in the work [Zheltikov, 2018]. It deals with the possibility of the existence of superposition states of ions, which are located on the outer and inner side of the membrane of the neuron and axon. The paper indicates the absence of experimental data and theoretical results confirming the possibility of existence of such quantum effects in the neural structures of the brain. At the same time, it is argued that the currently available experimental data on the presence of quantum effects in complex molecules do not allow reject this hypothesis categorically. It should be noted that despite the absence of experimental data, which confirms the existence of quantum effects in neural structures of the brain, there are currently experimental evidence of the quantum nature of the behavior of macromolecules [Gerlich, Eibenberger, et al, 2011], as well as the existence of quantum coherence in photosynthesis [Ishizaki, Fleming, 2009], [Wolynes, 2009]. Furthermore, by considering the superposition states, which may occur during the operation of ion channels, it is necessary to pay attention to the possibility of the existence of superposition states of the open-closed channel. It is possible that the existence of a superposition of these states in the simultaneous presence of synchronous operation of a large number of channels can lead to the emergence of macroscopic quantum states similar to laser. Despite the apparent difference between the laser and the brain, the analogies between them have deep enough grounds, because, firstly, both the brain and the laser belong to the class of open non-equilibrium systems, and secondly, in both objects the basis of functioning are microscopic quantum objects. In the laser — these are working atoms or ions, in the brain, as mentioned above, the functions of elementary quantum objects can be performed by ion channels and synaptic gaps, and their work ensures the appearance and distribution of the spike. Importantly, in the laser, despite the fact that it is a macroscopic object, there are purely quantum processes of spontaneous and induced emission, as well as coherent collective quantum processes. Collective quantum effects occur in lasers especially strongly at the lasing threshold, when superposition states of laser modes are observed, which can be considered as macroscopic objects

[Lamb, 1965], [Markelov, 1976]. Analogies in the brain and the laser function are considered in the work [Lee et al., 2018], where, particularly, the size of a quantum system with generation rate of 10 Hz, which lies in scope of the brain function and corresponds to the frequency of the alpha rhythm, is estimated. It is shown that the size of such system is about 10 microns, which is approximately equal to the typical size of the neuron. At the same time, a system of neurons connected to a neural network can be considered as an equivalent of a multimode laser. The paper [Danilov et al, 2016] discusses some effects associated with the synchronization of both longitudinal and transverse modes in lasers. Synchronization of longitudinal modes leads to the so-called self-synchronization mode, when the chaotic temporal dynamics of the generation goes into the mode of generation of ultrashort laser pulses. When the transverse modes are synchronized, the effect of laser beam scanning of the laser output aperture occurs. Time base of the produced superpositional mode (supermode) presented in the work [Danilov et al, 2016], demonstrates the manifestation of a macroscopic superposition state (the state of the field of the laser) in visual presentation, Figure 2.

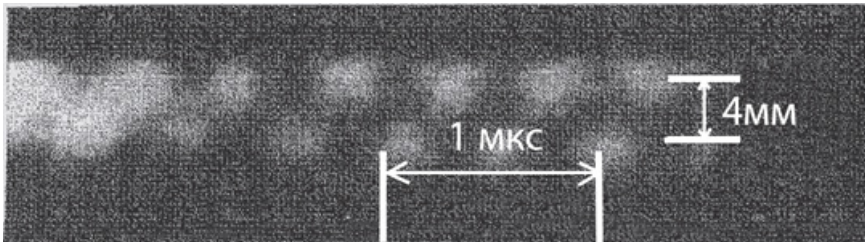

Figure 2. Time base of transportation of supermode in a flat resonator [Danilov et al, 2016]. (мм — mm, мкс — μs).

If we draw an analogy with the brain, we can assume that in the brain, the synchronization of the work of various neural networks can lead to both temporary bursts of activity, and to some "wandering" activity on various neural networks. This "wandering", however, is associated with the process of information processing, which should involve a large amount of different neural networks, which are in a superposition state. It should be noted that this quantum process of mode synchronization is very similar to the classical collective phenomena described in the work [Rabinovich, Muezinoglu, 2010]. However, as mentioned above, the existence of quantum effects is required to prove free will. Quantum effects would allow to produce a collapse of the superposition and choice of one current state from

a variety of potential states. In this sense, the hypothesis of the quantum process of mode synchronization in neural networks of the brain is more reasonable.

Currently, despite the existence of quite common analogies between laser and brain, there is no understanding of the details of the process that could provide the choice of alternatives when a person makes a decision. It seems that to describe the essence of freedom there is a lack of common principles by which a conscious choice is being made. It is appropriate to recall the ideas of von Neumann [Neumann von, 1964]. They come to this, that the collapse of the wave function of a closed system, which consists of microparticles, a macrodevice and an observer, carries out a non-physical "abstract I" of the observer. Of course, the idea that the observer chooses alternative states of the particle and the device seems too contrived. However, if we consider that that the human brain in the process of thinking and making unmotivated (or poorly motivated) decisions can be considered in some approximation as a closed system, which is not the subject of decoherence from the environment, the idea of the collapse of the wave function of the brain by "abstract I" after the phase of deterministic evolution of its superposition state, can be very fruitful. The only thing, condition that must be fulfilled, is the existence of degrees of freedom, which are isolated from external influence, which allows to realize the superposition of states. Such degrees of freedom can be superposition states of ion channels and (or) synaptic gaps. We do not consider tubulin microtubules on grounds mentioned above.

This hypothesis, of course, does not describe all the details of the process, however, it allows us to understand truly how in the presence of degrees of freedom, which are weakly interacting with the environment, it is possible to choose alternatives and observe the superposition macro-state of the brain. On the basis of the ideas of von Neumann, we can assume that the choice of alternatives and observation of the superposition state of the brain is carried out by an "abstract I", which in the paper [Solovyev, 2019] is called contemplative-control precisely because it performs the function of observing the content of consciousness (brain) and controlling the body. Since only the macro-state of the brain can carry some semantic information, which is observed by the contemplative-controlling I, and which serves as the basis for making meaningful decisions, it is clear that we have to say superpositions and collapse in the system of neural networks. Thus, von Neumann's ideas about the existence and role of the abstract I in the process of observation and choice of alternatives, allows, in general, to

solve the problem of the existence of free will and to rehabilitate the Cartesian model of consciousness [Solovyev, 2019]. It should be mentioned that the fundamental difference between a quantum computer and a human, from the point of view of information processing, is that the non-physical abstract or contemplative-controlling I can observe the superposition states of the brain, in which information is recorded (i.e., the content of consciousness), without the collapse of the wave function, and for the output of information in a quantum computer, the collapse of its wave function is necessary.

As mentioned above, the quantum macrostates in the laser appear at the lasing threshold. They are associated with both intensity fluctuations and the presence of a superposition of modes. If we talk about the analogies between the laser and the brain, in the brain it can be compared with making of unmotivated decisions, i.e. with the manifestation of free will in its pure form. In this case, we can assume that there is a certain fluctuation in the brain, which is a superposition of two or more states, this fluctuation is amplified and realized by the person (his abstract I). When a person makes a decision, one of the quantum alternatives is chosen, which then gets a classical appearance. This process, in principle, is similar to the process of choosing alternatives in quantum measurement:

$$(\alpha|N_a\rangle + \beta|N_b\rangle)|B_o\rangle \rightarrow \alpha|N_a\rangle\,|B_a\rangle + \beta|N_b\rangle\,|B_b\rangle$$

Here: $\alpha|N_a\rangle + \beta|N_b\rangle$ — superposition state of the neuron before triggering; B_o — unperturbed state of the part of the brain with which this neuron interacts; $\alpha|N_a\rangle\,|B_a\rangle + \beta|N_b\rangle\,|B_b\rangle$ — superposition state of the brain after interaction with a neuron N. When a person makes a decision, only one alternative is chosen and enhanced $\alpha|N_a\rangle\,|B_a\rangle$ with probability α^2, or $\beta|N_b\rangle|B_b\rangle$ with probability β^2.

In general, the described decision-making scheme coincides with the two-stage model described on The Information Philosopher [informationphilosopher]. In this model, the making of unmotivated decisions is carried out in two stages: the first stage is a random generation of various random thoughts (decisions), and the second finding of alternatives, pic. 3. In our approach, we assume that the generation of random solutions occurs in the form of a superposition of alternatives, which can then be processed (evolve) without the collapse of the wave function. The selection of an alternative takes place at the point of "Torn" Decision through the collapse of the wave function of the brain contemplating-controlling I.

Figure 3. Schematic representation of the decision-making process (free will) [informationphilosopher].

The presented theoretical scheme of choice of alternatives corresponds well with the well-known experiments of Libet [Libet, Gleason, 1983], which studied the neurobiological features of human decision-making. In these experiments, the test person at any time had to carry out a simple action, such as raising his hand. The experiments measured the preparedness potential, which is responsible for the preparation and fulfillment of the action, as well as the time when the test person, or, in our terminology, abstract or contemplative-controlling I of the test person, was aware of the internal individual wish to carry out the action. We emphasize that in these experiments, the contemplative-controlling I appeared, albeit indirectly, because it was possible to register the moment of realization of the processes by nonmaterial I, which are occurring in the test person's own brain. It was expected, that I of the test person must first realize the wish to raise his hand, and then there should be a potential preparedness, which, ultimately, would start the mechanism of raising the hand. However, the experiment showed, that 550 ms before the action occurs readiness potential appears; after 300 ms, or 250 ms before the action, a person realizes the wish to raise his hand; after another 200 ms, or 50 ms before the action, motor neurons are activated, and the process goes into an irreversible stage of fulfillment. These experiments caused a huge discussion, because, at first sight, they proved the absence of free will. However, later Libet pointed out that [Libet, 1999], the next 200 ms after the moment of realization of the wish to carry out the action, the test person can cancel it, i.e. he, speaking the language of Libet, has veto right. The possibility to cancel the action ends 50 ms before its fulfillment, when the activation of motor neurons begins. Furthermore, in discussions about Libet's experiments, it is believed that the test person carried out the free will at the time of consent (or non-consent) to participate in the experiment [Hallett, 2009]. If so, then we can assume that by choosing an alternative to "participate" an unconscious "random generator" of the preparedness potential activates in the brain of the test person, This generator later realizes

the contemplative-controlling I of the test person (see pic.3). Then, with the realization of the wish to carry out an action, the test person can again make a choice: to perform the action or to cancel it. This, in turn, means that at times when the test person can carry out the abolishment of the action, his psyche and brain are also in a superposition state. Thus, we can assume that basically mechanism of free will is based on the transition of the brain and psyche from a superposition state into one of the relevant alternatives, but the details of these processes require careful study.

If definitive theoretical solution to the problem of brain quantization has not been found yet, then there is an experimental evidence of the existence of quantum or, more carefully, quantum-like features of the human psyche. They appear in experiments on the research of choice under uncertainty, which were conducted at the end of the last century by Tversky and Kahneman (Tversky A., Kahneman D.) [Tversky, Kahneman, 1983].

The point of these experiments was that the test persons told a short and uncertain story about an imaginary girl Linda, and then asked quite specific questions: is Linda a bank teller and whether she is a feminist? It is important that there was no specific information about this in the story that was told by the test person. It turned out that the results of experiments were not described by the classical probability model. The experiments were explained on the basis of a formal quantum-like model, in which a certain state vector is attached to the state of psyche of the test person after hearing the story about Linda, by analogy with quantum formalism [Trueblood, Pothos et al, 2014].

In this case, the probabilities of the answers “yes” or “no” are calculated as the squares of the projections of this vector on the corresponding orthogonal axes: the axis “yes” or the axis “no”. An important feature of this model is that the orthogonal axes “yes”–”no” for the case of “feminist” and “teller” are located at some angle to each other. This is what allows us to describe an important feature of the Tversky and Kahneman experiments, which consists in the fact that the different sequence of answers to questions gives different results, i.e., speaking in terms of quantum mechanics, the answer operators do not commute with each other. This can be explained quite easy. Indeed, if we ask the test person a question: is the “girl Linda” bank teller, and the test person will give a certain answer, then the state vector describing his psyche, will be projected on a certain axis of the coordinate system “bank teller”. Then the next answer to the question, whether the “girl Linda” is the feminist, will be given from a new state, which, of course, will give other probabilities of

answers "yes" — "no" than the direct answer to the question, when the vector of the state of psyche was in the initial state.

From the point of view of quantum mechanics, the situation with the test person in the experiments of Tversky and Kahneman looks so as if the psyche firstly, and therefore the brain, are in a superposition state, and when replying a collapse of the wave function of the brain and the choice of one of the alternatives occurs. In other words, the collapse is one of the manifestations of the free will of human, although there is a question: is this choice always made consciously under the control of the contemplative-controlling I or it has (may have) an unconscious, spontaneous character? Irrational spontaneity when choosing under uncertainty does not allow in principle to talk about free will at the moment of choice in rational terms. The element of rationality in the quantum consideration of the issue of free will, apparently, should be sought in the set of deterministic evolution of the vector of the state of psyche (brain) and its probabilistic, but still indeterministic projection on the basic vector. The situation with the consideration of the problem of free will is complicated by the fact that in most cases, decision-making operators, speaking in quantum language, do not commute with each other, i.e. they can not (as quantum measurements) be carried out simultaneously, and the sequence of actions changes the result [Busemeyer, Pothos et al, 2011]. This shows that human thinking and decision-making are not subject to Boolean logic, and, consequently, the problem of free will cannot be solved within the framework of traditional rational discourse. It is quite possible that the efficiency of the brain is precisely associated with the fact that the brain can operate with superposition states similar to a quantum computer. Then the process of contemplation of images by our contemplative-controlling I can be considered as an analogue of parallel quantum calculations without the collapse of the wave function, and decision-making — as the output of the result in discrete form. This means that contemplation itself must also be included in the process of free decision-making.

Quantum-like effects in behavior can also be observed when choosing under uncertainty where there is "social pressure" [Gorbatov, Solovyev et al, 2019]. The paper shows that the tips presented by the test persons when answering questions with knowingly ambiguous answers, strongly affect the test result, shifting the probability of answers in the direction of the available tips. In this case, the generation of false hints is a tool of influence on the results of testing in the group. An important result of the presented experiments is that the test results can be described using laser analogies. The developed laser-like model

considers the process of answering an uncertain question by analogy with the decay of an excited atom into various underlying states, and the answer in the presence of hints as an analogue of the induced decay of the excited level, when the hint changes the probability of the answer of the test person, as well as the quantum of light flying past the excited atom affects the probability of the decay of the excited level into a certain underlying state. These data, as well as the quantum-like description of the Tversky and Kahneman experiments, shows that quantum analogies can be useful for describing human behavior, and this, in turn, requires the search for fundamental reasons for the existence of quantum-like effects in human behavior. Furthermore, the presented data on the study of social induction demonstrate that the influence of external information influence on decision-making can significantly limit the free will of a person.

The question of the essence of the process of contemplation and the division of the contemplative-controlling I and the contents of consciousness, as can be understood from the above, is important for understanding the decision-making process. In this regard, it is appropriate to dwell on the results of an experimental study of neurobiological activity of the brain in meditation or, more strictly speaking, in the process of controlled stopping of the internal monologue, i.e. in the absence of thoughts of test person [Moiseenko, Solovyev et al, 2019]. On pic.4 a tomogram of brain encephalographic activity of test person who was in a controlled state of stopping the internal monologue (inner silence, absence of thoughts) is presented. The state of absence of thoughts was determined by subjective reports, according to which in this state in the absence of the permanent flow of thoughts, from time to time the spontaneous formation of certain thoughts is observed, which, however, subsequently faded due to the fact that the test person was not concentrated on them and chose a state of silence. An important feature of the state of inner silence is that the test person, in the absence of thoughts, was aware of his subjectivity, i.e. his contemplative-controlling I. This confirms the fact that the abstract I cannot be associated with the content of consciousness [Solovyev, 2019]. An interesting feature of these experiments is that in the state of internal silence there is a significant activity in the gamma range. This is coincident with the results of work [Lee, Kulubya et al, 2018]. From the point of view of the study of free will, these experiments are of interest as a confirmation of the logical decision-making scheme described above and presented on pic.3. Namely, in this case there was a phase of spontaneous emergence of thoughts, a phase of their realization and a phase of the choice of a state of silence due to suppression of the appeared thought.

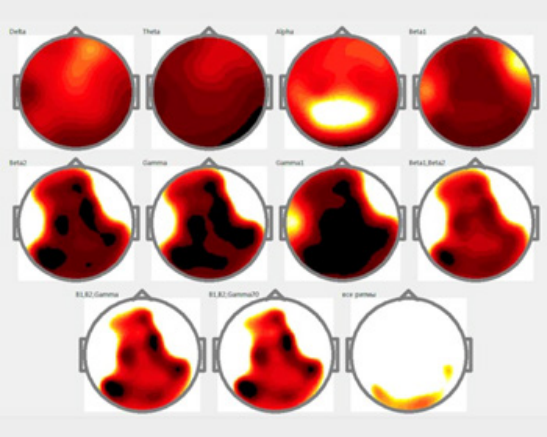

Figure 4. Topograms of neurobiological activity of the brain in a state of inner silence (open eyes).

Analyzing Libet's experiments, it should be noted that their important feature is the inclusion of a purely subjective phenomenon of awareness. It is noted in the work [Libet, 1999]: «Our own previous studies have indicated that *awareness* is a unique phenomenon in itself, distinguished from the contents of which one may become aware». In addition, Lisbet notices: «The content of an unconscious mental process (e.g. correct detection of a signal in the brain *without any awareness* of the signal) may be the same as the content *with awareness* of the signal. But to become aware of that same content required that stimulus duration be increased by about 400 msec». Comparing this conclusion with the results of the work [Moiseenko, Solovyev et al, 2019], we can say that awareness is connected not only with the specific content, but also with the awareness of its absence or the awareness of one's own contemplative-controlling I. In Libet experiments awareness occurs when the preparedness potentional gets to some certain value 400 msec after its spontaneous appearence. It can be assumed that in experiments [Moiseenko, Solovyev et al, 2019] the appearance of thoughts in a state of intelligent silence is also the result of random fluctuation, which is amplified to a certain level, and then faded, due to a certain effort by the test person. Thus, the process of suppressing thoughts in a state of intelligent silence or meditation confirms the possibility of veto right in decision-making, described by Libet in the work [Libet, 1999]. In this sense, we can consider the state of intelligent silence as a manifestation of free will, as a free choice of state without thoughts.

It should be noted that the described process of intelligent silence has much in common with the process of reflection, when a person calmly thinks about certain situation, "considers" some arguments and counterarguments. Usually in the process of thinking a person formulates vital attitudes for himself and makes goal-setting. Making subsequent decisions associated with a particular situation is carried out similar as illustrated on pic. 3. In the human brain, various options for responding to the situation are generated, and the person either allows the fulfillment of this response, or imposes a veto and proceeds to consider the next option of action, comparing it with his life settings and goal-setting. At the same time, awareness should play a key role in decision-making, because it allows you to track the momentum for action, check it with your own goal-setting and decide on the continuation of the action or on the imposition of a veto on it. In a stressful situation, actions are performed, as usual, unconsciously. This saves time on making vital decisions. However, this can lead to actions that are contrary to fundamental life attitudes.

In conclusion we note, that free will is an extremely complex phenomenon, which is very difficult to study by traditional methods, because they are somehow connected with the phenomenon of awareness and the phenomenon of the abstract or contemplative-controlling I. This means that the study of the phenomenon of freedom should combine the methods of objective instrumental research with the methods of research of the subjective inner world of human. It is important to note that free will is incompatible with the classical Descartes-Laplace determinism, and for its explanation it is necessary to involve the ideas of quantum mechanics to describe the brain activity

References

1. Abbott D., Davies P., Arun K. (Eds.), with foreword by Sir Roger Penrose. Quantum Aspects of Life, Imperial College Press, 2008, 581 pp.
2. Beck F., Eccles J. (1992)'Quantum aspects of brain activity and the role of consciousness', Proceedings of the National Academy of Sciences of the USA, Vol. 89 (23), pp. 11357–11361.
3. Busemeyer J., Pothos E., Franco R., Trueblood J. A quantum theoretical explanation for probability judgment "errors". Psychological Review. 2011. 118 (2): 193–218
4. Danilov O. B., Rozanov N. N., Solovyev N. A., Soms L. N. Multimode lasers as analogues of complex biological systems. Optics and spectroscopy. 2016. 120: 682–690.
5. Gerlich S., Eibenberger S., Tomandl M., Nimmrichter S., Hornberger K., Fagan P. J., Tuxen J., Mayor M., Arndt M. Quantum interference of large

organic molecules. Nature Communications, volume 2, Article number: 263 (2011). https://www.nature.com/articles/ncomms1263#f3
6. Gorbatov D., Solovyev N., Soms L. Social induction and a problem of choice in conditions of uncertainty. IEEE International Conference «Video and Audio Signal Processing in the Context of Neurotechnologies», SPCN-2019, May 27 — May 31, 2019, St.Petersburg, Russia
7. Hallett M. Physiology of volition. Downward causation and the neurobiology of free will. Eds. Murphy N., Ellis G., O'Connor T. 2009. Berlin: Springer-Verlag. 291 pp.
8. Informationphilosopher, Two-Stage Models for Free Will. http:// www.informationphilosopher.com/freedom/two-stage_models.html
9. Inwagen van P. The Incompatibility of Free Will and Determinism. Philosophical Studies, 1975, 27 (3), p.185–199
10. Ishizaki A., Fleming G. (2009) Theoretical examination of quantum coherence in a photosynthetic system at physiological temperature. Proc Natl Acad Sci USA106:17255–17260.
11. Klyucharev V.A., Free will: neuroeconomic approach, Journal of higher nervous activity, 2017, т. 67, № 6, с. 755–760
12. Lamb W. Theory of an optical maser. Phys. Rev. 1964. 134: 6A. A1429–A1450.
13. Lee D., Kulubya E., Goldin P., Goodarzi A. and Girgis F. (2018) Review of the Neural Oscillations Underlying Meditation. Front. Neurosci. 12:178. doi: 10.3389/fnins.2018.00178
14. Libet B. (1999)'Do we have free will?' Journal of Consciousness Studies, Vol. 9, pp. 47–57.
15. Libet B., Gleason, C.A., Wright, E.W., Pearl, D.K. (1983)'Time of conscious intention to act in relation to onset of cerebral activity (readiness-potential): The unconscious initiation of a freely voluntary act', Brain: A Journal of Neurology, Vol. 106 (3), pp. 623–642.
16. Maoz https://braininstitute.us/news/templeton-fetzer
17. Markelov V.A. Fluctuations of ring laser radiation in two-mode mode. Quantum electronics.1976. 3. 3: 571–575.
18. Moiseenko G., Solovyev N., Shelepin Yu. The state of inner silence as a conscious choice (neurophysiology of voluntary purposeful suppression of mental activity). IEEE International Conference «Video and Audio Signal Processing in the Context of Neurotechnologies», SPCN-2019, May 27 — May 31, 2019, St.Petersburg, Russia
19. Neumann von I. Mathematical foundations of quantum mechanics.M: Science, 1964. 367 c.
20. Penrose R. Shadows of the mind: a search for the missing science. M., Izhevsk: Institute of computer research, 2005.

21. Rabinovich M. I., Muezinoglu M. K. Nonlinear dynamics of the brain: emotion and cognition. Advances in Physical Sciences. 2010. 180: 371–387.
22. Solovyev N. A. Quantum neurophilosophy and rehabilitation of Cartesian model of consciousness // Journal of higher nervous activity. 2019. T. 69. № 1. C. 120–129.
23. Trueblood J., Pothos E., Busemeyer J. Quantum probability theory as a common framework for reasoning and similarity. Frontiers in Psychology. 2014
24. Tversky A., Kahneman D. Extensional versus intuitive reasoning: the conjunction fallacy in probability judgment. Psychological Review. 1983. 90: 293–315.
25. Wolynes P. Some quantum weirdness in physiology. PNAS October 13, 2009 106 (41) 17247–17248; https://doi.org/10.1073/pnas.0909421106
26. Zheltikov A. M. Critique of quantum mind: the dimension of consciousness, delayed choice and lost coherency // Advances in Physical Sciences. 2018. T. 188. № 10. C. 1119–1128.
27. Zurek W. H. 'Decoherence and the Transition from Quantum to Classical', Los Alamos Science, 2002, Vol. 27, pp. 86–109.

ARTIFICIAL NEURAL NETWORKS

Chapter 22.
Learning Video-sequence Enhancement with Synthetic and Real Data

A.A. Boiko

Introduction

The signal restoration problem can be represented as finding a certain inverse function of degrading model of the unknown clean image, applied to the unknown clean images. These degrading models break down into categories, such as blur, noise, compression artifacts, resolution loss, etc. Traditionally, it is required to prepare data for a reliable representation of the generated distortions and their statistical characteristics to train networks solving image reconstruction problems from clean-corrupted image pairs However, the preparation of the data might be hindered by non-trivial modeling of the image degradation process, which may be poorly correlated with actual distortion due to unknown statistical parameters [Liu et al., 2014].

In this paper, we considered the use of the corrupted data itself for inverting degradation that appears while shooting on Bayer filter matrix. This kind of noise is quite popular in researching [Nazari, 2017] due to natural dependence on the signal value. Previously, the various sets of images and data were presented, based on the various approaches — shooting a sequence of frames of the same scene, with permanent exposure and ISO settings [Hasinoff et al., 2016], shooting a scene with different exposure [Chen et al., 2018] and ISO [Anaya, Barbu, 2018]. In this work, for training noise suppression, two sets of images were used: [Chen et al., 2018], as a representation of images with real noise, and ImageNet [Russakovsky et al., 2015] with subsequent synthetic augmentation.

Experimental results

The residual neural network RED30 was chosen for training. This network contains symmetrically convolution layers that perform the encoding, and deconvolution layers for decoding. Convolutional layers eliminate noise and distortion, layers with deconvolution associate single input activation with multiple outputs and are used as learning layers that increase resolution

and detail. This network showed itself well in solving problems of noise suppression and image restoration [Mao et al., 2016, Lehtinen et al., 2018], however, the number of parameters used by it is significantly large [Tai et al., 2017].

In [Lehtinen et al., 2018], the approach was proposed in order not to have the need to prepare long-exposure data. In the case the input and the output of the network are both noisy images. It was shown that when using Gaussian noise, the training strictly converges to the same result as when using clean image as a target. The results we obtained during training in pairs "noise-to-noise" with synthetic augmentation of ImageNet images are shown in Figure 1.

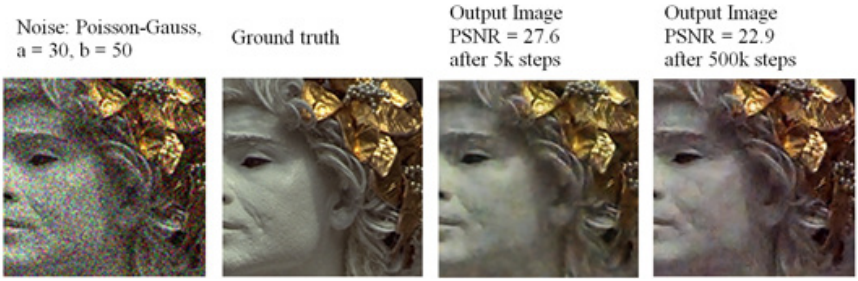

Figure 1. The results of synthetic augmentation and stable Gaussian noise source in a pair of "noise-to-noise".

In reality it takes assume that the Bayer image is subjected to Poisson-Gauss noise [Foi et al., 2008], so the noise term of augmented image is composed of two mutually independent parts (1):

$$\sigma\left(y(x)\right)\xi(x)=\eta_p y(x)+\eta_g(x) \tag{1}$$

σ — standard deviation, η_p — Poissonian signal-dependent component; η_g — Gaussian signal-independent component, $y(x)$ — the original image, $\xi(x)$ — zero-mean random with std equal 1. So, the augmented image might be described with model (2), where a is the varying variance of Poisson signal-dependent component $ay(x)=\mathrm{var}\left\{\eta_p y(x)\right\}$ and b is the constant variance of Gaussian component:

$$z(x)=\xi_1(x)\sqrt{ay(x)}+b\xi_2(x) \quad (2)$$

We trained the network with the stability of statistical characteristics of the Gaussian noise (the variance *a)* and randomly generated characteristics of Poisson noise (b). In this case the average metric PSNR for validation samples fell slightly compared with the results of the classical approach ("clean-to-noise") or previously presented concept, in which learning takes place in the "ideal" Gaussian noise model [Lehtinen et al., 2018].

However, in this case, it is still necessary to have pixel-aligned pairs of images with low exposure. Obtaining pixel-by-pixel aligned video sequences for video sequences is technically very difficult. This paper proposes the following solution. Under the assumption of the stability of the statistical characteristics of real noise in any part of the image, it is proposed to scatter the original image corrupted by real noise into parts according to the scheme shown in Figure 2.

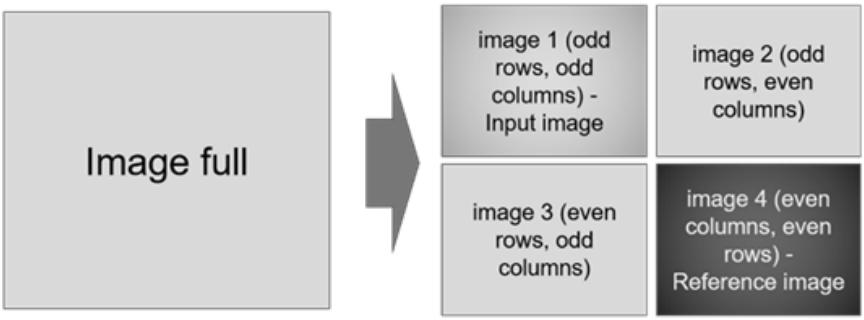

Figure 2. The scheme of scattering the image corrupted by real noise into pairs.

The resulting pairs are used in the training process of a neural network, which was slightly modified compared to the network in the previous experiment — there is added layer for depth conversion of tensor from 4 to 3, thereby changing a bit the concept of symmetry, and forcing the network to learn demosaicing. The result of the proposed solution is a denoised image in RGB color model. The detailed scheme is shown in Figure 3.

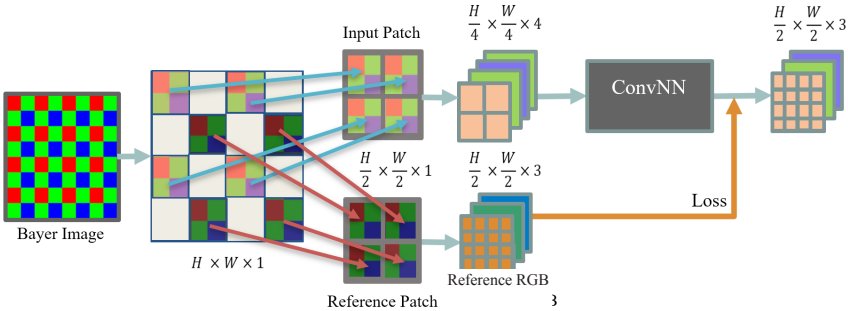

Figure 3. Image scattering scheme followed by feeding the resulting pairs into the neural network for training. Odd tiles represent pixels of input patch, the even ones are for tiles of reference patch, which is used in evaluating loss and comparison. The information of empty tiles is not used. H and W are for height and width respectively.

The result of training in the proposed scheme is presented in Table 1 and Figure 4.

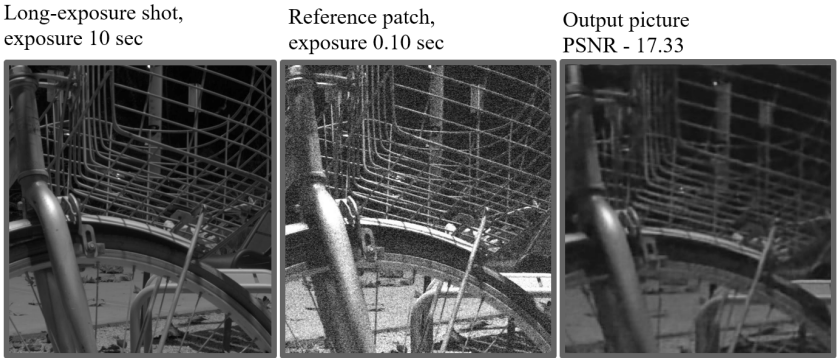

Figure 4. The results of training within the framework of the proposed concept.

In Figure 4 the validation triad of images are shown respectively: the target image shot with a long exposure is used in the PSNR calculation with output one, but for a neural network it is never shown; the noisy image shot with a low exposure enters the neural network; and the output result. The demosaicing algorithm with white balance settings was used to show the noisy image, since the contrast was naturally reduced by noise, its average brightness is much higher than the brightness of output one.

Table 1

Average PSNR on dataset [4] using RED30 network

Traditional approach (clean patch — noisy patch), real images	Noise-Noise [6], synthetic images	The proposed Scattering scheme, no reference frames are used, real images.
28.79	25.4	16.9

We can see that traditional approach outperform the proposed scattering scheme in PSNR. However, there is a serious issue with calculation of typical metrics in the case, and so far there are several assumptions about the reasons:

– the relocation of objects and their boundaries (pixel displacement of input-output pairs due to scattering);

– the complex demosaicing with non-trivial white balance;

– low average brightness compared to the ground truth picture.

Conclusions

In this work the approach of learning inverse degradation model for video sequence without clean images was proposed. The training method with simultaneous statistical parameters of noise was tested on samples with natural noise and proved to be visually effective, but now it requires further research of more relevant ways of evaluating itself to be compared with other solutions.

References

1. Anaya J., Barbu A. RENOIR — A Dataset for Real Low-Light Image Noise Reduction// in Journal of Visual Comm. and Image Rep, 2018.V. 51. № 2. P. 144–154
2. Chen C., Chen Q., Xu J., Koltun V., Learning to See in the Dark // in arXiv e-prints arXiv: 1805.01934, 2018.
3. Foi A., Trimeche M., Katkovnik V. and Egiazarian K. Practical Poissonian-Gaussian Noise Modeling and Fitting for Single-Image Raw-Data // in IEEE Transactions on Image Processing. 2008. V. 17. № 10. P. 1737–1754.
4. Hasinoff S. W., Sharlet D. et al. Burst photography for mobile cameras // in ACM Transactions on Graphics SIGGRAPH Asia. 2016. V. 35. № 6. P. 12.

5. Lehtinen N., et al, Noise2Noise: Learning Image Restoration without Clean Data // in arXiv e-prints arXiv: 1803.04189, 2018.
6. Liu X., Tanaka M. and Okutomia M. Single Noisy Image //in IEEE Transactions on Image Processing. 2014. V. 23. № 10 P. 4361–4371.
7. Mao X.—J., Shen C., Yang Y.—B. Image Restoration Using the Deep Convolutional Encoder-Decoder Networks with Symmetric Skip Connections// in arXiv e- prints arXiv: 1603.09056, 2016.
8. Nazari M. R. Denoising and Demosaicking of Color Images// applied for PhD degree. School of Electrical Engineering and Computer Science, Faculty of Engineering University of Ottawa. Canada. 2017, 157 p.
9. Russakovsky O., Deng J. et al, ImageNet Large Scale Visual Recognition Challenge// in IJCV, 2015.
10. Tai Y., Liu X., Image Super-Resolution via Deep Recursive Residual Network, IEEE Conference on Computer Vision and Pattern Recognition (CVPR). 2017. Honolulu.P. 2790–2798.

Chapter 23.
Efficient hardware implementation of neural networks

D. O. Malashin, R. O. Malashin

A large number of works is devoted to the development of new types of networks. A much smaller number of works is devoted to the implementation of neural networks in specific hardware (for example, [Baptista et al., 2018]). The purpose of the report is to tell about the ways of effective implementation of neural networks in the end device. This work is an attempt to offer some new solutions to maximize the capabilities of neural networks.

Hardware implementation of neural networks is an important part of modern development of artificial intelligence systems. It is payed much attention to such aspects as power consumption, computation rate, cost price of the solution, occupied space of the solution, etc. In particular, concrete parameters of the realization primary depend on levels of neural networks implementation: on-board implementation, on-chip implementation and implementation on the part of the chip. At the same time — the concrete type of neural network usually may make a strong adjustment to realization. In the work we consider convolutional neural networks (CNN), which at the moment are the most powerful tool for image analysis (for example [Malakhova et al., 2018; Malashin, Anisimov, 2016; Malashin, 2016]) and some other tasks.

A simplified scheme of implementation of the NN on a printed circuit board (PCB) can be represented as follows: There is some kind of host device (PC, phone, Android / IOS). The neural network is implemented on RAM, ROM and the main chip. In role of the main chip can be: processor device, FPGA, special custom chip (ASIC), microcontroller, etc. (Figure 1).

On figure 2 we can see the structure of on-chip NN implementation. In this case, in general, the entire neural network is implemented inside the chip, which serves as a hardware accelerator for a hardware solution, within the framework of which the use of the capabilities of neural networks is required. This NN chip interacts with other chips of this entire device using the standard protocol.

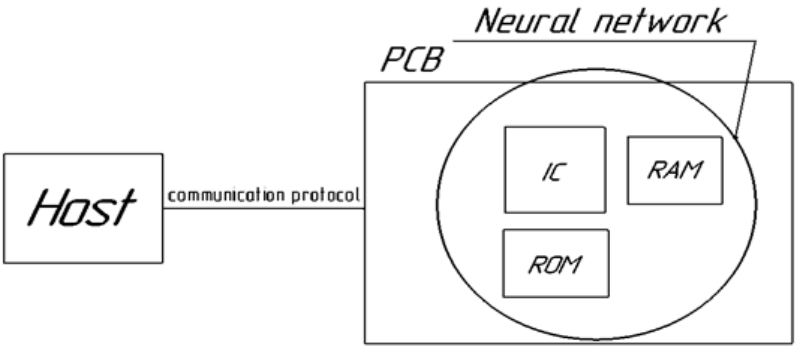

Figure 1. On-board implementation scheme.

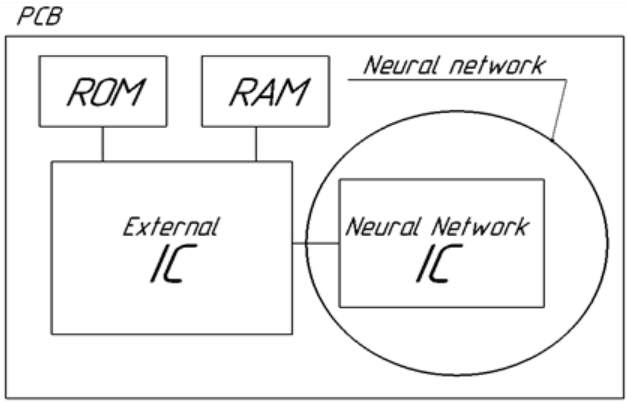

Figure 2. On-chip implementation scheme.

Probably, the most promising (and popular) version of implementation from the point of view of chip manufacturers is the implementation of the NN on a part of the crystal. Figure 3 structurally shows other hardware modules of the chip and the neural network is one of these hardware modules.

It is possible to highlight main difficulties in implementation of Convolutional Neural Networks (CNN), which are common to all levels of implementations:

- A lot of logical gates (logical elements) are required;
- High speed memory is required;
- Need in a great amount of mathematical operations to be parallelized.

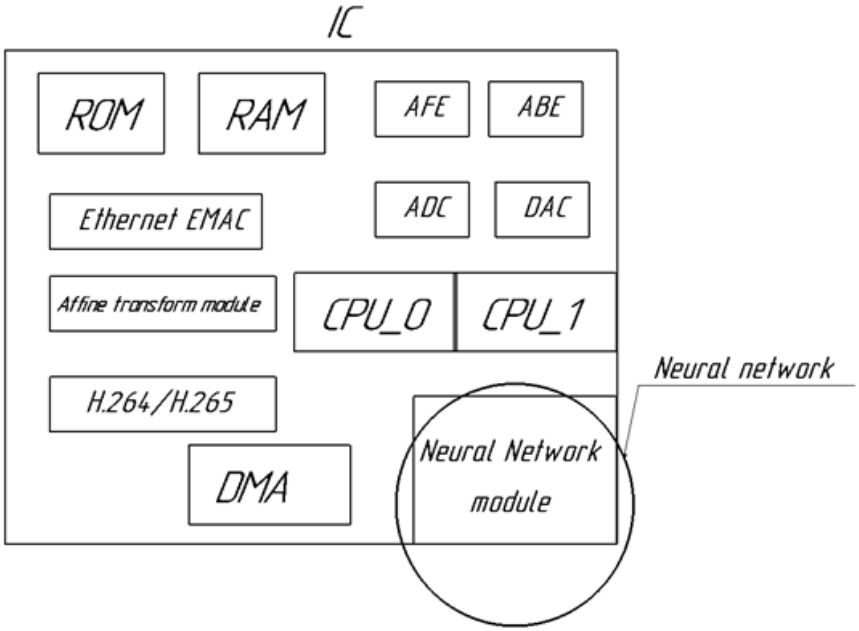

Figure 3. Part-chip implementation scheme.

Talking about efficient FPGA (field programmable gate arrays) implementation of large CNN's — the approach can be passed on the two main propositions. First, it is necessary to use compression for storing the coefficients of CNN to reduce the size of high-speed memory [Tatar, Holban, 2012; SongHan et al., 2016]. Second, CNN must exist only when there are tasks for neural network (use of dynamic reconfiguration or partial dynamic reconfiguration is a solution).

We propose the following. In the default FPGA configuration, we use a special neural network to determine from the input data (in our case, images) the best neural network at a particular point in time (or another algorithm) to solve this problem depending on changes in the conditions of the product (external, internal noise on the image, dynamic range, scenes, working temperature, etc.). Thus, it is essentially a network for choosing a neural network (or other solution). The only task of this network is to choose from a variety of algorithms — the best one solution according to the specified quality criteria (Figure 4).

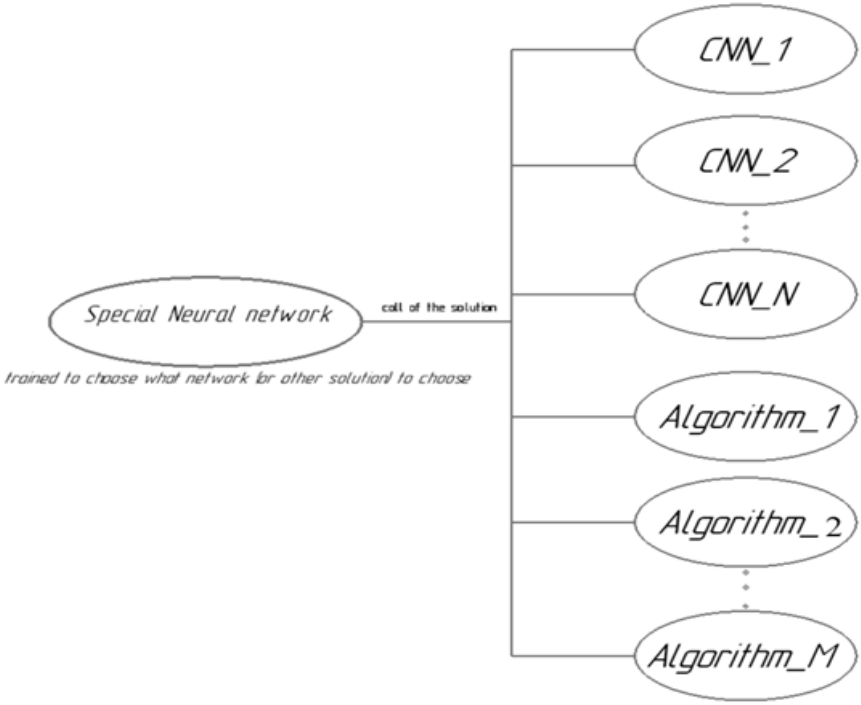

Figure 4. The proposed solution.

Let's look on the following example of our proposed solution (Figure 5). There is an FPGA with preloaded Special Neural Network (SNN) for choosing what CNN to use. It uses a small amount of chip space. The rest of chip space is free and turned off from static power consumption. The overall power consumption is low.

On the next step this SNN choses the best one solution according to the input data analyses and configures FPGA with the chosen configuration image from ROM. For example, it can be CNN_1 from Figure 4. Here the overall power consumption is higher comparing to the previous step.

Further, if the solution obtained by CNN_1 is not sufficient (does not satisfy some criteria), then the special SNN is loaded again to select a solution, and then it can load another configuration from the ROM, for example, Algorithm 2.

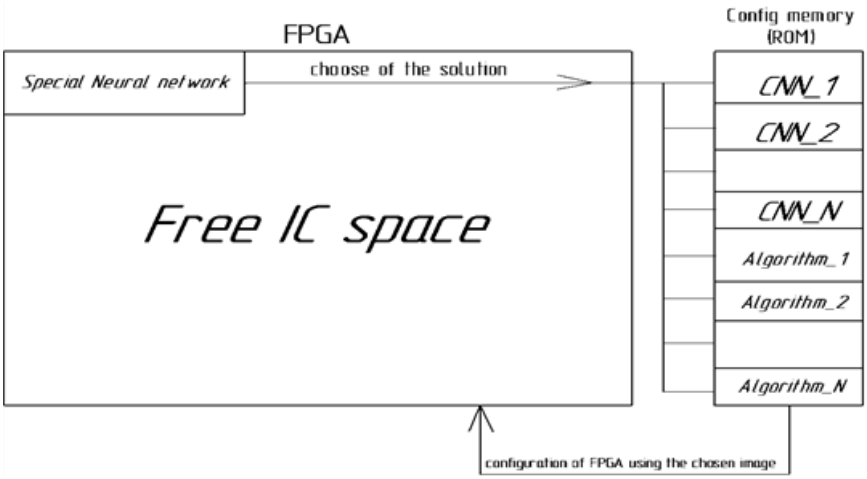

Figure 5. The proposed solution implementation.

One should admit that training SNN is a difficult task. In fact, it can be shown, that true optimal algorithm for SNN conditioned on input data should be as complex as networks that actually solves the task. But we consider usage of the approximation of optimal algorithm that can be magnitudes "cheaper" in terms of computational complexity. We are going to research the possible SNN architecture and its training strategy in future.

Anyway, there are many possible ways of using this approach. For example, it is possible, depending on the conditions, to directly call the algorithms sequentially, bypassing the call of a SNN. It is possible, as an option, to permanently have an operating SNN in the FPGA to constantly monitor the current decision and reduce the time to call another solution. A special neural network can also make decisions on loading several neural networks simultaneously (or other solutions in FPGAs) if it understands that the greatest probability is that it will be necessary to move to these solutions in the future according to the dynamics of changes in the input data. So, in general, the scope for creativity in the proposed approach is huge.

References

1. Malakhova E.Y., Shelepin E.Y., Malashin R.O. Temporal data processing from webcam eye tracking using artificial neural networks // Journal of Optical Technology. 2018. Vol. 85. No. 3. P. 186–188.

2. Malashin R. O., Anisimov N. A. Training Deep Neural Network for Accurate Age and Gender Recognition on Small Set of Data // Video and Audio Signal Processing in the Context of Neurotechnologies: book of abstracts. 2016. P. 19–22.
3. Malashin R. O. Extraction of object hierarchy data from trained deep-learning neural networks via analysis of the confusion matrix // Journal of Optical Technology. 2016. Vol. 83. No. 10. P. 599–603
4. Baptista Darío, Sheikh Shanawaz Mostafa, Lucas Pereira, Leonel Sousa and Fernando Morgado-Dias. Implementation Strategy of Convolution Neural Networks on Field Programmable Gate Arrays for Appliance Classification Using the Voltage and Current (V–I) Trajectory // Energies. 2018. V. 11. P. 2460
5. Tatar N., Holban S. A Bio Inspired Alternative to Huffman Coding // 11th International Conference on Development and Application Systems, Suceava, Romania. 2012, May 17–19. P. 179–182.
6. SongHan, Huizi Mao, William J. Dally. Deep Compression: Compressing deep neural networks with pruning, trained quantization and huffman coding // ICLR2016. P. 1–14.

Chapter 24.
Image enhancement with the use of object features

M.A. Titarenko, R.O. Malashin

Introduction

A common approach in computer vision is to separate low-level vision tasks, such as image enhancement, from high-level vision tasks, and solve them independently. In [Liu, Wen, 2019a], a method of teaching a deep neural network using high-level information as an additional quality control of noise suppression is proposed. In the case high-level information is extracted from another neural network that solves the problem of high-level computer vision [Liu, Wen, 2019a]. It is possible to extract high-level features in various ways. One can only use the network output as done in [Liu, Wen, 2019a]. Alternatively, it is possible to extract features from lower layers of the neural network [Liu, Wen, 2019b]. The current work uses the first approach.

The purpose of this work is to conduct a series of experiments on the training of a model consisting of two convolutional neural networks (the first solves the problem of image quality improvement, the second classifier) to solve the problem of classification in presence of noise and blur.

Experiments

In [Liu, Wen, 2019a], the cascade network architecture is proposed so that it processes the input of noisy images by successively combining a network for noise reduction (preprocess net) and another network for a high-level computer vision task (HL-network), with the goal to restore image that achieves maximum accuracy when performing various high-level tasks. A preprocess net is first applied to the input image, and then the reconstructed image is fed to the network performing a high-level task. In this work we have considered similar architecture.

During the experiment's dataset cifar10 was used. This dataset contains 60000 pictures of 10 object classes: cats, dogs, horses, etc. 50000 training sample images and 10000 test images were selected from the dataset.

Unet [Ronneberger et al., 2019] was used as preprocess net. Classification

was chosen as a high-level task. resNet20 [He et al., 2019] architecture was pretrained on cifar10 dataset (92.4 % accuracy). In further experiments with a cascade of two networks, weights of this trained model were used. The network training strategy is as follows: firstly, the high-level task network pretrained on clean images is initialized. In one pass the reconstructed image and high-level information is obtained. Image recovery quality and high-level information are used to change the weights of the network. Then classification and reconstruction loss are computed. Only weights in the preprocess net are updated by an error propagated back from the HL-network, which is similar to minimizing "perceptual" loss for the high-level task network. The weights of the HL-network do not change during the training. An important part of learning networks is the loss function, which is the subject of research of this work. Joint loss of denoiser and HL-network in the case is a weighted sum of the reconstruction loss and the high-level task loss. The reconstruction loss is the mean square error (MSE) between the output of the denoising network and the clean image. The classification loss is the cross-entropy between two vectors encoding the predicted label and the ground truth label.

The scheme of the cascade network and training strategy is depicted in figure 1.

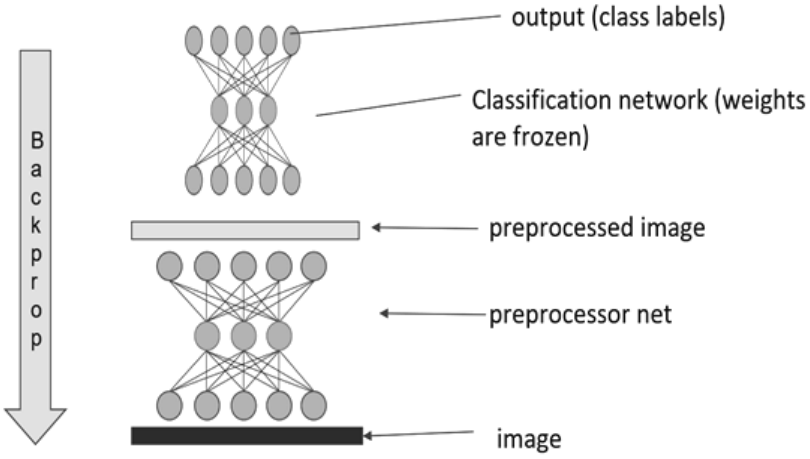

Figure 1. Cascade network architecture.

Two series of experiments with different types of distortions were carried out: with noise, and with blur. To complicate the task for preprocessor net, parameters of noise and blur were randomly picked from specific range. For

gaussian noise σ was in range from 3 to 80. Blur was generated with gaussian kernel with size in range from 1 to 7. Four experiments were performed in each series:

1. Single classifier. Only the classifier is trained with a classification loss.
2. Cascade of two networks. Only the Unet is trained with a classification loss.
3. Cascade of two networks. Only the Unet is trained with a low-level loss.
4. Cascade of two networks. Only the Unet is trained with a sum of classification and reconstruction losses.

Table 1 contains the results of the experiments with the accuracy (in percent) of the classification. For comparison we added the results of the network classifier, trained on clean images.

Table 1

Summary table with accuracy (in percent) of the classification of corrupted images for all trained models

Model	Type of experiment	Noise	Blur
Single classifier	Trained with distorted images	80.2	82.0
	Trained with clean images	52.2	70.6
Cascade of two networks	Classifier loss	53.1	20.1
	Reconstruction loss	73.2	44.1
	Sum of Classifier loss and Reconstruction loss	63.1	38.2

We've found out that training the cascade of networks on noisy images with classification loss provides unexpected dynamics. Figure 2 shows the training curves in that experiment.

According to graphs on figure 2 the model increases the classification accuracy throughout the course of training, but after 40th epochs, the quality (in terms of PSNR) of images starts to decline. This means that, in addition to solving the problem of denoising, Unet begins to introduce distortion into images that helps the classifier but reduces the PSNR.

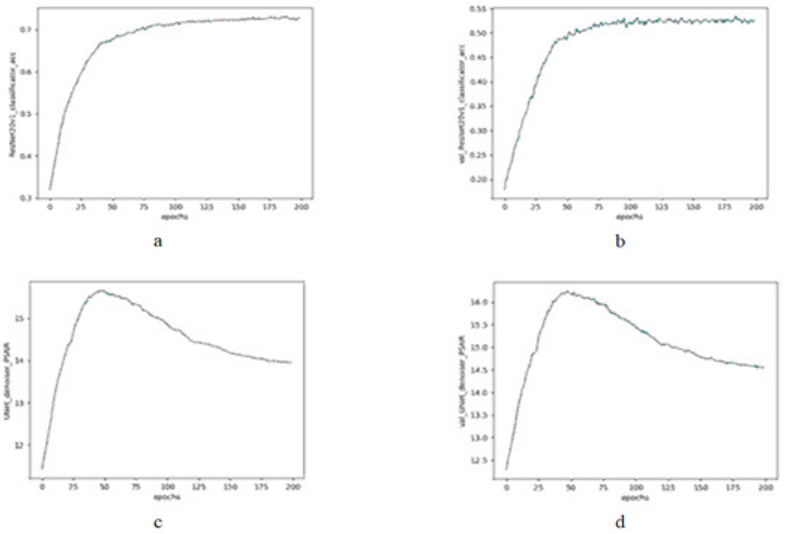

Figure 2. The training curves. (a) Classification accuracy on training sample. (b) Classification accuracy on test sample. (c) PSNR on training sample. (d) PSNR on test sample.

In order to check whether the Unet network can learn to repeat an image without distorting it by using high-level loss, an experiment was performed to learn preprocess net with clean images and classification loss only. In the process of learning the model overfits very quickly. As a result, the maximum accuracy of 36.4 % was achieved after the first epoch. Figure 3 show the accuracy on the test and training samples.

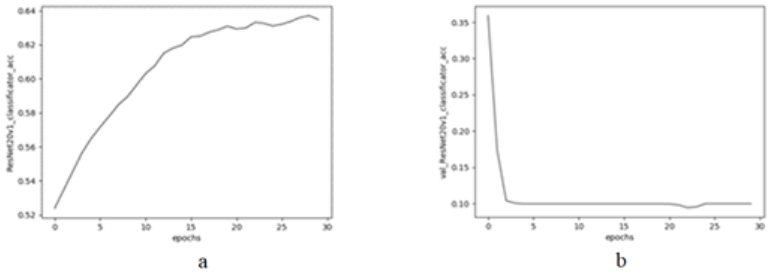

Figure 3. The training curves. (a) Classification accuracy on training set. (b) Classification accuracy on test set.

Conclusions

For all of the experiments with noise and blur cascade of networks showed results lower than single classifier network. For denoising experiments with two network maximum classification accuracy is obtained when training preprocessor network directly on corrupted-clean pairs of images with MSE. Propagating classification loss during training doesn't improve the result. To increase the accuracy, we are going to conduct a series of experiments backpropagating loss of the classifier network features computed on clean and corrupted images.

We have also shown that backpropagating high-level information from the top layer of classifier network when training preprocessor net can lead the latter to produce image distortion. The possible explanation is that preprocessor learns to reach some image space that is not covered by the training set. Exploiting this effect can help to find out some novel ideas on how to improve classifiers and how to fight adversarial attacks on them. We are going to investigate this in our future work.

It appeared to be more difficult to train cascade network with blurred images than with noisy images. For blurred images every experiment lead to overfitting. We've observed the same effect when training on clean images. That may be caused by too complex Unet model. We are going to investigate this in future experiments. However, the results show evidence that adding Gaussian noise to images in the scheme can have a regularization effect and prevent overfitting.

References

1. He Kaiming, Xiangyu Zhang, Shaoqing Ren and Jian Sun. Deep Residual Learning for Image Recognition. URL: https://arxiv.org/pdf/1512.03385.pdf (accessed: 29.06.2019).
2. Liu Ding, Bihan Wen. Connecting Image Denoising and High-Level Vision Tasks via Deep Learning. URL: https://arxiv.org/pdf/1809.01826.pdf (accessed: 29.06.2019b).
3. Liu Ding, Wen Bihan. When Image Denoising Meets High-Level Vision Tasks: A Deep Learning Approach. URL: https://arxiv.org/pdf/1706.04284.pdf (accessed: 29.06.2019a).
4. Ronneberger Olaf, Philipp Fischer, and Thomas Brox. U-Net: Convolutional Networks for Biomedical Image Segmentation. URL: https://arxiv.org/pdf/1505.04597.pdf (accessed: 29.06.2019).

Chapter 25.
Neural network models of second order visual filters

D.V. Yavna, V.V. Babenko, K.A. Ikonopistseva

Second-order visual filters decode spatial modulations of contrast, orientation, and spatial frequency. Using these mechanisms, we obtain the information necessary for figure-background segmentation, detection of textural boundaries, decoding monocular depth features, and reconstructing the three-dimensional surface structure [Dövencioğlu et al., 2013, Victor et al., 2017]. There are evidences that their outputs are involved in both bottom-up and top-down attention control [Barbot et al., 2012], and models may be of interest for the development of visual saliency maps. This makes their modeling especially relevant in theoretical and practical senses — both for a better understanding of fundamental perceptual mechanisms, and for developing algorithms for constructing visual salience maps and predicting an observer's attention shifts.

At the moment, there is a well-developed approach to modeling second-order mechanisms, based on both psychophysical and neurophysiological data [Graham, 2011]. Initially it was supposed and then was neurophysiologically confirmed (e.g. [Zhou, Baker, 1996]) the existence of special neural elements — second order filters, which combine the rectified outputs of the first order filters. Simple striate neurons are considered as these latter. First-order filters intrinsically may work as detectors of spatial brightness modulations, but are not able to detect periodic spatial changes in contrast, orientation, or spatial frequency. This requires rectification and second-order filtration at a lower spatial frequency — similar to principles of decoding modulations in analog radio communication. "Filter — rectify — filter" (FRF) is one of the generally accepted names of such models.

Different versions of the models well explain the experimental effects of perceiving spatial heterogeneities in artificial stimuli. However, the details of such models, as well as the results of different authors, may not coincide and even contradict each other. Thus, such issues as the organization of receptive fields of second-order filters, the ratio of orientation settings of first and second-order filters, the specificity of mechanisms to the modulated feature, and a number of other questions were discussed for a long time [Babenko,

Ermakov, 2013]. For a number of such issues, there is still no generally accepted point of view. Thus, despite the seeming simplicity of the modeling approach, the implementation of a realistic computer model using digital image filtering is difficult. This is explained both by the contradictions in the results of different studies, and by the need for an empirical fitting of a set of parameters that make the model quite architecturally and computationally complex.

Modern convolutional neural networks are universal tools for solving hard-to-formalize tasks. We believe that the modeling of second-order visual mechanisms using modern neural networks can be performed more efficiently in comparison with earlier approaches based on digital image filtering. The effect of modeling using neural networks is to eliminate the need for "manual" fitting of model parameters, as well as to significantly reduce development time and eliminate subjective factors. Also, in the common case, the convolutional neural network should be characterized by greater invariance to random changes and distortions in the image.

We investigated the trainability of the convolutional neural network in classification and demodulation of spatial modulations that are defined by periodic changes in contrast, orientation, and spatial frequency. Training was conducted using artificial textures which were randomly modified in modulated local feature, the slopes of the carrier and envelope axes, the carrier and envelope wavelengths, the phase shift of the modulations, and in average brightness and contrast (Figure 1). The texture synthesis algorithm is based on changing the parameters of the synthesized micropatterns depending on their location; it is described in detail by N. Prins and F. Kingdom [Prins, Kingdom, 2003].

Continuous trigonometric functions were used as modulators. Texture sizes were 256×256 pixels in grayscale. A total of 15000 images were generated, 5000 for each modulated attribute. 3500 images of these 5000 were taken for learning, the rest were used for validation and testing. Thus, the number of images in the training sample was 10500.

Training calculations were done using Keras and Tensorflow. Initially, the network was trained to classify the modulated feature. It was possible to train the network of five convolutional layers with 98 % accuracy. "Relu" activations were used all hidden layers. Filter sizes from first to last convlayer are 3×3, 3×3, 5×5, 5×5, 7×7, there were 64 filters on each layer. After each such layer, 2x2 pooling was performed. Networks with fewer convolutional layers could not be trained at an acceptable level of accuracy.

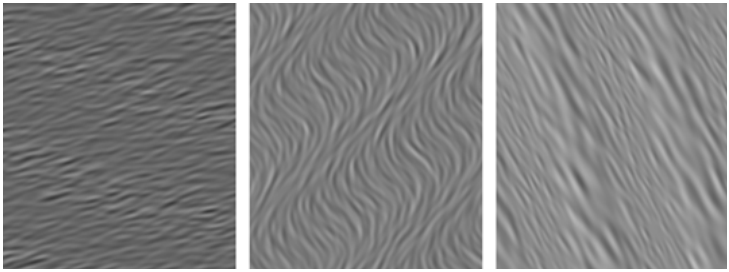

Figure 1. Modulated textures formed from Gabor micropatterns. From left to right: modulation of contrast, orientation, spatial frequency.

Visualization of filters learned by convolutional layers using gradient ascent in input space [Chollet, 2017] showed that the main operations for processing the input signal are performed in layers 1–4, and most of the filters specialize in the analysis of spatially distributed texture features. The network does not produce local detectors of oriented gradients which often learned by convnets being trained on object images. Special attention should be paid to the second layer, where the signal is likely splitting by spatial frequencies (Figure 2).

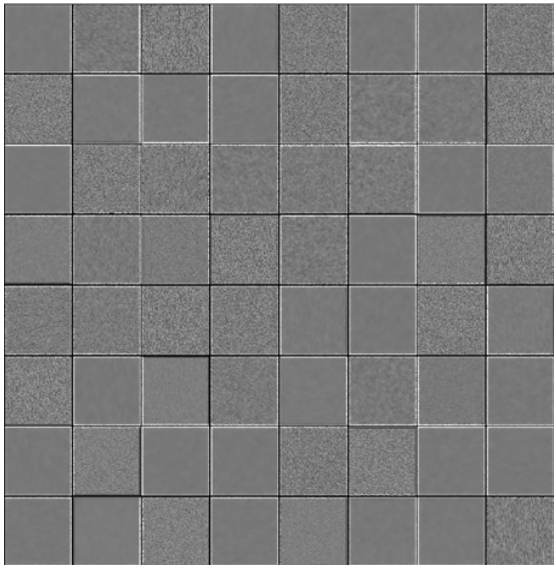

Figure 2. Patterns that cause the maximum response of filters in the second convolutional layer.

In contrast to the underlying ones, the filters of the fifth convolutional layer specialized mainly on “global stripes” [Graham, 2011], so it can be considered as a decision-making layer (Figure 3).

Thus, we were able to verify the possibility of training the simple convnet for classifying spatial modulations in a reasonable time with good accuracy.

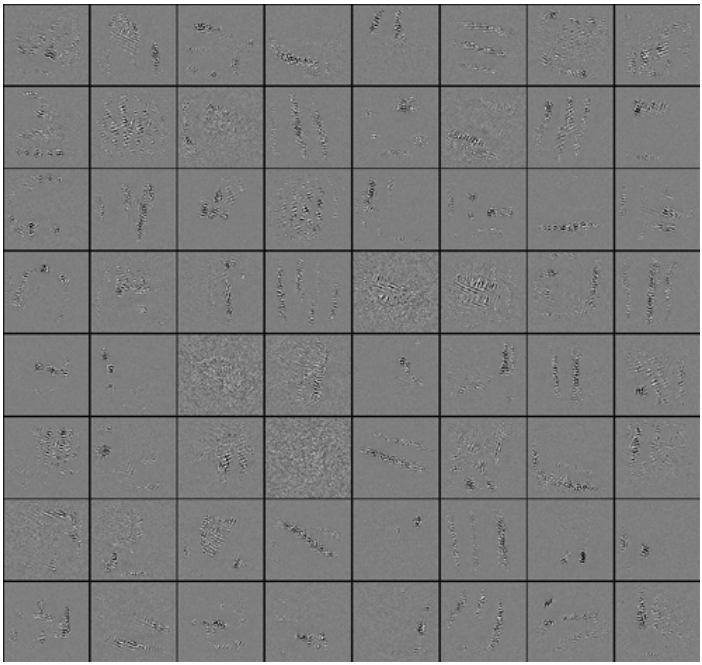

Figure 3. Patterns that cause the maximum response of filters in the fifth convolutional layer.

After training the classifier we proceeded to the develop of decoders which are architecturally similar to denoising autoencoders. We trained models specific to a particular modulation, as well as a non-specific model that decodes modulations regardless of modulated feature. For both specific and non-specific models, an acceptable demodulation quality was achieved with an eight-layer (4 encoding and 4 decoding layers) auto-encoder. It should be noted that the coding — decoding accuracy for specific models was slightly higher than for non-specific ones. An example of the texture processing using a model specific to spatial frequency modulations is shown in Figure 4.

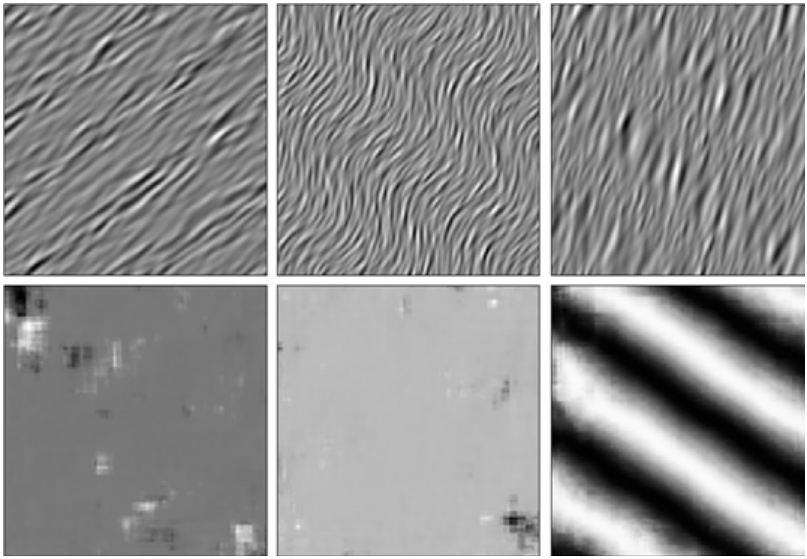

Figure 4. Modulated textures (top) and the results of the spatial frequency modulation decoder (bottom). From left to right: modulation of contrast, orientation, spatial frequency.

The results suggest that coding of spatial modulation requires less convolutional layers than classification, and it's possible to create the universal decoder of spatial heterogeneity signals using a more diverse training set.

Currently, convolutional neural networks, originally designed under the influence of the discoveries of D. Hubel and T. Wiesel [Malakhova, 2017], are of great interest among researchers of the visual system. However, it should be borne in mind that modern implementations of neural networks are based on tensor mathematics, but not on models of natural neurons, and the developers themselves warn about the dangers of direct analogies [Chollet, 2017]. Artificial neural networks should be considered first of all not as models of structures, but as models of functions, e.g. recognition of emotional faces [Shelepin, 2017]. Using the artificial networks for modeling the brain functions gives new possibilities in saliency maps development, making it possible to test hypotheses about the contributions of certain physical characteristics of the image to the "attractiveness" of a particular fragment of the scene.

Supported by RFBR, project No 18–29–22001.

References

1. Babenko V. V. and Ermakov P. N. Vision and the binding problem [in Russian]. Moscow: Credo Publishing, 2013.
2. Barbot A., Landy M. S., and Carrasco M. Differential effects of exogenous and endogenous attention on second-order texture contrast sensitivity // Journal of Vision, vol. 12, no. 8, pp. 6–6, Aug. 2012.
3. Chollet F. Deep Learning with Python, 1st ed. Greenwich, CT, USA: Manning Publications Co., 2017.
4. Dövencioğlu D. N., Welchman A. E., Schofield A. J. Perceptual learning of second order cues for layer decomposition // Vision Res., vol. 77, pp. 1–9, Jan. 2013.
5. Graham N. V. Beyond multiple pattern analyzers modeled as linear filters (as classical V1 simple cells): useful additions of the last 25 years // Vision Res., vol. 51, no. 13, pp. 1397–1430, Jul. 2011.
6. Malakhova E. Y. Presentation of information in neural networks when recognizing image semantics [in Russian] // Proceedings of the XXIII Congress of the P. Pavlov Physiological Society, Voronezh, 2017, pp. 1642–1644.
7. Prins N., Kingdom F. A. A. Detection and discrimination of texture modulations defined by orientation, spatial frequency, and contrast // J. Opt. Soc. Am. A, vol. 20, no. 3, pp. 401–410, 2003.
8. Shelepin Y. E. Introduction to neuroiconics [in Russian]. St. Petersburg: Trinity Bridge Publishing, 2017.
9. Victor J. D., Conte M. M., Chubb C. F. Textures as Probes of Visual Processing // Annu. Rev. Vis. Sci., vol. 3, no. 1, pp. 275–296, Sep. 2017.
10. Zhou Y. X., Baker C. L. Jr. Spatial properties of envelope-responsive cells in area 17 and 18 neurons of the cat // J. Neurophysiol., vol. 75, no. 3, pp. 1038–1050, 1996.

Chapter 26.
Gioconda's Smile — from biological to artificial neural networks

O. V. Zhukova, K. Yu. Malakhova, Yu. E. Shelepin

Introduction

The understanding of recognition of facial expressions by the human visual system and modeling of this process with artificial neural networks remains an important problem of the vision sciences. Existing algorithms quite successfully cope with recognition tasks in above-threshold conditions. When decision is made in the presence of uncertainty, the effectiveness of such models drops significantly. An example of the uncertainty in the perception of facial expressions is the "smile" of the Mona Lisa. Leonardo da Vinci perfected the change in the curve of the lips, imitating a smile, to a threshold value. At threshold values of the signal (smile), under the influence of the internal noise of the visual system, facial expressions cause the observer to be uncertain (if the smile is present or not). The most effective algorithms in computer vision are convolutional neural networks, their performance is comparable to humans or even exceeds it. In contrast to the algorithms of the previous generation, neural networks efficiently work with natural images, similar to those that are found on a daily basis, and do not require manual programming of features: the selection of image characteristics and identification of their relationship to the final task. Deep learning models learn features automatically during the training process. They also demonstrate the ability to work with images regardless of the lighting conditions, size and view angle of the captured object. Although architectures of the models evolve at unprecedented rates, the core principles remain the same: the perceptron learning [Rosenblatt, 1965] and the hierarchical processing of the visual signal [Hubel et al., 1962; Fukushima et al., 1982], both derived from the observations of neural activity in the brain. As a result, artificial neural networks inherit functional properties of the biological prototype and naturally become a model of the visual cortex, allowing for the exploration of recognition process based on the analogies between these systems.

In this study, we conduct a comparative analysis of the capabilities of biological and artificial neural networks in recognition of facial expressions in the conditions of uncertainty.

Experiments

Neurophysiology of emotion recognition

In the neurophysiological part of the study, we recorded neural activity of 24 subjects while they were performing emotion recognition task. The stimuli consisted of generated human faces (FaceGen — Singular Inversions, Canada) divided into two categories. The first category included images of 36 identities with pronounced facial expressions of joy or sadness and six-degree head turns from left to right on the built-in FaceGen scale (above threshold decision-making conditions). The second category included images of the same identities with neutral facial expressions and zero rotation (full face), thus, enforcing decision making under uncertainty. The stimuli were presented in four blocks: in blocks 1 and 3 images with neutral facial expression (category 2); in blocks 2 and 4 images with facial expression (category 1). The subjects were instructed to determine either the facial expressions or the direction of the head rotation of a virtual person. The responses were given by the left or right click of a mouse. The subjects were not instructed about the presence of images with a neutral facial expression and zero rotation. Such images were regarded as stimuli under a threshold for recognition. Thus, blocks 1 and 3 simulated extreme uncertainty conditions.

Modeling with artificial neural networks

In the second part of the study, we implementation the process of emotion recognition using a convolutional neural network selected because of it functional similarities to the processing in the ventral visual pathway [Guclu et al., 2015; Kriegeskorte, 2015]. As a base model we used VGG Face [Parkhi et al., 2015], trained to identify celebrities on a dataset of 2.6 million images collected on the Internet. The network was chosen because of its alleged ability to distinguish facial expressions learned implicitly as an augment for identification process. We retrain fully-connected layers on a dataset of 1000 images categorized into two facial expressions (happiness and sadness). As the output, the network predicts the probability with which an image belongs to the category ‘happiness’.

Convolutional neural networks process the image with filters that encode visual features in the form of weight matrices. The essence of the convolution operation is to define the matching of an input to the convolution filter (or kernel). Since the filter size is smaller than the image, it is applied sequentially with a small step to cover the entire image, and the result is summed and recorded in the same position of the output image. Thus, an activation map was formed, which reflected the correspondence of an image to a filter. Filters of the first convolutional layer highlight simple features signs such as color and slope of the line — they are universal for almost all networks working with images, regardless of the task being performed [Malakhova, 2018].

The neurons of subsequent convolutional layers have larger receptive fields of the image and respond to increasingly complex shapes of objects, resulting in the ability to discriminate among categories of objects. Nevertheless, in convolutional layers the role of spatial arrangement in the neuron's response is preserved. It is only in the fully connected layers, when neurons response become invariant to the position or size of an object. This property of invariance is achieved by the transmittance of signal from all neurons in a convolutional layer to a neuron in fully-connected layer. Thus, the receptive field covers the whole image and takes into account all possible spatial locations of objects.

Results

Results in a neurophysiological study series

Brain activity is studied using the functional magnetic resonance imaging. In the condition where images with explicit facial expression and head turns were presented, we observed two activation patterns indicated in Fig 1A by different colors. Yellow color indicates activation during performing the rotation identification, while the blue indicates the emotion recognition. Note that both turn and emotion there were clearly expressed in this category of generated images. It can be assumed that in the presence of both features, they are automatically compared and ranked, for example, according to the degree of relevance, significance, complexity. Apparently, the activation of the Default network mode can be associated with the task of determining of the head turn. During the task of emotion recognition, activation is observed in the areas of the brain that are responsible for the emotional perception of stimuli (e.g., in the insular cortex).

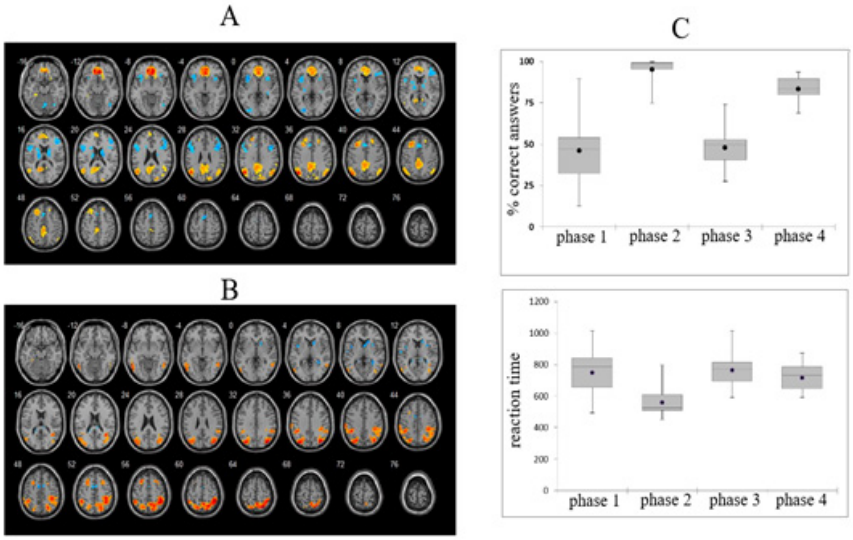

Figure 1. Activation maps obtained by comparison of neural response to stimuli of two categories. A) Subtraction of block 4 from block 2. Both blocks contain faces with facial expressions of joy or sadness and head rotation to the left or to the right. However, the instruction was changed: in block 2 subjects were asked to identify rotation, while in block 4 they determined facial expressions; B) Subtraction of block 3 from block 1. In both blocks images had neutral facial expressions and no head rotation. Likewise to A, the instruction was changed: in block 1 subjects responded to rotations, in block 3 — to the facial expressions. C) Comparison of reaction time and accuracy of the recognition in different blocks. The x-axis shows the block of the experiment. In the case of blocks 1 and 3, the percentage of clicks on the right and left mouse buttons was counted (responses 'head rotation to the right' and 'joy' facial expression were chosen as the references). The values in blocks 2 and 4 illustrate the percentage of correct answers. Black dots point to the average value for the group of subjects. Data are presented on a group of subjects (24 people) (without FDR-corr., $P < 0.001$).

Under the second condition both features were absent — images depicted faces with neutral emotions and no head rotation (Fig. 1B). As a result, two patterns of a large-scale neural network activation were observed. Orange color indicates activation in the rotation recognition task, which, as expected, involves the dorsal visual pathways responsible for the processing of spatial relationships. Blue color indicates activations during the task of emotion

recognition, characterized by the involvement of areas responsible for the emotional perception of stimuli (for example, the insular lobe as in previous condition).

Response time and accuracy of the subjects responses presented on the Figure 1C. It can be seen that the recognition of facial expressions and head rotations in blocks 1 and 3 (under conditions of uncertainty) was a significant difficulty for the subjects, and led to a slower reaction time. The likelihood of recognizing facial expressions decreased to the level of random guessing, about 50 %.

Thus, in the neurophysiological experiment, various patterns of large-scale neural network of the human brain were identified according to the experimental paradigm (alternating obvious and uncertain conditions for decision-making). In the case of simultaneous presence of such features as head rotations and facial expressions on a stimulus, it is likely that the features are automatically identified, semantically evaluated and discriminated despite the instruction. That results in the activation of the dorsal visual pathways responsible for the description of spatial relationships during emotion recognition. And, vice versa, in the task of identifying the head rotation, activation is seen in the medial prefrontal cortex, which is known for the conscious and unconscious empathy of the other person's emotional state.

Results in a neurotechnological study series

The architecture of the deep neural network consisted of 13 convolutional and 3 fully connected layers. We retrained fully-connected layers to categorize facial expressions on manually labelled dataset of 1000 images. The accuracy of categorization on a test set was 97 %. We then tested the model on the images with neutral facial expressions: the likelihood of image categorization into 'joy' class was in this case at the level of random guessing, about 50 %. For example, when recognizing the indefinite smile of the Mona Lisa, the model assigned a probability of 0.69 that the image belongs to the 'joy' class.

The Figure 2 visualizes the properties of the model and its response to the image. Filters of the first convolutional layer detect simple features such as color and orientation of a line (Fig. 2B); they are universal for almost all networks working with images, regardless of the performed task. Figure 2C depicts examples of matching the filters with the input image, so-called activation maps, where the light areas indicate high similarity between a filter and a fragment of the picture.

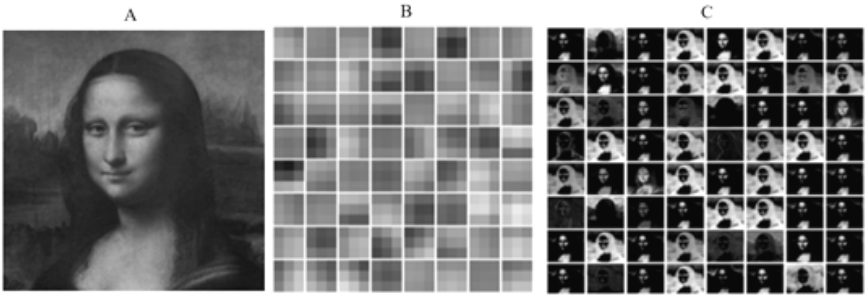

Figure 2. Visualization of the convolutional neural network analysing the Mona Lisa image. A) original image; B) filters of the first convolutional layer of size 3×3 pixels and 3 channels; C) activation maps obtained through application of the first convolutional layer filters to the image. Light areas indicate high similarity between the filter and the fragment of the picture, while dark areas denote the absence of activation.

Conclusions

The ability to recognize emotions and facial expressions, such as a smile, is a highly accurate process in normal conditions for both humans and artificial neural networks. However, under the conditions of uncertainty (threshold and noisy images) the performance decreases to the level of random guessing in both systems. Observed similarities in performance may arise as a result of the functional resemblance of the systems with the core principle of the matched filtering as a similarity measure between the presented stimuli and a pattern learned by the network (e.g. smile).

With the advantages obtained through mimicking the visual processing of biological systems, artificial neural networks inherit their fundamental limitations. On the other hand, the uncertainty of the model's decision on the Gioconda's smile (with probability 0.69 the image was categorized into the 'joy' category) may originate in the training dataset. If the dataset does not contain enough examples of uncertain images, the model cannot learn how to work with such cases. The latter, in turn, is limited by our ability to recognize emotions under near threshold conditions.

References

1. Fukushima K., Miyake S. Neocognitron. 1982. A self-organizing neural network model for a mechanism of visual pattern recognition. In Com-

petition and cooperation in neural nets. Berlin: Springer Heidelberg. P. 267–285.
2. Guclu U., van Gerven M.A. 2015. Deep neural networks reveal a gradient in the complexity of neural representations across the ventral stream. In J. Neuroscience: The official journal of the Society for Neuroscience. V. 35. P. 10005–10014
3. Hubel D.H., Wiesel T.N. 1962. fields, binocular interaction and functional architecture in the cat's visual cortex. In J. Physiology. V. 160. P. 106–154
4. Kriegeskorte N. 2015. Deep neural networks: A new framework for modeling biological vision and brain information processing. In Annual Review of Vision Sci. V. 1. P. 417–446.
5. Malakhova E. Yu. 2018. Processing of visual information in artificial and biological neural networks. In Neurotechnology. SPb .: ed. VVM. C. 338–349.
6. Parkhi O.M., Vedaldi A., Zisserman A. 2015. Deep face recognition In BMVC. V. 1 № 3. P. 6.
7. Rosenblatt F. 1965. Principles of neurodynamics (perceptron and theory of brain mechanisms). M.: World. 480 p.

NEURAL NETWORKS IN CLINICAL RESEARCH

Chapter 27.
Acupuncture as a Method of Neural Network Regulation

G. O. Andreeva, K. M. Naumov, D. V. Pechenchin

Acupuncture is a set of different methods for mechanical, physical, chemical or biological stimulation of biological active points which have been successfully in use to treat ailments for over 5,000 years. Today this form of treatment is officially recognized by healthcare systems of Eastern, as well as Western countries; the mechanisms of such stimulation, however, still remain unknown and are being intensively studied.

The plethora of published research and author's own investigations allow to claim for the efficacy of acupuncture, including with regard to enhanced neuroplasticity — the fact that allows to use this method in different stages of disease, i.e. prevention, relief of symptoms, and rehabilitation.

Traditional Oriental medicine suggests that acupuncture stimulation is based on a so-called system of meridians that interconnect all levels of human organism. Current knowledge about the structure and functions of nervous system allows to treat it as a multitude of neural networks of different complicity. Hereby, more complicated neural network structures rely on simpler neuronetworks of lower levels as a basis. This framework shows that in general, it is the ability of acupuncture to elicit a systemic response in central structures by stimulating peripheral points that underlies its mechanism of action.

In a generalized way acupuncture acts on the following levels: peripheral, segmental, and central.

The peripheral level (i.e. peripheral nerves and nerve plexuses) is the most well-studied and has been proved by various research evidence [Ma et al., 2005; Berger, 2008, Goldman et al. 2010, Stux, 2000, Takano et al., 2012]. Acupuncture mechanisms rely on the following effects:

- local reactions at the needle-tissue interface (aseptic inflammation);
- local relaxation of contracted muscles;
- locally enhanced microcirculation;
- local immune response (mediated by lymphatic system and mast cells);
- local adenosine release and improve antinociceptive effect;

- neural response to stimulation of A-delta and C-axons;
- modifications of neural plasticity on the level of afferent peripheral fibers and formation of new synaptic contacts with nerve terminals;
- stimulation of DNA synthesis to activate tissue recovery and replacement at sites of acupuncture-caused injuries.

On the Figure 1A some this effect are demonstrate very schematically. The Figure 1B demonstrate the technology of immersing a needle for acupuncture along the edge of a cube of tissue conditionally selected and presented in three-dimensional space is demonstrated.

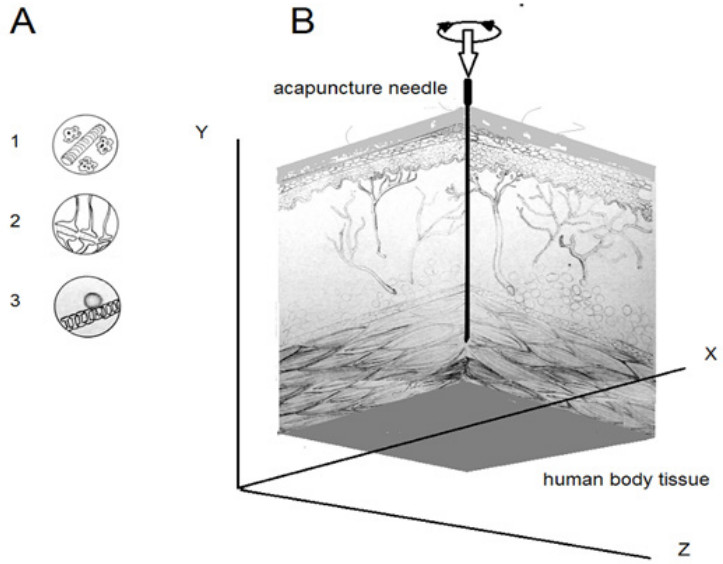

Figure 1. Peripheral effects (A) and technology (B) of acupuncture.

1 — aseptic inflammation, enhanced microcirculation, *2* — modification of neural activity, *3* — local adenosine release.

Segmental effects of acupuncture are associated with more complicated and multidirectional interactions [Ivanichev, 1999, Vasilenko, 2004]:

- 'gate control' mechanism and its relevance in suppressing pain impulses at peripheral receptor sites by means of selective activation of thick myelinated fibers and attenuation of impulse transduction via small poorly myelinated and unmyelinated fibers [Melzack R., Wall P. D., 1965];

- release of endorphins (enkephalins and dinorfine) in the dorsal horns of spinal cord, which also induces analgesic effect;
- activation of neurons in the spinal dorsal horns and transduction of stimuli to the brain stem via spinothalamic and spinoreticular tracts;
- activation of descending inhibitory pathways
- regulation of visceral organs through dermatovisceral reflex pathway.

The effects of acupuncture resulting from stimulation of spinal cord (SC) segmental levels are used for treating traumas and injuries of peripheral nerves, as well as regional pain and myotonic syndromes. More complicated mechanisms involve the autonomic nervous system that includes cerebral structures, as well as SC segmental apparatus, SC intermediolateral nuclei, the sympathetic column, vegetative ganglia, and plexuses of the thorax, abdomen, and lesser pelvis. Taken together with neural networks of individual organs (heart, bowel) known as the 'metasympathetic' nervous system, the autonomic nervous system reveals to us its staggering complexity. This system is most likely to be responsible for positive response to treatment of vegetative-vascular dystonia, gastrointestinal disorders, hypertension, bronchial asthma, and other systemic disorders.

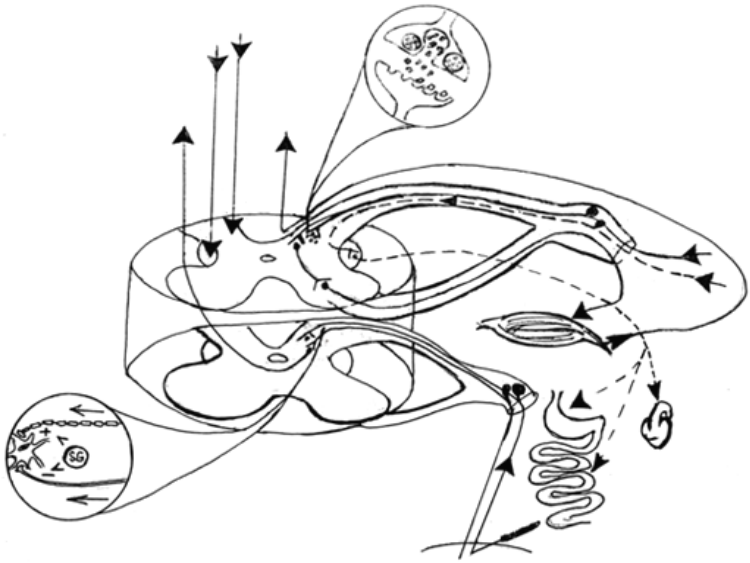

Figure 2. Segmental effects of acupuncture.

Electromyoneurography, laser doppler and electrical skin resistance measurements are relevant methods of control.

Central effects of acupuncture are mediated by neural networks of the cortex and basal ganglia. There are several underlying mechanisms:

- stimulation of central neuronetworks: systemic excitatory or inhibitory action on primary and secondary sensorimotor cortical fields, the areas of thalamus, the insular, frontal cingulate gyrus, and hippocampus [Wu et al., 2010; Lo et al., 2003; Lo et al., 2005];
- activation of primary cortical fields due to specificity of responses to stimulation of acupuncture points [Cho et al., 2013];
- mobilized limbic-paralimbic neuronetworks, including the caudate nucleus, amygdala, hippocampus, dorsal cingulate gyrus, and medial prefrontal cortex [Cho et al., 2013];
- activation of the hypothalamic-pituitary-adrenal axis along with ACTH production by hypothalamus and activated adrenal glands; the release of nonopioid neuropeptides, that regulate hypothalamic-pituitary axis [Cho et al., 2001; Ma et al., 2005], modifies pain perception and immune responses.

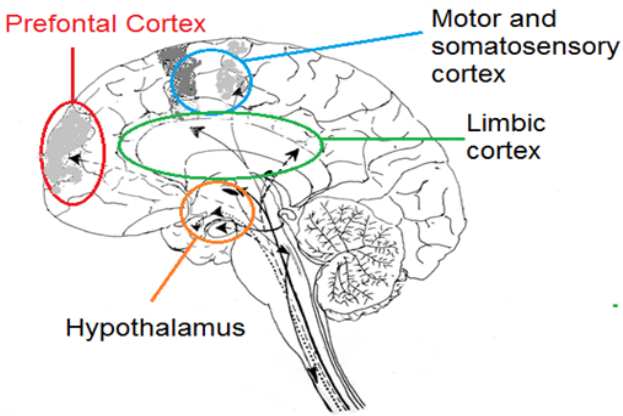

Figure 3. Central effects of acupuncture.

There is evidence that raphe nuclei, reticular formation of the brainstem, central grey matter, hypothalamus, thalamus, and cortex of the large hemispheres are intensively engaged in acupuncture stimulation at the central level [Pariente et al., 2005; Napadow, 2007; Berger, 2008]. The release of enkephalins,

monoamines, serotonin, and noradrenaline in the midbrain (periaqueductal gray) activates the descending antinociceptive system. This induces physiological analgesia and normalizes homeostasis, including activation of immunity, cardiovascular and respiratory system, which also accelerates tissue healing.

Neuronetworks of autonomic nervous system can be outlined with some degree of approximation. Thus, parasympathetic activity is believed to be regulated by hypothalamic nuclei (release of endorphins and nonopioid neuropeptides), the nuclei of the midbrain (glutamate) and medulla oblongata (opioids and GABA), whereas sympathetic activity is regulated by medulla oblongata structures. Prefrontal cortex is engaged in the activity of both parts of the ANS [Li et al, 2013].

Such methods as EEG and multipurpose transcranial duplex sonography are used to measure central effects of acupuncture. Cerebral spectroscopy and functional MRI also show promise [Hui et al., 2010].

Advanced functional MRI imaging provided evidence in favor of both general non-specific and regional specific responses generated by acupuncture stimulation in certain areas of the brain. In particular, it was demonstrated that stimulation of GB37 acupoint activates the visual area (BA18 and BA19) of the occipital lobe of the cerebral cortex [Cho et al., 2013]. The name of GB37 point — Guangming — means 'bright light'. It is located on the anterior side of the fibula and is used to treat vision-related disorders, i. e. farsightedness, nearsightedness, night blindness, and eye pain.

The central effects of acupuncture stimulation are used for treatment of sleep disorders, pain syndromes (especially in patients with secondary disfunction of thalamus), various behavioral spectrum disorders (anxiety disorders first and foremost).

Today spectral analysis of heart rate variability (HRV) offers the most accessible metrics to assess the effects of acupuncture stimulation. This method allows clinicians to gain control over acupuncture stimulation effect by adjusting the treatment scheme to every individual patient.

This method is exceptionally efficient in correcting vegetative disorders. Thus, it allows to prove that different modalities of stimulation applied to acupuncture points modify the activity of sympathetic and parasympathetic divisions of ANS. For example, acupuncture stimulation of the He gu points using tonification technique enhances sympathetic activity, whereas sedation technique applied to the Zu san li position enhances parasympathetic activity.

It is pivotal to continuously measure treatment efficacy, because central structures of the ANS may respond differently to acupuncture stimulation.

The case of a male patient, 21y, with no significant medical history remarkably demonstrates the effects of acupuncture on patient's vegetative state. He was treated with acupuncture using disposable sterile needles (0,3x25mm) inserted in the Qu chi (LI-11), Zu san li (St-36) positions at the depth of 25mm perpendicular to skin surface and retained for 20 min. Needles were rotated clockwise and counterclockwise at instant needling and by the end of needling. The HRV analysis was performed before needling and 10 min after needles were removed. Before an acupuncture procedure the HF component of HPV moderately dominated the LF component. After the procedure there was an increase in the total power (TP), VLF, LF/HF ratio, and LF, with a decreasing effect on HF, which supports the regulatory effect of acupuncture mediated by sympathetic and parasympathetic divisions of the ANS, as well as central structures.

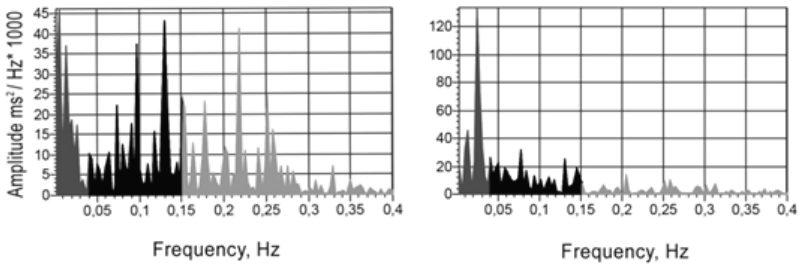

Figure 4. Spectral analysis of heart rate variability before and after acupuncture.

Conclusion: By modifying afferent flow patterns, different acupuncture techniques affect neural networks of different levels and complicity. This optimizes their performance and corrects functional disorders, which allows to treat both peripheral disorders and systemic diseases, provided that the modality of acupuncture treatment has been well-tailored. Such viewpoint is entirely compatible with the experience of using acupuncture in clinical practice (according to research studies and our own observations) and allows to use unbiased methods to monitor efficacy of treatment.

References

1. Berger P. Acupuncture in a western medical context / P. Berger // Journal of pain the South African. 2008. Vol. 3, № 1. P. 9–13.

2. Cho Z. H. Functional magnetic resonance imaging of the brain in the investigation of acupuncture / Z. H. Cho, C. S. Na, E. K. Wong [et al.] // In: Stux G., Hammerschlag R. (Ed.) Clinical Acupuncture. Berlin: Springer-Verlag, 2001. 227 p.
3. Cho Z. H., C. S. Na. E. K. Wang. S. H. Lee I-K. Hong Functional Magnetic Resonance Imaging of the Brain in the Investigation of Acupuncture, 2013.
4. Hui K. K.S. Monitoring acupuncture effects on human brain by fMRI / K.K.S. Hui, V. Napadow, J. Liu et al. 2010. http: // www. jove. Com / details.php?id = 1190, doi: 10.3791/1190.
5. Ivanichev G. A. Sensornoye i reflektornoye vzaimodeystviye v mekhanizmakh akupunktury / G. A. Ivanichev. Kazan': Matbugat yorty, 1999. 144 s .
6. Li Q. Q. Acupuncture effect and central autonomic regulation / Q. Q. Li, G. X. Shi, Q. Xu [et al.] Evid Based Complement Alternat Med. 2013; 2013: 267959. Published online 2013 May 26. doi: 10.1155/2013/267959.
7. Lo Y. L., Cui S..L, Fook-Chong S. The effect of acupuncture on motor cortex excitability and plasticity. Neuroscience Letters. 2005; 384 (1–2):145–149. doi: 10.1016/j.neulet.2005.04.083.
8. Lo Y. L., Cui S. L. Acupuncture and the modulation of cortical excitability. NeuroReport. 2003; 14 (9):1229–1231. doi: 10.1097/00001756–200307010–00008.
9. Ma Y. T. Peripheral mechanisms of acupuncture / Y. T. Ma, M. Ma, Z. H. Cho // Biomedical acupuncture for pain management: an integrative approach. Elsevier Churchill Livingston USA, 2005. Vol. 3. P. 26–34.
10. Melzack R. Pain mechanisms: a new theory / R. Melzack, P. D. Wall // Science. 1965. Vol. 150, № 3699. P. 971–979.
11. Napadow V. Hypothalamus and amygdala response to acupuncture stimuli in carpal tunnel syndrome / V. Napadow N. Kettner, J. Liu [et al.] // Pain. 2007. Vol. 130, № 3. P. 254–266.
12. Pariente J. Expectancy and belief modulate the neural substrates of pain treated by acupuncture / J. Pariente, P. White, R. S. Frackowiak [et al.] // Neuroimage. 2005. Vol. 25, № 4. P. 1161–1167.
13. Stux G. Clinical acupuncture / G. Stux, R. Hammerschlag // Springer-Verlag Berlin Heilderberg, 2001. 223 p.
14. Vasilenko A. M. Neyroendokrinoimmunologiya boli i refleksoterapiya / A. M. Vasilenko // Refleksoterapiya. 2004. № 1(8). S. 7–19.
15. Wu P. Acupuncture in poststroke rehabilitation: a systematic review and meta-analysis of randomized trials / P. Wu, E. Mills, D. Moher [et al.] // Stroke. 2010. Vol. 41, № 4. P. 171–179. doi: 10.1161/strokeaha.109.573576.

16. Yoshimoto K. Acupuncture stimulates the release of serotonin, but not dopamine, in the rat nucleus accumbens / K. Yoshimoto, F. Fukuda, M. Hori [et al.] // Tohoku J. Exp. Med. 2006. Vol. 208, № 4. P. 321–366.

Chapter 28.
Identification of visual and spatial disorders in Parkinson's disease

P. S. Dynin, K. M. Naumov, I. V. Litvinenko, M. R. Alizade

Research objective

A research of frequency of occurrence of visual and spatial disorders at patients with Parkinson's disease

Introduction

Impaired cognitive functions are an integral part of the clinical picture of the late stages of Parkinson's disease (PD) [Litvan et al., 2018]. As the disease progresses, there is a regular increase in cognitive deficit due to mild disorders, such as problems with operative memory and attention, up to severe forms reaching the level of dementia [Dawson et al., 2018]. In a number of works, special attention is paid to such a form of cognitive impairment as visual and visual-spatial impairment (VSI) [Weintraub et al., 2018]. This type of disorder is characterized by a number of manifestations that adversely affect the social adaptation of patients with PD. These include a violation of spatial orientation and understanding of the proportions of surrounding objects, color perception, changes in the perception of the contrast of objects, facial recognition, visual illusions and hallucinations [Weintraub et al., 2018]. In turn, the most frequent manifestation of the considered symptoms are visual illusions and hallucinations, constituting about 30 % of the incidence among all VSI [Litvan et al., 2018]. According to modern data, the visual-spatial deficit manifests itself to the greatest extent in patients with the presence of dementia, which is characteristic mainly for the late stages of the disease [Lee et al., 2014]. In addition, a number of authors have shown that VSI in combination with other moderately severe cognitive impairments may be a predictor of the development of dementia in PD [Lee et al., 2014].

Taking into account the urgency of the above-described problem, it is of particular interest to diagnose and establish the mechanisms for the occurrence of VSI in PD, as well as the search for possible patterns of their formation and progression. Taking into account the specificity of the considered symptom complex,

the most important is to determine the degree of involvement of various structures of the visual analyzer at the stages of PD progression. Taking into account the presence of dopaminergic neurons in the retina and dopamine participation in retinal neurophysiology, it is necessary to determine the role of changes in the functional activity of the retinal neurotransmitter network and possible degenerative changes in its inner and outer layers in the pathogenesis of the formation of VSI in PD [Frederick et al., 1982]. These changes can be identified using the optical coherence tomography (OCT) of the retina. Recently, a number of authors have presented the results of the study of the organ of vision in patients with PD, in which this technique was applied [Satue et al., 2016].

In addition, it is advisable to determine the possible relationship of changes in directly different parts of the retina with the degeneration of the cortex. This can be identified using the MR-morphometry method, which is actively used in the diagnosis of neurodegenerative and vascular diseases manifested by cognitive impairment.

Materials and methods

To verify how frequent visual and spatial disorders in Parkinson's disease may occur, we examined 62 patients with the established diagnosis Parkinson's disease. Middle age was 65.26±5.23 years. The disease stage at patients made from 2.0 to 3.0 (Hoehn a Jahr scale). The following examinations were conducted: The UPDRS, the clinical and neuropsychological testing including the Poppelreyter test (Figure 1), the Raven test, Rupp's test, visual examination of an organ of vision, a retina research by method of an optical coherent tomography for the purpose of assessment of its thickness and an exception of the accompanying ophthalmologic diseases leading to formation of visual and spatial disorders.

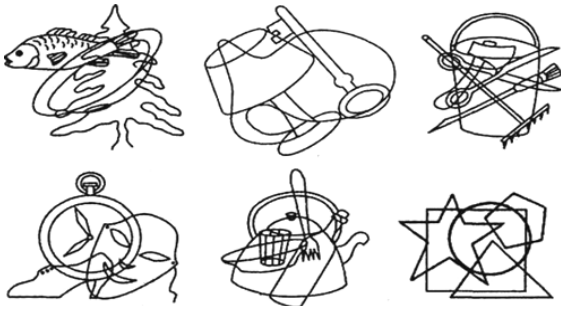

Figure 1. Poppelreuter test (example).

Criteria of an exception of group of a research was presence of ophthalmologic diseases, except for an initial age cataract, craniocerebral injuries, intense violation of brain blood circulation in the anamnesis.

Results and discussion: visual and spatial disorders were revealed at 47 patients from the examined group that made 75,81 %. Such as objective and simultaneous agnosia, the difficulty of orientation in space and in assessing the distance to objects. The following variants of illusory phenomena (17 people) were identified: exometamorphic — "merging" and "blurred" letters when reading, periodic doubling in the eyes — in 13 patients, various pareidolias — in 6 patients (often identified with PD) [Uchiyama et al., 2015]. The visual illusions established at 17 patients (36,17 %) were the most frequent of the revealed symptoms. Difficult subject visual hallucinations were revealed at 11 patients (18,03 %). Simple visual hallucinations, feeling of the stranger, flashing of "front sights" were revealed at 9 (14,75 %) patients. At the same time, at patients with presence of an initial age cataract, visual disorders came to light more often than at group without its existence. Those ophthalmological disorders were excluded by optical coherence tomography (Figure 2).

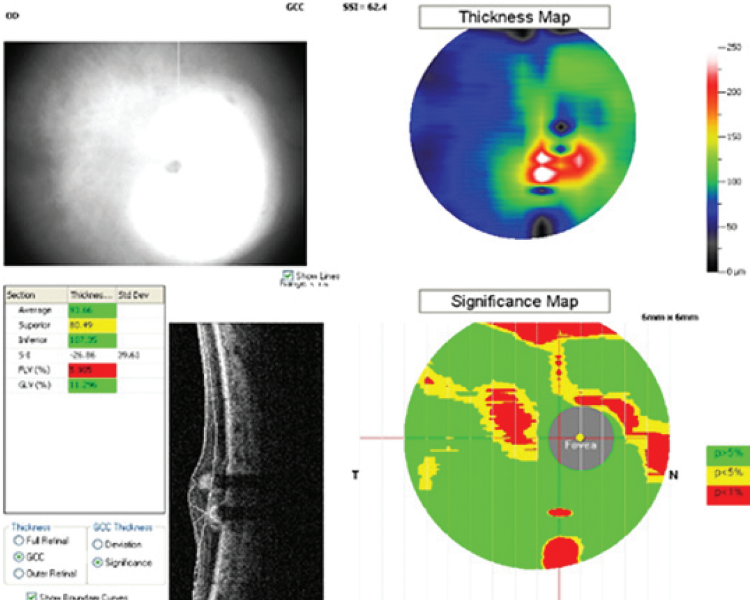

Figure 2. Example of GCC OCT protocol results (the patient with PD had a complaints to visuo-spatial deficit. OCT reveals ophthalmological pathology).

Hallucinatory phenomena of varying severity were detected in 27 people. It should be noted that in most of these patients the criticism of hallucinations was preserved and they perceived them precisely as hallucinations. Many of them had elementary visual hallucinations: "points", "sparkles", "spots". Of the complex phenomena were established: in 8 people — optical receptor hallucinosis, in 6 people — subject hallucinations, and these violations were detected mainly in the increased cognitive impairment group.

Conclusion: Thus, visual and spatial disorders take the important place among not motor manifestations of Parkinson's disease. The most frequent of the found disorders are the hallucinations revealed at most of patients. Also it is necessary to pay attention to presence at patients with Parkinson's disease of the accompanying visual pathology which can lead to formation of visual and spatial disorders. In this regard the research of interrelation of therapeutic and surgical treatment of ophthalmologic diseases at the patients with Parkinson's disease having visual and spatial disorders and dynamics of change of manifestations of this symptomatology at successfully carried out treatment of pathology of an organ of vision seems perspective. Correction of motor complications, carried out, in particular, by dopamine receptor agonists, is undoubtedly the basis of successful treatment of PD, but their ability to cause visual hallucinations and other mental symptoms must be taken into account.

References

1. Dawson B. K., Fereshtehnejad S., Anang J. B.M. et al. Office-Based Screening for Dementia in Parkinson Disease. The Montreal Parkinson Risk of Dementia Scale in 4 Longitudinal Cohorts. JAMA Neurol. Published online March 26, 2018. doi:10.1001/jamaneurol.2018.0254.
2. Frederick J. M., Rayborn M. E., Laties A. M. et al. Dopaminergic neurons in the human retina. Comp. Neurol. 1982; 210(1): 65–79. doi.org/10.1002/cne.902100108
3. Lee J. Y., Kim J. M., Ahn J. et al. Retinal nerve fiber layer thickness and visual hallucinations in Parkinson's Disease. Movement Disorders 2014; 29 (1): 61–67. doi: 10.1002/mds.25543
4. Litvan I., Kieburtz K., Tröster A. I. and Aarsland D. Strengths and challenges in conducting clinical trials in Parkinson's disease mild cognitive impairment. Mov Disord. 2018; 33: 520–527. doi:10.1002/mds.27345.
5. Satue M., Obis J., Rodrigo M. J. et al. Optical Coherence Tomography as a Biomarker for Diagnosis, Progression, and Prognosis of Neurodegenerative Diseases. Journal of Ophthalmology. 2016;2016: 8503859. doi:10.1155/2016/8503859.

6. Uchiyama M., Nishio Y., Yokoi K. et al. Pareidolia in Parkinson's disease without dementia: a positron emission tomography study. Parkinsonism Relat. Disord.— 2015.—Vol. 21.—P. 603–609. doi: 10.1016/j.parkreldis.2015.03.020.
7. Weintraub D., Tröster A. I., Marras C. and Stebbins G. Initial cognitive changes in Parkinson's disease. Mov Disord. 2018; 33: 511–519. doi:10.1002/mds.27330.

Chapter 29.
Genetics of visual perception: clinical aspects

A. P. Gerasimov, D. Yu. Shalygin

Neuroophthalmology is the section of clinical medicine between neurology and ophthalmology, studying the pathology of the visual pathway and oculomotor system. In Soviet Union and Russia it is associated with classical works of E. J. Tron, but his monographs were published near 50 years ago [Bing, Bruckner, 1959; Tron, 1966; 1968].

There are many medical advances in recent years. Neuroimaging techniques are widely available in technical and economic aspects. Method of visual evoked potentials has been improved through computer processing. There are many successes of paediatric, including neonatal, neurology. The spectrum of diseases that require neuro-ophthalmic counseling changes (disappearing of syphilitic and decreasing of toxic atrophies of the optical nerve).

It is necessary to accent fundamental advances: intensive progress of the physiology of vision and the rapid progress of molecular genetics [Gerasimov, Shalygin, 2017]. Physiology, including physiology of visual perception, has molecular background. Physiological processes are provided by the proteins (receptors, signal molecules, ion channels, ion pumps, enzymes, etc.). The structure and function of these proteins are determined by genes, which affect many organs and tissues (pleiotropic effect). Errors of the genetic apparatus lead to the insufficiently quantitatively or defectively qualitative corresponding proteins.

Now basic instrument of both theoretical and practical genetics is Online Mendelian Inheritance in Men — OMIM (https://omim.org/) [Online Mendelian Inheritance in Men, 2019]. This open data base contains detailed information about known genes and diseases with genetic associations. Both genes and diseases have unique numbers and cross-links.

Search in OMIM was executed twice: 20.11.17 (first discussion of these problems) [Gerasimov, Shalygin, 2017] and 30.05.19. Result includes both genes, and diseases, and dynamic was very significant. Request «visual perception» leaded to 62 entries in 2017, but to 1,416 in 2019. Request «visual disorders» leaded primary to 398 entries, but 1,5 years later there were 8,885 entries!

Diseases as "the experiment, performed by nature" are illustrating associations between genetic and physiology.

Several diseases are associated with retinal pathology.

Retinitis pigmentosa has 85 (79 at 2017) genetic variants. Variants are mainly associated with disorders of visual perception: RP76 (OMIM: 606822), RP74 (OMIM: 606151), RP69 (OMIM: 615757), PRP6 (OMIM: 613979), RP20 (OMIM: 180069), RP59 (OMIM: 608172), RP64 (OMIM: 614477), C2orf71 (OMIM: 613425), ARL2BP (OMIM: 615434) at al. These genes are from different functional groups.

NARP syndrome (Neuropathy, Ataxia, and Retinitis Pigmentosa) (OMIM: 551500) is the mitochondrial disease. It is linked with mutation in gene *MTATP6*, coding subunit 6 of mitochondrial H(+)-ATPase. Major mutation is missens-mutation 8993T-G, leading to substitution LEU156ARG.

Different variants of retinal receptors damage were described. Cone-rod retinal dystrophy with loss of color vision and of visual acuity is followed by nyctalopia (night blindness) and loss of peripheral visual fields. Genetic variants, associated with associated with disorders of visual perception: CORD2 (OMIM: 602225), CORD8 (OMIM: 605549), CORD16 (OMIM: 614477).

Retinal dystrophy and iris coloboma with or without congenital cataract—RDICC (OMIM: 610942) is associated with *MIR204* gene, encoding microRNA.

Retinal dystrophy, iris coloboma, and comedogenic acne syndrome: RDCCAS (OMIM: 615147) is associated with disorders of visual perception too.

Leber Hereditary Optic Neuropathy—LHON (OMIM: 535000)—is the mitochondrial disease. There are 18 allelic variants, partially overlapping with retinitis pigmentosa, including mutation in gene of tRNA of Leu or disorders in Complex I, III, and IV polypeptides in the respiratory chain. Genes associated with visual perception are: *LCA12* (OMIM: 180040), *LCA15* (OMIM: 602280), *LCA2* (OMIM: 180069), *MTTL1* (OMIM: 590050) etc.

Many neurodegenerative diseases are associated with different forms disorders of visual perception and oculomotor functions.

Pontocerebellar hypoplasia has phenotype: cerebral and cerebellar atrophy, atrophy of the pons (in some patients), oculomotor apraxia, nystagmus, poor visual attention. Variants are associated with visual perception: PCH1B (OMIM: 614678), PCH2A (OMIM: 277470), PCH4 (OMIM: 608755), PCH5 (OMIM: 608755), PCH2F (OMIM: 608756), PCH9 (OMIM: 102771), PCH6 (OMIM: 611524).

Spinocerebellar ataxia in ophthalmology context has in phenotype not only optic atrophy and pigmentary retinal degeneration, but supranuclear ophthalmoplegia. Variants are associated with visual perception: SCA7 (OMIM: 164500), SCA17 (OMIM: 607136) etc.

Different forms of epilepsy are associated with genes, involved in perceptive functions.

Familial temporal lobe epilepsy, 4 type, (ETL4, OMIM: 611631) is remarkable example of focal genetic epilepsy.

Early infantile epileptic encephalopathy is big (> 70 variants) group of progressive neurodegenerative diseases with pharmacoresistant seisures with different ophthalmology disorders from atrophy of optical nerve up to cortical blindness. Association with visual perception was described for the type 5 (EIEE5, OMIM: 182810) and 31, (EIEE31, OMIM: 602377).

With visual perception and its disorders are associated myoclonic epilepsy of Unverricht and Lundborg (EPM1A, OMIM: 254800) and generalized epilepsy with febrile seizures plus, type 7 (GEFSP7, OMIM: 613863).

There are many other forms of epilepsy, associated with genes necessary for visual perception. More then, new associations are describing rapidly.

We have two possible interpretations of this fact:

1. Disorder of visual perception may be nonspecific associated with damage to the brain tissue during the progress of encephalopathy.

2. The same time, visual perception is associated with short-term memory, which is based on the reverberation of nerve impulses along closed neural circuits. Paroxysmal processes have a similar mechanism.

Role of mitochondria (including examples of NARP and LHON) is important because:

- Conduction and synaptic transmission are energy consuming processes.
- Mitochondrial diseases are caused by mutations of more than 200 genes.
- The distribution of modified mitochondria in the tissues is random, and the presence of clinical manifestations depends on their share in the cell (the phenomen of heteroplasmy).
- A significant part of cases are soft forms with minimal signs [Gerasimov et al., 2018]

As the example of disorder without clear molecular basis may be discussed hereditary prosopagnosia, OMIM: 610382. Almost all reported cases are of the acquired form, but there is evidence for a familial form as well. But there is no molecular description in OMIM, and the last publication was in 2008.

In our previous publication (2017) [Gerasimov, Shalygin, 2017] we performed analysis of cytogenetic localisations of described genes. We selected 3 locuses:

- 1p31.3 — LCA2 and RP20, 1p34.1 RP76, 1p36.11 — RP59,
- 9q21.12 — RDICC, 9q21-q22 — ETL4,
- 9q34.11 — EIEE31 and EIEE5.

Now analysis of distribution and interactions of many thousands genes needs especially bioinformative and interactomic algorithms.

Conclusions:

- Visual perception at various levels is associated with genes, the damage of which is associated with retinitis pigmentosa, retinal dystrophy, LHON, pontocerebellar hypoplasia and spinocerebellar ataxia, early infantile epileptic encephalopathy.
- Often they may be grouped in common loci (1p31–36; 9q21–22, 9q34) and can be inherited together
- On the visual pathway different genes have different localizations of functional activity 1.in receptor zone (retina), 2.in visual tract with subcortical centers and 3.in cortex.

References

1. Bing R., Bruckner R. Brain and aye. Bases of neuroophthalmology. Russ. ed. — L., Medgis, 1959. (Бинг Р., Брюкнер Р. Мозг и глаз. Основы офтальмоневрологии. Перевод с немецкого и редакция Е. Ж. Трона. — Л., Медгиз, 1959).
2. Gerasimov A. P., Shalygin D. Yu. Genetics of visual perception: clinical aspects // Clinical neurophysiology and neurorehabilitation / Materials of the 5th scientific conference with the international participation. — SPb, 22–24 nov. 2017, p. 94. (Герасимов А. П., Шалыгин Д. Ю. Генетика зрительного восприятия: клинические аспекты // Клиническая нейрофизиология и нейрореабилитация / Материалы Пятой научно-практической конференции с международным участием. — СПб, 22–24 ноября 2017. С. 94)

3. Gerasimov A. P., Ushanov V. V., Shalygin D. Yu. Pathophysiology mechanisms of mitochondrial diseases of the visual pathway // Clinical neurophysiology and neurorehabilitation / Materials of the 6th scientific conference with the international participation. — SPb, 22–23 nov. 2018, p. 99–100. (Герасимов А. П., Ушанов В. В., Шалыгин Д. Ю. Патофизиологические механизмы митохондриальных заболеваний зрительного пути // Клиническая нейрофизиология и нейрореабилитация / Материалы Шестой научно-практической конференции с международным участием. — СПб, 22–23 ноября 2018. — С. 99–100)
4. Online Mendelian Inheritance in Men — OMIM (open database) https://omim.org/ (available 2019)
5. Tron E. J. Aye and neurosurgery pathology. — L., Medicine, 1966. (Трон Е. Ж. Глаз и нейрохирургическая патология. — Л., Медицина, 1966).
6. Tron E. J. Diseases of the visual pathway. Second edition. — L., Medicine, 1968. (Трон Е. Ж. Заболевания зрительного пути. Изд. 2-е, перераб. и доп. — Л., Медицина, 1968).

Chapter 30.
Modern achievements in cochlear and brainstem auditory implantation

I.V. Koroleva, E.A. Ogorodnikova

According to the WHO, 466 million people suffer from hearing loss, 34 million of them are children [WHO, 2018]. There are more than 5 million total deaf people in the world. Various hearing loss occurs in 1 % of people aged 20 years. The number of age-related hearing impairments doubles every 10 years. Among people over 65, at least 24 % of the population is affected by hearing impairment [Koroleva, 2012]. As WHO estimates, 1.1 billion young people aged 12–35 are at risk of hearing loss due to prolonged exposure to loud sounds when listening to music [WHO, 2018].

Hearing loss in adults leads to impaired communication and therefore causes problems of interaction in the family and at work, limited learning opportunities and professional duties, and to the disability due to significant hearing impairment [Koroleva, 2012]. Person with hearing loss often cannot fully perceive speech or distinguish other surrounding sounds. As a result, they experience anxiety and irritability, which, in the absence of rehabilitation, leads to various psychological changes and identity crisis, especially in people with late deafness: increased anxiety, depression, irritability, egocentrism, social isolation, etc. Their order varies depending on the personality type, the degree of hearing loss and the character of hearing impairment compensation, support for the immediate social environment.

In children, hearing loss is often congenital or occurs at an early age. In such cases, even a slight decrease in hearing leads to impaired speech development, and with a deep decrease in hearing — to muteness. The consequences of hearing impairment in children are various secondary disorders of mental processes: perception, attention, memory, thinking, imagination, emotional-volitional sphere, etc. All of this limits the child's ability to learn, and in adulthood to gain a profession, find a job [Vygotskiy, 2000; Koroleva, 2012]. The child with severe degree of hearing loss receives disability status.

At present a whole arsenal of rehabilitation methods for people with hearing impairments is used. All these methods can be divided into 3 groups [Korol-

eva, 2012, Koroleva et al., 2018]:

1. medical methods (conservative and surgical treatment of the pathology of individual peripheral structures of the auditory system),
2. technical methods (different devices for restoration of auditory function or compensation of hearing impairment based on undamaged analyzer characteristics),
3. psychological and pedagogical methods (methods of development, training, psychological assistance to people with hearing impairment due to compensatory mechanisms of the brain and creating favorable conditions for their social adaptation).

In some cases, there is a combination of medical, technical and pedagogical methods at integrated medical-technical-pedagogical rehabilitation technologies [Koroleva, 2018]. Such technologies include rehabilitation methods associated with the use of hearing aids and implants. In general, the technical means of rehabilitation of people with hearing impairment can be divided into two large groups (Figure 1).

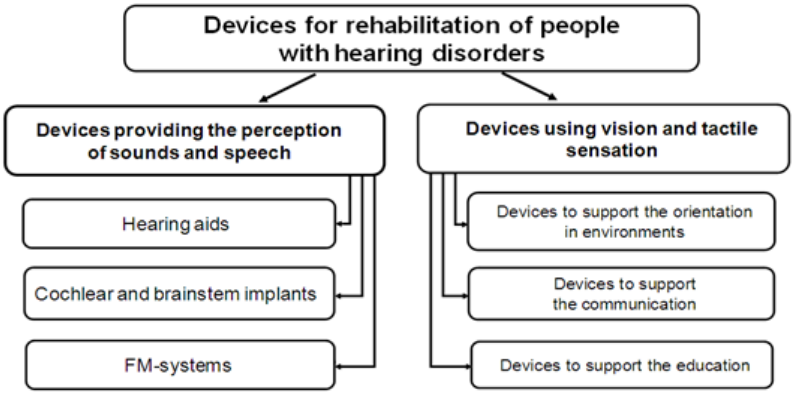

Figure 1. Rehabilitation equipment for people with hearing impairment [Koroleva et al., 2018].

The modern approach to the rehabilitation of people with hearing impairments involves a partial or full restoration of a subject's ability to perceive sounds and speech. Today various technical devices are used to provide an opportunity to recognize surrounding sounds and speech for people with varying degrees and type of hearing loss (Figure 2):

1. Traditional hearing aids (HA)
2. Implantable hearing aids
3. Cochlear implants (CI)
4. Auditory brainstem implants (ABI)
5. FM systems

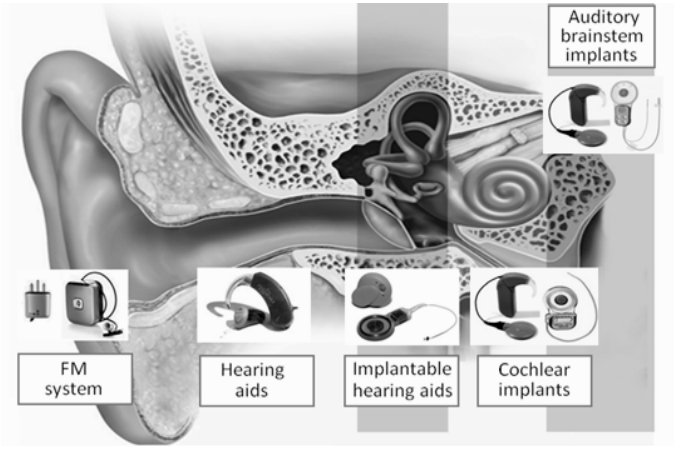

Figure 2. Modern hearing devices and their location in auditory system structures [Koroleva, 2012].

Due to damage of the structures of the outer, middle, inner ear, the external sounds come to the auditory system weakened. As a result, children and adults with hearing impairments do not hear quiet sounds, sounds of medium and significant volume are perceived as illegible, or do not recognized at all. Hearing aids (HA) amplify the sounds transmitted to the hearing system of a hearing-impaired person. These devices for amplifying speech and other sounds that provide the ability to hear ambient sounds and speech to people with mild, moderate, severe hearing loss and part of people with hard hearing loss [Handbook, 2009; Koroleva, 2012; Tavartkiladze, 2013].

However, for deaf people with the majority of auditory receptors damaged (hair cells), HAs are not effective for speech perception. Deaf patients are advised to use a cochlear implant (CI) [Cochlear implants, 2006; Koroleva, 2012; Tavartkiladze, 2013]. The effect of CI is based on the fact that in case of sensorineural hearing loss with destruction of the cochlear receptors (hair cells) the neurons of the spiral ganglion and their axons forming the auditory

nerve remain intact for a long time. A significant portion of the auditory nerve fibers are retained even with a very long period of deafness or hearing loss due to meningitis. Unlike HA, which only enhances sounds, CI replaces dead cochlear receptors and converts sounds into electrical impulses that stimulate the dendrites of spiral ganglion neurons. These impulses are transmitted through the auditory nerve to the subcortical and cortical auditory centers of the brain causing auditory sensations and deaf person assumes the ability to hear speech, surrounding sounds, music.

CI consists of 2 parts — implantable and external. The implantable part includes receiver, chain of active electrodes (from 8 to 22), and reference electrode (Figure 3). It is completely autonomous and has not any external outputs and batteries or other parts requiring replacement. The receiver case is made of titanium or ceramic, depending on the CI model. The implanted part of the CI is intended for life-long use without substitution, including under the growth of the child.

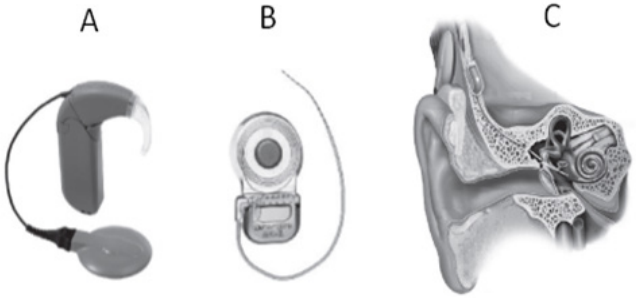

Figure 3. The device of cochlear implant [Koroleva, 2016].

A — the external part of CI with the speech processor, transmitter, microphone, power supply; B — the inner part of CI, including the receiver and the chain of active electrodes; C — the location of CI parts on the head and in the ear.

The external part of modern CI models from different companies includes a microphone, sound processor, battery placed in a boot similar to a behind-the-ear HA, as well as a transmitter with a magnet. The transmitter locates behind the ear under the hair. It is attracted to the implanted part through the skin by magnet. There are CI models in which all components of the external part are packed in one block. For some CI, it is possible to temporarily remove the magnet from the receiver of the implantable part. It is necessary for nuclear magnetic tomography scanning. Recent CI models allow carry out such examinations without removing the magnet.

The sound processor located in the outer part of the CI is a small-sized specialized computer. On the outer casing of the CI processor there are regulators that allow you to adjust the volume of sounds, choose a program for their processing, etc. There are also special indicators that control the operation of the CI, and the discharge of batteries. In addition, various external devices can be connected with this part of CI through a special connector — a phone, a player, an FM system, etc. In the modern models of CI systems, the regulators are located on the panel of remote control. It makes easier for the patient to manage them, and excludes the possibility of accidentally switching regulators in children. Using the remote control, patient can simultaneously change the parameters of two CI processors in bilateral implantation.

The CI power source is rechargeable batteries or disposable batteries located in the battery block near the processor. The outer part of CI is removed during sleep or bathing, as HA. With the latest CI models, the patient can swim without removing the external part.

Scheme of the work of cochlear implant (Figure 4, I):

- Speech and other sounds enter the microphone of the external part of the CI and are converted into electrical signals.
- Electrical signals are transmitted to the CI processor.
- In the CI processor the entire spectrum of the audio signal is frequency filtering in accordance with the number of channels / electrodes. Then, in each channel, signal processing (with different strategies) is performed and the signals are converted into encoded sequences of electrical pulses.
- The electrical pulses are transmitted by transmitter (held on the patient's scalp using a magnet) in the form of radio signals to a radio receiver located under the skin in the temporal bone;
- The implanted receiver decodes the signal and sends it as a sequence of electrical signals to the electrodes in the cochlea;
- Electrical impulses stimulate the auditory nerve fibers. Different parts of the nerve are stimulated by different electrodes in accordance with the spectrum of sound entering the microphone. The electrodes in the initial part transmit information about low-frequency sounds to the apical part of the cochlea. Electrodes located closer to the receiver transmit information about high-frequency sounds to the basal part of the cochlea. Thus, the principle of tonotopic organization of the cochlea and the auditory system as a whole is respected;

- The fibers of the auditory nerve transmit information further to the auditory centers of the brain, where information about speech and non-speech signals is processed in the same way as in a normally hearing person and patient perceives diverse sounds, including speech and music.

The intelligibility of speech, perceived with CI, substantially depends on the coding strategy (conversion) of speech signals into electrical impulses. The following basic strategies of signal coding in CI system are used:

- strategies for highlighting speech characteristics;
- SPEAK strategy (spectral maximum detection strategy);
- CIS strategy and other advanced versions based on it;
- ACE strategy.

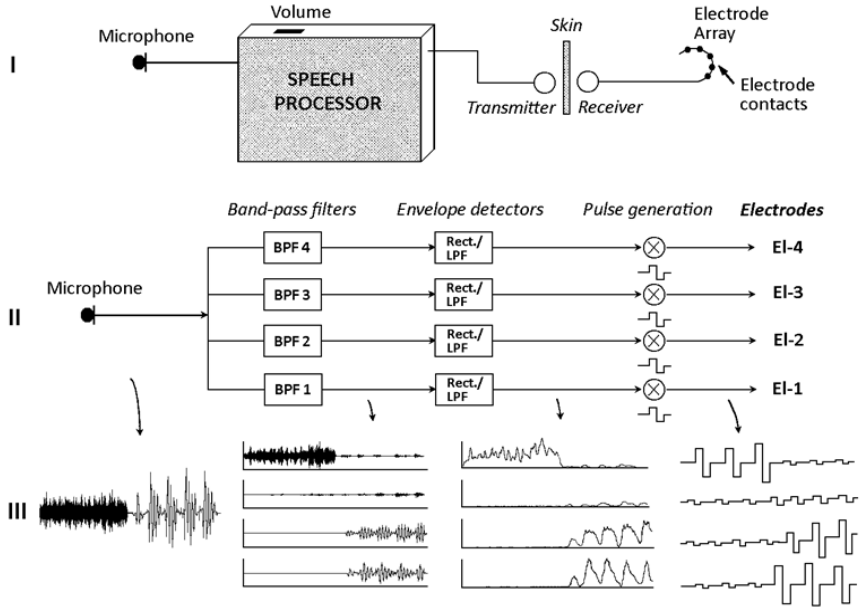

Figure 4. Schematic representation of the CI functioning [Loizou, 1998]. I — schematic representation of the device of the CI system. II — detail of the processing of audio / speech signals in CI models with CIS coding strategy. III — schematic representation of the conversion of sound signals into biphasic electrical pulses at different stages of processing in the CI processor.

CIS-strategy (Continuous Interleaved Sampling — continuous alternating strategy of fast coding) is the standard of application in modern CI systems (Figure 4, II). Under the CIS strategy, all electrodes are stimulated for each cycle, but not simultaneously [Wilson et al., 1991]. This allows to achieve a high frequency of stimulation of the auditory nerve (up to 83000 imp / s) and to avoid the application of electric fields during stimulation of adjacent electrodes. As a result, not only spectral, but also temporal characteristics of speech signals are transmitted, including information on transients, the envelope of signals. This provides a better transmission of both segmented (phonemes) and suprasegmental (intonational-rhythmic) characteristics of speech. At that the main parameters of stimulation, the change of which affects the intelligibility and sound quality of speech and other sounds, are the frequency of stimulation, the duration of the pulses, the order of stimulation of the electrodes, the compression parameters of input signals (Figure 4, III).

In recent years, special attention has been paid to the development of new coding strategies based on the CIS strategy for advancing transmitting spectral information and information of the fine temporal structure in speech signals, including the low-frequency range, which is important for the perception of music and speech in noise, the prosodic characteristics. In most CI systems, it is possible to use different coding strategies. This allows audiologist to choose the optimal strategy for the patient or to help for experienced CI user independently changes the strategy, according to signal category (speech, music) and acoustic environment (quiet or noisy conditions).

In spite of some differences in the design of implantable part of different CI models surgical approaches for their implantation are similar [Koroleva, 2016]. The operation of implanting of the internal part of CI into the ear of a deaf patient consists of the following main stages (Figure 5):

1. cut of the skin behind the ear to provide access through the bone to the inner ear (before surgery, the hair behind the ear is shaved off);
2. preparation of the recess for the CI receiver in the temporal bone;
3. mastoidectomy;
4. drilling a cochleostomy to insert an electrode carrier (for some methods)
5. introduction of the electrode carrier into the cochleostomy or through the hole in the round window into the scala tympany;
6. installation and fixation of the CI receiver in the temporal bone, fixation of the electrode carrier;
7. skin suturing behind the ear.

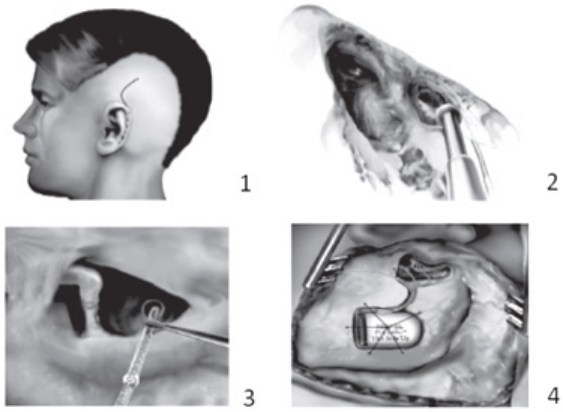

Figure 5. Stages of the surgery of cochlear implantation [Koroleva, 2016].

1 — incision of the skin on the head; *2* — mastoidectomy and posterior tympanotomy; *3* — introduction of an electrode carrier into a cochleostomy; *4* — location and fixation of the CI receiver in the temporal bone.

After surgery, as a rule, computed tomography of the temporal bones is done to control the completeness of the electrode chain introduction into the cochlea. Most patients, including children, after the end of the action of anesthesia can get up and communicate. The day after surgery, the patient can independently move with almost no restrictions, although the bandage on their head remains for several days to protect the incision. Usually patients are discharged from the clinic 7–10 days after surgery. Most of adult patients report that they fully recover from surgery in less than two weeks. After surgery, the patient does not hear. He begins hearing only after connecting and programming the processor located in the external part of CI.

However, cochlear implantation is not only a surgical operation. It is a complex system of measures which includes 3 main components:

1. *preoperative diagnostic examination and selection of patients*: a comprehensive audiological examination, computed tomography of the temporal bones, MRI of the cochlea, consultations with audiologist and psychologist, a standard set of preoperative examinations. These measures are carried out in regional deaf centers or in the center of cochlear implantation (takes 2–5 days).
2. *surgical operation*, which performed by otosurgeon at the center of

cochlear implantation (the duration of 40–90 minutes).

3. *postoperative auditory-speech rehabilitation* of a patient with CI. The initial procedures include connecting the external part of the CI, programming and setting up the CI processor (usually 3–4 weeks after the operation), classes with a special teacher and speech therapist to restore / develop auditory perception of sounds and speech with CI. For deaf children it also embraces the training of understanding of speech and developing of own oral speech with the skills of communication. In addition, psychological support of patient and all family, audiological observation, technical aid and assistance in social adaptation are realized. The measures carried out in the center of cochlear implantation (initial period), regional audiological and rehabilitation centers, educational institutions for children with hearing impairment. The duration of postoperative rehabilitation for postlingually deaf adult patients is 1–3 months, for prelingually deaf children, up to 5 years.

Cochlear implantation is performed for adults and children with bilateral sensorineural deafness or hard hearing loss. The earliest age of implantation in children is 6 months. For adult patients, the maximum age is limited only by the somatic state of the patient. By 2019, more than 550 thousand people use CI in the world.

Cochlear implantation refers to medical rehabilitation methods with a high economic effect. In terms of the indicator "financial costs / improving the quality of life", it takes 3rd place after "intensive care for newborns" and "cardiovascular surgery" [Koroleva, 2016]. Most patients use 1 CI (implant for one ear) because of the high cost of the device. Some patients are exposed to bilateral cochlear implantation. First of all, these are patients who have lost hearing due to meningitis, and deaf-blind children. In a number of economically developed countries, bilateral implantation is performed for all children. Bilateral cochlear implantation may be performed simultaneously or sequentially [Litovsky et al., 2004; Peters et al., 2010]. In the latter case, the interval between the first and second operation may vary from 6 months up to 20 years, and after implantation on the second ear, the patient also needs postoperative auditory-speech rehabilitation [Koroleva et al., 2019; Peters et al., 2010].

Thanks to cochlear implantation the ability to perceive the speech and communicate is restored in postlingually deaf adults. They can return to work and social activities. Prelingually deaf children with CI get the chance to learn and understand the speech and start speaking. The best results are achieved

in children implanted under the age of 2 years. With properly organized post-operative auditory-speech rehabilitation their level of speech development approaches to the normal, which allows to study in a main-stream school and to receive any profession. In deaf children with complex impairments owing to CI, the possibilities of communication and learning are expanding. In all cases, the use of CI improves not only the quality of life of the patient, but also his family [Koroleva, 2016; Faulkner, Pisoni, 2013].

However, if the auditory nerves of the patient are damaged or the cochlea is fully ossified, then even CI will not help. For such patients, the method of auditory brainstem implantation has been developed [Colleti et al., 2009; Tavartkiladze, 2013; Koroleva, 2016]. The auditory brainstem implant (ABI) is inserted into the cochlear nuclei of the brain stem above the auditory nerve (Figure 6, I).

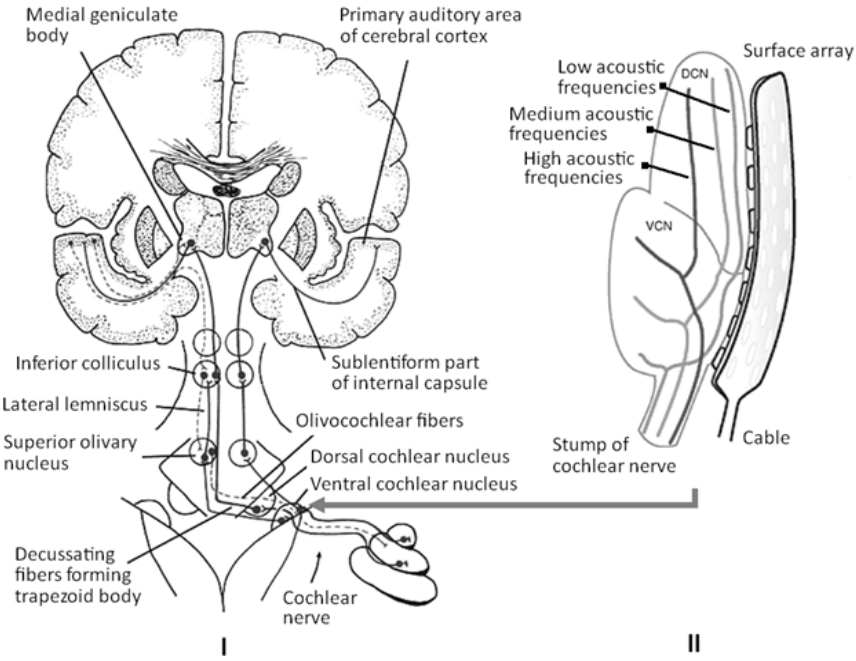

Figure 6. Scheme of the auditory system with the location of the ABI electrode carrier on the ventral cochlear nucleus (I), the tonotopic organization of cochlear nuclei with the surface arrangement of electrodes (II).

ABI also consists of the implantable and external parts. The outer part of the ABI is the same as for the CI, the inner part as a whole is also similar, but the shape of the electrode carrier is different — in correspondence of the size and shape of the cochlear nucleus (Figure 7).

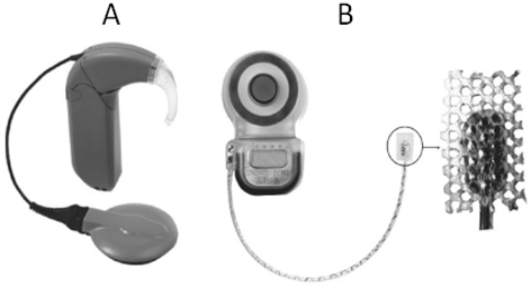

Figure 7. The device of the auditory brainstem implant [Koroleva, 2016].

A — the external part of the ABI, including a sound processor, transmitter, microphone, power supply ("Opus 2", "MED-El"); B — the internal part of the ABI, including the receiver and the carrier of the electrodes ("Mi1000 Concerto ABI", "MED-El")

Auditory brainstem implantation includes the same components as cochlear implantation, but with certain features:

1. *Preoperative diagnostic examination and selection of patients for surgery* consists of standard set of measures for cochlear implantation + MRI of the cochlea and brain in the area of the cerebellar angle. It is carried out in a neurosurgical hospital or in the center of cochlear implantation.
2. *Neurosurgical surgery of brain stem implantation* carried out in a neurosurgical hospital. The duration of the operation is 5–8 hours. An important part of the surgery is the electrophysiological control of the location of the electrodes on the cochlear nuclei by recording brain stem potentials.
3. *Postoperative rehabilitation* is realized in the center of cochlear implantation. The content of postoperative rehabilitation of patients with ABI is the similar to rehabilitation of patients with CI.

The number of ABI users is much less than the CI users. Up to 2018, only about 1,700 people with ABI were registered in the world. It is accounted by the fact that cases of auditory nerve damage as a cause of deafness are rela-

tively rare. As well the ABI implantation is a more complex surgery, which can have serious consequences for the patient. In addition, the results of using ABI are inferior to success of the cochlear implantation. The small size of cochlear nuclei in comparison to the cochlea makes difficult the selectively stimulate individual frequency-specific zones of the nuclei. It is also more difficult to configure the processor of ABI and training of patients to perceive sounds and speech with ABI. Therefore, for a long time, such rehabilitation was single and performed only for adult patients with a diagnosis of neurofibromatosis II, when after removing the tumors it was not possible to preserve the auditory nerves. But in recent years, due to the improvement of the carrier of ABI electrodes, sound processors, and surgical methods, brainstem implantation is performed also for adults and children with full ossification of the cochlea, aplasia of the cochlea and auditory nerve, disturbances of the auditory nerves by a trauma.

In Russia, the first auditory brainstem implantations were performed to 3 patients (2 adults and 1 child) in 2014 with the participation of specialists from the St. Petersburg Research Institute of Ear, Throat, Nose and Speech, Polenov Russian Neurosurgical Research Institute, Department of Neurosurgery of the Fulda Clinic and the University Hospital of Marburg (Prof. R. Behr) [Yanov et al., 2017].

It has been shown that in the majority of ABI users improves auditory-visual perception of speech. But some patients can only detect the sounds, while others become able to perceive and distinguish speech, reaching 50 % of speech intelligibility [Skarzynski et al., 2000; Behr et al., 2007; Colleti et al., 2009; Matthies et al., 2013]. The quality of auditory perception and speech intelligibility in patients with ABI depends on:

- the cause of hearing loss (after removal of the tumor the results are generally worse),
- the degree of brain damage as a result of compression by the tumor and during surgery,
- the location of the electrodes in the cochlear nuclei of brain stem and the number of activated electrodes,
- the age of the patient at the time of surgery. In children the development of auditory perception with ABI is better than in adults. It is due to the plasticity of the nervous system in childhood, especially under implantation up to 2 years..

Difficulties in recognizing of sounds and slowly learning in patients with ABI relative to CI users is determined of narrower frequency range of perception.

The cochlear nuclei have a layered structure — afferent fibers of the high-frequency part of the auditory nerve pass deep in the nuclei, and on the surface — low-frequency (Figure 6, II). So, when using a flat surface electrode, mainly low-frequency afferents are stimulated. There are 2 hypotheses to explain lower speech intelligibility with ABI — the hypothesis of selectivity and the distortion hypothesis.

The hypothesis of selectivity — ABI cannot provide selective contact with frequency-specific zones of cochlear nuclei in accordance with their tonotopic organization. Firstly, in the ABI the number of independent channels transmitting spectral information is limited. Secondly, each electrode of ABI activates large populations of neurons, the excitation fields of which overlap each other. As a result, the excitation boundaries of the frequency-specific region are blurred.

The distortion hypothesis — ABI distorts the activation of specific neural circuits in cochlear nuclei. Cochlear nuclei are complex structures with several types of specialized neurons that perform different functions. The projections of these neurons go to the ipsi- and contralateral superior structures in auditory system. In addition, there are numerous connections between neurons inside the cochlear nuclei. With surface stimulation of nuclei, competing pathways are excited simultaneously and effect of interference distorting the efficient functioning of cochlear nuclei. At the same time, under stimulating of cochlear nuclei through the auditory nerve with CI, they function closer to the natural way.

Cochlear and brainstem implantation are constantly evolving technologies. The device and characteristics of the internal and external parts of the CI / ABI, surgical technique of implantation, methods of tuning the implant processor and postoperative auditory-speech rehabilitation, methods of assessing the quality of fitting settings and the effectiveness of rehabilitation are constantly improving [Koroleva, 2016].

Various parameters in CI systems are modernized:

- Reducing the size of CI;
- Design of fully implantable devices;
- Developing of strategies for processing acoustic signals;
- Improving the intelligibility of speech transmitted by CI (in different conditions, including in noise);
- Improving the perception of music with CI;
- Decrease of energy consumption;

- Modification of electrodes for implantation under ossification or abnormality of cochlear;
- Perfection of electrode carrier to improve the quality of sound signals transmission, reduce trauma to the cochlea, etc .;
- Reducing the size of the implantable receiver, allows to simplify the surgical procedure and reduce its duration;
- Development of CI models combined with a hearing aid (electro-acoustic correction);
- Development of objective methods for tuning the CI processor;
- Development of binaural implantation;
- Design of CI models with minimization of the life limitations for CI users (swimming, MRI).

Auditory implantation is an example of a comprehensive medical-technical-pedagogical technology, where the final result depends on the success of each component [Koroleva, 2016].

Fitting of the CI / ABI processor is crucial for transmitting relevant features of different categories of sound signals, including linguistic elements of speech, which is necessary for their adequate speech perception and recognition by the CI / ABI users [Tavartkiladze, 2013; Vaerenberg et al., 2014; Koroleva, 2016]. For the processors' fitting the manufacturers are developing special equipment and programs that provide primary parameters of electrical stimulation at the initial stage of using CI / ABI, and conditions of their correction according to auditory perception experience of patient under adaption to new conditions of hearing. The optimal parameters of electrical stimulation are individual and depend on a number of difficultly controlled factors — the state of the structures of the cochlea, auditory nerve, subcortical and cortical auditory centers of the brain, patient's sensory experience, peculiarities of the location of the electrodes in the cochlea, etc.

Assessment of the CI / ABI processor settings is carried out by subjective and objective methods [Cochlear implants, 2003; Koroleva et al., 2013; Tavartkiladze, 2013; Koroleva, 2016]. Subjective methods include assessing of patient's reactions to stimulation — the minimum (threshold) and maximum comfortable levels of electrical stimuli, parameters of the volume balance for the ensemble of electrodes. A part of the comprehensive procedure of processor settings checking is testing the patient's perceptual responses to acoustic stimulation, including determining tonal hearing thresholds with CI / ABI, speech intelligibility in silence and in noise, a subjective assessment of the quality of speech with CI / ABI, using questionnaires.

Objective methods include recording physiological responses of the auditory system to electrical stimulation: stapedial reflexes (ESRT), auditory nerve potential (ART), brainstem and cortical evoked potentials [Lorens et al., 2004; Kosaner et al., 2009; Shapiro et al., 2012; Bakhshinyan, 2014; Gransier et al., 2016]. These methods are primarily used during the initial period of use of the CI / ABI in young children or prelingually deaf teens without auditory experience. However, even in these patients with growing auditory experience with CI / ABI, the subjective assessment methods are gaining more importance for the fitting of the parameters of electrical stimulation [Lorens et al., 2004; Koroleva et al., 2013; Calvino et al., 2016]. The role of the perceptual assessment of the processor fitting quality also increases due to the development of CI systems and transmitting the new cues of acoustic signals that are important for the perception of prosodic information and melody in speech or in music. These measures help to maximize the approximation of auditory perception with CI to the natural one. This determines the need to analyze the capabilities of CI users to adequately identify all diverse acoustic information.

To ensure such assessment of the quality of processor fitting a special battery of psychoacoustic tests was developed in addition to the traditional methods (recording ESRT, ART, tonal hearing thresholds, discomfort thresholds) and on the basis of the experience in using the training program "Learn to Listen" [Koroleva et al., 2003; Ogorodnikova et al., 2005; Ogorodnikova et al., 2008; Koroleva et al., 2013]. Tests allow evaluate the patient's perception of temporal and spectral characteristics of sounds with CI at different stages of rehabilitation [Ogorodnikova et al., 2008; Koroleva et al., 2013].

The developed battery includes 2 test blocks. The first of them is focused on checking the quality of the initial fitting of the CI processor according to the results of the perception of the basic characteristics of sound signals: duration, time structure, timbre. The tasks of block have a limited linguistic nature and, in general, reflect the universal character of audition. They are used at the beginning and at the end of the first rehabilitation session to control the settings of the processor in accordance with new auditory skills with CI (the daily auditory training). The second block is aimed to assess auditory perception and quality of processor fitting in patients with experience of CI using (of 6 months). This block includes more complex tasks with pronounced linguistic component for training of the perception of dynamically changing speech signals, target speech signal in a complex acoustic scene (speech competition, background noise) and to develop skills of acoustic orientation, etc. The approbation of test battery confirmed its efficiency, which is relying on

the possibility of adequate assessment of individual characteristics of the patient's auditory perception at different stages of rehabilitation. It is especially important for patients with problems of processor fitting by only traditional methods and with serious deficit of speech environment.

Thus, in recent decades, the technical, medical and rehabilitation components of auditory implantation that provide a comprehensive solution for people with hard hearing loss and deafness have shown significant progress and essential achievements based on the use of innovations in hearing aid technologies and new data of studies on hearing and speech physiology. Now the new perspectives in compensation of sensory and cognitive dysfunctions are associated with the heavy development of modern neurotechnologies in the field of artificial neural networks and artificial intelligence.

References

1. Bakhshinyan V. V. Sovremennyye tendentsii i perspektivy primeneniya metoda telemetrii nervnogo otveta v reabilitatsii patsiyentov posle kokhlearnoy implantatsii. Vestnik otorinolaringologii. 2014; 2:21–25. (In Russ)]
2. Behr R. et al. The High Rate CIS Auditory Brainstem Implant for Restoration of Hearing in NF-2 Patients. Skull Base. 2007, V.17. N2. P. 91–107.
3. Calvino M., Gavilán J., Sánchez-Cuadrado I., Pérez-Mora R.M., Muñoz E., Lassaletta L. Validation of the Hearing Implant Sound Quality Index (HISQUI19) to assess Spanish-speaking cochlear implant users' auditory abilities in everyday communication situations. Acta Oto-Laryngologica. 2016; 136(1):48–55. https://doi: 10.3109/00016489.2015.1086021.
4. Cochlear implants / Ed. Waltzman SB, Roland JT / N-Y-Stuttgart.: Thieme Medical Publishers, 2006.
5. Cochlear implants. Objective measures / Ed. Cullington H. E. / Whurr publishers. London — Philadelphia. 2003.
6. Colleti V. et al. Outcomes in nontumor adults fitted with the auditory brainstem implant: 10 years' experience. Otol Neurotol. 2009. V.30. N5. P. 614–8.
7. Faulkner K. F., Pisoni D. B. Some observations about cochlear implants: challenges and future directions. Neuroscience Discovery. 2013; 1(9):1–9. https://doi.org/10.7243/2052–6946–1–9.
8. Gransier R., Deprez H., Hofmann M., Moonen M., van Wieringen A. W. Auditory steady-state responses in cochlear implant users: Effect of modulation frequency and stimulation artifacts. Hearing Research. 2016; 335:149–160. https://doi: 10.1016/j.heares.2016.03.006. PMID: 2699466.

9. Handbook of clinical audiology/ Ed. Katz J., Medvedstsky L., Burkard R., Hood L. Philadelphia, PA [etc.]: Wolters Kluwer/Lippincott Williams & Wilkins. 2009.
10. Koroleva I. V. Reabilitatsiya glukhikh i vzroslykh posle kokhlearnoy i stvolomozgovoy implantatsii.— SPb.: KARO, 2016. 872 s. (In Russ)].
11. Koroleva I. V. Vliyaniye tekhnicheskogo progressa i kokhlearnoy implantatsii na razvitiye surdopedagogicheskoy pomoshchi detyam s narusheniyem slukha/ Kafedra surdopedagogiki v zerkale vremen: Kollektivnaya monografiya. Sankt-Peterburg: Izd-vo RGPU im.A.I.Gertsena, 2018. S.68–84. (In Russ)]
12. Koroleva I. V. Vvedeniye v audiologiyu i slukhoprotezirovaniye.— SPb.: KARO, 2012.— 400 s. (In Russ)]
13. Koroleva I. V., Kuzovkov V. Ye., Levin S. V., Ogorodnikova E. A., Yanov YU.K., Astashchenko S. V. Posledovatel'naya bilateral'naya kokhlearnaya implantatsiya s dlitel'nym intervalom mezhdu operatsiyami u slepoglukhogo patsiyenta. Vestnik otorinolaringologii, 2019. T.84. № 2. S.29–35. (In Russ)]
14. Koroleva I. V., Kuzovkov V. Ye., Yanov Yu.K. Tekhnicheskiye sredstva reabilitatsii patsiyentov s narusheniyem slukha. V kn.: Reabilitatsiya invalidov: natsional'noye rukovodstvo/ pod red. G. N. Ponomarenko.— M.: GEOTAR-Media, 2018. S.401–407. (In Russ)]
15. Koroleva I. V., Lyublinskaya V. V., Ogorodnikova E. A., Pak S. P., Stolyarova E. I., Pudov V. I. Sposob slukho-rechevoy reabilitatsii i yeye otsenki u patsiyentov s kokhlearnymi implantami. Patent na izobreteniye № 2209057, 2003. (In Russ)]
16. Koroleva IV, Ogorodnikova EA, Pak SP, Levin SV, Balyakova AA, Shaporova AV. Metodicheskiye podkhody k otsenke dinamiki razvitiya protsessov slukhorechevogo vospriyatiya u detey s kokhlearnymi implantami. Rossiyskaya otorinolaringologiya. 2013; 3:75–85. (In Russ)].
17. Kosaner J., Anderson I., Turan Z., Deibl M. The Use of ESRT in Fitting Children with Cochlear Implants. Int Adv Otol. 2009; 5:(1) 70–79.
18. Litovsky R. Y., Parkinson A., Arcaroli J., Peters R., Lake J., Johnstone P., Yu G. Bilateral cochlear implants in adults and children. Arch Otolaryngol Head Neck Surg. 2004 May 130(5), P. 648–55. https://doi.org/10.1001/archotol.130.5.648.
19. Loizou P. Mimicking the human ear: an overview of signal processing strategies for converting sound into electrode signals in cochlear implants// IEEE Signal Processing Magazine. 1998. V.98. P. 101–130.
20. Lorens A., Walkowiak A., Piotrowska A., Skarzynski H., Anderson I. eSRT and MCL correlations in experienced pediatric cochlear implant users. Cochlear Implants Int. 2004; 5: 28–37.

21. Matthies C. et al. Auditory brainstem implants in neurofibromatosis Type 2: is open speech perception feasible? J Neurosurg. 2013. V.120. N2. P. 546–58.
22. Ogorodnikova E.A., Koroleva I.V., Pak S.P. Sposob reabilitatsii funktsii akusticheskoy oriyentatsii i yeye otsenki u patsiyentov s kokhlearnym implantom. Patent na izobreteniye № 2265426, 2005. (In Russ)]
23. Ogorodnikova E.A., Koroleva I.V., Lyublinskaya V.V., Pak S.P. Komp'yuternaya trenazhernaya sistema dlya reabilitatsii slukhorechevogo vospriyatiya u patsiyentov posle operatsii kokhlearnoy implantatsii. Rossiyskaya otorinolaringologiya. 2008; Prilozheniye 1: 342–347. (In Russ)].
24. Peters B.R., Wyss J., Manrique M. Worldwide trends in bilateral cochlear implantation. Laryngoscope. 2010 May;120 Suppl 2: S17–44. https://doi.org/10.1002/lary.20859
25. Shapiro W., Tamala H., Bradham S. Cochlear Implant Programming. Otolaryngologic Clinics of North America. 2012; 45(1): 111–127. https://doi.org/10.1016/j.otc.2011.08.020.
26. Skarzynski H. et al. First Auditory brainstem implant in Poland: Auditory perception results over 12 months. J. Laryngol Otol., Suppl. 2000. V.27. P. 44–45.
27. Tavartkiladze G.A. Rukovodstvo po klinicheskoi audiologii. M.: Meditsina; 2013. (In Russ.)].
28. Vaerenberg B., Smits C., De Ceulaer G., Zir E., Harman S., Jaspers N., Tam Y., Dillon M. et al. Cochlear Implant Programming: A Global Survey on the State of the Art. The Scientific World Journal. 2014; Article ID501738, 12 pages http://doi.org/10.1155/2014/501738.
29. Vygotskiy L.S. Psikhologiya M.: Aprel'-Press, 2000. (In Russ)]
30. WHO. Deafness and hearing loss. Updated March 2018 // Available at: http://www.who.int/mediacentre/factsheets/fs300/en/ and https://www.who.int/news-room/fact-sheets/detail/deafness-and-hearing-loss.
31. Wilson B.S., Finley C.C., Lawson D.T. et al. Better speech recognition with cochlear implants // Nature. 1991. N352. P. 236–238.
32. Yanov Yu.K., Koroleva I.V., Kuzovkov V. Ye., Levin S.V., Behr R., Levina Ye.A., Sugarova S.B., Lilenko A.S. Novyye tekhnologii v otorinolaringologii: stvolomozgovaya implantatsiya. Rossiyskiy meditsinskiy zhurnal. 2017, № 23. S.1695–1698. (In Russ)].

Chapter 31.
Structural and functional features of the macula organization in schizophrenia

K. E. Kozub

Schizophrenia is a severe mental illness that affects more than 21 million people worldwide, according to WHO. Schizophrenia is characterized by impaired thinking, perception, emotions, language, self-perception and behavior.

The history of the study of visual functions in schizophrenia began with the work of E. Kraepelin and E. Bleiler. E. Kraepelin was the first to be able to obtain experimental evidence of impaired visual perception in schizophrenia [Cohen, Servan-Schreiber, 1992]. However, E. Bleiler was unable to confirm them and came to the conclusion that the main visual disturbances in schizophrenia are "unprovable" [Cohen, Servan-Schreiber, 1992]. The authoritative opinion of E. Bleiler was one of the reasons for the decrease in researchers' interest in studying visual functions in schizophrenia up to the 1950s and 1960s. XX century. Progress in research was probably constrained by the fact that visual impairment is subtle and not as obvious as high-level cognitive problems. A study of the basic visual functions of patients with psychosis (visual acuity, accommodation, visual field, color perception) in Russia was first conducted by A. Shamshinova. She showed a significant effect of psychotropic pharmacological drugs on the visual functions of patients and the need for further study of this problem [Shamshinova, 1972]. Later Goldovskaya I. L. side effects of psychotropic drugs on the organ of vision were analyzed in detail, a set of restrictions on the conduct of this therapy and measures to prevent such complications were revealed [Goldovskaya, 1989].

The first experimental evidence of a violation of the processes of visual perception in schizophrenia was obtained in the course of psychophysical studies, allowing to evaluate both sensory function and decision-making mechanism. From the 2nd half of the 20th century, neurophysiologists are actively studying this issue. The analysis of spatial visual information at lower hierarchical levels, starting from the retina, involves two parallel channels of transmission of qualitatively different information. The magnocellular (M-path) is stimulated by low-contrast, low spatial frequency, images, small stimulus size and movement. Parvocellular (P-path), in contrast, is stimulated by high-contrast

images with high spatial frequency, large stimulus size and color. The responses of the magnocellular system (approximately 10 % of nerve fibers) are faster and shorter than those of the parvocellular system (80 % of fibers). Most clearly, these paths are distinguishable at the level of the external articulated body, where they pass through different layers of cells — large (M-path) and small (P-path), forming two tracts. At the level of the cortex, the P-cells give connections mainly to the temporal cortex, and the M-cells to the parietal. Usually the first tract is called the ventral, and the second — dorsal, but between them there are cross-links (fig.1). The responses of the visual pathways to stimulation are examined using electroretinography, functional magnetic resonance imaging (fMRI), electroencephalography (EEG), which includes a wide range of event-related potentials, as well as in psychophysical experiments [Simonova et al., 2014].

In schizophrenia, persistent sensory impairments are observed, accompanied by a mismatch in the mechanisms of local and global analysis, which manifests itself in a change in the functional state of the magnocellular and parvocellular visual systems (fig.2). These changes are recorded using electroretinography, functional magnetic resonance imaging (fMRI), electroencephalography (EEG), as well as in psychophysical experiments.

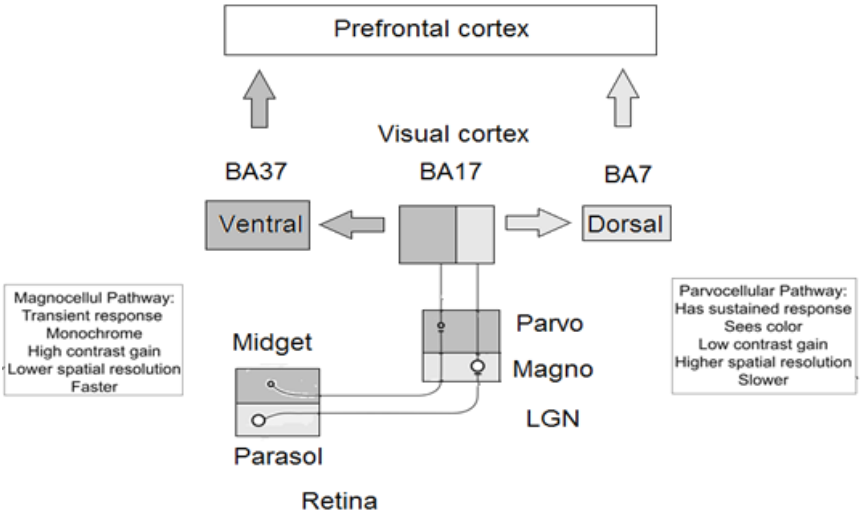

Figure 1: Visual representation of the parvocellular and magnocellular pathways.

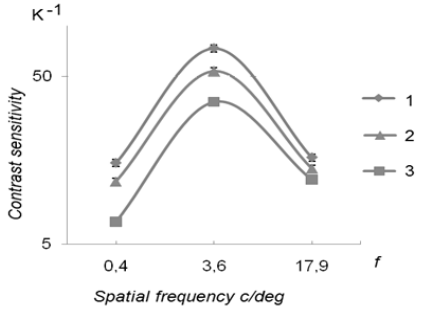

Figure 2: Change in contrast sensitivity in patients with schizophrenia depending on the type of antipsychotic therapy. *1*— normal, *2*— atypical antipsychotics, *3*— typical antipsychotics [Shoshina, Shelepin, 2016].

Patients treated with atypical antipsychotics, blocking mainly dopamine and serotonin receptors, showed a decrease in contrast sensitivity, compared with a mentally healthy control, in the range of low and medium spatial frequencies. While patients receiving typical antipsychotics, blocking mainly dopamine receptors — in the range of low and high spatial frequencies [Shoshina, Shelepin, 2016].

Thus, the results of the analysis allow to say that the type of antipsychotics produced has the effect on the degree of reduction, compared with the norm, of the threshold contrast sensitivity only in the range of low spatial frequencies, to which the magnocellular channels providing global image analysis are most sensitive. [Shoshina, Shelepin, 2016; Shelepin, 2017].

The axons of the retinal ganglion cells form the optic nerve and, leaving the retina, form synapses in the lateral geniculate body, where they provide a separate signal path for the magno- and parvocellular visual pathways. Therefore, the study of the retinal structure can be especially useful in schizophrenia, which is characterized by a disorder in both these systems.

Optical coherence tomography of the retina (OCT) is a non-contact method of visualization of the retina`s structure, based on the principle of light interferometry, in which the infraded light is projected both onto the fundus and the reference mirror. The difference between the spectral frequency composition of the light reflected from the fundus of the eye is compared with the constant spectrum of light reflected from the reference mirror and is used to visually reconstruct the retinal layers by analogy with ultrasound. OCT allows non-invasive assessment of the state of the neurons of the visu-

al analyzer. The main protocols for OCT studies are the macular mode and the mode of examination of the optic nerve head, which determines both the disk morphology and the thickness of the retinal peripapillary nerve fiber layer (RNFL).

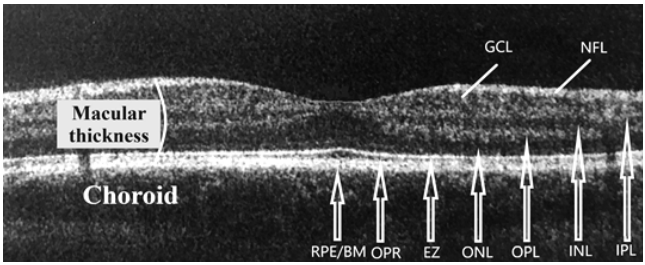

Figure 3: OCT image of the normal macula, retinal layers including:

NFL — retinal nerve fiber layer; GCL — ganglion cell layer; IPL — inner plexiform layer; INL — inner nuclear layer; OPL — outer plexiform layer; ONL — outer nuclear layer; OPR — outer segments of photoreceptors; RPE/BM — retinal pigmented epithelium/ Bruch`s membrane complex; EZ — ellipsoid zone

OCT studies of retina performed in patients with schizophrenia are few and tend to show thinning of the retinal peripapillary nerve fiber layer (RNFL) or macula. Curiously, in the study from Spain [Ascaso at al. 2015], thinning of the macula was found in a subgroup of patients who had not had a psychotic episode in the last 6 months, suggesting that acute psychosis may be associated with inflammation and swelling of the retinal tissues, which prevents the detection of her atrophy. A similar conclusion had previously been confirmed in a study from Malaysia by Dr. Lee et al. (Table 1), where the thinning of the macula was found in patients with a longer duration of the disease, while in patients with a disease experience of less than 2 years, it did not differ from the control.

One of the latest research by Silverstein et al. (2018), including 32 patients with schizophrenia and 32 control faces, correlated by sex and age, taking into account their comorbidities and dose of antipsychotic drugs, showed no deviations in the thickness of the macula and RNFL, but revealed increased parameters of the Cup volume and the Cup to disk ratio. The latter conclusion requires a recheck taking into account the data on patient refraction, since changes in this index may be due to the anatomical features of the eyes, in particular myopia (an increase in disk excavation in megalodisks, provided that glaucoma is excluded).

Table.1

Comparisons between control group and schizophrenia subgroups according to chronicity or illness [Lee, 2013]

	N	Mean	SD
Overall peripapillary RNFL thickness, μm			
Control	30	103.53	6.53
Acute	5	103.60	6.35
Chronic	13	94.15	6.63
Long term chronic	12	91.58	12.15
Macula average thickness, μm			
Control	30	284.83	9.76
Acute	5	278.20	8.07
Chronic	13	271.08	10.25
Long term chronic	12	263.58	14.28
Macula volume, mm^3			
Control	30	10.17	0.35
Acute	5	9.94	0.31
Chronic	13	9.69	0.36
Long term chronic	12	9.44	0.52

* The mean difference is statistically significant at the 0.05 level.

Findings:

The detection of reliable markers of schizophrenia using the OCT method, which is objective, fast, and non-invasive, could make a significant contribution to the system of diagnosis and monitoring of patients with schizophrenia. Finally, it may be fundamentally important to establish a link between peripheral changes in the structure of the visual analyzer (thickness and geometry of the macular zone) and functional changes at all stages of the transmission and analysis of visual information.

References

1. Cohen J.D., Servan-Schreiber D. Context, cortex, and dopamine: a connectionist approach to behavior and biology in schizophrenia // Psychol

Rev. 1992.Vol. 99. P. 45–77.
2. Goldovskaya I. N. Psychotropic therapy and organ of vision. Dissertation abstract, 1989.
3. Joe P. A pilot study assessing retinal pathology in psychosis using optical coherence tomography: Choroidal and macular thickness // Psychiatry Res. 2018.
4. Lee W. W., Tajunisah I., Sharmilla K., Peyman M., Subrayan V. Retinal nerve fiber layer structureabnormalities in schizophrenia and itsrelationship to disease state: evidencefrom optical coherence tomography // Invest Ophthalmol Vis Sci.2013;54:7785–7792.
5. Shamshinova A. M. Changes in the organ of vision in patients with schizophrenia during treatment with neuroleptics of the phenothiazine series (chlorpromazine, triftazine). Dissertation abstract, 1972.
6. Shelepin Y. E. Introduction to neuroeconics. Spb. ITK Troitsky bridge LLC, 2017. P. 92–106, 122–132.
7. Shoshina I. I., Shelepin Y. E. Mechanisms for global and local analysis of visual information in schizophrenia. Spb. BBM, 2016. P. 58–59, 97–101, 227–228.
8. Simonova N. A., Garah J. V., Zaitseva Y. S., Shmukler A. B. Neurophysiological mechanisms of visual impairment in schizophrenia // Social and Clinical Psychiatry 2014, Vol. 24, No. 1
9. Silverstein S. M., Paterno D., Cherneski L., Green S. Optical coherence tomography indices of structural retinal pathology in schizophrenia // Psychological Medicine, Vol. 48, Issue 12. September 2018.

Chapter 32.
Modern angle of view of the problem of restoration of vital functions

D. I. Krivenchuk, A. S. Zamaro, V. A. Kulchitsky

The title of the article to some extent reflects the importance of the visual analyzer for the analysis of facts and the generation of hypotheses in scientific research. Face-to-face scientific discussions among professionals are a necessary step in verifying various assumptions. The authors of the article looked at the problem of correction of control of vital functions. Mortality statistics reflect the fact of insufficient effectiveness of modern methods of diagnosis and treatment of diseases that are accompanied by a violation of the control of the activity of the heart and blood vessels, as well as the respiratory system [Wang et al., 2019].

One of the fatal conditions is respiratory arrest, especially when apnea develops during sleep. Why during sleep? In a sleeping state, there is no possibility of arbitrary regulation of respiration. During wakefulness, a person consciously, when trying to hold a long breath, ultimately decides to resume inhaling and exhaling. Therefore, if a person has impaired automatic control of breathing regulation, then due to arbitrary regulation, correction of inhalation and exhalation is possible. However, during sleep with a violation of the central regulation of respiration and the absence of arbitrary control of inspiration and expiration, the mechanism of chemoreceptor regulation remains. Receptors of the vascular bed and especially the carotid body detect a lack of oxygen in the blood, and medullary receptors (on the ventral surface of the medulla oblongata) respond to the growth of carbon dioxide in the brain tissue [Schläfke et al., 1975; Chernigovsky, 1976; Nattie, Li, 2012] and contribute to the activation of respiratory movements when breathing is held. And if a pathological process develops in the area of these receptors, which is accompanied by inhibition of the functional state of peripheral (in the vessels) and central (in the brain) chemoreceptors? In this case, the chemoreceptor mechanism will not work and sleep apnea will actually become fatal for a person. Therefore, for the prevention of such fatal conditions, it is advisable to determine the effectiveness of the functioning of peripheral and central chemoreceptors. This technique of “return breathing” was developed in ex-

periments [Sato et al., 1994; Dahan et al., 2007; Bruce, White, 2015] and proposed in clinical practice [Kulchitsky et al., 2014; Kaliadzich et al., 2014], in particular for the treatment of patients with obstructive sleep apnea syndrome [Kulchitsky et al., 2018].

So, the complex issue of timely diagnosis and timely treatment of sleep apnea is considered. Nevertheless, what is seen on the horizon in the technologies for the prevention and treatment of diseases that are manifested by pathological processes in brain tissue due to brain ischemia, hemorrhage or brain injury? Until now, the restoration of the performance of patients of different ages after a stroke is a problem in virtually all countries of the world. As a result of the pathological process in the nervous tissue, the functioning of the neural networks of the brain is disrupted. Clinical practice has shown that after a sudden violation of the structure and functioning conditions of neural networks, even in a local area of the brain, a process of restoring control of impaired functions develops over a long period. But, unfortunately, depending on many conditions, the reparative process is very slow and often the patient remains disabled for life. In the course of experiments on laboratory rodents, it was possible to prove high efficiency for the restoration of brain neural networks of manipulations on the implantation of mesenchymal stem cells (MSCs) into the brain. The authors of the article, together with neurosurgeons Yuri Shanko and Valeria Novitskaya (Republican Scientific and Practical Center for Neurology and Neurosurgery, Minsk, Belarus), demonstrated that the best implantation efficiency is achieved using the perineural stem cell migration technique after injection of the suspension with MSCs into the submucous layer of the nasal cavity [Shanko et al., 2018a; 2018b, 2018c; Kulchitsky et al., 2018]. In this case, MSCs migrate in the perineural spaces of the olfactory and trigeminal nerves to the cranial cavity (*Figure 1*) and then directly to the site of brain damage [Shanko et al., 2018a; 2018b, 2018c; Kulchitsky et al., 2018]. In the area of damage to the neural networks of the brain, MSCs secrete neurotrophic factors that form the conditions for the restoration of the functions of neural networks. In three clinics in Minsk, more than 75 patients who have suffered an ischemic stroke or brain injury have been effectively treated [Shanko et al., 2019a; Zamaro et al., 2018].

Unfortunately, the problem of restoring brain functions is especially difficult to solve in the presence of massive damage to the neural networks of the brain. In such situations, clinicians sometimes dreamed of methods by which they could replace the destroyed parts of the brain with healthy neural networks.

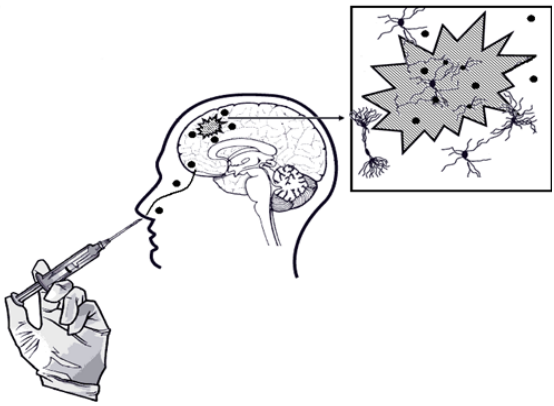

Figure 1. Scheme of migration of mesenchymal stem cells along the olfactory and trigeminal nerves from the nasal cavity to the injured brain.

These dreams begin to come true. Bioprinting technologies appeared in the 21st century. Such technologies make it possible to construct various biological structures in organoids, scaffolds, and in three-dimensional space. The authors are primarily interested in the technology of bioprinting of nervous tissue. The complexity of the structure of neural networks, their interaction with glial elements, the intercellular matrix, blood vessels, cerebrospinal fluid, and various signaling molecules that are secreted at the synapse level and extrasynaptically makes the solution to this problem extremely difficult [Shanko et al., 2019b; Zamaro et al., 2018]. The appearance of the first bioprinters and excessive advertising of new technologies only emphasized the complexity and unresolved nature of this problem. Suppose, using bioprinting, a three-dimensional biological object has been created, including neural networks, glial elements, and the intercellular matrix. It becomes clear that such a design is not viable after placing it in damaged areas of the brain. In this design, there are no blood vessels and other elements of the nervous tissue that are vital for the normal functioning of the implanted neural networks. That is why we sadly sometimes look at the next designed model of a bioprinter. Nevertheless, our small team is looking to the future with hope.

References

1. Bruce R.M., White M.J. (2015) The ventilatory response to muscle afferent activation during concurrent hypercapnia in humans: central and

peripheral mechanisms. Exp. Physiol. 100(8):896–904. doi: 10.1113/EP085024.
2. Chernigovsky V.N. (1976) Tissue receptors. Historical scope. Modern view. Perspectives. Prog. Brain Res. 43: 3–14.
3. Dahan A., Nieuwenhuijs D., Teppema L. (2007) Plasticity of central chemoreceptors: effect of bilateral carotid body resection on central CO_2 sensitivity. PLoS Med. 4(7): e239.
4. Kaliadzich Z., Semenik T., Riazechkin A., Furmanchuk D., Andrianova T., Zaikina N., Pashkevich S., Gudny G., Kulchitsky V. (2014) Chemoreceptor control of gas homeostasis in patients with obstructive sleep apnea. Act. Nerv. Super. Rediviva 56(3–4): 73–78.
5. Kulchitsky V., Zamaro A., Koulchitsky S. (2018) Hypoxia and Hypercapnia: Sensory and Effector Mechanisms. Biomedical Journal of Scientific & Technical Research. 8(4): 1–3. DOI: 10.2671/BJSTR.2018.08.001692.
6. Kulchitsky V., Zamaro A., Krivenchuk D., Koulchitsky S. (2019) Can Nerve Trunks Serve as Railroads for Stem Cells? Biomedical Journal of Scientific & Technical Research. 15(1): 1–3.
7. Kulchitsky V., Zamaro A., Shanko Y., Koulchitsky S. (2018) Prospects of Perineural Implantation of Stem Cells in Recovery of Neural Networks' Functions in Brain Diseases. Biomedical Journal of Scientific & Technical Research. 10(3): 1–4.
8. Kulchitsky V., Semenik T., Kaliadzich Z., Andrianova T., Tsishkevich K. (2014) The analysis of chemosensitive structures contribution to obstructive sleep apnea development. Clin. Neurophysiol. 125 (1): S330-S331.
9. Nattie E., Li A. (2012) Central chemoreceptors: locations and functions. Compr. Physiol. 2(1): 221–254.
10. Sato M., Severinghaus J.W., Bickler P. (1994) Time course of augmentation and depression of hypoxic ventilatory responses at altitude. J. Appl. Physiol. 77(1):313–316.
11. Schläfke M.E., Pokorski M., See W.R., Prill R.K., Loeschcke H.H. (1975) Chemosensitive neurons on the ventral medullary surface. Bull. Physiopathol. Respir. (Nancy) 11(2): 277–284.
12. Shanko Y., Navitskaya V., Zamaro A., Krivenko S., Zafranskaya M., Pashkevich S., Koulchitsky S., Takalchik-Stukach Y., Denisov A., Kulchitsky V. (2018c) Prospects of Perineural Administration of Autologous Mesenchymal Stem Cells of Adipose Tissue in Patients with Cerebral Infarction. Biomedical Journal of Scientific & Technical Research, 10(1) 1–3.
13. Shanko Y., Krivenchuk D., Zamaro A., Koulchitsky S., Navitskaya V., Kulchitsky V. (2019b) Mutual Issues of Bioprinting and Stem Cell Technologies in Neural Tissue Repair. Biomedical Journal of Scientific & Technical Research. 16(5): 1–3.

14. Shanko Y., Navitskaya V., Zamaro A., Krivenko S., Koulchitsky S., Kulchitsky V. (2019a) Application of stem cells perineural migration in patients with stroke. J. Neurol. Stroke. 9(2):111–112.
15. Shanko Y., Navitskaya V., Zamaro A., Zafranskaya M., Krivenko S., Koulchitsky S., Takalchik-Stukach Y., Smeyanovich A., Nizheharodova D., Pashkevich S., Dosina M., Denisov A., Kulchitsky V. (2018b) Somatotopic principle of perineural implantation of stem cells in patients with brain injuries. J. Neurol. Stroke. 8(5):259–261.
16. Shanko Y., Zamaro A., Takalchik-Stukach Y., Koulchitsky S., Pashkevich S., Panahova E., Navitskaya V., Dosina M., Denisov A., Bushuk S., Kulchitsky V. (2018a) Mechanisms of Neural Network Structures Recovery in Brain Trauma. Biomedical Journal of Scientific & Technical Research. 7(5):1–2.
17. Wang F., Harel-Sterling L., Cohen S., Liu A., Brophy J.M., Paradis G., Marelli A.J. (2019) Heart failure risk predictions in adult patients with congenital heart disease: a systematic review. Heart. pii: heartjnl-2019–314977. doi: 10.1136/heartjnl-2019–314977.
18. Zamaro A., Krivenchuk D., Denisov A., Koulchitsky S., Kulchitsky V. (2018) Topical Issues of Bioprinting Technology. Biomedical Journal of Scientific & Technical Research. 12(1): 1–3.

Chapter 33.
The functional connectivity's alterations among patients with Alzheimer's disease

K. V. Markin, D. A. Tarumov, K. M. Naumov, V. U. Lobzin, A. V. Temniy, N. A. Puchkov

Introduction

Alzheimer's disease (AD) is a chronic neurodegenerative disease manifested by progressive deterioration of memory, speech, and other higher cortical functions. Today, according to the WHO, it is the main (60–80 %) cause of all dementias [The Global Dementia Observatory Reference Guide, 2018]. The pathogenesis of the disease is based on impaired metabolism of beta-amyloid which accumulates in brain tissues and vessel walls in the form of senile plaques. Also, formations of neurofibrillary tangles consisting of bound hyperphosphorylated tau-protein leading to accelerate the neurodegenerative processes of white and gray brain's matter [Lobzin et al., 2018]. The macropathogenesis of the disease is characterized by a sequential neurodegenerative process of the cortical divisions, which begins with the medial divisions of the cortex, then moves to the temporal and parietal lobes, then the frontal lobes and lastly captures the occipital lobes [Emelin et al., 2017].

Based on this, the earliest symptom of the following clinic is memory impairment in the form of progressive amnesia (first forgetfulness to current events, then fixation amnesia, then complete anamnestic disorientation). Along with memory disorders, all types of cognitive activity are disturbed (attention, comprehension, analysis, synthesis, abstraction). Later, violations of orientation in space and perception (recognition of faces, identification of objects) appear. The late stage of AD is characterized by a global neurodegenerative process with manifestations of behavioral and psychotic disorders, progressive disturbances of posture, gait, muscle stiffness. [Emelin et al., 2016]

For early detection and accurate diagnosis of AD, it is necessary to understand the degree of dysfunction of the brain systems involved in the process of memory ensure. Neuroimaging is one of the best methods in this case because of its informativeness and minimally invasiveness in comparison with others. fMRI is the method of neuroimaging which is using to assess the dynamics

of functional disorders based on changes in the main brain networks. Resting state Functional magnetic resonance imaging (rs-fMRI) is the registration of the BOLD signal (Blood Oxygen Level Dependent) from the volume points of the brain called voxels. The similarity of the frequency characteristics of the recorded BOLD signal in anatomically distant parts of the brain is called functional connectivity (FC) [Piradov et al., 20165]. It is assumed that this coactivation of brain structures during the resting state reflects the functional relationships that underlie brain's readiness to respond to incoming external stimuli. Therefore, the FC reflects the similarity of the characteristics of the pattern of neural activity of brain structures anatomically distant from each other [Van den Heuvel et al., 2010]. Modern methods allow us to analyze the GM as a single network, a connection consisting of subnets, and also to evaluate the topology of functional connections. The most common mathematical method for evaluating a "macroconnectom" and the main theoretical approach to studying its structural and functional organization is graph theory, according to which the whole brain is represented as a set of nodes (anatomical regions) interconnected in varying degrees [Van den Heuvel et al., 2011; Achard et al., 2007].

According to the theory of neural systems (Figure 1), the work of the brain is represented as a changing activity of neural networks depending on the activity being performed. Brain networks are constellation formations of large neural ensembles of various parts of the cortex and subcortical structures. Today were allocated 32 brain networks [Rosazza et aql., 2011] which can be divided into two large groups: "task-positive" (task performance) and "task-neg-

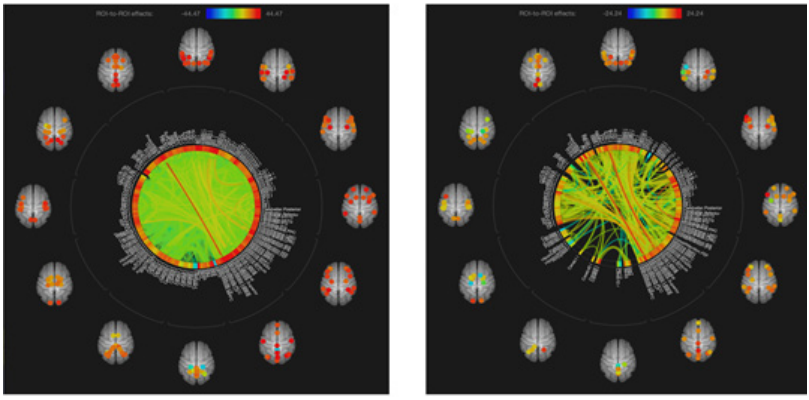

Figure 2. General FC of HC (left) and AD patients (right).

ative" (passive mode of the brain). In accordance with Stanford University's manual, Salience Network (SN) has a switching function between these two types of brain networks [Menon et al., 2015]. Default Mode Network (DMN) is the main task-negative network which is represented by Medial Prefrontal Cortex (MPFC), Posterior Cingulate Cortex and the Lateral Occipital Cortex right and left division (LOC l/r) [Horn et al., 2013]. These components are anatomically closely related to the parahippocampal gyrus, angular gyrus, hippocampus, that apparently determines one of the main functions of the DMN — mental "scrolling" of recent memorable exciting events that we call a passive brain mode [Davey et al., 2016; Mars et al., 2012]. Moreover, binding the time continuum [Ostby et al., 2012], absorbing distractions [Ziaei et al., 2014], activating the chains of "social connections" [Li et al., 2014] and others are the DMNs functions too.

The main "task-positive" network is the Executive Control Network (ECN). It consists of Lateral Prefrontal Cortex (LPFC) on the right and left sides, and Posterior Parietal Cortex (PPC), also both divisions. The function, based on the name, of this network is any initiation and control of cognitive activity [Marek et al., 2018; Zanto et al., 2013]. The Salient Network is represented by the Anterior Insular Lobe (AI) and the Anterior Cingulate Cortex

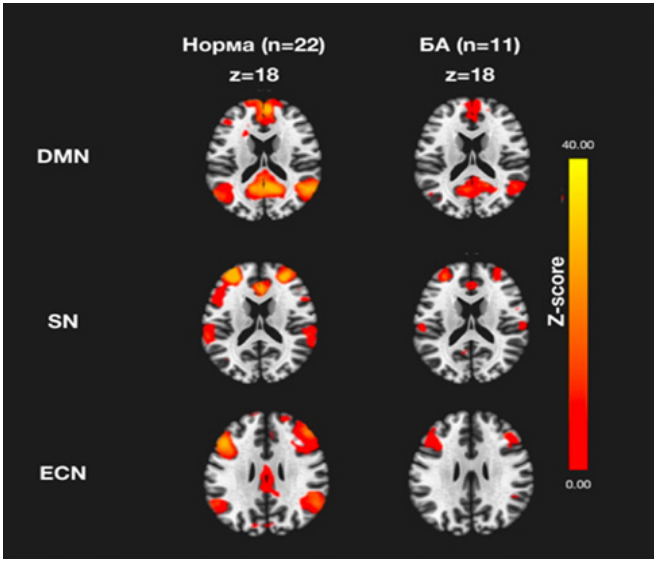

Figure 3. Main alterations of FC among AD patients.

(ACC) and regulates switching between “task-positive” and “task-negative” networks [Menon et al., 2015; Menon et al., 2011]. So, the FC alterations of these brain networks within it or with other brain structures could serve as a basis for identifying the causes of the appearance of certain symptoms in patients with AD. According to the first meta-analysis conducted by Jacobs in 2013 (53 studies / 1196 patients / 1255 healthy), FC decrease in the DMN among patients with AD can be predictor of the disease long before the first symptoms appear, immediately after its compensatory amplification [Jacobs et al., 2013].

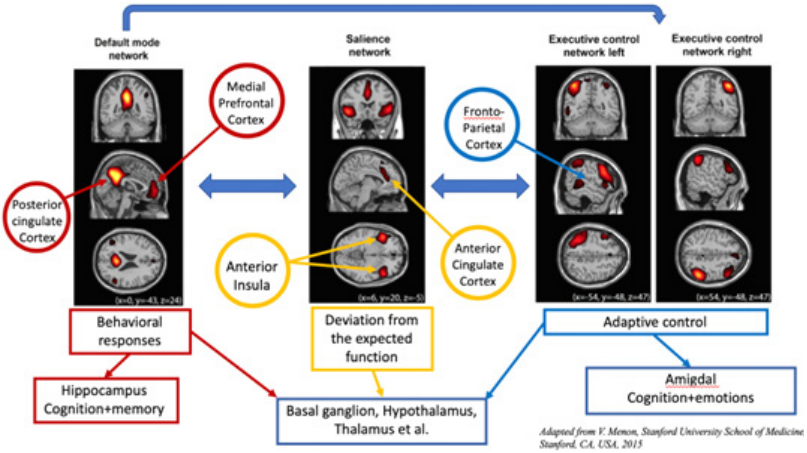

Figure 1. The scheme of the Brain Network theory.

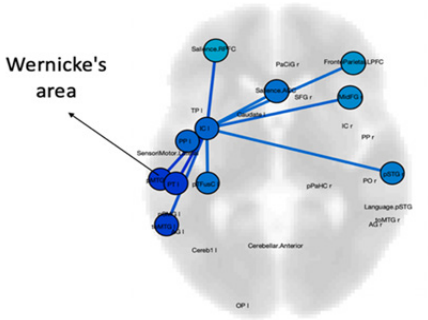

Figure 4. Comparison of alterations in FC of Networks.

A meta-analysis of 75 sources on this topic in 2015 showed that a decrease in FC among patients with AD was observed in all brain networks in comparison with patients with mild cognitive impairment (MCI), which alterations of FC in similarly brain networks were lower [Li et al., 2015]. Having analyzed 34 sources for 2017, Badhwar came to the conclusion that patients with AD and MCI have a significant decrease in FC in the DMN and ECN amid an increase in FC in the SN. In this case, the compensatory function is attributed to the Salience Network [Badhwar et al., 2017].

The purpose of our study is to identify changes in functional connectivity in patients with Alzheimer's disease.

Materials and methods

An experimental group included 11 (70±4 years of age) patients from Neurology Department with AD; control group consisted of 22 healthy controls. Resting functional magnetic resonance imaging was performed on each subject. The next stage — postprocessing (motion correction, spatial normalization, image smoothing) and statistical analysis were carried out on the basis of MATLAB, using the CONN Functional Connectivity Toolbox 18.a package.

Results

General FC of patients is significantly reduced in comparison with the control group (Figure 2). When considering the results of data processing according to the graph theory method, the main nodes with reduced FC are in the temporal and parietal lobes, which fully correspond to the previously described etiopathogenesis of the disease. The significant differences in FC during intergroup comparison (p-FDR <0.05) were determined mainly by decreased FC, although regions were also observed with its increase. The main node with reduced PK in patients with BA was the Insula Cortex in left division (ICl), which lies anatomically between the medial and convexity parts of the temporal-parietal-frontal junction, and communicates with the nuclei of the thalamus and the amygdala through the white matter pathways. Previous studies have associated a decrease in the IC FC with episodic memory impairments in patients with MCI [Bushara et al., 2001], and also describe the correlation between the connection of the insular lobe with various elements of the GM brain and neuropsychological studies [Seghier et al., 2012].

In our study decreasing in the FC of the insular lobe was observed with the following nodes: the temporal plane, the temporal pole and the posterior part of the superior temporal gyrus, which together represent the Wernicke's area,

which may be the reason for the difficulty in processing multimodal sensory information [Bushara et al., 2001]; angular gyrus, which function is to extract traces of memory [Seghier et al., 2012]; the anterior prefrontal cortex responsible for extracting prospective memory [Volle et al., 2011]. These FC changes are consistent with the results (the average result of the experimental group was 18.25–3.45, with a norm of no less than 26 points) of the neuropsychological testing of MoCA (Montreal Cognitive Assessment) aimed at identifying dementia by examining the functions of attention, memory, and concentration in patients' executive functions, speech, optical-spatial activity, conceptual thinking, counting and orientation (Figure 3). At the same time, a decrease in FC between the insular lobe and the medial frontal gyrus, as well as the worm-like gyrus, clearly indicates a violation of the recognition of faces by patients, which is confirmed by the results (average quality rating = 38–20 %; quantitative characteristic = 32–10 %) of neuropsychological testing on face recognition (using pictures of the illusory nature of Giuseppe Archimboldo and Oleg Shuplyak).

Comparison of the FC of brain networks in patients with AD and the control group showed that its decline is observed in both task-positive and task-negative networks (Figure 4). A decrease in the DMN FC within the network, and to a greater extent in relation to other nodes, corresponds to the data described in the literature [Horn et al., 2013; Davey et al., 2016; Qin et al., 2016; Mars et al., 2012; Ostby et al., 2012; Jacobs et al., 2013; Li et al., 2015; Badhwar et al., 2017] and manifests itself clinically in the form of the absence of memories of recent events and the "scrolling" of related information the mental continuum of patients in comparison with a healthy person. In patients, predominantly, there is a residual memory for events of old years or a momentary, emotionally weakly colored reaction to events occurring around, with no compartments with memory traces due to their absence. This is clearly manifested in the repeated questions of patients about their location, forgetting the distance traveled, the repetition of the same phrases with indistinguishable semantic content in relation to the current situation. At the same time, the gap in connectivity between the DMN elements and the islet lobe, which is part of the SN, observed in patients with asthma may indicate the impossibility of switching between work modes and rest of the brain, and therefore, turning on / off DMN or ECN, depending on the prevailing functional mode (Figure 5). Perhaps this explains the increase in FC between the anterior cingulate gyrus — the SN element and elements of the visual network (primary fields) (Figure 6). In this case, SN assumes the function of the DMN and proceeds to the processing of the incoming picture of the world from the

visual network — a compensatory function, but not coping with the amount of information, does not include its flow into the circulation in the GM, and therefore there is no comparison. At the same time, other elements of the visual network, as well as individual "Cuneus" nodes covering the secondary visual fields reflect a decrease in FC, which once again confirms the flow of information that has not been completely processed by the visual analyzer to the salient network.

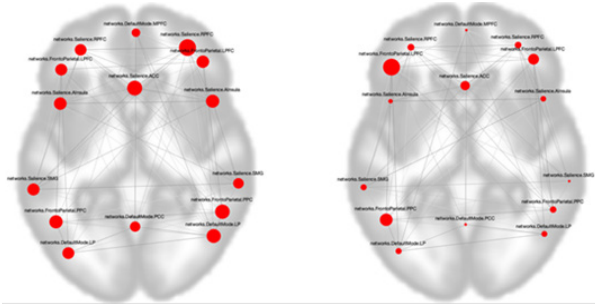

Figure 5. Internetwork alterations of FC among HC (left) and AD (right).

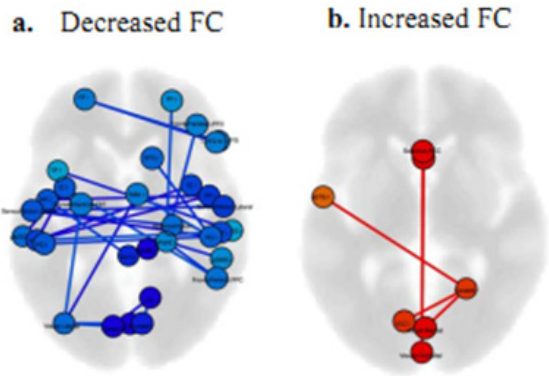

Figure 6. Intergroup comparison of FC.

Conclusion

In conclusion, alterations of functional connectivity among patients with Alzheimer's disease can be a good predictor of early stages and an evidence base for neuropsychological tests. Also, it could be helpful for studying pathogen-

esis of the disease.

References

1. Achard S. Efficiency and Cost of Economical Brain Functional Networks / S. Achard, E. Bullmore // PLoS Comput Biol — 2007. — № 3(2). — e17.
2. Badhwar A. P. Resting-state network dysfunction in Alzheimer's disease: A systematic review and meta-analysis / A. P. Badhwar [et al.] // Alzheimer's & Dementia: Diagnosis, Assessment & Disease Monitoring — 2017. — Vol. 8. — P. 73–85.
3. Bushara K. Neural correlates of auditory-visual stimulus onset asynchrony detection / K. Bushara [et al.] // J Neurosci — 2001. — Vol 13. — P. 300–304.
4. Davey C. G. Mapping the Self in the Brain's Default Mode Network / C. G. Davey, J. Pujol, B. J. Harrison // NeuroImage — 2016. — Vol. 132. — P. 390–397.
5. Emelin A. Yu. Bolezn' Al'tsgeymera: uchebnoye posobiye / A.YU. Yemelin, V.YU. Lobzin, I. S. Zheleznyak, I. V. Boykov. — SPb: VMedA, 2016. — 75 s.
6. Emelin A. Yu. Kompleksnaya differentsial'naya diagnostika kognitivnykh narusheniy / A.YU. Yemelin, V.YU. Lobzin // Zhurn. nevrologii i psikhiatrii imeni S. S. Korsakova. — 2017. — № 6, Vyp.2. — S. 33–39.
7. Horn A. The structural-functional connectome and the default mode network of the human brain / A. Horn, D. Ostwald, M. Reisert, F. Blankenburg // NeuroImage. — 2013. — Vol. 102. — P. 142–151.
8. Jacobs H. I.L. Meta-analysis of functional network alterations in Alzheimer's disease: Toward a network biomarker / H.I.L. Jacobs, J. Radua, H. C. Lukmann, A. T. Sack // Neuroscience and Biobehavioral Reviews — 2013. — Vol. 37. — P. 753–765.
9. Li H. J. Toward Systems Neuroscience in Mild Cognitive Impairment and Alzheimer's Disease: A Meta-Analysis of 75 fMRI Studies / H. J. Li [et al.] // Human Brain Mapping — 2015. — Vol. 36. — P. 1217–1232.
10. Li W. The Default Mode Network and Social Understanding of Others: What Do Brain Connectivity Studies Tell Us / W. Li, X. Mai, C. Liu // Frontiers in Human Neuroscience — 2014. — Vol. 8. — P. 74.
11. Liu X. Altered Functional Connectivity of Insular Subregions in Alzheimer's Disease / X. Liu [et al.] // Frontiers in Aging Neuroscience — 2018. — Vol. 10. — P. 1–12.
12. Lobzin V. Yu. Novyy vzglyad na patogenez bolezni Al'tsgeymera: sovremennyye predstavleniya o klirense amiloida / V.YU. Lobzin, K. A. Kolmakova, A.YU. Yemelin // Obozreniye psikhiatrii i meditsinskoy psikhologii. — 2018. — № 2 — S. 22–28.

13. Marek S. The frontoparietal network: function, electrophysiology and importance of individual precision mapping / S. Marek, U. F. Nico // Dialogues Clin Neurosci — 2018. — Vol. 20, № 2. — P. 133–140.
14. Mars R. B. On the Relationship between the 'Default Mode Network' and the 'Social Brain' /R.B. Mars [et al.] // Frontiers in Human Neuroscience — 2012. — Vol. 6. — P. 189.
15. Menon V. Large-scale brain networks and psychopathology: a unifying triple network model / V. Menon // Trends in Cognitive Sciences — 2011. — Vol. 15, № 10. — P. 483–506.
16. Menon V. Salience Network / V. Menon, A. W. Toga // Brain Mapping: An Encyclopedic Reference — 2015. — Vol. 2. — P. 597–611.
17. Ostby Y. Mental Time Travel and Default-Mode Network Functional Connectivity in the Developing Brain / Y. Otsby [et al.] // Proceedings of the National Academy of Sciences — 2012. — Vol. 109, № 42. — P. 16800–16804.
18. Piradov M. A. Vozmozhnosti sovremennykh metodov neĭrovizualizatsii v izuchenii spontannoĭ aktivnosti golovnogo mozga v sostoyanii pokoya / M. A. Piradov [i dr.] // Nevrologicheskiĭ zhurnal — 2016. — Vyp. 21, № 1. — S. 4–12.
19. Qin P. Spontaneous Activity in Default-Mode Network Predicts Ascription of Self-Relatedness to Stimuli / P. Qin, S. Grimm [et al.] // Social Cognitive and Affective Neuroscience — 2016. — Vol. 11, № 4. — P. 693–702.
20. Rosazza C. Resting-state brain networks: literature review and clinical applications / C. Rosazza, L. Minati // Neurol Sci — 2011. — Vol. 32, № 5. — P. 773–785.
21. Seghier, M. L. The Angular Gyrus: Multiple Functions and Multiple Subdivisions / M. L. Seghier // The Neuroscientist — 2012. — Vol. 19, № 1. — P. 43–61.
22. The Global Dementia Observatory Reference Guide. Geneva, Switzerland: World Health Organization, 2018.
23. Van den Heuvel M. P. Exploring the brain network: a review on resting-state fMRI functional connectivity / M. P. Van den Heuvel, H. E. Hulshoff Pol // European Neuropsychopharm — 2010. — № 20(8). — P. 519–534.
24. Van den Heuvel M. P. Rich-Club Organization of the Human Connectome / M. P. Van den Heuvel, O. Sporns // Journal of Neuroscience — 2011. — № 31(44). — P. 15775–15786.
25. Volle E. The role of rostral prefrontal cortex in prospective memory: A voxel-based lesion study / E. Volle [et al.] // Neuropsychologia — 2011. — Vol. 49, № 8. — P. 2185–2198.

26. Xie C. Abnormal insula functional network is associated with episodic memory decline in amnestic mild cognitive impairment / C. Xie [et al.] // NeuroImage — 2012. — Vol. 63, № 1. — P. 320–327.
27. Zanto, P. T. Fronto-parietal network: flexible hub of cognitive control / P. T. Zanto, A. Gazzaley // Trends in Cognitive Sciences — 2013. — Vol. 17, № 12. — P. 602–603.
28. Ziaei M. Brain Systems Underlying Attentional Control and Emotional Distraction During Working Memory Encoding / M. Ziaei, N. Peira, J. Persson // NeuroImage — 2014. — Vol. 87. — P 276–286.

Chapter 34.
Violation of visual information processing in patients with schizophrenia and depression and their correction with the help of cognitive tasks in a virtual environment

S. V. Murav'eva, Yu. E. Shelepin

Introduction

The aim of this study was to evaluate the effectiveness of the application of neurotechnology with an interactive virtual environment for the correction of cognitive impairment in patients with schizophrenia and depression (focused activity in a virtual environment). In the Vision Physiology Laboratory was created a neurotechnology using virtual reality for the rehabilitation of patients with neurocognitive disorders. The task was to create a technology for the rehabilitation of patients by activating the work of the spatial-frequency channels of the visual system associated with cognitive functions.

Methods

This paper describes research data that evaluated the effect of a course of visual stimulation with a cognitive task in an interactive virtual environment on the functioning of the magno- and parvo systems in patients with schizophrenia and depression. The virtual environment used at the second stage of the analysis represented a video of natural scenes that simulated a bike ride through the landscape with a varying relief completely synchronized with the movement of the patients. To demonstrate the images, a large angular size monitor was used, which provided a more complete immersion of the subjects into a virtual environment. The observer's task included a thorough review of both spatial images (magno-system) and separate objects (parvo-system) presented on the panoramic monitor, but also the fulfillment of the cognitive task. For example, focusing on individual video elements in order to search and account objects with certain characteristics set at the beginning of the session.

To assess the effectiveness of the technique, we used the analysis of the amplitude of the components of cognitive visual evoked potentials in the demonstration of images that differ in physical features (spatial-frequency spectrum)

for selective activation of low-frequency (magno) and high-frequency (parvo) channels and semantic features (objects of living and nonliving)

The study involved 30 patients with paranoid schizophrenia (F20 for ICD—10) with disease duration of 1 to 10 years—17 men and 13 women and 14 patients with depression (F32; F33 for ICD—10)—8 men and 6 women aged 21 to 34 years. The control group consisted of 30 healthy subjects aged from 18 to 30 years old—16 men and 14 women. All observers had visual acuity of at least 0.9, refraction corresponded to the norm. All patients who participated in the studies were in the hospital and received antipsychotic therapy.

At the primary stage, when comparing the results obtained in patients with schizophrenia and the control group and patients with depression and the control group before the course of focused activity in a virtual environment, the following significant changes were identified.

Results and Discussion

Comparative analysis of evoked potentials amplitude during the perception of images, that filtered via digital filtration for selective effect on the magno- (low frequency) and parvo- (high frequency)—channels of the visual system was used. It was shown that in patients of both groups a decrease in the amplitude of the components of evoked potentials to stimuli, filtered mainly by high spatial frequencies (parvo system), is observed.

In patients with schizophrenia, a significant decrease in the amplitude of the components of visual evoked potentials P100 (N100) and P250 (N250) in the occipital (O1; O2), central (C3; Cz; C4), anterior (Fp1; Fp2) and posterior frontal areas (F3; Fz; F4). A decrease in the amplitude of N170 is observed in the occipital (O1; O2) and temporal region (T5; T6), P300- P500—in the parietal (P3; Pz; P4), central (C3; Cz; C4) and frontal region (Fp1; Fp2 and F3; Fz; F4) compared with healthy subjects. This effect did not depend on the content of images (live or inanimate objects). When comparing the ratio of the amplitudes of the components, the following differences in patient and the control group are observed. In the control group, the amplitude of the P170 component in the parietal, in the central lead (Cz) and the frontal leads is not significantly different, in the central leads (C3, C4)—at high frequencies higher than at low frequencies. And patients have the opposite picture: the amplitude of this component is significantly higher at low spatial frequencies than at high ones. In the control group, the amplitude of the N250 (P250) components in the occipital, central, and frontal leads to high-frequency stimuli was significantly higher than the low, and the patients did not differ

significantly. In the control group, the amplitude of the P300- P500 component in the parietal, central, and frontal leads to high-frequency stimuli was significantly higher than low. And in patients with schizophrenia, this pattern is observed only in the central parietal abduction (Pz). In the other leads is not significantly different.

In patients with depression upon presentation of images containing the high-frequency part of the spectrum, a significant decrease in the amplitude of the components of visual evoked potentials was recorded. The amplitude of component P100 (N100) is significantly reduced in the anterior (Fp1; Fp2) and posterior frontal region (F7; F3; Fz; F4; F8), the central region (C3; Cz; C4) and the parietal region (P3; Pz; P4). This effect did not depend on the content of images (live or inanimate objects). The amplitude of component N170 (P170) was significantly reduced in the frontal region (Fp1; Fp2) and (F7; F3; Fz; F4; F8), central (C3; Cz; C4) and the parietal region (P3; Pz; P4) upon presentation of images animate and inanimate nature. The amplitude of the N250 component is reliably reduced in the anterior and posterior frontal, central and parietal regions only upon presentation of images of wildlife.

When comparing the ratio of the amplitudes of the components in all the above areas, the following significant differences in these patients from the control group are observed. In the control group, the amplitude of the P170 component in the parietal, frontal leads is not significantly different, in the central leads it is higher at high frequencies than at low ones. This effect did not depend on the content of images (live or inanimate objects). And in patients with images of inanimate nature, the opposite is observed: the amplitude of this component is significantly higher at lower spatial frequencies than at high parietal, central and frontal leads, when only live images are presented in parietal leads. In the control group, the amplitude of the N250 component (P250) in the occipital, central and frontal leads to high-frequency stimuli was significantly higher than the low, and in patients the opposite was true. The ratio of the amplitudes of the P300- P500 component upon presentation of images of high and low frequency frequencies in patients with depression corresponds to the data of the control group in all leads.

When analyzing the data before and after the stimulation course by an interactive virtual environment with a cognitive task, the following significant differences were obtained. In patients with schizophrenia, a significant increase in the amplitudes of the N170 (P170) components in the occipital (O1 and O2) and central areas (Cz), P250 (N250) in the occipital (O1 and O2) and central parietal (Pz) areas and P350 — P500 in the frontal (F3, Fz, F4), central

(Cz, C3, C4) and parietal (P3, Pz, P4) areas upon presentation of images of living and nonliving objects filtered by high spatial frequencies. The most pronounced changes are characteristic of the late components P300 — P500 (Figure 1).

In patients with depression, a significant increase in the amplitude of components is observed: P100 in the occipital-temporal (T5, T6), P170 (N170) in the central parietal, central and central frontal region (Pz, Cz and Fz), component P250 (N250 a) the occipital-temporal (T5, T6), central (Cz) and frontal region (F3, Fz, F4) in response to stimuli of living and nonliving objects of high spatial frequencies. (Figure 1).

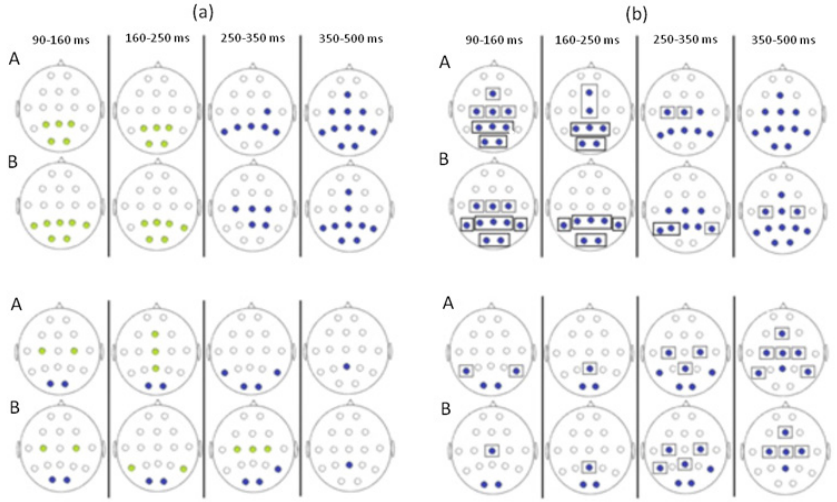

Figure 1. Comparative analysis of the amplitude of components of cognitive visual evoked potentials in patients with depression and schizophrenia before (a) and after (b) sensorimotor load (according to the Wilcoxon test, $p < 0.05$).

Data of patients with depression — top row; of patients with schizophrenia — bottom row.

Green indicates areas where significant differences in the amplitude of evoked potentials were detected when the amplitude in response to images of low spatial frequencies above amplitude in response to images of higher spatial frequencies. Blue indicates areas where significant differences in the amplitude of evoked potentials were detected when the amplitude in response to images of high spatial frequencies above the amplitude in response to images of low spatial frequencies (corresponds to the norm). Without the color — of the area where there were no significant differences. A) — living objects; B) — nonliving objects.

Data were obtained, that patients with schizophrenia experienced violations of the processing of visual information, both in the early and late stages. In depressed patients, only the early stages of visual processing are affected. After a course of exposure to interactive virtual environments with a cognitive task, patients with schizophrenia experience an improvement in the processing of visual information, both in the early and late stages. In depressed patients — in the early stages of the processing of visual information. In patients of both groups, a significant increase in the amplitude of the components of cognitive visual potentials at high spatial frequencies (parvo-system) is observed. Thus, the result of applying the course of exposure is a pronounced activation of the parvo-system, namely the system that is more affected.

When analyzing clinical manifestations when comparing the results obtained only on the background of drug therapy and therapy in combination with neurotechnology with a cognitive task, a more pronounced and rapid decrease in anxiety, a pathological dominant, improvement of structured thinking and emotional state of patients.

Chapter 35.
Mechanisms of visual agnosia in patients with Alzheimer's disease

A. N. Simarev, K. M. Naumov, K. V. Markin, V. U. Lobzin, A. U. Emelin

Alzheimer's disease is a degenerative disease of the nervous system, characterized by a gradual, unobtrusive onset of presenile or senile (> 65 years) age, the steady progression of mental disorders in combination with other cognitive disorders. In the development of BA, a certain staging is observed: in the preclinical stage, neurodegeneration covers the parahippocampal area, then goes to the frontal cortex area, after which the process is generalized, covering the entire cerebral cortex. As a rule, asthma in the initial stages gives a very poor clinical picture, which makes it difficult to carry out early diagnosis. In turn, this leads to a late start of treatment, and, accordingly, its low effectiveness. Development of methods for early diagnosis based on the identification of malfunctions of complex functional systems is considered as a promising direction for solving this problem. One of the particular tasks is to assess the characteristic patterns of visual perception disorders in the early stages of Alzheimer's disease, as a reflection of the defeat of the neural networks for collecting and processing information in the visual system [Belaspova et al., 2016; Emelin, Lobzin, 2017].

Main part

Age-related neurodegeneration is an irreversible process of atrophy of the brain substance that every person will face sooner or later.

Today in Russia about ¼ of the population belonging to the category of persons over working age: men aged 60 years and older, women aged 55 years and older [Population census, 2010] are at risk of developing neurodegenerative diseases, one of whose manifestations is visual impairment.

The most significant role in the pathogenesis of Alzheimer's disease is played by vascular factors, genetic predisposition, disregulation of the blood-brain barrier, and other causes leading to the development of metabolic disorders of β-amyloid and its amyloid precursor protein (APP), which leads to the forma-

tion of amyloid precursor protein (APP) beta amyloid deposits and neurofibrillary tangles. [Vlasenko et al., 2010; Lobzin et al., 2018] A certain stage is observed in the development of BA: in the preclinical stage, neurodegeneration covers the parahippocampal site (mild BA), then spreads to the parietal lobes, then to the frontal cortex area, after which the process is generalized, covering the entire cerebral cortex. Despite the fact that obvious violations of visual perception are considered typical for severe asthma, early signs of visual impairment are also detected at early stages. A number of researchers believe that a special case of Alzheimer's disease is posterior cortical atrophy ("posterior" or "visual" version).

In general, violations of visual perception can lead to violations in any part of the optical path: be it the retina of the eye, the pathways, or the areas of the visual cortex of the brain. Neurodegeneration processes can capture all levels where there are neurons.

Visual perception is not as simple as it seems at first glance. For a long time, it was believed that he was exclusively afferent (centripetal) character, being a passive process, i.e. resulting from stimulation of the senses by agents coming from outside. For the first time denied this hypothesis I.M. Sechenov in his "reflex concept of perception", according to which perception is an active process. [Sechenov, 1947]. He pointed out that "… every act of visual perception includes, along with centripetal (afferent) mechanisms, also centrifugal (efferent) mechanisms. The eye, perceiving objects of the surrounding world, actively "gropes" them, and these "feeling" movements, along with proprioceptive signals from the eye muscles, are included as elements in the visual perception" [Luria, 1962].

A.R. Luria based on the works of A.L. Yarbus [Yarbus, 1961] designated "that the visual perception of an object or its image is a complex active process consisting of extracting individual signs of this object or image, synthesizing them into complexes or groups, and finally choosing a value from a number of alternatives. Sensory and motor devices are involved in this process, in particular, an eye movement device that performs orienting-exploratory activity" [Luria, 1962]. This determines the relevance of the state of associativity of the visual centers of the cerebral cortex.

The process of visual perception itself is carried out at several stages: peripheral, cortical and systemic. In the first case, perception disorders will be associated with degenerative processes of retinal neural networks, in which the number of rods and cones will decrease, as well as ganglion cells, in the second — the defeat of the primary cortical fields of the visual analyzer (decrease

in the number of neurons in the corresponding areas of the cerebral cortex), in the third — defeat of the neural network structures of secondary and tertiary cortical fields responsible for the functions of a conscious gnosis.

Optical image perception is the main step in coding optic information into the nervous system. In photoreceptors, the process of photon absorption and triggering the response of neural structures occurs. After that, from the bipolar cells of the intermediate layer of the retina, the signal is transmitted to the ganglion cells. The latter are the initial stage of neural network processing of visual information, generating propagating impulses. These are the "output" neurons of the retina, their axons form the optic nerve, the axons of the ganglion cells are sent to the subcortical visual centers, mainly in the external articular body. In turn, from the subcortical structures, information enters the cerebral cortex (primary visual cortex, 17 Brodmann field). It is noteworthy that starting from the retinal ganglion cells, neurons are divided into 2 types: large and small. They are associated with overlying structures strictly adhering to a certain regularity — large (Magna) cells with large, and small (Parvo) with small. Thus, the formation of interconnected parvo-and magnosystems [Shelepin, 2017].

After processing, in the primary visual cortex, the magnetic and parvosystems transmit visual information in 2 final streams: the ventral (V) — paravocellular tract and the dorsal (D) — magnocellular tract.

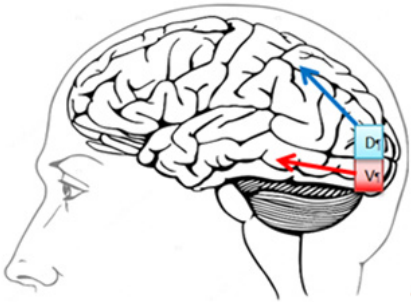

Figure 1. The ventral and dorsal tracks as the "prolongation" of magno- and parvocellular pathways.

The first path starts from 17 fields according to Brodman, passes through 18, 19 and 37 fields heading to the lower temporal field, which is considered to be the repository of image descriptions. Information passing through this path provides object recognition. The magnocellular tract, in turn, is directed to the

parietal cortex, responsible for analyzing the nature of dynamic changes and the position in space of the visual object [Shelepin, 2017].

Both streams are directly related to the prefrontal cortex of the frontal lobe, which plays an important role in both visual and spatial perception, and, along with this, influences the formation of episodic and semantic memory. In addition, the ventral flow has a functional relationship with the hippocampal and parahippocampal regions, which suggests the possibility of comparing and comparing the resulting visual image with the accumulated experience due to semantic memory [Dynin, 2016].

Thus, the presence of a direct relationship between the cortex areas responsible for memory, attention and visual perception explains the possible cumulative impairment of these functions during primary degeneration of both primary and secondary or tertiary cortical fields of the visual analyzer.

Initially it was assumed that it is the degeneration of the ventral flow that is responsible for the "images of memory" that underlies visual agnosia. However, this theory, proposed by Charcot in 1887, was refuted by A. R. Luria, proposing his hypothesis of "amorphosynthesis", i. e. synthesis of individual traits into a single structure. He believed that visual agnosia is a complex visual disorder of the synthesis of isolated elements of visual perception, a violation of the combination of these elements into "simultaneous-perceived groups", which is the basis of the normal recognition of objects [Luria, 1962]. In this regard, it would be wrong to give one of the two streams a leading role in the organization of visual perception disorders.

Clinical studies and experimental observations have made it possible to identify various variants of agnosia.

The initial separation of agnosias was aimed at distinguishing occipital from parietal forms: the so-called lower and upper sections of the "wide visual sphere." The narrower differentiation of clinical forms of agnosia implies the following variations:

1) Predominantly temporal;
2) Temporal-occipital;
3) Predominantly parietal;
4) Parietal-occipital.

Temporal syndrome is characterized by a defect in the recognition of individual subject images (figures, letters or numbers). There is a slowness of

perception of the image, fragmentation with a tendency to complement the perceived fragment to the whole by conjecture, without visual control, a tendency towards excessive generalized perception of the subject. Visual memorization and recognition of a familiar object is impaired. The ability to draw may also be impaired due to the patient's inability to grasp the drawing as a whole and to control itself [Kok, 1967]. For diagnostics tests are used "noisy images", the Popelreyter technique [Poppelreuter, 1923; Shelepin et al., 2009; Sells, Larner, 2011].

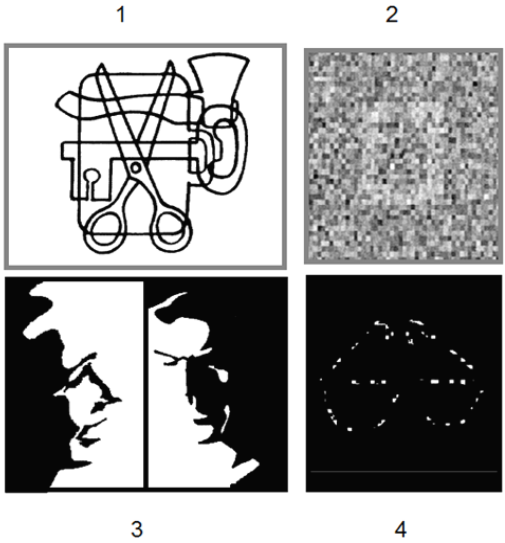

Figure 2. Examples of noisy images used in psychophysiology *1* — Popelreyter test, *2* — wait noise test, *3* — Moony test, *4* — Gollin test [Shelepin et al., 2009].

The temporal-occipital syndrome differs from the previous one by the addition of facial recognition and, sometimes, color disorders. A characteristic feature of agnosia on the face is fragmentation and excessive generalization of the perception of individuals. Also, with this form of visual agnosia, optical alexia can be observed (reading disorder) [Kok, 1967]. For the diagnosis of high performance tests show with illusions using painting of Octavio Ocampo [Painting «Family of birds» and Painting «General's Family», 2019].

The parietal and parietal-occipital syndromes are distinguished by the presence of simultaneous agnosia — the inability to assess the meaning of the picture due to the fragmentary perception of the spatial situation with the

intimate recognition of individual objects. Drawing skills are impaired due to the violation of visual control, due to the inability to cover the spatial relationships of the details as a whole. Sometimes there is an apraxia of dressing.

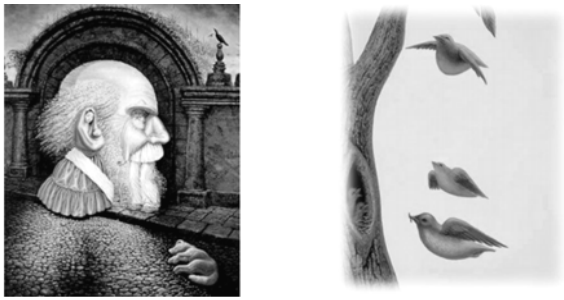

Figure 3. Examples of optical illusions used to assess facial recognition [Painting «Family of birds» and Painting «General's Family», 2019].

The method of assessing the ability to recognize emotional facial expressions is of great interest. Photographs of familiar faces or relatives are a more sensitive stimuli.

Figure 4. Examples of typical images of emotions (own images).

Great expectations are associated with the use of using the Gollin test (measurement of recognition thresholds for fragmented outline images during gradual construction of the outline). [Shelepin et al., 2009]. The possibility of using this method in clinical practice is currently being studied.

In the diagnosis of disorders of visual perception, we use the following approach, determined from the results of a preliminary analysis of the literature and our own experience:

1. Standard techniques: MOCA, FAB, MMSE, clock drawing test — used to confirm and evaluate the severity of cognitive deficit.
2. Ophthalmological methods aimed at assessing the state of the fundus (examination, EAST), neurophysiological VEP — to assess the state of the pathways of the visual analyzer.
3. Special methods for the detection of agnosias: subject gnosis ("noisy image" technique, Popplereyter technique), the Gollin test, face detection, emotion estimation, letter definition, color definition, test images for the diagnosis of simultaneous and optical-spatial gnosis.

With the introduction of modern methods of examining patients in perspective, the following methods of early diagnosis of BA:

1. Functional magnetic resonance imaging is a technique that registers special BOLD-signals (blood oxygen level dependent) from the volume points of the brain, thus reflecting changes in the neural networks of the brain.
2. Eye-tracking — a method of registration of eye movement when viewing images shown.
3. Tachystoscopy — a technique for studying the speed of visual perception.
4. Determination of the coefficient of efficiency of visual perception reflects the value of the image contrast energy necessary for recognizing the presented image in comparison with the ideal model [Danko et al., 1999].

Conclusion

1. The proposed theory of the development of visual agnosia in patients with BA takes into account the possibility of suffering of all parts of the visual tract. The most critical areas should be considered the retinal ganglion cells, spur neurons, parietal-occipital sulcus, lateral occipital sulcus, hippocampus and parahippocampal gyrus, prefrontal regions of the frontal lobe.
2. The clinical manifestations of visual agnosia are highly variable and depend on the location and stage of the neurodegenerative process. In the early stages of Alzheimer's disease, the most sensitive methods are the detection of agnosia: the subject gnosis is the "noisy image" technique and the Popelreiter technique; making faces out of illusions;

definition of superimposed letters; color definition; simultaneous gnosis; optical spatial gnosis.

3. Further research is needed to identify early clinical patterns of the development of visual impairment in Alzheimer's patients using instrumental neurophysiological techniques based on recording oculomotor disorders and evaluating the complex synthetic functions of the neural networks of the visual analyzer that determine the quality of gnostic functions.

References

1. Belaspova A. V. Posterior cortical atrophy — a variant of progressive local atrophy of the brain / A. V. Belaspova E. S., Berdnikovich A. S., Kadykav, Kashin E. M. // Annals of Clinical and Experimental Neurology.— 2016.— № 3.— p. 61–66.
2. Danko R. E. Efficiency ratio of visual perception in healthy observers and in patients with neurosis / R. E. Danko, N. N. Krasilnikov, A. V. Kuznetsov, S. V. Litvintsev, Y. K. Malakhova, Y. E. Shelepin // Optical journal.— 1999.— № 10.— p. 65–67.
3. Dynin P. S. Features of the visual-perception ofspace consisting of a nstvennogo in Alzheimer's disease: dis. Cand. honey. Sciences: 14.01.11 / Dynin Pavel Sergeevich.— VMA them. S. M. Kirov, Department of Nervous Diseases, 2016.— 149 p.
4. Emelin A. Y. Complex differential diagnosis of cognitive impairment / A. Y. Emelin, V. Y. Lobzin // Journal of Neurology and Psychiatry named after SS. Korsakov.— 2017.— № 6 — p. 33–39.
5. Kok E. P. Visual agnosia / E. P. Cock.— Medicina Publishing House, Leningrad Branch, 1967.— 224 p.
6. Lobzin V. Y. A new look at the pathogenesis of Alzheimer's disease: current understanding of amyloid clearance / V. Y. Lobzin, K. A. Kolmakova, A. Y. Emelin // Review of Psychiatry and Medical Psychology.— 2018.— № 2 — P. 22–28.
7. Luria A. R. Higher human cortical functions and their abnormalities in local brain lesions / A. R. Luria.— Moscow: Moscow University Press, 1962.— 431 p.
8. Painting «Family of birds» by Octavio Ocampo // https:// www.visionsfineart.com/ocampo/family_of_birds.html (available 2019)
9. Painting «General's Family» by Octavio Ocampo // https:// www.visionsfineart.com/ocampo/generals_family.html (available 2019)
10. Poppelreuter W. Zur Psychologie und Pathologie der optischen Wahrnehmung / W. Poppelreuter // Zeitschrift für die Gesamte Neurologie und

Psychiatrie.— 1923.—Vol. 83.—P. 26–152.
11. Population census // Federal State Statistics Service.— 2010, access mode http:// www.gks.ru/free_doc/new_site/perepis2010/croc/Documents/portret-russia.pdf, free.
12. Sechenov I. M. Selected works: in 2 tons. / I. M. Sechenov.—Moscow: Publishing House of the Academy of Science of the USSR, 1947.— 1718 p.
13. Sells R. The Poppelreuter figure visual perceptual function test for dementia diagnosis / R. Sells, A. J. Larner // Prog. Neurol. Psychiatry.— 2011.—Vol. 15, № 2.—P. 17–21.
14. Shelepin Yu. E. Introduction to neuroiconics: Monograph / Yu. E. Shelepin.—St. Petersburg: Trinity Bridge, 2017.— 839 p.
15. Shelepin Yu. E. Chikhman, V.N., Foreman N. Analysis of the studies of the perception of fragmented images: global description and perception using local features // Neurosci Behav Physiol.— 2009.—Jul; 39(6).— P. 569–80.
16. Vlasenko A. G. Regional characteristic of beta-amyloid accumulation at the preclinical and clinical stages of Alzheimer's disease / A. G. Vlasenko, M. A. Minton, D. K. Morris // Annals of Clinical and Experimental Neurology.— 2010.— № 4.—p. 10–14.
17. Yarbus A. L. Eye movement when examining complex objects / A. L. Yarbus.—Moscow: "Biophysics", 1961.— 346 p.

Chapter 36.
Non-pharmacological methods of neuroprotection and neurorehabilitation

M.V. Zueva

Glaucoma, being a multifactorial disease, has many signs of neurodegenerative disorder and involves disruption of neural networks in the brain [Calkins, Horner, 2012; Gupta N. et al., 2006; Lawlor et al., 2018]. Common mechanisms of neurodegeneration in the retina and brain include ischemia, inflammation, mitochondrial dysfunction, oxidative stress, etc. [Cordeiro, 2016]. Three main objectives of neuroprotective therapy for glaucoma considered depending on the timing of the start of treatment, the target and the mechanisms of action include protection of not yet affected axons of retinal ganglion cells (RGCs), salvage of minimally damaged axons or regeneration of RGCs and their axons [Parisi et al., 2008]. The concepts of neuroprotection and neurorehabilitation (or neurorestoration) are attributed as various aspects of the "modifying disease" treatment. A modifying treatment is one that slows down the clinical evolution to the late stages of neurodegenerative diseases, achieving this result either by suppressing primary events (neuroprotection) or by enhancing the compensatory and regenerative mechanisms in the brain (neurorehabilitation) [Francardo et al., 2017].

The neuroprotective activity is inherent of such drugs as glutamate antagonists, ginkgo biloba extract, neurotrophic factors, antioxidants, calcium channel blockers, brimonidine, and antihypertensive drugs with the effect of regulating blood flow, nitric oxide synthase inhibitors [Doozandeh, Yazdani, 2016]. In glaucoma, the problem of deficiency of neurotrophic factors is proposed to be solved using gene therapy with delivery of retinal plasmid DNA encoding neurotrophic factors [Foldvari et al., 2016; Lebrun-Julien, Di Polo, 2008]. In neurodegenerative diseases of the retina and brain, non-drug methods are also used to protect and restore the structure and function of the nervous tissue [Alwis, Rajan, 2014; Baroncelli et al., 2010; Rosa et al., 2013]. Today, special attention is focused on internal restorative strategies based on brain plasticity. Experience-dependent plasticity allows the brain to respond flexibly to changes in inputs from the external environment. The structural-functional plasticity of the neocortex networks in adults is realized

through strengthening, weakening, breaking, or adding synaptic connections in response to environmental challenges. Structural changes in the CNS occur through the Hebbian mechanisms of synaptic and non-synaptic plasticity. In the rehabilitation of patients with neurodegenerative pathology, the role of physical activity and cognitive training was shown. Many methods of activation of neuroplasticity were created in the framework of the concept of "environmental enrichment" [Pascual-Leone et al., 2011]. The structural, cellular and molecular effects of environmental enrichment have been shown in animal research [Baroncelli et al., 2010; Mora et al., 2007]. Not exhausting physical activity is now considered an efficient paradigm of neuroprotection and neurorestoration in the preclinical and advanced stages of Parkinson's disease (PD) [Francardo et al., 2017]. It has been shown in animals that non-stressful physical training regimes have a neuroprotective effect on the dopaminergic and non-dopaminergic systems [Howells et al., 2005; Petzinger et al., 2010; Ryan, Kelly, 2016]. Physical activity can reduce the risk of PD development and improve the quality of life of patients [Hirsch et al., 2016; LaHue et al., 2016; Macpherson et al., 2017]. However, carefully conducted studies on large cohorts have shown a very weak effect for cognitive and physical training in neurodegenerative disorders. The crucial reason for the lack of effectiveness of cognitive and physical training is a progressive and steady decrease in the plasticity potential of the adult brain [Maya-Vetencourt, Origlia, 2012], the rate of which is individual and depends on person-specific genetic, biological, and environmental factors [Pascual-Leone et al., 2011].

For neuroprotection and neurorestoration of the visual system in cases of brain injuries and retinal diseases, several methods of non-drug therapy have been proposed. Bernhard Sabel divides the training for visual rehabilitation in homonymous vision loss caused by post-chiasm damage into two strategies: "compensation" and "recovery" [Dundon et al., 2015; Sehic et al., 2016]. These include visual scanning training (VST), audiovisual scanning training (AViST), and vision restoration therapy (VRT). VST and AViST are aimed at compensating for the loss of the visual field through visual and audiovisual training of scanning eye movements, while the VRT improves visual functions by activating residual vision sites by training the recognition of visual stimuli.

Neuroprotective possibilities of non-invasive brain stimulation (NIBS) are also discussed. Transcranial electro- and magnetostimulation have numerous effects on the structure and function of nervous tissue, EEG, cognitive functions, motor activity, and behavioral responses in patients with neurological

disorders, trauma, and cerebral strokes [Henrich-Noack et al., 2017]. However, the positive and negative effects of NIBS are still insufficiently studied, the mechanisms of their action are not well-understood, and the optimal therapeutic doses and parameters of transcranial stimulation are not determined, so it does not allow yet recommending this method in widespread clinical practice.

Non-invasive strategies of transcorneal, transorbital, and transpalpebral electrostimulation (ES) have been studying for more than 25 years in animal and clinical research. Non-invasive ES is considered a promising approach to preserve and restore vision in certain diseases of the retina and optic nerve. The mechanisms underlying the neuroprotective effects of transcorneal ES include an increase in the production of neurotrophic factors, an improvement in the chorioretinal blood circulation, inhibition of pro-inflammatory cytokines [Sehic et al., 2016]. Transorbital repetitive ES with the alternating current improved visual fields after the optic nerve damage [Gall et al., 2016]. The rhythmic stimulation with light flashes and sound tones, adequate to the visual and auditory system, is considered to be a most promising method of brain stimulation. The rehabilitation effects of rhythmic sensory stimulation are based on the phenomenon of "brainwave entrainment" and synchronization in cortical activity. The brain is highly sensitive to the rhythms of the external environment and adapts the rhythms of its activity with the temp of repeated audio- and visual signals, changing the power of the dominant rhythms in the EEG [Barlow, 1960].

However, the evidence showed that periodic rhythms can only locally improve cortical activity in specific EEG ranges, but are not able to restore the complex fractal dynamics characteristic of healthy brain activity (for review see [Zueva, 2015]). A typical sign of normal physiological processes is their fractal dynamics, the power spectrum of which corresponds to 1/f. The fractal complexity of brain activity is lost in neurodegenerative diseases [Al-Nuaimi et al., 2018; Dauwels et al., 2011; Jeong, 2004]. In pathology, fractal dynamics is replaced by ordered fluctuations of physiological parameters or completely random (stochastic) behavior [Goldberger et al., 2002; Hausdorff et al., 1996; Lipsitz, Goldberger, 1992; Manor, Lipsitz, 2013]. Evidence has been collected of the fractal anatomy of the vascular network and neural networks of the eye and brain and their lost in various retinal diseases, for example, in diabetic retinopathy [Tălu et al., 2015] and primary open-angle glaucoma (POAG) [Ciancaglini et al., 2015]. Glaucoma first causes an increase in the fractal complexity of the RGC's dendritic tree for three weeks, and then its progressive decrease [Kalesnykas et al., 2012]. A decrease in the fractal complexity

of dendritic branching in experimental glaucoma was found also for neurons in lateral geniculate body [Ly et al., 2011].

Because the potential of neuroplasticity is significantly reduced with aging and diseases, the effectiveness of any methods of neurorehabilitation based on brain plasticity is objectively limited. On the other hand, stimulation therapies usually apply regular stimuli of a constant frequency, which are not able to restore the normal fractal pattern of the physiological rhythms, and can further remove the system from the dynamics that characterize healthy processes. We hypothesized that for the best effectiveness of any strategies for restoring the structure and activity of the retina and the brain, an activation of adaptive neuroplasticity is necessary.

Considering this, we have developed a new approach to stimulation, based on the use of complex-structured signals with fractal dynamics. We propose that fractal modes in sensory stimulation can improve the effectiveness of various therapeutic strategies aimed at restoring the brain by activating the potential of neuroplasticity. A model range of fractal stimulators is created, which generate complex-structured optical signals with given properties and different FDs based on Weierstrass functions (Patent RU2671199, 2018 and Patent RU2680185, 2019). We hypothesized that fractal optical stimulation could be a promising non-pharmacological approach in the neuroprotective therapy. The effect of low-intensity fractal phototherapy on sensitivity in the visual field (Humphrey perimetry) was evaluated in patients with suspected glaucoma and primary open-angle glaucoma (POAG) [Zueva, 2018]. In the photostimulator, the LED emitter built in the case of virtual reality glasses formed the optical signal with the maximum brightness of on the cornea $10-12\ Lx$ and $FD=1.4$.

The group of comparison used a relaxation video program twice a day for 10 days instead of phototherapy (https://www.youtube.com/watch?v=8LFTTULcqD4). In the video program, the observer was presented with a computer-simulated image — a geometric fractal set with the effect of the illusion of movement. The duration of each relaxing video training session is 30 minutes. The positive effect of fractal stimulation was found both in the suspected glaucoma group and in eyes with an early and developed stage of POAG. Two-week low-intensity fractal phototherapy significantly improved the MD indices in the main group. In contrast, after the video-course, there was only a tendency to improve the sensitivity, but MD indices did not change much [Zueva, 2018].

Thus, we obtained the first evidence of the neuroprotective effect of fractal phototherapy for glaucoma. Low-intensity stimulation with signals with a fractal dimension of 1.4 improved the values of MD in all groups with POAG

and suspected glaucoma. The results allow suggesting that in advanced glaucoma, a decrease in visual functions is associated not only with the death of RGCs but also with dysfunction of surviving cells that are yet at the stage of reversible plastic changes. These results also substantiate the advisability of administering neuroprotective therapy to patients with any stage of glaucoma, including pre-perimetric and far-advanced POAG. The mechanism of the neuroprotective effect of fractal optical stimulation may be associated with the activation of synaptic and dendritic plasticity. Fractal stimulation can have effects at the cellular and molecular levels, activating neurotrophic factors and enhancing the expression of genes that control protein synthesis and neural signaling. We concluded that manifestations of adaptive plasticity at the preclinical stage for some RGCs in glaucoma may underlie the neuroprotective effects of fractal phototherapy. The modifying disease impacts of fractal photostimulation can apparently be reflected in the suppression of primary events in the development of POAG.

References

1. Al-Nuaimi A. H. et al. Complexity Measures for Quantifying Changes in Electroencephalogram in Alzheimer's Disease. Complexity. 2018; Art. 8915079.
2. Alwis D. S., Rajan R. Environmental enrichment and the sensory brain: the role of enrichment in remediating brain injury. Front. Syst. Neurosci. 2014; 8:156.
3. Barlow J. S. Rhythmic activity induced by photic stimulation in relation to intrinsical activity of the brain in man. Electroencephalogr Clin Neurophysiol. 1960; 12: 317–26.
4. Baroncelli L. et al. Nurturing brain plasticity: impact of environmental enrichment. Cell Death Different. 2010; 17:1092–103.
5. Calkins D. J., Horner P. J. The cell and molecular biology of glaucoma: Axonopathy and the brain. IOVS. 2012; 53(5): 2482–84.
6. Ciancaglini M. et al. Fractal dimension as a new tool to analyze optic nerve head vasculature in primary open angle glaucoma. In Vivo. 2015; 29:273–80.
7. Cordeiro M. F. Eyeing the brain. Acta Neuropathologica. 2016; 132(6):765–6.
8. Dauwels J. et al. Slowing and Loss of Complexity in Alzheimer's EEG: Two Sides of the Same Coin? Int. J. Alzheim. Dis. 2011; 2011, Art ID539621, 10 pages.
9. Doozandeh A., Yazdani S. Glaucoma Neuroprotection. J Ophthalmic Vis Res.2016; 11:209–20.

10. Dundon N.M. et al. Visual rehabilitation: visual scanning, multisensory stimulation and vision restoration trainings. Front Behav Neurosci. 2015; 9, Art.192.
11. Foldvari M., Ding Wen Chen D.W. The intricacies of neurotrophic factor therapy for retinal ganglion cell rescue in glaucoma: a case for gene therapy. Neural Regen Res. 2016;11(6):875–7.
12. Francardo V. et al. Neuroprotection and neurorestoration as experimental therapeutics for Parkinson's disease. Exp Neurol. 2017; 298; 137–47.
13. Gall C. et al. Alternating current stimulation for vision restoration after optic nerve damage: A randomized clinical trial. PLoS ONE. 2016; 11(6): e0156134.
14. Goldberger A.L. et al. Fractal dynamics in physiology: Alterations with disease and aging. PNAS (USA). 2002; 99(Suppl 1):2466–72.
15. Gupta N. et al. Human glaucoma and neural degeneration in intracranial optic nerve, lateral geniculate nucleus, and visual cortex. Br J Ophthalmol. 2006; 90: 674–8.
16. Hausdorff J.M. et al. Fractal dynamics of human gait: stability of long-range correlations in stride interval fluctuation. J Appl Physiol. 1996; 80:1448–57.
17. Henrich-Noack P. et al. Non-invasive electrical brain stimulation: from acute to late-stage treatment of central nervous system damage. Neural Regen Res. 2017; 12: 1590–94.
18. Hirsch M.A. et al. Exercise-induced neuroplasticity in human Parkinson's disease: what is the evidence telling us? Parkinsonism Relat Disord. 2016;22(S.1):78–81.
19. Howells F.M. et al. Stress reduces the neuroprotective effect of exercise in a rat model for Parkinson's disease. Behav Brain Res. 2005; 165:210–20.
20. Jeong J. EEG dynamics in patients with Alzheimer's disease. Clin Neurophysiol. 2004 Jul; 115(7):1490–505.
21. Kalesnykas G. et al. Retinal ganglion cell morphology after optic nerve crush and experimental glaucoma. Invest Ophthalmol Vis Sci. 2012 Jun 22; 53(7):3847–57.
22. LaHue S.C. et al. The best medicine? The influence of physical activity and inactivity on Parkinson's disease. Mov Disord. 2016; 31: 1444–54.
23. Lawlor M. et al. Glaucoma and the brain: Trans-synaptic degeneration, structural change, and implications for neuroprotection. Surv Opthalmol. 2018; 63: 296–306.
24. Lebrun-Julien F., Di Polo A. Molecular and cell-based approaches for neuroprotection in glaucoma. Optom Vis Sci. 2008; 85(6): 417–24.
25. Lipsitz L.A., Goldberger A.L. Loss of 'complexity' and aging. Potential

applications of fractals and chaos theory to senescence. JAMA. 1992; 267:1806–09.
26. Ly T. et al. Dendrite plasticity in the lateral geniculate nucleus in primate glaucoma. Vision Res. 2011; 51(2): 243–50.
27. Macpherson H. et al. A life-long approach to physical activity for brain health. Front Aging Neurosci. 2017; 9, p. 147.
28. Manor B., Lipsitz L.A. Physiologic complexity and aging: implications for physical function and rehabilitation. Prog Neuropsychopharmacol Biol Psychiatry. 2013; 45:287–93.
29. Maya-Vetencourt J. F., Origlia N. Visual cortex plasticity: a complex interplay of genetic and environmental influences. Neural Plasticity. 2012, Article ID631965, 14 pages.
30. Mora F. et al. Aging, plasticity and environmental enrichment: structural changes and neurotransmitter dynamics in several areas of the brain. Brain Res Rev. 2007;55(1):78–88.
31. Parisi V. et al. Evidence of the neuroprotective role of citicoline in glaucoma patients. Prog Brain Res. 2008; 173:541–54.
32. Pascual-Leone A. et al. Characterizing brain cortical plasticity and network dynamics across the age-span in health and disease with TMS-EEG and TMS-fMRI. Brain Topogr. 2011; 24:302–15.
33. Petzinger G.M. et al. Enhancing neuroplasticity in the basal ganglia: the role of exercise in Parkinson's disease. Mov Disord. 2010; 25(Suppl. 1): 141–45.
34. Rosa A.M. et al. Plasticity in the human visual cortex: an ophthalmology-based perspective. Biomed. Res. Int. 2013; 2013:568354.
35. Ryan S.M., Kelly A.M. Exercise as a pro-cognitive, pro-neurogenic and anti-inflammatory intervention in transgenic mouse models of Alzheimer's disease. Ageing Res Rev. 2016; 27:77–92.
36. Sabel B.A. et al. Vision Restoration in Glaucoma by activating Residual Vision with a Holistic, Clinical Approach: A Review. J Curr Glaucoma Pract. 2018;12(1):1–9.
37. Sehic A. et al. Electrical stimulation as a means for improving vision. Am J Pathol 2016, 186: 2783–97.
38. Tălu S. et al. Characterisation of human non-proliferative diabetic retinopathy using the fractal analysis. Int J Ophthalmol. 2015; 8(4):770–76.
39. Zueva M. Fractality of sensations and the brain health: the theory linking neurodegenerative disorder with distortion of spatial and temporal scale-invariance and fractal complexity of the visible world. Front Aging Neurosci. 2015; 7:135.
40. Zueva M. et al. Fractal optical stimulation improves visual fields in glaucoma patients. Doc Ophthalmologica. 2018; 136(Suppl.1):35.

AUTHORS

Aleksandrov A.A. – St.Petersburg State University, St. Petersburg, Russia
Alizade M.R. – Kirov Medical Military Academy, St. Petersburg, Russia
Andreeva G.O. – Kirov Medical Military Academy, St. Petersburg, Russia
Andreeva I.G. – I.M. Sechenov Institute of Evolutionary Physiology and Biochemistry, Russian Academy of Sciences, St. Petersburg, Russia
Babenko V.V. – Southern Federal University Rostov-on-Don, Russia
Boiko A.A. – Pavlov Institute of Physiology Russian Academy of Sciences, St. Petersburg, Russia; ITMO University St. Petersburg, Russia
Bondarko V.M. – Pavlov Institute of Physiology Russian Academy of Sciences, St. Petersburg, Russia
Chikhman V.N. – Pavlov Institute of Physiology Russian Academy of Sciences, St. Petersburg, Russia
Danilichev S.N. – "Federal State Budgetary Institution Scientific Research Institute of CPC named after Yu.A. Gagarin", Russia
Dmitrieva E.S. – St.Petersburg State University, St. Petersburg, Russia
Dobrov A.V. – AIIRE St. Petersburg, Russia
Dynin P.S. – Kirov Medical Military Academy, St. Petersburg, Russia
Emelin A.U. – Kirov Medical Military Academy, St. Petersburg, Russia
Glasman K.F. – St.Petersburg University of Film and Television, St. Petersburg, Russia
Gerasimov A.P. – Almazov National Medical Research Centre, St. Petersburg, Russia
Gorbatov D.S. – St. Petersburg State Institute of Psychology and Social Work, St. Petersburg, Russia
Grinenko E.N. – St.Petersburg University of Film and Television, St. Petersburg, Russia
Gvozdeva A.P. – I.M. Sechenov Institute of Evolutionary Physiology and Biochemistry Russian Academy of Sciences, St. Petersburg, Russia

Harauzov A. K. – Pavlov Institute of Physiology Russian Academy of Sciences, St. Petersburg, Russia

Ikonopistseva K. A. – Southern Federal University Rostov-on-Don, Russia

Ivanova L. E. – Pavlov Institute of Physiology Russian Academy of Sciences, St. Petersburg, Russia

Knyazeva V. M. – St.Petersburg State University, St. Petersburg, Russia

Koroleva I. V. – St. Petersburg Scientific Research Institute of Ear, Throat, Nose and Speech

Kozub K. E. – Pavlov Institute of Physiology Russian Academy of Sciences, St. Petersburg, Russia

Krasilnikov N. N. – Petersburg State University of Aerospace Instrumentation, St. Petersburg
NNKrasilnikov@yandex.ru

Krasilnikova O. I. – Petersburg State University of Aerospace Instrumentation, St. Petersburg

Krivenchuk D. S. – Brain Center and Institute of Physiology, National Academy of Sciences, Minsk, Belarus

Kulchitsky V. A. – Brain Center and Institute of Physiology, National Academy of Sciences, Minsk, Belarus

Labutina O. V. – Pavlov Institute of Physiology Russian Academy of Sciences, St. Petersburg, Russia

Litvinenko I. V. – Kirov Medical Military Academy, St. Petersburg, Russia

Lobzin V. U. – Kirov Medical Military Academy, St. Petersburg, Russia

Malakhova K. Yu. – Pavlov Institute of Physiology Russian Academy of Sciences, St. Petersburg, Russia

Malashin D. O. – Pavlov Institute of Physiology Russian Academy of Sciences, St. Petersburg, Russia
The Joint-Stock Company "Ural Optical and Mechanical Plant named after Mr. E. S. Yalamov" (UOMZ), Branch "Ural-GOI"
malashindo@yandex.ru

Malashin R. O. – Pavlov Institute of Physiology Russian Academy of Sciences, St. Petersburg, Russia
ITMO University St. Petersburg, Russia

Markin K. V. – Kirov Medical Military Academy, St. Petersburg, Russia

Merkulyeva N. S. – Pavlov Institute of Physiology Russian Academy of Sciences, St. Petersburg, Russia
mer-natalia@yandex.ru

Michalkin A.A. – Pavlov Institute of Physiology Russian Academy of Sciences, St. Petersburg, Russia

Moiseenko G.A. – Pavlov Institute of Physiology Russian Academy of Sciences, St. Petersburg, Russia

Murav'eva S.V. – Pavlov Institute of Physiology Russian Academy of Sciences, St. Petersburg, Russia
muravsvetlana@mail.ru

Naumov K.M. – Kirov Medical Military Academy, St. Petersburg, Russia
naumov_k@list.ru

Ogorodnikova E.A. – Pavlov Institute of Physiology Russian Academy of Sciences, St. Petersburg, Russia

Pavlov A.V. – ITMO University St. Petersburg, Russia

Pechenchin D.V. – Kirov Medical Military Academy, St. Petersburg, Russia

Podvigina D.N. – Pavlov Institute of Physiology Russian Academy of Sciences, St. Petersburg, Russia

Pronin S.V. – Pavlov Institute of Physiology Russian Academy of Sciences, St. Petersburg, Russia

Puchkov N.A. – Kirov Medical Military Academy, St. Petersburg, Russia

Shalygin D.Yu – Mechnikov North-Western State Medical University, St. Petersburg, Russia

Shelepin E.Yu. – Pavlov Institute of Physiology Russian Academy of Sciences, St. Petersburg, Russia

Shelepin Yu.E. – Pavlov Institute of Physiology Russian Academy of Sciences, St. Petersburg, Russia

Shchemeleva O.V. – Pavlov Institute of Physiology Russian Academy of Sciences, St. Petersburg, Russia

Shepeleva I.P. – Pavlov Institute of Physiology Russian Academy of Sciences, St. Petersburg, Russia

Simarev A.N. – Kirov Medical Military Academy, St. Petersburg, Russia

Skuratova K.A. – St.-Petersburg State University St.—Petersburg, Russia

Smirnova V.A. – I.M. Sechenov Institute of Evolutionary Physiology and Biochemistry, Russian Academy of Sciences

Solnushkin S.D. – Pavlov Institute of Physiology Russian Academy of Sciences, St. Petersburg, Russia

Solovyev N.A. – St. Petersburg State Institute of Psychology and Social Work, St. Petersburg, Russia
solovyovnikita@yandex.ru

Soms L. N. – Vavilov State Optical Institute, University ITMO St. Petersburg, Russia
AIIRE LLC- Artificial Intelligence Information Retrieval Engine, St. Petersburg, Russia

Soms N. L. – Vavilov State Optical Institute, University ITMO St. Petersburg, Russia
AIIRE LLC- Artificial Intelligence Information Retrieval Engine, St. Petersburg, Russia

Stankevich L.N. – St.Petersburg State University, St. Petersburg, Russia

Tarumov D.A. – Kirov Medical Military Academy, St. Petersburg, Russia

Temniy A.V. – Kirov Medical Military Academy, St. Petersburg, Russia

Titarenko M. A. – ITMO University St. Petersburg, Russia;
Pavlov Institute of Physiology Russian Academy of Sciences, St. Petersburg, Russia

Varovin I.A. – Pavlov Institute of Physiology Russian Academy of Sciences, St. Petersburg, Russia

Vasiljev P.P. – Pavlov Institute of Physiology Russian Academy of Sciences, St. Petersburg, Russia

Yavna D.V. – Southern Federal University Rostov-on-Don, Russia

Zamaro A.S. – Brain Center and Institute of Physiology, National Academy of Sciences, Minsk, Belarus

Zhukova O.V. – Pavlov Institute of Physiology Russian Academy of Sciences, St. Petersburg, Russia

Zueva M.V. – Moscow Helmholtz Research Institute of Eye Diseases Moscow, Russia

Научное издание

НЕЙРОННЫЕ СЕТИ И НЕЙРОТЕХНОЛОГИИ

Коллективная монография

Под редакцией Ю. Е. Шелепина, Е. А. Огородниковой, Н. А. Соловьева, Е. Г. Якимовой

Компьютерная верстка: *Мещерин В. В.*

Подписано в печать 03.09.2019. Формат 60 × 84 1/16.
Бумага офсетная. Гарнитура Times. Печать цифровая.
Усл. печ. л. 17,20. Тираж 500 экз. Заказ № 996.

Отпечатано в Издательстве ВВМ .
198095, Санкт-Петербург, ул. Швецова, 41.